The diamagnetic angular momentum of an electron

Colin R. Greenshields

M.Sci. (Hons)

Submitted in fulfilment of the requirements for the

Degree of Doctor of Philosophy

School of Physics and Astronomy

College of Science and Engineering

University of Glasgow

January 2016

Abstract

Diamagnetism is the magnetism exhibited by all materials, even those not normally considered magnetic, in the presence of an applied magnetic field. On a microscopic level, it is associated with the angular momentum acquired by individual electrons in the magnetic field. Recently discovered electron vortices, meanwhile, possess orbital angular momentum even in field-free space.

In this thesis, I consider the angular momentum of an arbitrary electron wavefunction in a uniform magnetic field. I show that the kinetic orbital angular momentum of the electron can be represented as a sum of three components: the canonical angular momentum associated with a vortex, the angular momentum associated with a cyclotron orbit of the wavefunction as a whole, and a "diamagnetic" angular momentum associated with an internal rotation of the wavefunction that is induced by the magnetic field.

I show that the diamagnetic angular momentum depends on the moment of inertia of the electron's probability distribution, which for free electrons has interesting consequences. Whereas diamagnetism in materials is normally very small compared to the effects of intrinsic magnetic moments, a free electron – for example, in an electron microscope – can have a probability distribution with a much larger average radius. This means that the diamagnetic component can be the dominant contribution to the electron's angular momentum. On the other hand, the diamagnetic angular momentum may instead be of a similar magnitude to the canonical and/or cyclotron components, in which cases the current density strongly depends on the relative magnitudes and directions of these components.

Further, diffraction and interference of the electron's wavefunction lead to interesting dynamical effects. I demonstrate that the kinetic angular momentum of the electron can vary with time, which seems at first sight to violate angular momentum

conservation. The diamagnetic angular momentum also gives rise to a "Faraday effect" for electrons, analogous to the rotation of the polarization of light in a magnetic field. All of this behaviour is a surprising departure from the simple cyclotron orbit predicted by classical theory.

Contents

List of Figures

Acknowledgements

First and foremost I would like to thank my supervisors Bob Stamps and Sonja Franke-Arnold. I have been very lucky to have had two excellent supervisors who have both contributed so much to my work and my personal development. They have complementary strengths, and make a great team!

A number of other researchers have had a significant impact on my PhD. Steve Barnett helped enormously in bringing clarity to my half-formed ideas on angular momentum conservation. I also learned a great deal from Konstantin Bliokh, during the three months I spent at RIKEN in Japan. Franco Nori welcomed me warmly into his research group at RIKEN, and was a valued mentor when my supervisors were on the other side of the world. (Or I thought they were, at least. A few days after I arrived Bob appeared unexpectedly in the same building, on completely unrelated business!) A special mention should also go to Donald MacLaren and Stephen McVitie, for helping to keep my ideas grounded in reality.

The research I describe here was made possible by funding from the UK EPSRC, through a Scottish Universities Physics Alliance Prize Scholarship. It has been a privilege to have had financial support that allowed me to pursue whatever ideas interested me. I am also grateful for the support and encouragement I received from Bob and Sonja in making the most of the freedom this scholarship provided. My internship at RIKEN was supported by a Postgraduate Research Mobility Scholarship from the College of Science and Engineering, as well as by RIKEN.

It has made a great difference that I've had such a strong support network around me in Glasgow. Working with colleagues who have come from all across the globe, I have felt very lucky to meet regularly with friends I have known since primary school, and to have dinner with my family every weekend. At the same time, one of the most enriching aspects of my time at university has been the many new friends and

acquaintances I have made.

To my parents

Author's declaration

I hereby declare that this thesis is the result of my own work, except where explicit reference is made to the work of others, and has not been presented in any previous application for a degree at this or any other institution.

Publications and data

The following publications and data have arisen from the work described in this thesis:

1. C. Greenshields, R. L. Stamps and S. Franke-Arnold, Vacuum Faraday effect for electrons, *New Journal of Physics* 14, 103040 (2012) doi:10.1088/1367-2630/14/10/103040.

2. C. R. Greenshields, R. L. Stamps, S. Franke-Arnold and S. M. Barnett, Is the angular momentum of an electron conserved in a uniform magnetic field?, *Physical Review Letters* 113, 240404 (2014) doi:10.1103/PhysRevLett.113.240404.

3. C. R. Greenshields, S. Franke-Arnold and R. L. Stamps, Parallel axis theorem for free-space electron wavefunctions, *New Journal of Physics* 17, 093015 (2015) doi:10.1088/1367-2630/17/9/093015.

4. C. Greenshields, *Mathematica* program for the numerical solution of the time-dependent Schrödinger equation in the presence of a magnetic field [Data Collection], doi:10.5525/gla.researchdata.199 (2015).

 In this thesis I have adapted and reused elements of these articles. The published versions of the articles are reprinted in Appendix B.

When I was a young child I conceived the idea of an infinite series of universes, the solar system being an atom in a larger universe on the one hand, and the mundane atom a universe to a smaller atom, and so on. I do not go so far as that now, but only observe that there is a tendency to make the electrons indivisible, and all exactly alike. But they must have size and shape, and be therefore divisible. Unless, indeed, they are infinitely rigid. Or they may vary in shape without dividing...

— Oliver Heaviside, *The Radiation from an Electron describing a Circular Orbit* [3]

Chapter 1

Introduction

1.1 Background

1.1.1 Angular momentum of matter and fields

The concept of angular momentum is important for describing systems that possess rotational symmetry. This includes electrons orbiting an atomic nucleus and, on a larger scale, the planets in the solar system. Free rotations, whether of a fundamental particle or of a macroscopic body, are also fruitfully analysed in terms of angular momentum. So is the motion of an electron in a uniform magnetic field, where the symmetry is cylindrical.

The connection between angular momentum and rotational symmetry is one instance of the general principle that is Noether's theorem [4]. Noether showed that for any

symmetry a system possesses, there exists an associated conservation law [5, 6]. For example, the conservation of momentum can be deduced from translational symmetry, and the conservation of energy is related to symmetry in time. In the same way, symmetry under rotation implies that the angular momentum of a system is conserved. In quantum mechanics, this is reflected by the rotational symmetry of the angular momentum eigenstates of a particle.

It is not only massive particles that can possess angular momentum. Electromagnetic fields contain a momentum density, which is proportional to the Poynting vector, and the moment of this momentum defines an angular momentum [7]. This is the case, for example, with the spin angular momentum of the photon, which is associated with the circular polarization of an electromagnetic wave [8, 9].

A subtlety arises when matter interacts with an external electromagnetic field. In this case, the momentum of a massive particle, and therefore its angular momentum, can be defined in different ways [10]. The particle's mechanical motion is described by its *kinetic* momentum. On the other hand, it is the *canonical* momentum that is related to the symmetry of the system. The difference between these quantities can be ascribed to the momentum exchanged between the particle and the field [11]. The distinction between kinetic and canonical momenta is at the heart of the Abraham-Minkowski dilemma, a long-running debate over the amount of momentum light transfers to a material through which it passes [12, 13, 14]. This issue is also of significance when charged matter interacts with an external magnetic field [15, 16, 17, 18].

Photons do not possess electrical charge, and therefore do not interact directly with an external magnetic field. Nonetheless, the polarization of light can be affected by a magnetic field, through the mediation of a magneto-active medium. This was first observed by Michael Faraday, and was the first experimental evidence of a connection between light and electromagnetism [19]. When linearly polarized light propagates parallel to a magnetic field, the polarization direction rotates – an effect that now

bears Faraday's name. Faraday rotation arises as a result of changes to the angular momentum of electrons in the medium, which cause right and left handed circularly polarized light – photons with opposite spin – to travel at different speeds [20].

1.1.2 Optical and electron vortices

It is now well established that, in addition to their spin, photons can possess orbital angular momentum [21, 22]. Whereas a photon's spin is related to polarization, its orbital angular momentum is associated with twisted wavefronts, in an "optical vortex" [23, 24]. Such a vortex coincides with a singularity in the phase of an electromagnetic wave, at which the intensity vanishes [25]. In contrast to the spin, a measurement of which can yield one of only two values, the photon's orbital angular momentum can be an arbitrary multiple of $\hbar$. Over the last two decades optical angular momentum has become a large and very active research field, with numerous emerging technological applications [22, 26].

In a similar way that differing propagation speeds of photons with opposite spin gives rise to a rotation of the linear polarization of light, an orbital angular momentum dependent dispersion results in a rotation of the intensity distribution [27]. Such a dispersion can be induced by rotating the medium through which the light propagates [28, 29, 30], and the image rotation that follows can be interpreted as a "mechanical" Faraday effect [31]. However, a magnetic Faraday effect for optical angular momentum has not been observed. This is consistent with findings that light's orbital angular momentum, in contrast to its spin, does not interact strongly with the internal degrees of freedom of atoms [32], or with chiral media [33, 34, 35].

Electrons possessing quantized orbital angular momentum are familiar from atomic physics. It is only a few years ago, however, that *free* electrons possessing such angular

momentum were predicted and then observed [1, 36, 37, 38]. This angular momentum is associated with a singularity in the phase of the electron's wavefunction, around which the probability current density circulates [39, 40]. In some ways these free electron vortices resemble vortices in fluids; whether classical [41] or quantum [42, 43, 44]. However, in an electron vortex state the angular momentum is associated with a single particle. As with photons, or electrons in atoms, the total angular momentum of a free electron is the sum of its spin and orbital components [45, 46, 47]. Since electrons possess charge, this angular momentum is associated with a magnetic moment [36, 45]. Progress in the understanding of electron vortices, and spatially structured electron states more generally, has been described in a recent review article [48].

Electron vortices have mostly been studied using transmission electron microscopes. These instruments are designed to image materials and structures that are smaller than the wavelength of light [49]. In experiments involving electron vortices, however, the microscope often simply provides a convenient source of highly coherent electron states. The most common technique that has been used to create vortices has been transmitting the electron beam through a special diffraction grating that contains a fork dislocation [1, 38, 50, 51]. This method has been adapted for use with electrons after widespread use in optics. An example of a forked diffraction grating is shown in Fig. 1.1, taken from [1]. Such a grating splits the incident beam into a series of diffraction orders, each of which possesses a different value of orbital angular momentum. The resulting probability distribution can be imaged on the microscope's CCD camera, by detecting the positions of a large number of electrons that pass through the microscope column one after another [52, 53].

It is anticipated that electron vortex beams will have a number of applications, in both fundamental physics and technology. In microscopy, they could be used to map magnetic information at the atomic level [54, 55, 56, 57], as well as to probe chiral properties of molecules and nanostructures [58]. Other potential applications include nanomanipulation [59, 60] and, by exploiting spin-orbit coupling, an efficient method of producing spin-polarized electron beams [61, 62]. Further, electron orbital angular

momentum could be exploited to extract greater information from particle physics collisions [63, 64], and to investigate the radiation produced by magnetic moments [65].

In addition to this, the demonstration of electron vortices has led to an interest in wavefunctions that are sculpted in other ways, and the use of these in specific applications. Recently Airy beams, previously realised with light, were demonstrated for electrons [66]. These have intensity maxima that propagate along a curved trajectory, even though no external force is applied, and open up new possibilities for steering electron wavepackets. Similarly, Bessel beams, the transverse distributions of which do not spread upon free propagation, have recently been realised [67]. These could find application in electron tomography, where images at different planes of depth are needed. Note that a Bessel beam can posses a vortex, but that this is not necessarily the case. Another development is that calculations have shown that electron magnetic circular dichroism can be performed without using a vortex probe, by tailoring the symmetry of the electron phase distribution using abberation-correction optics [68].

1.1.3 Interaction of electrons with a magnetic field

The orbital motion of an electron is influenced by a magnetic field. This can be most simply understood by considering the Lorentz force of classical physics, which in a uniform magnetic field gives rise to a circular orbit of the electron in a plane perpendicular to the field. This is commonly known as the cyclotron orbit, after the early particle accelerator developed by Ernest Lawrence [69]. If the electron also has motion parallel to the field, its trajectory is a helix. In the absence of an external electrical potential, the electron's orbital motion is independent of its spin, of which the component in the direction of the magnetic field is conserved [70].

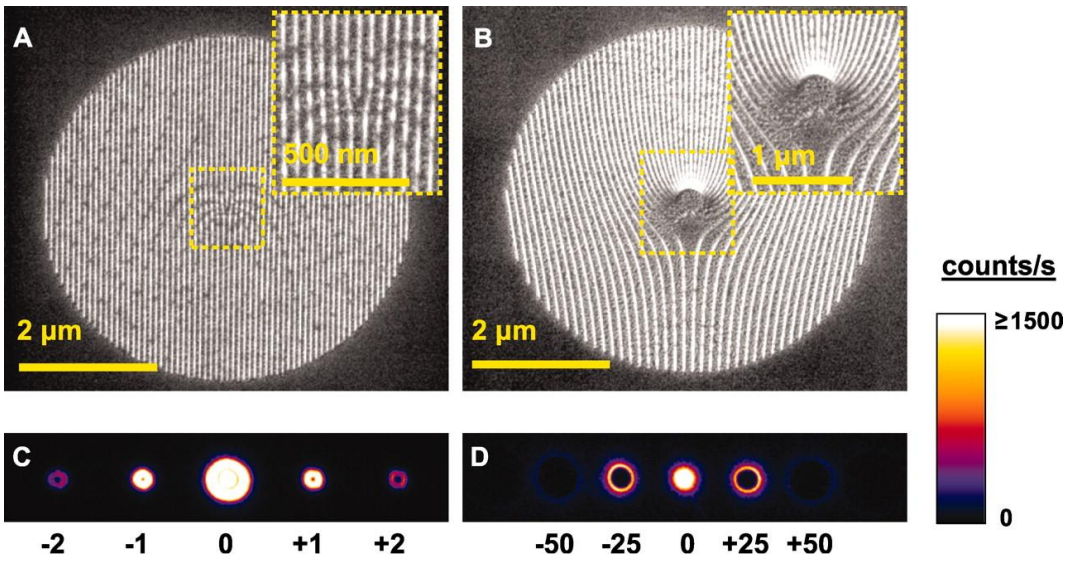

Figure 1.1: **Diffraction gratings used to generate electron vortex beams (top row), and the associated probability distributions (bottom row).** From [1], available at `http://www.sciencemag.org/content/331/6014/192.abstract`, and reprinted with permission from AAAS. An electron beam transmitted through one of the gratings is split into a series of components, which have the orbital angular momentum quantum numbers shown. The diffraction spots corresponding to zero orbital angular momentum are ordinary non-rotating electron states, while the ring-shaped distributions are those of vortex states. The orbital motion of the electron in a vortex state means that there is zero probability of the electron being detected at the centre. The quantum number is equal to a multiple of the number of prongs in the fork dislocation of the grating, which here is equal to 1 (left) and 25 (right).

Interestingly, a uniform magnetic field does not define a unique rotation axis. This is a consequence of the translational symmetry of the field. Rather, the symmetry axis of a cyclotron orbit depends on both the initial position and the initial transverse momentum of the electron.

The situation is different for electrons in atoms. Even when spin-orbit coupling [71, 72] is ignored, the atomic potential has the important effect of constraining the electron's translational motion. The effect of a magnetic field is therefore appropriately described in terms of a perturbation to the atomic energy eigenstates [73, 74]. To first order in the magnetic field strength, the observed energy shifts can be explained using Larmor's theorem: the effect of the external magnetic field is equivalent to a rotation of the coordinate system, with respect to the symmetry axis of the fields, at the Larmor angular velocity [75]. This angular velocity is half of the value for free cyclotron motion [76].

Another consequence of the Larmor rotation of atomic electrons is diamagnetism [77, 78]. This is the small magnetization exhibited by all materials in the presence of an external magnetic field that opposes, and partially cancels, the applied field. Diamagnetism was first explained quantitatively by Langevin, who considered the magnetic moment associated with the Larmor rotation of each electron orbital [79]. The magnetic moment is proportional to the cross-sectional area of the orbital, which is the reason why, in the case of atomic electrons, the magnetization is weak. Typical diamagnetic susceptibilities (the magnetization per unit field strength) are $\sim -10^{-5}$, compared with susceptibilities of 10^{-5}–10^{-3} for paramagnetic materials and 10^{2}–10^{4} for ferromagnets [80].

Diamagnetism can also arise from the motion of free electrons within a material [81, 82]. This is observed in metals and semiconductors, when the temperature is low enough to sufficiently limit scattering [83]. Such a magnetization cannot be understood classically: classical orbits would be reflected at the boundaries of the material, resulting in a net

magnetization of zero [82]. It is explained instead in terms of the energy eigenstates of the system [81]. Known as Landau states, these possess quantized angular momentum. Landau's theory has been successful in explaining the properties of condensed matter in the presence of a magnetic field [84, 85]. However, in such systems the precise state of each electron, including its probability density and current density, remains obscured.

1.2 Outline of thesis

In this thesis, I consider the interaction of a single electron with a uniform magnetic field. I show that, like in condensed matter, the electron possesses a "diamagnetic" angular momentum. I compare and contrast this angular momentum with the canonical angular momentum of a vortex state, and with the angular momentum of the classical cyclotron orbit. My results are of a general nature, and are largely independent of the particular experimental geometry. However, I refer throughout to experiments that can be performed in electron microscopes.

I demonstrate that for a quantum state described by a wavefunction it is meaningful and useful to decompose the electron's total kinetic angular momentum with reference to the centre of mass for the wavefunction. The centre of mass follows a classical cyclotron orbit. The rotation relative to the centre of mass (in the absence of a vortex), meanwhile, exhibits properties familiar from Langevin's and Landau's theories of diamagnetism. For these reasons, I label the corresponding angular momentum components as "cyclotron" and "diamagnetic" respectively.

I show how simultaneous rotations can occur with respect to more than one parallel axis. These parallel-axis rotations are possible with or without the presence of canonical angular momentum, but are particularly striking where there is a superposition of vortices that have different values of this angular momentum. The identification of two

distinct rotation axes does, however, depend on there being an extended probability distribution. In the classical limit, the diamagnetic angular momentum vanishes.

Surprisingly, the diamagnetic angular momentum, and therefore the electron's total kinetic angular momentum, can vary with time. This happens when, due to diffraction, the moment of inertia of the electron's probability distribution varies. Noether's theorem seems to require, however, that the angular momentum of the electron is conserved, since the magnetic field is rotationally symmetric. This apparent paradox is resolved by taking into account the radial electric field of the electron. I show that the combination of this field with the external magnetic field gives rise to an electromagnetic angular momentum, the change in which compensates for that of the familiar mechanical angular momentum. This means that the total angular momentum, including that of the electromagnetic field, is indeed conserved.

The diamagnetic angular momentum has no direct counterpart in optics, since, as already noted, photons do not interact with an external magnetic field. Nonetheless, I show that the rotation of the electron's probability density is closely analogous to the rotation of the polarization of light in the optical Faraday effect. Even in free space, an electron beam experiences a Zeeman interaction with a longitudinal magnetic field. This results in a dispersion that depends on the total angular momentum, including its orbital component. As was predicted for optical angular momentum, such a dispersion gives rise to a rotation of the probability density of a vortex superposition. At the same time that our paper on electron Faraday rotation [86] was published, the same effect, termed Larmor rotation, was predicted by others [87].

My results demonstrate that the rotational dynamics of a single electron can be significantly different from those of a photon, as well as from what is predicted by classical theory for a point particle. In addition to being of fundamental interest, this is likely to be of importance in future applications of electron orbital angular momentum. For a start, magnetic fields are used to manipulate electrons' trajectories, meaning that it

is essential to understand their effect on the electron's angular momentum. Further, understanding such basic interactions with external fields is a necessary first step towards a detailed picture of interactions with matter. While I consider only one very simple field configuration, the concepts I describe apply more generally, and my results could be used to make intuitive predictions and order of magnitude calculations in a variety of situations.

The remainder of the thesis is organised as follows. The next chapter contains background material: both theory and relevant details of experiments. In Chapter 3, I describe the decomposition of the electron's kinetic angular momentum using the parallel axis theorem. Although this research was performed last, it is presented first here as it provides an overview of the different angular momentum components. In Chapter 4, I consider wavefunctions that have a time-varying radius, leading to the aforementioned conservation paradox. This is followed, in Chapter 5, by my results on Faraday rotation, which can be viewed as a consequence of the earlier theory and suggest practical applications. A summary of the thesis and ideas for future research are provided in Chapter 6.

Chapter 2

Electron wavefunctions in a uniform magnetic field

I introduce well-established concepts and results upon which my own work will build. This includes ideas that were established almost a century ago, in the early days of quantum theory, as well as much more recent developments. I first concentrate on theory, and then consider experiments in electron microscopes.

2.1 Theory

2.1.1 Hamiltonian

The motion of an electron in a uniform magnetic field is commonly described within the framework of non-relativistic quantum mechanics [70]. This is appropriate whenever

the electron has a velocity much less than the speed of light. This condition is satisfied, for example, by conduction electrons in metals [81] and semiconductors [88], and electrons trapped in quantum dots [89] or Penning traps [90]. Similarly, free electrons in low energy [91] and photoemission [92] electron microscopes have a non-relativistic velocity, as do electrons emitted in slow ion-atom collisions, where vortices were recently observed [40].

Electrons in transmission electron microscopes typically have an energy $\sim 100\,\mathrm{keV}$, meaning that relativistic effects need to be taken into account. Once a relativistic correction is made to the electron's energy, however, its motion is accurately described by the Schödinger equation [2, 93]. The reason for this is that the transverse component of the electron's momentum is relatively small, and, as a consequence, spin-orbit coupling is negligible [45]. In this thesis, for simplicity, I do not consider relativistic energy corrections. Where accurate quantitative predictions relating to transmission electron microscopy are required, however, these corrections could be applied to my results in the usual manner. The separation of spin and orbital angular momenta in the non-relativistic approximation greatly simplifies the description of the electron's motion.

The Hamiltonian for an electron with non-relativistic energy interacting with an arbitrary magnetic field $\mathbf{B}$, described by a vector potential $\mathbf{A}$, is

$$H = \frac{(\mathbf{p}^{\mathrm{kin}})^2}{2m} - \mathbf{B}\cdot\boldsymbol{\mu}_{\mathrm{s}}. \tag{2.1}$$

Here $\mathbf{p}^{\mathrm{kin}} = m\mathbf{v}$, where $\mathbf{v}$ is the velocity, is the electron's kinetic momentum, which describes its mechanical motion. The kinetic momentum is related to the canonical momentum, $\mathbf{p}^{\mathrm{can}} = -i\hbar\boldsymbol{\nabla}$, by

$$\mathbf{p}^{\mathrm{kin}} = \mathbf{p}^{\mathrm{can}} - e\mathbf{A}. \tag{2.2}$$

As will be described in sections 2.1.3 and 2.1.4, the canonical momentum is an abstract variable that depends on the gauge chosen and does not have a definite physical meaning. In the second term of (2.1) $\boldsymbol{\mu}_{\mathrm{s}} = -g\mu_{\mathrm{B}}\boldsymbol{\sigma}/2$ is the magnetic moment associated

with the electron's spin, $\mu_{\rm B} = -\hbar e/(2m)$ is the Bohr magneton, $\boldsymbol{\sigma} = (\sigma_x, \sigma_y, \sigma_z)$ is the Pauli matrices vector,

$$\sigma_x = \begin{pmatrix} 0 & 1 \\ 1 & 0 \end{pmatrix} \quad \sigma_y = \begin{pmatrix} 0 & -i \\ i & 0 \end{pmatrix} \quad \sigma_z = \begin{pmatrix} 1 & 0 \\ 0 & -1 \end{pmatrix}, \tag{2.3}$$

and $g \approx 2$ [94] is the gyromagnetic ratio. The first term in (2.1) is the kinetic energy of the electron's motion in the magnetic field, while the second term describes the Zeeman interaction of its spin angular momentum with the field. In general, this Zeeman interaction will result in a coupling of the electron's spin and spatial degrees of freedom, even at non-relativistic velocities [61, 95, 96]. However, if the magnetic field is uniform, this coupling vanishes.

In this thesis I consider a uniform magnetic field, the direction of which is taken to define the z axis:

$$\mathbf{B} = B\hat{\mathbf{z}}. \tag{2.4}$$

The vector potential is chosen as

$$\mathbf{A} = -\frac{1}{2}By\hat{\mathbf{x}} + \frac{1}{2}Bx\hat{\mathbf{y}} = \frac{1}{2}B\rho\hat{\boldsymbol{\phi}}, \tag{2.5}$$

where I have introduced cylindrical polar coordinates $\mathbf{r} = (\rho, \phi, z)$. This choice of vector potential is convenient to exploit the rotational symmetry of both the magnetic field and of the electron states I consider. The effect of choosing a different gauge is described later in this chapter. With the magnetic field (2.4) and vector potential (2.5), the Hamiltonian (2.1) becomes

$$H = H_\perp + H_z + H_{\rm s}, \tag{2.6}$$

where

$$H_\perp = \frac{1}{2m}(\mathbf{p}_\perp^{\rm kin})^2 = \frac{1}{2m}(\mathbf{p}_\perp^{\rm can})^2 + \frac{1}{2}m\omega_{\rm L}^2\rho^2 + \omega_{\rm L}L_z^{\rm can}, \tag{2.7}$$

$H_z = (p_z^{\rm kin})^2/(2m)$ and $H_{\rm s} = g\omega_{\rm L}S_z$ [95, 97]. Here S_z is the z component of the electron's spin, which has the eigenvalues $\pm\hbar$.

The component $H_\perp$ describes the energy of the motion of the electron in the plane perpendicular to the magnetic field. Here $\omega_{\rm L} = -eB/(2m)$ is the Larmor angular

velocity and

$$L_z^{\text{can}} = (\mathbf{r} \times \mathbf{p}^{\text{can}})_z = -i\hbar \frac{\partial}{\partial \phi} \tag{2.8}$$

is the z component of the canonical orbital angular momentum. The quadratic position dependence of the second term in (2.7) indicates the similarity of this system to a two dimensional harmonic oscillator, with a frequency equal to the Larmor angular velocity [76], while the final term here describes a rotation of the coordinate system at this angular velocity [75]. Note that for a uniform magnetic field, in the non-relativistic approximation, the Hamiltonian (2.7) is correct to all orders in the magnetic field strength.

The total energy of the electron depends additionally on its linear motion in the z direction and on the Zeeman interaction of its spin. Since the vector potential (2.5) has no z component, the z components of the kinetic and canonical momenta are equal: $p_z^{\text{kin}} = p_z^{\text{can}} = -i\hbar\,\partial/\partial z$. This momentum commutes with the Hamiltonian (2.6), which does not depend explicitly on the z coordinate, and is therefore a constant of motion [81, 97]. This reflects the fact that classically an electron moving parallel to a uniform magnetic field experiences no Lorentz force. Similarly, the z component of spin, S_z, is a constant of motion. This means that it is straightforward to separate the transverse motion of the electron, described by the Hamiltonian (2.7), from its longitudinal motion and spin.

2.1.2 Landau states

As Landau demonstrated in [81], the energy of the orbital motion of a free electron in a uniform magnetic field is quantized. This is a direct consequence of the harmonic effective potential that appears in the Hamiltonian (2.7). Landau quantisation has a significant effect on the properties of condensed matter systems at low temperatures in the presence of a strong magnetic field. It gives rise to the de Haas-van Alphen effect, which can be used to image Fermi surfaces, as well as related behaviour including

Schubnikov-de Haas oscillations [84]. Further, Landau quantisation plays a key role in the quantum Hall effects [85]. Landau levels are highly degenerate, and their effect on condensed matter is associated with a large number of electrons occupying each energy level. The Landau levels of a single electron, and transitions between these, have however been detected using a Penning trap [90]. Very recently the probability density and internal rotational dynamics of Landau states were imaged directly for the first time using electron vortex beams [2].

The Landau wavefunctions are the solutions to the time-independent Schrödinger equation

$$H_\perp \psi_\perp(\mathbf{r}_\perp) = E_\perp \psi_\perp(\mathbf{r}_\perp), \tag{2.9}$$

where $\mathbf{r}_\perp$ denotes the position within the plane perpendicular to the magnetic field. In cylindrical coordinates, the transverse gradient operator, to which the canonical momentum $\mathbf{p}_\perp^{\text{can}}$ is proportional, is $\boldsymbol{\nabla}_\perp = \partial/\partial\rho\,\hat{\boldsymbol{\rho}} + (1/\rho)\partial/\partial\phi\,\hat{\boldsymbol{\phi}}$. The Hamiltonian (2.7) can therefore be expressed as

$$H_\perp = -\frac{\hbar^2}{2m}\frac{1}{\rho}\frac{\partial}{\partial\rho}\left(\rho\frac{\partial}{\partial\rho}\right) - \frac{\hbar^2}{2m}\frac{1}{\rho^2}\frac{\partial^2}{\partial\phi^2} + \frac{1}{2}m\omega_{\text{L}}^2\rho^2 - i\hbar\omega_{\text{L}}\frac{\partial}{\partial\phi}. \tag{2.10}$$

The wavefunctions that satisfy the equation (2.9) are found to be the following products of ρ and ϕ dependent contributions:

$$\psi_{\perp\,n,\ell}^{\text{Lan}} = N_{n,|\ell|}\left(\frac{\rho\sqrt{2}}{\rho_{\text{B}}}\right)^{|\ell|}\exp\left(-\frac{\rho^2}{\rho_{\text{B}}^2}\right)L_n^{|\ell|}\left(\frac{2\rho^2}{\rho_{\text{B}}^2}\right)\exp\left(i\ell\phi\right) \tag{2.11}$$

[70]. Here $n = 0, 1, 2, ...$ is the radial quantum number, $\ell \in \mathbb{Z}$ is the quantum number for the z component of orbital angular momentum, $L_n^{|\ell|}$ is an associated Laguerre polynomial,

$$\rho_{\text{B}} = 2\sqrt{\frac{\hbar}{|eB|}} \tag{2.12}$$

is a characteristic radius and $N_{n,|\ell|} = \sqrt{2n!/[\pi(n+|\ell|)!]}/\rho_{\text{B}}$ is a normalisation constant. The wavefunction is normalised such that $\int \mathrm{d}^2\mathbf{r}_\perp\,|\psi_{\perp\,n,\ell}^{\text{Lan}}|^2 = 1$. As will be discussed in subsequent chapters, the Landau wavefunctions (2.11) closely resemble the Laguerre-Gaussian functions used to describe optical and electron vortices.

The probability density, $|\psi^{\rm Lan}_{\perp n,\ell}|^2$, and probability current density,

$$\mathbf{j}^{\rm Lan}_{\perp n,\ell} = \frac{1}{m}{\rm Re}(\psi^{\rm Lan}_{\perp n,\ell}{}^{*}\mathbf{p}^{\rm kin}_{\perp}\psi^{\rm Lan}_{\perp n,\ell}) = |\psi^{\rm Lan}_{\perp n,\ell}|^2\left(\frac{\ell\hbar}{m\rho}+\omega_{\rm L}\rho\right)\hat{\boldsymbol{\phi}} \tag{2.13}$$

[98], of Landau states with $n = 0$ and $n = 1$ are shown in Figs. 2.1 and 2.2. The corresponding energy eigenvalues are

$$\begin{aligned} E^{\rm Lan}_{\perp N} &= (2n+|\ell|+1)\hbar|\omega_{\rm L}| + \ell\hbar\omega_{\rm L} \\ &= (N+\frac{1}{2})\hbar|\omega_{\rm c}| \end{aligned} \tag{2.14}$$

where $N = n + [1+{\rm sign}(\ell B)]\,|\ell|/2 = 0, 1, 2, \ldots$ and $\omega_{\rm c} = 2\omega_{\rm L} = -eB/m$ is the cyclotron angular velocity. These energy levels are equally spaced with an interval $\hbar|\omega_{\rm c}|$, with a minimum value of $E^{\rm Lan}_{\perp 0} = \hbar|\omega_{\rm c}|/2$, as illustrated in Fig. 2.3. There is also a degeneracy of the energy of the eigenfunctions $\psi^{\rm Lan}_{\perp n,\ell}$, with different combinations of n and ℓ corresponding to the same value of N. Of particular note, all states for which ℓ has the opposite sign to B have the energy quantum number $N = n$, which is independent of the magnitude of ℓ. It will be seen later that this is a consequence of a partial cancellation of the canonical and diamagnetic components of the electron's orbital angular momentum. Reversing the direction of the magnetic field raises or lowers the energy quantum number N by an amount equal to $|\ell|$.

In general, an electron in a magnetic field will not be in a stationary pure Landau state, but rather in a superposition of a large number of these. This is certainly the case in electron optics, where the probability density of the electron varies upon propagation, and where an arbitrary initial state can be defined using components such as holograms [99]. Even if the electron's probability density is rotationally symmetric, and has a radial distribution resembling a Laguerre-Gaussian function, it may be that there is a net transverse momentum, resulting in motion of the centre of mass of the distribution. I consider the consequences of such a transverse momentum in Chapter 3. Another possibility is that the radial distribution is either more spread out or more tightly focused than that of the corresponding Landau state, which has a mean-square radius determined by the magnetic field. This is the situation I consider in Chapter 4. Also, Landau states with different values of ℓ can be superposed, breaking the rotational symmetry of the probability density. Such superpositions will be considered in both

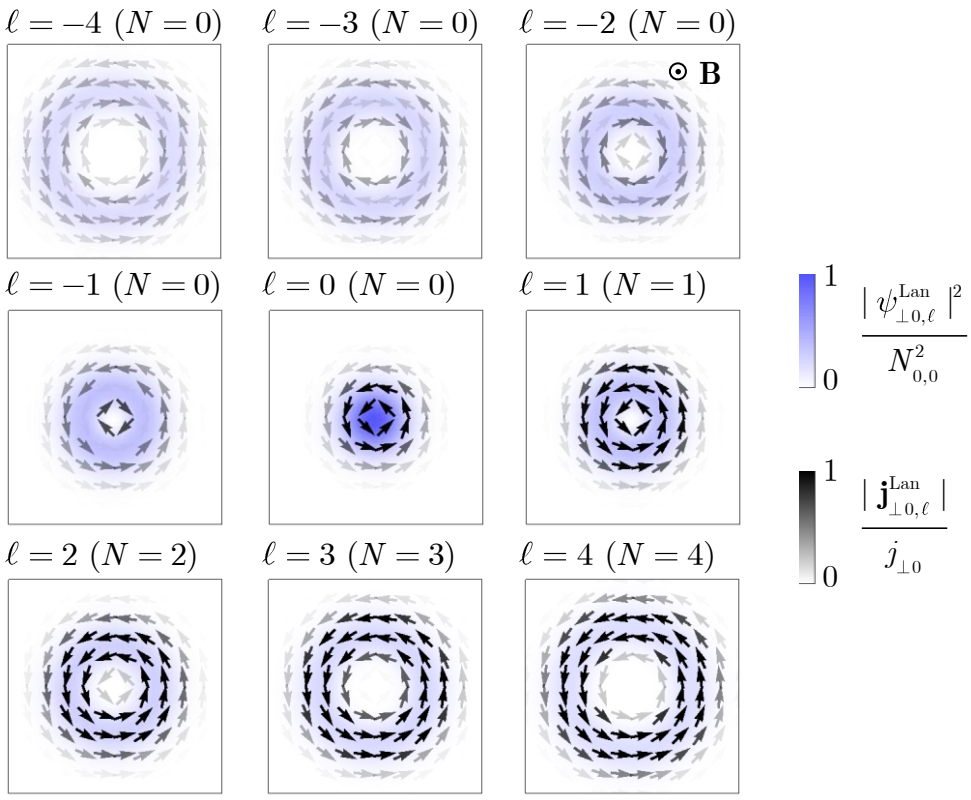

Figure 2.1: **Probability density and current density for Landau states with $n = 0$.** These are shown for $B > 0$, meaning that the magnetic field is in the positive z direction. Each tile is a square in the x-y plane of side length $5\rho_{\mathrm{B}}$. In this and subsequent images the current density is scaled with respect to the maximum value for the Landau state $\psi^{\mathrm{Lan}}_{\perp 0,0}$, $j_{\perp 0} = \mathrm{Max}\left[|\mathbf{j}^{\mathrm{Lan}}_{\perp 0,0}|(\mathbf{r}_\perp)\right]$. In the areas where the current density is strongest, the colour scale representing it is saturated. The states are labelled by both ℓ and the energy quantum number N that appears in (2.14).

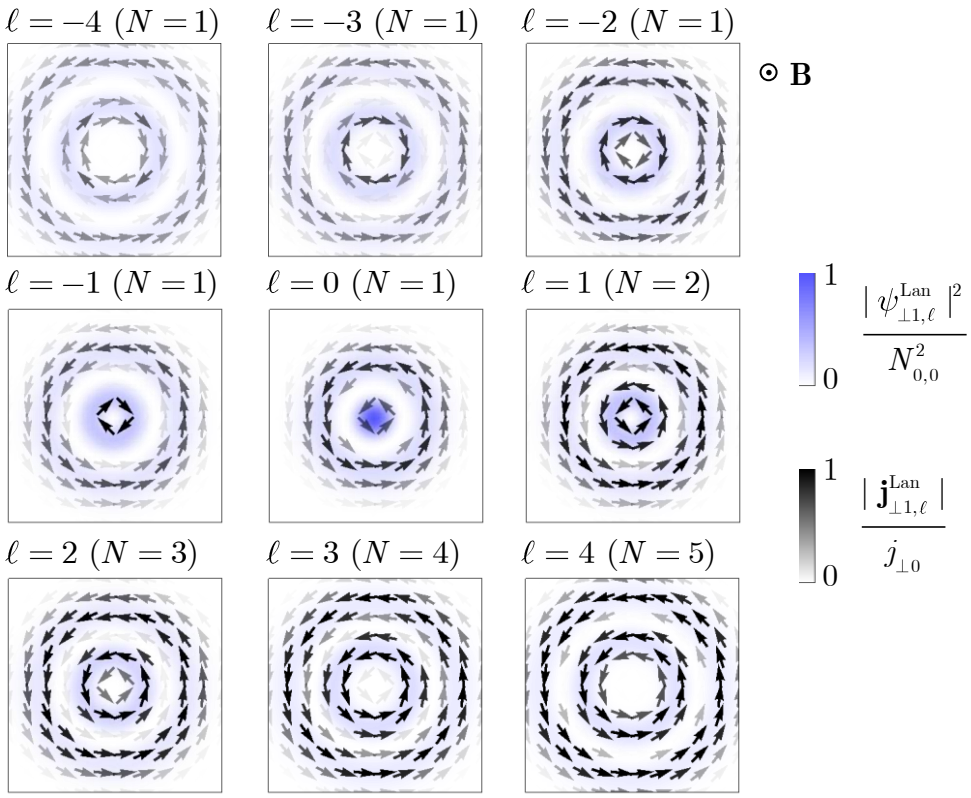

Figure 2.2: **Probability density and current density for Landau states with $n = 1$.** As in Fig. 2.1, the magnetic field is in the positive z direction and the tiles have a side length of $5\rho_{\mathrm{B}}$.

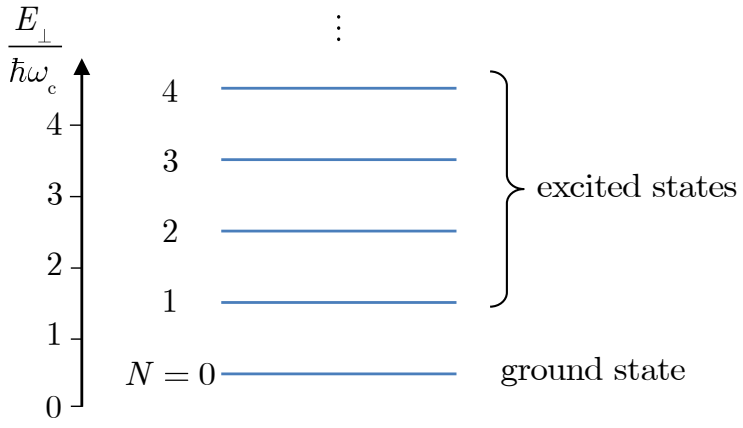

Figure 2.3: **The Landau energy levels of an electron in a uniform magnetic field.** These are equally spaced by an energy difference of $\hbar|\omega_{\mathrm{c}}|$. The ground state has the zero-point energy $\hbar|\omega_{\mathrm{c}}|/2$.

Chapter 3 and Chapter 5.

2.1.3 Canonical and kinetic angular momenta

The mass of a particle multiplied by its velocity, $m\mathbf{v}$, is the *kinetic* momentum of the particle [93]. This is a physical observable, and describes the mechanical motion of the particle.

In Hamiltonian mechanics, on which Schrödinger's quantum theory is based, the term "momentum" is additionally used in a more general sense. Hamilton's theory is formulated in terms of "canonical coordinates" and "canonical momenta", which may or may not correspond to physical positions and momenta [93]. These quantities can be chosen in a way that simplifies calculations and are related, via Noether's theorem [5, 6], to symmetries of the system. The quantum mechanical operator $-i\hbar\boldsymbol{\nabla}$ represents a canonical momentum [10].

For an electron moving in an the absence of a magnetic field, the kinetic and canonical momenta are equivalent. However, as seen in (2.2), when there is an interaction with a magnetic field these quantities differ by the amount $e\mathbf{A}$. The canonical momentum in this case depends on the gauge chosen. This is demonstrated explicitly in the next section. I note that regardless of which definition of momentum is used, the commutation relations between the coordinates of position and momentum are the same. This is because the vector potential commutes with the position. For example:

$$[x, p_x^{\text{kin}}] = [x, p_x^{\text{can}}] - e[x, A_x] = i\hbar, \tag{2.15}$$

since $[x, A_x] = -B[x, y]/2 = 0$.

Orbital angular momentum is defined as a cross product of position and momentum

vectors. If the canonical momentum is chosen, the result is a canonical angular momentum, as in (2.8). Here it is the z component of the angular momentum that is of interest as this describes the rotational motion of the electron in a plane perpendicular to the magnetic field. The canonical angular momentum $L_z^{\rm can}$ is related to symmetry under azimuthal rotation [4]. The Landau wavefunctions (2.11) are eigenstates of this angular momentum, with eigenvalues $\ell\hbar$. However, like the canonical momentum $\mathbf{p}^{\rm can}$, $L_z^{\rm can}$ depends on the choice of gauge. The mechanical motion of the electron is described by the *kinetic* angular momentum [87, 10]

$$\begin{aligned} L_z^{\rm kin} &= (\mathbf{r}\times\mathbf{p}^{\rm kin})_z \\ &= (\mathbf{r}\times\mathbf{p}^{\rm can})_z - e(\mathbf{r}\times\mathbf{A})_z \\ &= L_z^{\rm can} + m\omega_{\rm L}\rho^2. \end{aligned} \tag{2.16}$$

For a Landau state, the kinetic angular momentum has the expectation value

$$\begin{aligned} \langle L_z^{\rm kin}\rangle_{n,\ell}^{\rm Lan} &= \int {\rm d}^2\mathbf{r}_\perp\, {\psi_{\perp\, n,\ell}^{\rm Lan}}^* L_z^{\rm kin}\psi_{\perp\, n,\ell}^{\rm Lan} \\ &= \ell\hbar + m\omega_{\rm L}\langle\rho^2\rangle_{n,\ell}^{\rm Lan} \\ &= \ell\hbar + {\rm sign}(B)(2n+|\ell|+1)\hbar \\ &= {\rm sign}(B)(2N+1)\hbar, \end{aligned} \tag{2.17}$$

since the mean-square radius of the probability distribution for this state is

$$\langle\rho^2\rangle_{n,\ell}^{\rm Lan} = \int {\rm d}^2\mathbf{r}_\perp\,\rho^2|\psi_{\perp\, n,\ell}^{\rm Lan}|^2 = \frac{1}{2}(2n+|\ell|+1)\rho_{\rm B}^2 \tag{2.18}$$

[87, 98]. These allowed values of the kinetic angular momentum are illustrated in Fig. 2.4. They are closely related to the Landau energy levels, with the energy and kinetic angular momentum satisfying the classical relation for a particle in a circular orbit with an angular velocity $\omega_{\rm c}$:

$$E_{\perp N}^{\rm Lan} = \frac{1}{2}\omega_{\rm c}\langle L_z^{\rm kin}\rangle_{n,\ell}^{\rm Lan}. \tag{2.19}$$

The canonical and kinetic angular momenta, as well as the probability density and current density, for a Landau state with $n=0$ and $\ell=1$ are illustrated in Fig. 2.5. It is the kinetic angular momentum that is associated with the circulation of the electron's

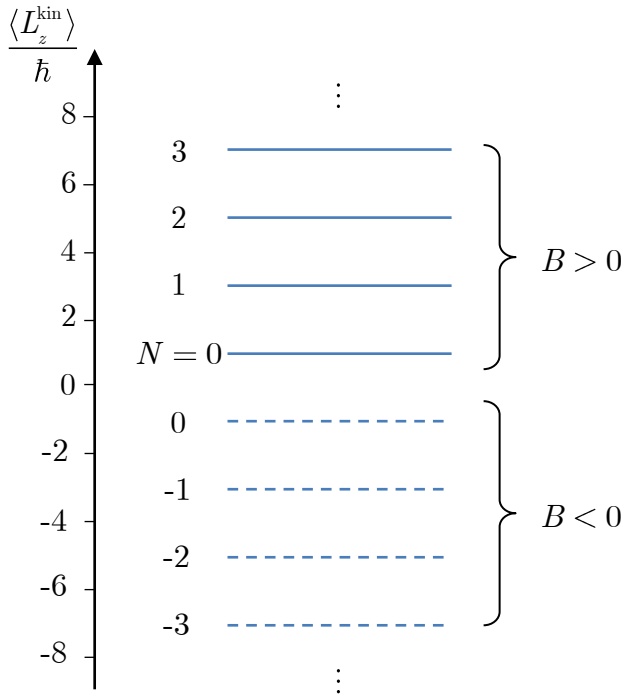

Figure 2.4: **Kinetic orbital angular momentum of the Landau states.** The expectation value of this angular momentum always has the same sign as the magnetic field, and assumes only odd multiples of $\hbar$.

probability current density:

$$\langle L_z^{\rm kin}\rangle_{n,\ell} \equiv m\int \mathrm{d}^2\mathbf{r}_\perp\,\rho j_\phi \tag{2.20}$$

[87].

The angular momentum of a charged particle is associated with a magnetic moment. The magnetic moment corresponding to the electron's kinetic orbital angular momentum is

$$M_z = \frac{e}{2m}L_z^{\rm kin} \tag{2.21}$$

[10]. Using (2.20) and (2.21), the expectation value of this magnetic moment can be expressed as an integral over the *electrical* current density, $\mathbf{j}_\perp^{\rm elec} = e\mathbf{j}_\perp$:

$$\begin{aligned}\langle M_z\rangle &= \frac{e}{2m}\langle L_z^{\rm kin}\rangle \\ &\equiv \frac{e}{2}\int \mathrm{d}^2\mathbf{r}_\perp\,\rho j_\phi \\ &= \frac{1}{2}\int \mathrm{d}^2\mathbf{r}_\perp\,\rho j_\phi^{\rm elec}.\end{aligned} \tag{2.22}$$

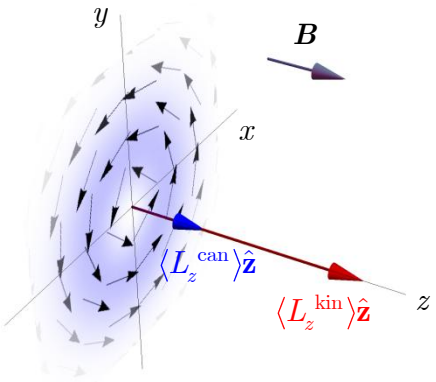

Figure 2.5: **Geometry of the canonical and kinetic angular momenta, and probability and current densities, for a Landau state with $n = 0$ and $\ell = 1$.** Here the canonical angular momentum has the expectation value $\langle L_z^{\rm can}\rangle_{0,1}^{\rm Lan} = \hbar$ and, as $B > 0$, the kinetic value obtained from (2.17) is $\langle L_z^{\rm kin}\rangle_{0,1}^{\rm Lan} = 3\hbar$.

Since the electron has negative charge, the magnetic moment is in the opposite direction to the angular momentum. For a Landau state the expectation value of the kinetic angular momentum is given by (2.17), and therefore the first line of (2.22) evaluates to

$$\langle M_z\rangle_{n,\ell}^{\rm Lan} = \frac{e}{2m}\langle L_z^{\rm kin}\rangle_{n,\ell}^{\rm Lan} = -\ell\mu_{\rm B} - {\rm sign}(B)(2n + |\ell| + 1)\mu_{\rm B}. \tag{2.23}$$

The first term here is the magnetic moment corresponding to the canonical angular momentum. The second term, which has the opposite direction to the magnetic field, is the diamagnetic contribution to the electron's magnetic moment [10]. Summing over a large number of such magnetic moments yields the diamagnetic response of a free electron gas that is described in Chapter 1.

In this thesis I characterise the diamagnetic response of an electron wavefunction in terms of its angular momentum. It should be remembered, however, that the diamagnetic angular momentum is always related, through (2.21), to a magnetic moment. The specific form of the diamagnetic moment in (2.23), and the corresponding angular momentum in (2.17), are particular to Landau states. In subsequent chapters, I shall consider the diamagnetic angular momentum of other wavefunctions.

2.1.4 Gauge transformations

Care must be taken, when describing interactions between matter and fields, to identify which quantities depend on the choice of gauge. All physically meaningful variables are of course gauge-invariant. Here, the gauge has been fixed through the choice of the vector potential in (2.5). However, this vector potential could be transformed according to

$$\mathbf{A} \rightarrow \mathbf{A} + \frac{\hbar}{e}\boldsymbol{\nabla}\chi, \tag{2.24}$$

for any smoothly varying function $\chi(\mathbf{r})$, without affecting the magnetic field $\mathbf{B} = \boldsymbol{\nabla}\times\mathbf{A}$. The Schrödinger equation is invariant under such a transformation if the local phase of the wavefunction is changed as follows:

$$\psi \rightarrow \psi' = \exp\left[i\chi(\mathbf{r})\right]\psi \tag{2.25}$$

[100, 101]. This means that under a gauge transformation the gradient of the phase – and therefore the canonical momentum, $\mathbf{p}^{\text{can}}$ – changes. The action of the canonical momentum operator on the wavefunction becomes:

$$\mathbf{p}^{\text{can}}\psi \rightarrow -i\hbar\boldsymbol{\nabla}\exp(i\chi)\psi = \exp(i\chi)(-i\hbar\boldsymbol{\nabla} + \hbar\boldsymbol{\nabla}\chi)\psi. \tag{2.26}$$

This change in the canonical momentum is counterbalanced by the transformation of the vector potential such that the kinetic momentum $\mathbf{p}^{\text{kin}}$ is unaffected by the gauge transformation. The current density, which is defined in terms of the kinetic momentum, is similarly unaffected. The change in the phase of the wavefunction under a transformation of the vector potential is illustrated in Fig. 2.6. The canonical angular momentum transforms in a similar manner to the canonical momentum, with its action on the wavefunction becoming:

$$L_z^{\text{can}} \rightarrow -i\hbar\frac{\partial}{\partial\phi} + \hbar\frac{\partial\chi}{\partial\phi}. \tag{2.27}$$

I note that for a state with a rotationally symmetric probability density, the *expectation value* of the canonical angular momentum is gauge-invariant. If the probability density

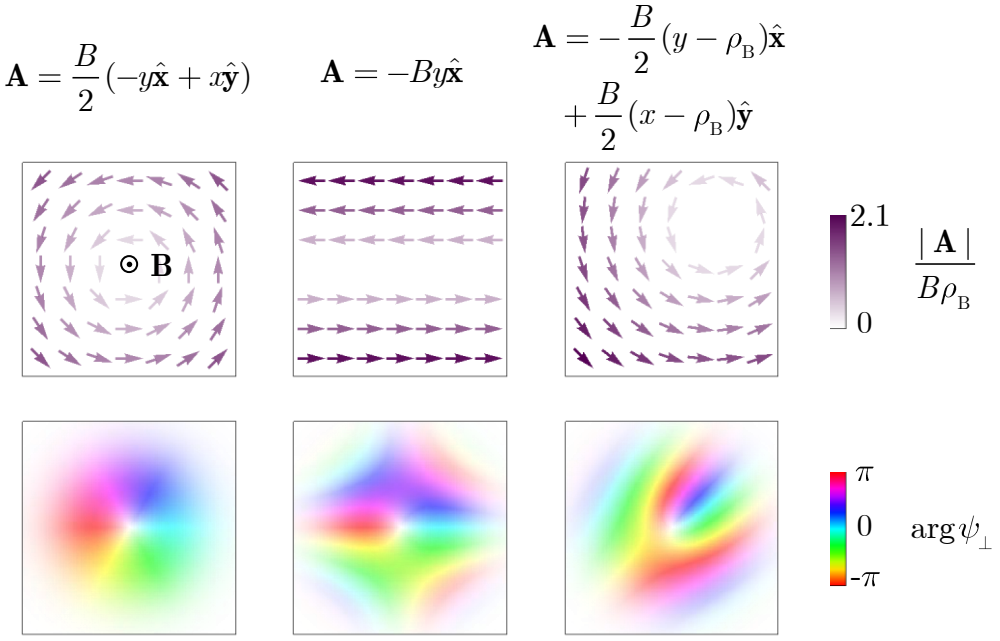

Figure 2.6: **Different choices of vector potential to describe a uniform magnetic field in the z direction and the phase of the Landau wavefunction $\psi^{\mathbf{Lan}}_{\perp\,0,1}$ in each case.** Each tile has a side length of $4\rho_B$. The opacity of the colours representing the phase of the wavefunction is modulated by the wavefunction amplitude. It is the vector potential on the left, introduced in (2.5), which is used in the rest of this thesis.

$|\psi|^2 = |\psi'|^2$ is independent of ϕ then the expectation value of the second term in (2.27) is

$$\left\langle \hbar \frac{\partial \chi}{\partial \phi} \right\rangle = \hbar \int_0^\infty \rho \mathrm{d}\rho \, |\psi|^2 \int_0^{2\pi} \mathrm{d}\phi \, \frac{\partial \chi}{\partial \phi} = 0, \tag{2.28}$$

since χ is smoothly varying and therefore the integral of $\partial\chi/\partial\phi$ is zero. Whatever the gauge, therefore, a rotationally symmetric state has $\langle L_z^{\mathrm{can}} \rangle = \ell\hbar$. I will provide a physical interpretation for this quantity in Chapter 4. The variables that depend on the gauge chosen, and those that do not, are summarised in Table 2.1.

Table 2.1: Variables that depend on the gauge chosen, and the corresponding physical observables that are gauge-invariant. For a rotationally symmetric state, the expectation value $\langle L_z^{\mathrm{can}} \rangle = \ell\hbar$ is gauge-invariant.

Depends on gauge	Independent of gauge
A	**B**
$\mathbf{p}^{\mathrm{can}}$	$\mathbf{p}^{\mathrm{kin}}$
L_z^{can}	L_z^{kin}
$\arg\psi$	$\lvert\psi\rvert^2$, $\mathbf{j}$

2.2 Experimental realisation in a transmission electron microscope

The influence of a magnetic field on the motion of electrons can be studied using a transmission electron microscope. In fact, the interaction of electrons with a magnetic field is key to the function of most electron microscopes, as it underlies the operation of magnetic electron lenses [102, 103]. Transmission electron microscopes are also used to image the magnetic field distributions within magnetic materials, using Lorentz microscopy [104] or electron holography [105]. It is interesting to note as well that conclusive experimental proof of the existence of the Aharonov-Bohm effect [101, 106], which is a non-local interaction between electrons and a magnetic field, was obtained using a transmission electron microscope [107, 108].

Recently, the interaction of electron vortices with magnetic fields has been investigated using transmission electron microscopes. It has been demonstrated that particular configurations of spatially varying magnetic fields can be used to convert the spin angular momentum of electrons into orbital angular momentum, and vice versa [61, 62]. Similarly, astigmatic magnetic lenses have been shown to produce transformations between states with different orbital angular momenta [109, 110, 111]. Meanwhile, the interaction of an electron beam with a nanofabricated magnetic needle, which produces a field resembling that of a monopole, has been shown to impart orbital angular momentum to the electrons [112, 113]. The potential to use vortex beams for imaging magnetic materials using magnetic dichroism measurements has also been considered [38, 56, 68, 114]. Of particular interest in the context of this thesis, vortex beams in electron microscopes have been used to image the rotation of electron wavefunctions, including those of Landau states, in uniform, or quasi-uniform, magnetic fields [2, 99, 115].

In this section, I shall describe some important characteristics of experiments involving vortex beams in transmission electron microscopes, and in particular their interaction with the magnetic field provided by the objective lens of the microscope.

2.2.1 Wavepackets

Many aspects of the operation of an electron microscope can be understood in terms of classical mechanics. In geometrical electron optics, classical electron trajectories are identified with rays [93, 116]. As with the description of light, however, some aspects of image formation require a wave description. In electron optics this is normally based on the time-independent Schrödinger equation [93, 117]. In order to make a connection with the behaviour I will describe in subsequent chapters, much of which involves time-dependent effects, here I explain how an electron microscope beam can instead be understood in terms of propagating wavepackets.

The electron beam in a transmission electron microscope is formed by accelerating electrons through a large potential difference Φ, which is typically of the order of 100 kV [49]. This results in each electron leaving the electron gun with a kinetic (and total) energy of $E = e\Phi \sim 100\,\text{keV}$. For a classical particle following a straight-line trajectory in the z direction (and ignoring relativistic effects), this corresponds to a velocity of $v_z = \sqrt{2E/m}$. At an energy of 100 keV, this velocity has the magnitude $v_z = 1.88 \times 10^8\,\text{m s}^{-1}$. Unlike a classical particle, however, an electron emitted by the electron source in an electron microscope has a degree of uncertainty in its energy; typically this energy spread, ΔE, is of the order of 1 eV [49]. This means that there is an uncertainty in the electron's longitudinal position that is described by the Heisenberg relation $\Delta z \Delta p_z \geq \hbar/2$, where $\Delta p_z = (\partial p_z/\partial E)\Delta E = \Delta E/v_z$ is the uncertainty of the momentum $p_z = mv_z$ [103]. For the state with minimum uncertainty, the uncertainty in the electron's z coordinate is therefore equal to $\Delta z = v_z\hbar/(2\Delta E)$. With the values of v_z and ΔE given above, this spread in position would be $\Delta z = 61\,\text{nm}$.

The average distance between successive electrons can be determined from the beam current. This current, I, may be of the order of $1\,\mu$A [49], which corresponds to an average time interval between electrons of $\tau = e/I = 16\,\text{ps}$. For electrons with an energy of 100 keV, this corresponds to a spatial separation of $d = v_z\tau = 20\,\mu\text{m}$. This is 2–3 orders of magnitude larger than the spread in position for a single electron, Δz, which is derived above. Therefore, the overlap between successive wavepackets is negligible, as illustrated in Fig. 2.7. This means that the interaction between electrons is negligible, justifying the use of the single particle Schrödinger equation.

In an electron microscope, it is the transverse probability density of the electron, $|\psi_\perp|^2$, that is measured. This is imaged by recording on a CCD camera the signals associated with a large number of electrons being detected at different transverse positions [52, 103]. The probability distribution of a single electron, the position of which has not yet been measured, evolves with time, and, since the electron is propagating along the z axis, also with the z position. For an electron travelling with a constant longitudinal velocity, v_z, the z position of the centre of mass of the wavepacket, $\langle z \rangle(t)$, is simply

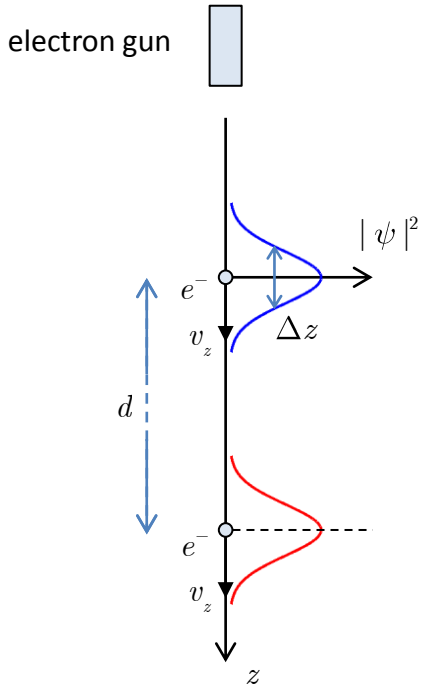

Figure 2.7: **Schematic illustration of electron wavepackets in a transmission electron microscope.** The longitudinal probability density, that is, the probability density as a function of the z coordinate, is shown for two different electrons. Each electron has the same average velocity, v_z, and uncertainty in position, Δz. The average spatial separation between electrons is $d \gg \Delta z$.

proportional to the time of flight: $\langle z \rangle = v_z t$. Therefore, the evolution of the electron's wavefunction can be described more easily by eliminating one of these variables, either the propagation distance or the time.

As has already been mentioned, in electron optics it is conventional to eliminate the time coordinate, and use the time-independent Schrödinger equation. Effectively, this means considering a time-average over a very large number of propagating wavepackets, each of which has a different arrival time. Such a time-average is what is normally detected on the microscope's CCD camera. In Chapter 5 I follow the conventional electron optical approach of using the time-independent Schrödinger equation.

In Chapters 3 and 4, on the other hand, I am concerned less with the specific application to electron optics, and I have found it preferable to use a time-dependent description. This means that my results are equally applicable whether the electrons are propagating along the z axis or not. The time-dependent description is particularly appropriate when discussing the fundamental concept of angular momentum conservation, in Chapter 4. This means that I simply solve the two dimensional time-dependent Schrödinger equation for the wavefunction in the $\mathbf{r}_\perp$ plane. For a wavepacket propagating along the z axis, this can be understood as describing the wavefunction at the z position of the centre of mass of the wavepacket, that is, in the plane $z = \langle z \rangle = v_z t$ [36].

2.2.2 Manipulating the electron's wavefunction

Recent advances in nanofabricated diffractive optics for electrons have greatly increased the control that can be exercised over an electron's wavefunction, and particularly its orbital angular momentum. The first demonstration of electron beams carrying orbital angular momentum, five years ago, used stacks of thin graphite films, carefully

arranged to form a spiral phase plate [37]. This was quickly followed by the introduction of specially designed holographic diffraction gratings, a technique that is far more accurate, reproducible and versatile [1, 38].

A particular strength of the holographic method is that it is not restricted to the generation of eigenstates of canonical angular momentum, which have a rotationally symmetric probability density; in principle, the wavefunction of the electron can be sculpted into any state that is desired [66, 115, 118]. Early efforts were limited in practice as they utilised only binary gratings, such as that shown in Fig. 1.1, which either transmit or block electrons depending on their position. The most advanced gratings, however, now allow the phase of the electron to be manipulated directly, through a spatial variation of the thickness of the grating material [50, 51]. This means that a net transverse momentum can be imparted to the electron, with a greater proportion of the beam intensity being directed into the first diffraction order. Phase gratings of this type can also be machined with smaller feature sizes, which allows beams with larger values of orbital angular momentum to be generated; at the time of writing, the record appears to be $\ell = 200$ [51].

While hologram patterns that are calculated by superposing the desired wavefunction with that of a plane wave result in diffraction orders that are separated transversely, a longitudinal separation can be obtained by replacing the plane wave with one that is spherical [119, 120]; this may be advantageous for applications in scanning transmission electron microscopy. An alternative approach to holography is instead to manipulate the electron's wavefunction by utilising the interaction with a spatially varying magnetic field [109, 110, 111, 112, 113].

2.2.3 Propagation through a magnetic lens

Electron microscope beams are normally focused using magnetic lenses [102, 103], which consist of a current-carrying coil producing a magnetic field that is directed along the optical axis. That such a magnetic field will focus an electron beam can be understood qualitatively by considering the classical cyclotron trajectories in geometrical electron optics: electrons are confined to circular orbits, the radii of which depend on the strength of the magnetic field. Unlike a glass lens focusing light, magnetic lenses also result in a rotation of the image; normally this is considered a background effect, however, and may be partially compensated by combining lenses that have opposite current directions [103]. In the Schrödinger formalism, the focusing of the electron beam can be associated with a change in the phase of the wavefunction, due to the magnetic field, which depends quadratically on the radial position [121].

The field of a magnetic lens is not uniform, but rather varies in strength along the optical axis, and, consequently, also has a radial component. An arbitrary rotationally symmetric magnetic field may be expressed as a series expansion in the axial component $B_{\mathrm{ax}}(z)$ as follows:

$$\begin{aligned}\mathbf{B}(\rho,z) &= \left[B_{\mathrm{ax}}(z)-\frac{1}{4}\frac{\mathrm{d}^2B_{\mathrm{ax}}(z)}{\mathrm{d}z^2}\rho^2+\frac{1}{64}\frac{\mathrm{d}^4B_{\mathrm{ax}}(z)}{\mathrm{d}z^4}\rho^4+\mathcal{O}(\rho^6)\right]\hat{\mathbf{z}}\\ &\quad+\left[-\frac{1}{2}\frac{\mathrm{d}B_{\mathrm{ax}}(z)}{\mathrm{d}z}\rho+\frac{1}{16}\frac{\mathrm{d}^3B_{\mathrm{ax}}(z)}{\mathrm{d}z^3}\rho^3+\mathcal{O}(\rho^5)\right]\hat{\boldsymbol{\rho}}\end{aligned} \tag{2.29}$$

[93]. Close to the z axis, the approximation

$$\mathbf{B}(\rho,z)\approx B_{\mathrm{ax}}(z)\hat{\mathbf{z}}-\frac{1}{2}\frac{\mathrm{d}B_{\mathrm{ax}}(z)}{\mathrm{d}z}\rho\hat{\boldsymbol{\rho}} \tag{2.30}$$

can be used. The axial magnetic field in an electron lens is commonly approximated by the bell-shaped function $B_{\mathrm{ax}}(z)=B_0/\left[1+(z/a)^2\right]$ where B_0 is the field at the centre of the lens and $2a$ is the full-width at half-maximum [122]. This field is illustrated schematically in Fig. 2.8. While a transmission electron microscope has a number of lenses, it is the objective lens that can produce by far the strongest magnetic field. For an objective lens, B_0 can have values up to $\approx 2\,\mathrm{T}$ [49].

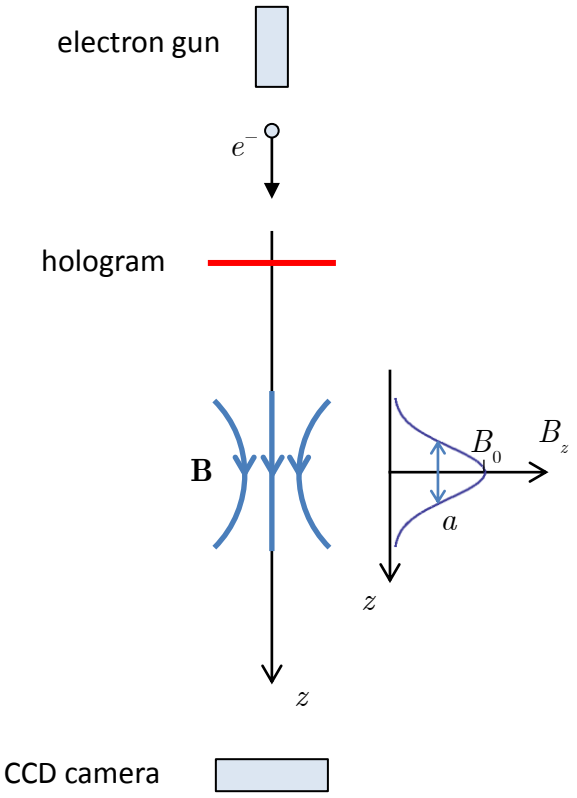

Figure 2.8: **Schematic illustration of an electron beam propagating through the objective lens of a transmission electron microscope.** In this case, prior to it entering the lens, the wavefunction of the electron is shaped by a hologram. The probability density of the electron is subsequently imaged on a CCD camera. A real microscope contains many components that are not shown here, including additional lenses for which the maximum magnetic field is much weaker.

Close to the centre of the lens, the field is approximately uniform, and in this region free electron Landau states have recently been observed [2, 99]. This is shown in Fig. 2.9, taken from [2]. The evolution of the electron's wavefunction upon propagation through the entire lens field, meanwhile, can be obtained by integrating over the function $B_{\mathrm{ax}}(z)$ [115, 121, 123]. Although in principle a spatially varying magnetic field produces a spin-dependent force on electrons, in an electron microscope lens the effect of this is negligible [93, 124]. More significant, but beyond the scope of this thesis, are the spherical, chromatic and other aberrations of the lens [103, 125].

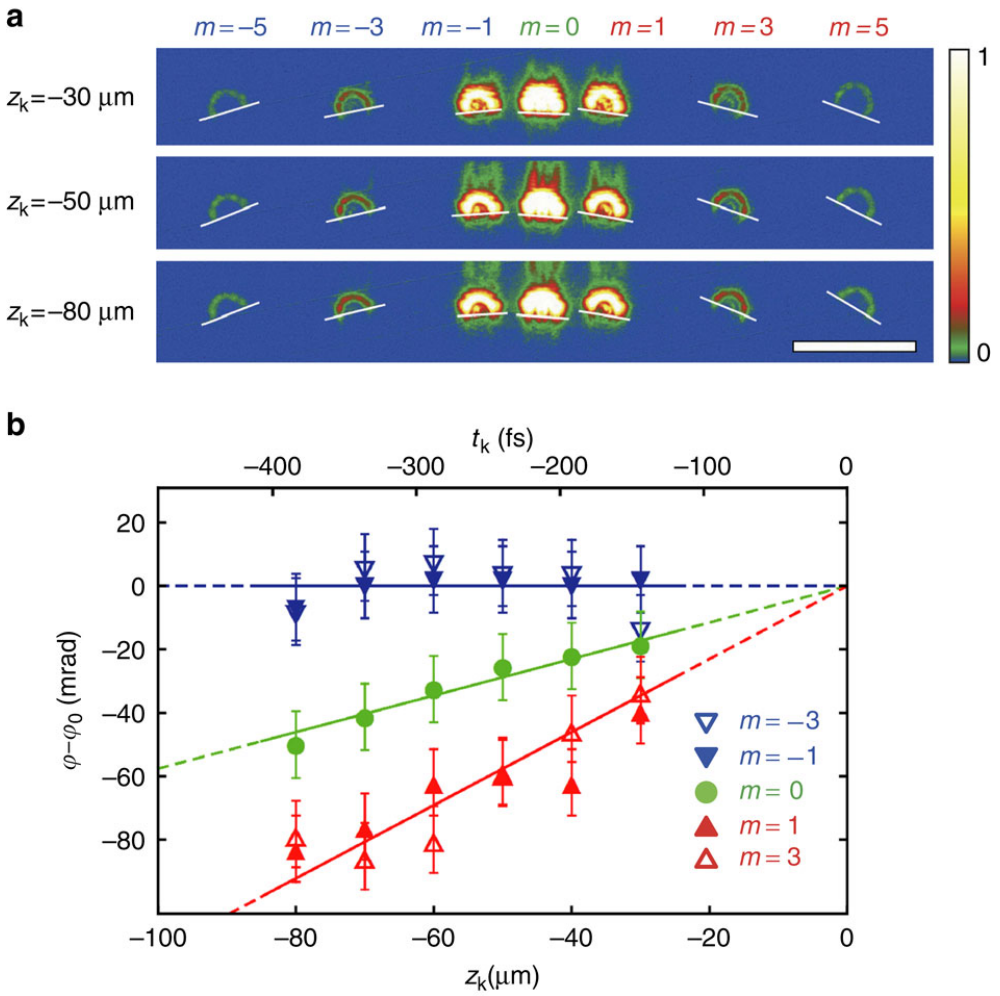

Figure 2.9: **Imaging free electron Landau states in an electron microscope.** From [2], available at `http://www.nature.com/ncomms/2014/140808/ncomms5586/full/ncomms5586.html` and licensed under Creative Commons Attribution 4.0 International. In this experiment a forked diffraction grating was used to create a series of vortex states in the same way as shown in Fig. 1.1; here m denotes the angular momentum quantum number for these states. Then, each diffraction order was truncated using a knife-edge, breaking the symmetry of the probability density, and therefore allowing the rotation of the electron to be imaged. In agreement with theoretical predictions for the Landau states, rotations at either the classical angular velocity, ω_c, the Larmor angular velocity, $\omega_{\mathrm{L}} = \omega_{\mathrm{c}}/2$, or an angular velocity of zero, were measured, in the cases where $m > 0$, $m = 0$ and $m < 0$ respectively. Note that part (a) also shows an additional rotation due to the Gouy phase, associated with the focusing of the electron beam; this Gouy rotation has been subtracted in (b). The variable z_{k} is the propagation distance from the knife-edge, and t_{k} is the corresponding time. The scale bar is 50 nm.

2.2.4 Measuring the orbital angular momentum and current density

The simplest property of the electron to measure in an electron microscope is its probability distribution in the plane perpendicular to the optical axis. As has already been mentioned, this is given by the intensity pattern captured on the CCD camera. The orbital angular momentum of electron vortex beams, however, is associated with the transverse current density and the transverse phase gradient, which are more difficult to measure.

One way to reveal the phase distribution of an electron beam is to interfere it with a known reference wave – this is electron holography [53, 105]. Using the measured probability density of the interference pattern, it is possible to reconstruct the unknown phase distribution. This technique has been used to experimentally map the spiral phase of an electron vortex beam propagating in field-free space [112]. However, holographic imaging is time-consuming and requires specialist equipment.

Recently a number of techniques for more easily characterising the orbital angular momentum of electron beams have been under investigation. Each of these is an adaptation of a method used to measure optical angular momentum. Perhaps the simplest is the obstruction of part of the beam by an opaque knife-edge [115, 126, 127]. This breaks the rotational symmetry of the probability density of a canonical angular momentum eigenstate, and the subsequent propagation of the truncated beam visualises the circulation of the current density. For electrons in a magnetic field, this provides information about the *kinetic* angular momentum of the electron [2]. The canonical angular momentum, meanwhile, can be determined from the intensity pattern recorded after transmission through a second hologram [128] or different forms of geometrical aperture [129, 130], as well as by using an astigmatic lens [129, 131].

Another technique, besides holography, that is widely used to image the spatial variation of the current density of an electron beam is differential phase contrast [132, 133, 134, 135, 136]. This involves scanning a tightly focused electron probe across the area of interest, and measuring the deflection of this probe. A related technique, that, instead of scanning, involves recording two slightly defocused images, allows the current density to be determined from the so-called transport of intensity equation [137, 138, 139].

In this chapter, I have presented background material that sets the context for my own research. Now, I shall begin to describe my results.

Chapter 3

Parallel axis theorem for free-space electron wavefunctions

I consider the orbital angular momentum of a free electron vortex moving in a uniform magnetic field. I identify three contributions to this angular momentum: the canonical orbital angular momentum associated with the vortex, the angular momentum of the cyclotron orbit of the wavefunction, and a diamagnetic angular momentum. The cyclotron and diamagnetic angular momenta are found to be separable according to the parallel axis theorem. This means that rotations can occur with respect to two or more axes simultaneously, which can be observed with superpositions of vortex states.

The chapter is structured with the main results presented first, followed by additional material that complements these. This allows the key ideas to be highlighted, while greater depth and detail is available for those who want it.

3.1 Main results

3.1.1 Introduction

In this chapter I consider an electron wavefunction that exhibits centre of mass motion, in addition to possessing canonical orbital angular momentum. I demonstrate that the total kinetic angular momentum of the wavefunction is described by the parallel axis theorem. This angular momentum comprises the canonical and diamagnetic components, which are associated with rotation relative to the centre of mass of the wavefunction, and a cyclotron component that has expectation value equal to that for the classical orbit. Interestingly, for free electrons all three of these components can have similar magnitude. This means that the trajectory of the electron is strongly dependent on how these angular momenta add and subtract. Further, I show that different cyclotron orbits can be superposed, leading to rotations with respect to multiple parallel axes, and periodic interference. These results suggest novel means of structuring electron beams for use in specific applications, such as probing magnetic and chiral materials.

3.1.2 Model

I consider an otherwise free electron moving under the influence of a uniform magnetic field. I take the direction of this magnetic field to define the z axis, and consider the motion of the electron within the x-y plane. The electron may also be moving in the z direction; however, as already noted in section 2.1.1, the component of its momentum in this direction is a constant of motion, and will not affect my results. I consider non-relativistic energies, meaning that the spin angular momentum is also constant, and can be separated from the orbital motion of the electron. In what follows, I shall

consider only the electron's orbital angular momentum. The magnetic field and vector potential are described by (2.4) and (2.5) respectively. The Hamiltonian of the system is therefore (2.7).

I am interested in the evolution of non-stationary states of the system, described by the time-dependent Schrödinger equation

$$i\hbar\frac{\partial\Psi_\perp(\mathbf{r}_\perp,t)}{\partial t} = H_\perp\Psi_\perp(\mathbf{r}_\perp,t). \tag{3.1}$$

Throughout this thesis the capital letter Ψ is used to denote a time-dependent wavefunction, whereas the lower-case ψ denotes a wavefunction that is time-independent. As discussed in section 2.2.1, if the electron is moving along the z axis with a velocity v_z, the Schrödinger equation (3.1) describes the state of the electron after a propagation distance of $z = v_z t$.

An electron with momentum transverse to the magnetic field will exhibit cyclotron motion. This is conventionally described in a classical context. Here I will derive the cyclotron motion by assuming an electron wavefunction

$$\Psi_\perp(t=0) = \Psi_{\perp,0} = u(\rho)\exp\left[i\left(\ell\phi + \frac{p_\mathrm{c}}{\hbar}x\right)\right], \tag{3.2}$$

where $\ell \in \mathbb{Z}$. I have defined the x axis as the direction of the transverse kinetic momentum at $t = 0$. This state has a rotationally symmetric probability density $|\Psi_{\perp,0}|^2 = |u(\rho)|^2$, and an expectation value of canonical angular momentum $\langle L_z^{\mathrm{can}}\rangle = \ell\hbar$. We shall see that the momentum $\langle\mathbf{p}_\perp^{\mathrm{kin}}\rangle_0 = p_\mathrm{c}\hat{\mathbf{x}}$ results in a cyclotron orbit of the wavefunction.

Note that in my model the canonical orbital angular momentum is not collinear with the instantaneous direction of propagation of the wavefunction. This is illustrated in Fig. 3.1. The angular momentum is in the direction of the magnetic field, while the kinetic momentum has a component perpendicular to the magnetic field. This contrasts with vortex states, either in field-free space or in a magnetic field, which are energy eigenfunctions, as these have momentum and angular momentum that are

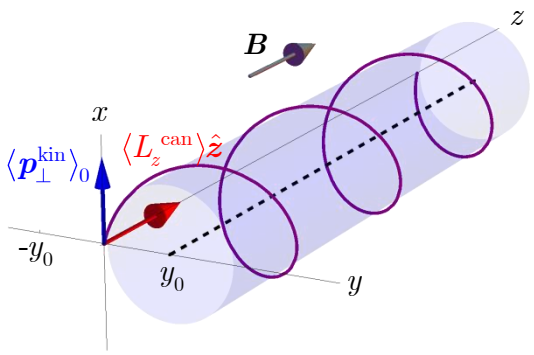

Figure 3.1: **Cyclotron trajectory of the centre of mass of the wavefunction.** This orbit occurs with respect to the axis $y = y_0$, the position of which depends on the initial transverse momentum $\langle \mathbf{p}_\perp^{\text{kin}} \rangle_0$ as well as the magnetic field. Also indicated is the direction of the canonical orbital angular momentum $\langle L_z^{\text{can}} \rangle \hat{\mathbf{z}}$.

collinear [60, 87]. Electrons in non-stationary states can have angular momentum at an arbitrary angle to their direction of propagation, however [39, 76, 140]. Here, as a result of the cyclotron orbit, the *time-averaged* expectation value of kinetic momentum is collinear with the angular momentum $\langle L_z^{\text{can}} \rangle$.

3.1.3 Electron trajectories and angular momentum

In the following I will show that the different forms of angular momentum give rise to rotations with respect to more than one axis. This can be seen by examining the "trajectories" associated with the electron's probability distribution and current density.

First, I will consider the expectation value of the electron's position, which is equivalent to the centre of mass of its probability distribution. Differentiating twice with respect

to time, I obtain the equation of motion

$$\begin{aligned}\frac{\partial^2\langle\mathbf{r}_\perp\rangle(t)}{\partial t^2} &= -\frac{1}{\hbar^2}\left\langle[[\mathbf{r}_\perp, H_\perp], H_\perp]\right\rangle(t)\\ &= -\omega_\mathrm{c}^2\left\langle\mathbf{r}_\perp - \left[x + p_y^\mathrm{kin}/(eB)\right]\hat{\mathbf{x}} - \left[y - p_x^\mathrm{kin}/(eB)\right]\hat{\mathbf{y}}\right\rangle(t)\\ &= -\omega_\mathrm{c}^2\left(\langle\mathbf{r}_\perp\rangle(t) - y_0\hat{\mathbf{y}}\right), \end{aligned} \tag{3.3}$$

where $y_0 = p_\mathrm{c}/(|e|B)$. Here I have used the fact that the quantity $\left[x + p_y^\mathrm{kin}/(eB)\right]\hat{\mathbf{x}} + \left[y - p_x^\mathrm{kin}/(eB)\right]\hat{\mathbf{y}}$, which is the centre of the orbit of a classical particle that has position $\mathbf{r}_\perp$ and momentum $\mathbf{p}_\perp^\mathrm{kin}$ [98], has the constant expectation value $y_0\hat{\mathbf{y}}$. The initial position and velocity of the centre of mass of the probability distribution are given by $\langle\mathbf{r}_\perp\rangle(0) = \mathbf{0}$ and

$$\frac{\partial\langle\mathbf{r}_\perp\rangle(0)}{\partial t} = -\frac{i}{\hbar}\left\langle[\mathbf{r}_\perp, H_\perp]\right\rangle(0) = \frac{p_\mathrm{c}}{m}\hat{\mathbf{x}} \tag{3.4}$$

respectively, and substituting these into (3.3) yields the trajectory

$$\langle\mathbf{r}_\perp\rangle(t) = y_0[\sin\omega_\mathrm{c}t\hat{\mathbf{x}} + (1 - \cos\omega_\mathrm{c}t)\hat{\mathbf{y}}]. \tag{3.5}$$

This trajectory, illustrated in Fig. 3.1, is a circular orbit with radius

$$\sigma = |y_0| = \left|\frac{p_\mathrm{c}}{eB}\right| \tag{3.6}$$

and angular velocity ω_c – the cyclotron orbit of a classical particle with the momentum p_c. The trajectory of the centre of mass of the probability distribution is therefore independent of the canonical angular momentum of the electron.

The canonical angular momentum is instead associated with a circulation of current within the electron's probability distribution. This can be seen by examining the probability current density

$$\mathbf{j}_\perp(\mathbf{r}_\perp, t) = \frac{1}{m}\mathrm{Re}(\Psi_\perp^*\mathbf{p}_\perp^\mathrm{kin}\Psi_\perp). \tag{3.7}$$

To do so I have solved the time-dependent Schrödinger equation (3.1) numerically using the Chebyshev method [141, 142, 143], as described in section 3.2.1. I must first specify the radial distribution, $u(\rho)$, of the initial wavefunction (3.2). Here I will set this to be the same as that of a Landau state:

$$u(\rho) = u_{n,|\ell|}^\mathrm{Lan}(\rho) = \psi_{\perp\, n,\ell}^\mathrm{Lan}(\rho, \phi = 0), \tag{3.8}$$

with $\psi^{\mathrm{Lan}}_{\perp n,\ell}$ defined by (2.11). This means that if $p_{\mathrm{c}} = 0$, the electron would be in a Landau state. An arbitrary radial distribution could be decomposed in terms of the eigenfunctions $u^{\mathrm{Lan}}_{n,|\ell|}$.

The time-evolution of the probability density $|\Psi_\perp|^2$ and the current density $\mathbf{j}_\perp$ are shown in Fig. 3.2. Here the transverse momentum p_{c} has been chosen such that the radius of the cyclotron orbit is approximately equal to the width of the probability distribution. In (a) and (b) the electron has no net canonical orbital angular momentum, while in (c) and (d) it has a canonical orbital angular momentum $\ell = 1$. The evolution of these states is shown for different directions of the magnetic field, which result in different directions of the cyclotron orbit. Whereas the probability density follows a straightforward classical orbit, the current density is seen to depend in a non-trivial manner on both the wavefunction and the magnetic field. In particular, in contrast to the classical cyclotron trajectory, and also to orbital angular momentum eigenstates in the absence of a magnetic field, the current distribution here is not rotationally symmetric. The rotational symmetry of the probability distribution, with respect to its centre of mass, is preserved, however. This reflects the fact that the magnetic field is rotationally symmetric, and the canonical angular momentum L_z^{can} is conserved. This means that the canonical orbital angular momentum of the electron is associated with a rotation axis at the centre of mass of the probability distribution, and is independent of the cyclotron orbit.

More surprising, perhaps, is that rotations in fact occur with respect to the cyclotron axis *and* the centre of mass axis even when the electron does not possess any net canonical angular momentum. This is as a result of the diamagnetic angular momentum of the wavefunction. In section 2.1.3 I described the diamagnetic angular momentum of a Landau state, which has the value $m\omega_{\mathrm{L}}\langle\rho^2\rangle^{\mathrm{Lan}}_{n,\ell}$. For the more general wavefunction I consider here, I define the diamagnetic angular momentum as $L_z^{\mathrm{dia}} = I'\omega_{\mathrm{L}}$, where

$$I' = m\langle\rho'^2\rangle \tag{3.9}$$

is the moment of inertia of the electron's probability distribution, in the reference

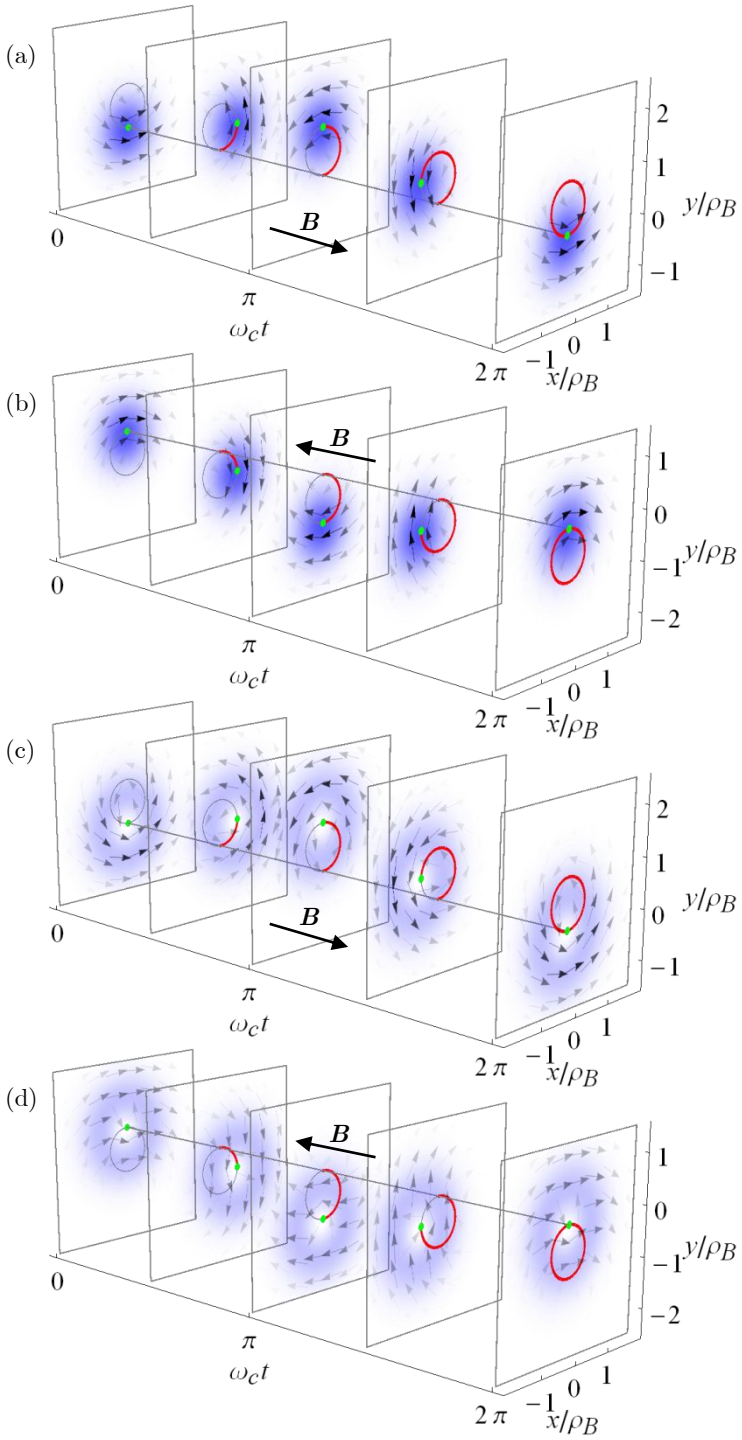

Figure 3.2: **Probability density $|\Psi_\perp|^2$ and current density $\mathbf{j}_\perp$ for wavefunctions with canonical orbital angular momentum $\ell = 0$ (a, b) and $\ell = 1$ (c, d), for opposite directions of the magnetic field.** In each case the transverse momentum is $p_c = 2\hbar/\rho_B$ and the wavefunction has the radial distribution $u^{\mathrm{Lan}}_{0,|\ell|}$. The red arcs indicate the trajectory of the centre of mass of the probability distribution, which is highlighted in green.

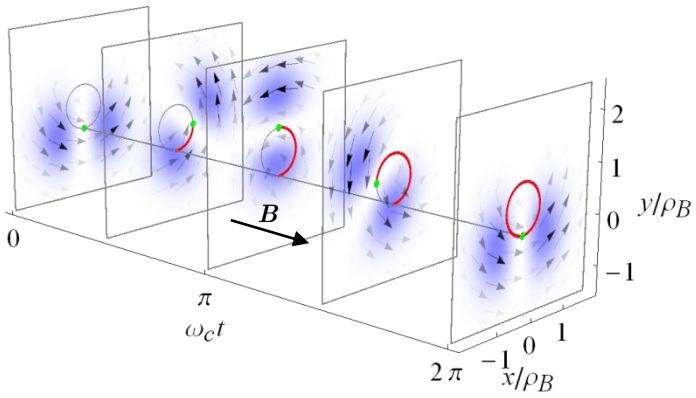

Figure 3.3: **Probability density and current density for an equally weighted superposition of wavefunctions that both have transverse momentum $p_c = 2\hbar/\rho_B$, but have opposite values of canonical angular momentum $\ell = \pm 1$.** The constituent states have the same radial distributions as in Fig. 3.2.

frame of its centre of mass. Here $\rho' = |\mathbf{r}_\perp - \langle \mathbf{r}_\perp \rangle|$ is the radial coordinate in this reference frame. This angular momentum arises as a result of the circulating current the magnetic field induces within the wavefunction, and is associated with a rotation of the probability density at the Larmor angular velocity ω_L [2, 115]. In contrast to cyclotron motion, the diamagnetic rotation depends on there being an extended probability distribution, and vanishes in the classical limit. The effect of the diamagnetic angular momentum becomes clear when considering a superposition of opposite values of canonical orbital angular momentum, such as that shown in Fig. 3.3. As this superposition has no net canonical angular momentum, the rotation of the electron's probability density with respect to its centre of mass is due entirely to the diamagnetic angular momentum.

In general, the orbital angular momentum with respect to the centre of mass axis will be given by a sum of canonical and diamagnetic contributions. The motion is thus described by two independent rotations: the cyclotron orbit, and the rotation around the instantaneous centre of mass axis due to the canonical and diamagnetic angular momenta.

3.1.4 Parallel axis theorem

The rotation of the electron's wavefunction is reminiscent of a classical rigid body. I will explore this analogy further by considering the total kinetic angular momentum of the electron. Here this angular momentum has the z component given by (2.16), with an expectation value of

$$\langle L_z^{\mathrm{kin}} \rangle = \ell\hbar + I\omega_{\mathrm{L}} \tag{3.10}$$

for any state with a canonical orbital angular momentum $\ell\hbar$. Here $I = m\langle\rho^2\rangle$ is the moment of inertia of the electron's probability distribution for rotation with respect to the z axis. Just as with a rigid body, I can use the parallel axis theorem to express the moment of inertia I as a sum of two components:

$$I = m\rho_0^2 + I', \tag{3.11}$$

where $\rho_0 = |\langle \mathbf{r}_\perp \rangle| = \sqrt{2(1-\cos\omega_{\mathrm{c}}t)}\,\sigma$, with σ defined by (3.6), is the radial coordinate of the centre of mass, and I' is the moment of inertia with respect to the centre of mass axis, given by (3.9). These two components correspond to the cyclotron orbit of the wavefunction and its diamagnetic angular momentum respectively. The total kinetic angular momentum of the electron, which I obtain from (3.10) and (3.11), can therefore be expressed as

$$\langle L_z^{\mathrm{kin}} \rangle = \ell\hbar + L_z^{\mathrm{cyclo}} + L_z^{\mathrm{dia}}, \tag{3.12}$$

where $L_z^{\mathrm{cyclo}} = m\omega_{\mathrm{L}}\rho_0^2 = (1-\cos\omega_{\mathrm{c}}t)m\omega_{\mathrm{c}}\sigma^2$ is the angular momentum associated with the cyclotron orbit. While the relation between the kinetic and canonical angular momenta in (2.16) is true also for a classical point particle [103], the decomposition into separate cyclotron and diamagnetic components that follows from (3.11) is only meaningful for an extended probability distribution.

Unlike the canonical and diamagnetic components, the cyclotron angular momentum depends on the choice of reference axis. A natural choice is to consider the angular momentum with respect to the centre of the cyclotron motion. In this reference frame, which we reach by making the transformation $y \to \tilde{y} = y - y_0$, the cyclotron angular

momentum has the constant value

$$\tilde{L}_z^{\text{cyclo}} = m\omega_c\sigma^2. \tag{3.13}$$

Irrespective of the reference frame, of course, the total kinetic angular momentum will be equal to the sum of the three components described.

One may expect that the cyclotron angular momentum, which exists classically, would be the dominant contribution to the electron's kinetic angular momentum. However, this need not be the case, as can be seen by considering typical parameters for free electrons in electron microscopes. For example, if an electron beam that is initially propagating parallel to a magnetic field is transmitted through a diffraction grating with a period $d = 100\,\text{nm}$, the first diffraction order will have a net transverse momentum of $p_c = \hbar(2\pi/d) = h/d$, which corresponds to an energy of $p_c^2/(2m) = h^2/(2md^2) = 0.15\,\text{meV}$. In a magnetic field of $B = 1\,\text{T}$, the resulting cyclotron orbit, which has radius 41 nm, will have an angular momentum of $2.6\hbar$. This is of the same order of magnitude as the canonical angular momentum of the lowest order vortex states, and considerably smaller than that of vortex beams recently generated with a winding number of $\ell = 200$ [51]. Indeed, in a given magnetic field, the cyclotron angular momentum can in principle have any size, ranging from zero to macroscopic values, depending on the net transverse momentum p_c. The diamagnetic angular momentum can also take a wide range of values, as the mean square radius of the probability distribution is varied [144], although this has a lower limit due to the uncertainty principle and a maximum due to the requirement of spatial coherence. This means that the different rotations I have described can indeed occur on the same length scale, justifying the choices of parameters in the figures.

3.1.5 Superposition of cyclotron orbits

So far I have considered rotations with respect to two different axes – the cyclotron axis, as well as the centre of mass axis. The position of the cyclotron axis was defined

by the transverse momentum p_c that appears in a plane wave factor in the wavefunction (3.2). Suppose, however, that we have a superposition of different transverse momenta. Arbitrary distributions of transverse momentum could be created using appropriately designed holograms, as described in section 2.2.2. A simple example would be the following superposition of two momenta, $p_{\mathrm{c},1}$ and $p_{\mathrm{c},2}$, which may also be associated with different canonical orbital angular momenta, ℓ_1 and ℓ_2:

$$\Psi_{\perp,0} = \frac{u^{\mathrm{Lan}}_{n,|\ell_1|}(\rho)}{\sqrt{2}} \exp\left[\mathrm{i}\left(\ell_1\phi + \frac{p_{\mathrm{c},1}}{\hbar}x\right)\right] + \frac{u^{\mathrm{Lan}}_{n,|\ell_2|}(\rho)}{\sqrt{2}} \exp\left[\mathrm{i}\left(\ell_2\phi + \frac{p_{\mathrm{c},2}}{\hbar}x\right)\right]. \tag{3.14}$$

This is similar to the wavefunction formed when a plane wave is transmitted through a forked diffraction grating [1]. For the discussion here the particular form of the radial distribution is not important, and the Landau function has been chosen with numerical efficiency in mind. The evolution of such a state, here with equal and opposite values of both the transverse momentum and canonical angular momentum, is shown in Fig. 3.4. It can be seen that there are now two cyclotron orbits, which have different rotation axes. These are associated with different directions of the initial momentum p_c. As a result, the two components of the superposition move apart, before recombining and interfering.

Taken together, the cyclotron orbits in Fig. 3.4 describe a rotation, with respect to the z axis, at the Larmor angular velocity ω_L. This is consistent with the predictions of classical electron optics regarding image formation in rotationally symmetric magnetic lenses [93]. Interestingly, though, in the case here the axis of the Larmor rotation is not defined by a symmetry of the magnetic field – a uniform magnetic field is rotationally symmetric with respect to an infinite number of axes. Rather, here the Larmor rotation occurs with respect to the centre of mass of the electron's probability distribution. This is the case both in Fig. 3.3, where the centre of mass follows a cyclotron orbit, and in Fig. 3.4, where the centre of mass is stationary. Further, it must be remembered that I am considering here a single electron that is in a state of superposition. This means, for example, that if one of the two cyclotron components in Fig. 3.4 underwent an interaction that modified its phase, this could be detected through its effect on the subsequent interference pattern.

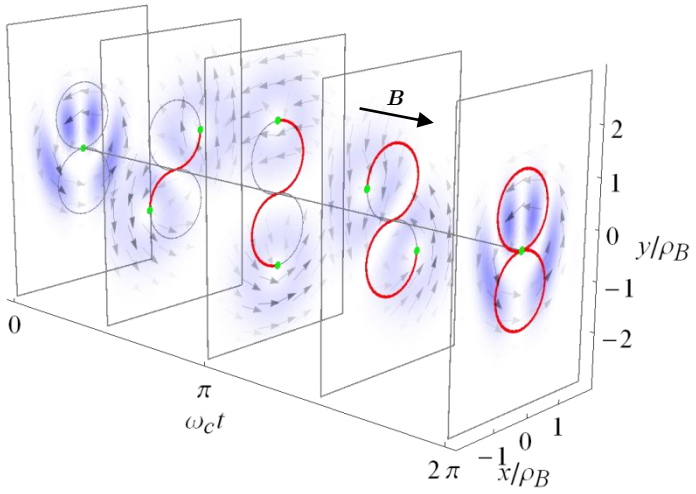

Figure 3.4: **Probability density and current density for an equally weighted superposition of a wavefunction with $p_c = 3\hbar/\rho_B$ and $\ell = -1$ and a wavefunction with $p_c = -3\hbar/\rho_B$ and $\ell = 1$.** The constituent states have the same radial distributions as in Figs. 3.2 and 3.3. The centre of mass of the superposition remains stationary in the x-y plane, while the individual components follow the cyclotron trajectories indicated.

3.1.6 Summary and outlook

In summary, I have shown that in a magnetic field an electron can rotate around more than one axis simultaneously. The wavefunction of the electron follows a cyclotron orbit, and superposed onto this is a rotation around the instantaneous centre of mass. The rotation with respect to the centre of mass axis arises as a result of the diamagnetic angular momentum, as well as any canonical orbital angular momentum the electron possesses. The kinetic angular momentum of the electron is therefore described by the parallel axis theorem.

My results show that canonical orbital angular momentum and cyclotron motion provide separate degrees of freedom for shaping electron current distributions. This could allow electron beams to be structured for use in specific applications. For example, the symmetry of the current distribution could be optimised to probe specific transitions in materials [68, 145]. It may also be possible to utilise cyclotron trajectories in novel

forms of interferometry. Moreover, here I have only considered the case in which the canonical angular momentum and magnetic field are parallel, so that the rotation is confined to a plane. With canonical angular momentum and magnetic fields that are in different directions to one another, the angular momentum and current density could be shaped in three dimensions.

Further, if the angular momenta were in different directions, it appears that they would become coupled. Canonical orbital angular momentum that is at an angle to a uniform magnetic field would be expected to precess around the direction of the field [39, 76]. The canonical angular momentum is also not conserved when the rotational symmetry of the magnetic field is broken, such as in astigmatic magnetic lenses [109, 110, 111]. Not only this, but in non-uniform magnetic fields the spin and orbital degrees of freedom of an electron with non-relativistic velocity are no longer independent [61, 95]. The nature of the coupling between all of these angular momenta is an interesting avenue for future investigation.

3.2 Complements to section 3.1

The remainder of this chapter consists of additional details and considerations that complement the material already presented. This begins with the use of the Chebyshev method to solve the time-dependent Schrödinger equation.

Following that, I provide a detailed derivation of the equation of motion for the centre of mass of the probability distribution. This is a rather lengthy calculation, which was only briefly outlined in section 3.1.3. To begin with, I consider the equation of motion for the expectation value of an arbitrary operator, in the presence of a uniform magnetic field, and obtain a result that I will reuse in Chapter 4. This general expression is then evaluated for the position operator; first for an arbitrary initial wavefunction and then

for the particular form of wavefunction I consider in this chapter.

The results of further numerical calculations of the electron's probability density and current density are then presented. This allows me to illustrate more fully how the orbital motion of the electron depends on the two degrees of freedom p_{c} and ℓ, including how different superpositions of these variables evolve.

The chapter is concluded with some additional details of the Chebyshev polynomial expansion on which the numerical calculations are based. Specifically, the expansion coefficients given by (3.21) are derived, and the exponential decay of these coefficients with increasing q is demonstrated. While these results can be found in some of the publications cited, it will be helpful for anyone wishing to reproduce the work described here to have a complete and self-contained description of exactly how my own calculations have been performed. This is especially true as many authors have used an alternative, "complex", form of Chebyshev polynomial, in which case the expansion coefficients are different.

3.2.1 Numerical solution of the Schrödinger equation

The time-dependent Schrödinger equation can be solved numerically with high accuracy and efficiency by expanding the time-evolution operator in a series of Chebyshev polynomials. In this section, I describe how this method can be applied to the two-dimensional Schrödinger equation for an electron interacting with an external magnetic field. For generality, I shall consider here a Hamiltonian of the form

$$\begin{aligned} \mathcal{H}(x,y) &= S_2\left(\frac{\partial^2}{\partial x^2}+\frac{\partial^2}{\partial y^2}\right)+\mathrm{i}S_{1x}(x,y)\frac{\partial}{\partial x} \\ &\quad +\mathrm{i}S_{1y}(x,y)\frac{\partial}{\partial y}+S_0(x,y) \end{aligned} \tag{3.15}$$

[143]. In the case of the Hamiltonian used in the rest of this chapter, I would have $S_2 = -\hbar^2/(2m)$, $S_{1x} = -\hbar eBy/(2m)$, $S_{1y} = \hbar eBx/(2m)$ and $S_0 = e^2B^2(x^2+y^2)/(8m)$. The *Mathematica* code I have written to perform these calculations is described in Appendix A, and is also available online at [146].

Since the Hamiltonian (3.15) is independent of time, I can write the solution of the Schrödinger equation as

$$\Psi_\perp(t+\Delta t) = \exp\left(-\frac{\mathrm{i}}{\hbar}\mathcal{H}\Delta t\right)\Psi_\perp(t). \tag{3.16}$$

In order to evaluate this numerically, first I must represent the wavefunction, and the coefficients S_2 etc., on a two-dimensional grid. If this grid covers an area $L_x \times L_y$, and contains $N_x \times N_y$ points, then the maximum spatial frequencies represented are $k_{x,\max} = \pi N_x/L_x$ and $k_{y,\max} = \pi N_y/L_y$. The maximum and minimum values of energy represented on the grid are then

$$\begin{aligned} E_{\max} &= -S_2(k_{x,\max}^2 + k_{y,\max}^2) + \mathrm{Max}(S_{1x})k_{x,\max} \\ &\quad + \mathrm{Max}(S_{1y})k_{y,\max} + \mathrm{Max}(S_0) \end{aligned} \tag{3.17}$$

and

$$E_{\min} = -\left[\mathrm{Max}(S_{1x})k_{x,\max} + \mathrm{Max}(S_{1y})k_{y,\max}\right] + \mathrm{Min}(S_0). \tag{3.18}$$

I shall now introduce a new operator

$$\tilde{\mathcal{H}} = \frac{\mathcal{H}-b}{a}, \tag{3.19}$$

where $a = (E_{\max} - E_{\min})/2$ and $b = (E_{\max} + E_{\min})/2$. This operator has eigenvalues represented on the grid that lie in the range $[-1, 1]$. I can then expand the time-evolution operator in a series of Chebyshev polynomials $T_q(\tilde{\mathcal{H}})$:

$$\begin{aligned} \Psi_\perp(t+\Delta t) &= \exp(-\frac{\mathrm{i}}{\hbar}b\Delta t)\exp(-\frac{\mathrm{i}}{\hbar}a\tilde{\mathcal{H}}\Delta t)\Psi_\perp(t) \\ &\approx \exp(-\frac{\mathrm{i}}{\hbar}b\Delta t)\sum_{q=0}^{M}\alpha_q(a\Delta t)T_q(\tilde{\mathcal{H}})\Psi_\perp(t). \end{aligned} \tag{3.20}$$

Chebyshev polynomials are chosen as these minimise the error associated with truncating the expansion at a finite order M [141]. The expansion coefficients are given

by

$$\alpha_q(a\Delta t) = \begin{cases} (-\mathrm{i})^q J_q(a\Delta t/\hbar), & q = 0 \\ 2(-\mathrm{i})^q J_q(a\Delta t/\hbar), & q \neq 0 \end{cases} \tag{3.21}$$

where J_q is a Bessel function. For $q > \mathrm{e}a\Delta t/(2\hbar)$, where e, in roman font, denotes the mathematical constant, the magnitudes of these coefficients decay exponentially with increasing q [147, 148]. This means that the error due to truncating the series at order M, which can be estimated by $|\alpha_M(a\Delta t)|$, can be made arbitrarily small. If I set

$$M = \frac{\mathrm{e}}{2\hbar} a\Delta t + \delta, \tag{3.22}$$

δ can be adjusted so that this error is less than machine precision. The numerical error resulting from the Chebyshev expansion is then negligible.

In order to evaluate the individual terms in the expansion (3.20), the action of the Chebyshev polynomial $T_q(\tilde{\mathcal{H}})$ on the initial wavefunction $\Psi_\perp(t)$ must be calculated. Using the recurrence relation for the Chebyshev polynomials, I obtain

$$T_q(\tilde{\mathcal{H}})\Psi_\perp(t) = 2\tilde{\mathcal{H}}T_{q-1}(\tilde{\mathcal{H}})\Psi_\perp(t) - T_{q-2}(\tilde{\mathcal{H}})\Psi_\perp(t), \tag{3.23}$$

for $q > 0$, with the initial conditions $T_0(\tilde{\mathcal{H}})\Psi_\perp(t) = \Psi_\perp(t)$ and $T_1(\tilde{\mathcal{H}})\Psi_\perp(t) = \tilde{\mathcal{H}}\Psi_\perp(t)$. The action of the Hamiltonian on the wavefunction can be efficiently calculated by evaluating the spatial derivatives in Fourier space [147, 149]. That is,

$$\begin{aligned} \mathcal{H}\Psi_\perp(t) \;\approx\; & S_2 \mathrm{FT}^{-1}[(-k_x^2 - k_y^2)\mathrm{FT}\Psi_\perp] + \mathrm{i}S_{1x}\mathrm{FT}^{-1}(ik_x\mathrm{FT}\Psi_\perp) \\ & + \mathrm{i}S_{1y}\mathrm{FT}^{-1}(ik_y\mathrm{FT}\Psi_\perp) + S_0\Psi_\perp, \end{aligned} \tag{3.24}$$

where k_x, k_y are the coordinates in Fourier space and FT denotes a discrete Fourier transform and FT^{-1} the corresponding inverse transform.

3.2.2 Centre of mass trajectory

In this section I provide additional details of the derivation of the centre of mass of the electron's probability distribution; that is, the expectation value $\langle \mathbf{r}_\perp \rangle$.

Equation of motion for the time-evolution of an arbitrary operator

The time-derivative of the expectation value of an operator can be related to its commutation with the Hamiltonian of the system. For any operator $\mathcal{O}$, which I will assume does not depend explicitly on time, this derivative can be expressed as

$$\begin{aligned}\frac{\partial\langle\mathcal{O}\rangle(t)}{\partial t} &= \int \mathrm{d}^2\mathbf{r}_\perp \left(\frac{\partial\Psi_\perp^*}{\partial t}\mathcal{O}\Psi_\perp + \Psi_\perp^*\mathcal{O}\frac{\partial\Psi_\perp}{\partial t}\right) \\ &= \frac{i}{\hbar}\int \mathrm{d}^2\mathbf{r}_\perp \left(H_\perp\Psi_\perp^*\mathcal{O}\Psi_\perp - \Psi_\perp^*\mathcal{O}H_\perp\Psi_\perp\right) \\ &= -\frac{i}{\hbar}\langle[\mathcal{O}, H_\perp]\rangle \end{aligned} \tag{3.25}$$

[150]. In the second line I have substituted in the time-dependent Schrödinger equation

$$i\hbar\frac{\partial\Psi_\perp}{\partial t} = H_\perp\Psi_\perp \tag{3.26}$$

and also its complex conjugate $i\hbar\,\partial\Psi_\perp^*/\partial t = -H_\perp\Psi_\perp^*$.

Here I am interested in a quantity that evolves periodically with time, and as such will be described by a differential equation that is second order in time. Therefore, I require an expression for the second derivative of the operator with respect to time, which I can obtain in a similar manner to above:

$$\frac{\partial^2\langle\mathcal{O}\rangle(t)}{\partial t^2} = -\frac{1}{\hbar^2}\langle[[\mathcal{O}, H_\perp], H_\perp]\rangle\,. \tag{3.27}$$

Position operator

These expressions will now be used to evaluate the expectation value of $\mathbf{r}_\perp = (x, y)$. I will work in Cartesian coordinates here as this is convenient for evaluating the commutation relations. Using Cartesian coordinates, the Hamiltonian $H_\perp$ is expressed as

$$H_\perp = \frac{1}{2m}\left[\left(p_x^{\mathrm{can}}\right)^2 + \left(p_y^{\mathrm{can}}\right)^2\right] + \frac{1}{2}m\omega_{\mathrm{L}}^2(x^2+y^2) + \omega_{\mathrm{L}}(xp_y^{\mathrm{can}} - yp_x^{\mathrm{can}}). \tag{3.28}$$

The commutator of x with this Hamiltonian is

$$\begin{aligned}[x, H_\perp] &= \left[x, \frac{1}{2m}(p_x^{\mathrm{can}})^2 - \omega_{\mathrm{L}} y p_x^{\mathrm{can}}\right] \\ &= \frac{1}{2m}\left[x, (p_x^{\mathrm{can}})^2\right] - \omega_{\mathrm{L}}\left[x, y p_x^{\mathrm{can}}\right] \\ &= i\hbar\left(\frac{p_x^{\mathrm{can}}}{m} - \omega_{\mathrm{L}} y\right), \end{aligned} \tag{3.29}$$

where I have used

$$\left[x, (p_x^{\mathrm{can}})^2\right] = p_x^{\mathrm{can}}\left[x, p_x^{\mathrm{can}}\right] + \left[x, p_x^{\mathrm{can}}\right]p_x^{\mathrm{can}} = 2i\hbar p_x^{\mathrm{can}} \tag{3.30}$$

and

$$\left[x, y p_x^{\mathrm{can}}\right] = y\left[x, p_x^{\mathrm{can}}\right] + [x, y]p_x^{\mathrm{can}} = i\hbar y. \tag{3.31}$$

Here, and in subsequent calculations, the identities $[AB, C] = A[B, C] + [A, C]B$ and $[A, BC] = B[A, C] + [A, B]C$ prove useful. The standard commutations relations for the position and canonical momentum, $[x, p_x^{\mathrm{can}}] = [y, p_y^{\mathrm{can}}] = i\hbar$ and $[x, p_y^{\mathrm{can}}] = [y, p_x^{\mathrm{can}}] = 0$, are also used.

The double commutator, which will be used to evaluate the second time-derivative, is

$$[[x, H_\perp], H_\perp] = -2\hbar^2\omega_{\mathrm{L}}\left(\omega_{\mathrm{L}} x + \frac{p_y^{\mathrm{can}}}{m}\right) = -\hbar^2\omega_{\mathrm{c}}^2(x - \tilde{x}). \tag{3.32}$$

Here

$$\tilde{x} = x + \frac{p_y^{\mathrm{kin}}}{eB} \tag{3.33}$$

is the x coordinate of the centre of the orbit of a classical particle that, when located at the position x, has a y component of kinetic momentum p_y^{kin} [98]. The expectation value of the x coordinate therefore obeys the equation of motion

$$\frac{\partial^2\langle x\rangle(t)}{\partial t^2} = -\omega_{\mathrm{c}}^2\left(\langle x\rangle(t) - \langle\tilde{x}\rangle\right), \tag{3.34}$$

which describes a harmonic oscillation with respect to the value $\langle\tilde{x}\rangle$.

The y coordinate can be obtained in a similar manner. The commutation relations are

$$\begin{aligned}[y, H_\perp] &= \left[y, \frac{1}{2m}(p_y^{\mathrm{can}})^2 + \omega_{\mathrm{L}} x p_y^{\mathrm{can}}\right] \\ &= \frac{1}{2m}\left[y, (p_y^{\mathrm{can}})^2\right] + \omega_{\mathrm{L}}\left[y, x p_y^{\mathrm{can}}\right] \\ &= i\hbar\left(\frac{p_y^{\mathrm{can}}}{m} + \omega_{\mathrm{L}} x\right) \end{aligned} \tag{3.35}$$

using

$$\left[y,(p_y^{\mathrm{can}})^2\right] = p_y^{\mathrm{can}}\left[y,p_y^{\mathrm{can}}\right] + [y,p_y^{\mathrm{can}}]p_y^{\mathrm{can}} = 2i\hbar p_y^{\mathrm{can}}, \tag{3.36}$$

$$\left[y,xp_y^{\mathrm{can}}\right] = x\left[y,p_y^{\mathrm{can}}\right] + [y,x]p_y^{\mathrm{can}} = i\hbar x \tag{3.37}$$

and

$$[[y,H_\perp],H_\perp] = 2\hbar^2\omega_{\mathrm{L}}\left(\omega_{\mathrm{L}}y - \frac{p_x^{\mathrm{can}}}{m}\right) = -\hbar^2\omega_{\mathrm{c}}^2(y-\tilde{y}). \tag{3.38}$$

Here $\tilde{y}$ is the y coordinate of the classical orbit centre, defined similarly to (3.33):

$$\tilde{y} = y - \frac{p_x^{\mathrm{kin}}}{eB}. \tag{3.39}$$

The equation of motion for the expectation value $\langle y\rangle$ therefore has the same form as that for the x coordinate:

$$\frac{\partial^2\langle y\rangle(t)}{\partial t^2} = -\omega_{\mathrm{c}}^2\left(\langle y\rangle(t) - \langle\tilde{y}\rangle\right). \tag{3.40}$$

Equations (3.34) and (3.40) can be expressed more compactly as

$$\frac{\partial^2\langle\mathbf{r}_\perp\rangle(t)}{\partial t^2} = -\omega_{\mathrm{c}}^2\left(\langle\mathbf{r}_\perp\rangle(t) - \langle\tilde{\mathbf{r}}_\perp\rangle\right), \tag{3.41}$$

where $\tilde{\mathbf{r}}_\perp = (\tilde{x},\tilde{y})$. Note that $[\tilde{\mathbf{r}}_\perp, H_\perp] = 0$, so that the expectation value $\langle\tilde{\mathbf{r}}_\perp\rangle$ is independent of time [98].

The solution of this equation of motion, for any initial wavefunction $\Psi_{\perp 0}$, can be written as

$$\langle\mathbf{r}_\perp\rangle(t) = \langle\mathbf{r}_{\perp 0}\rangle + \langle\mathbf{r}_\perp\rangle(0)\cos\omega_{\mathrm{c}}t + \frac{1}{\omega_{\mathrm{c}}}\frac{\partial\langle\mathbf{r}_\perp\rangle(0)}{\partial t}\sin\omega_{\mathrm{c}}t. \tag{3.42}$$

Evaluation for the initial state considered in section 3.1

Now consider the wavefunction

$$\Psi_\perp(t=0) = \Psi_{\perp 0} = u(\rho)\exp\left[i\left(\ell\phi + \frac{p_{\mathrm{c}}}{\hbar}x\right)\right]. \tag{3.43}$$

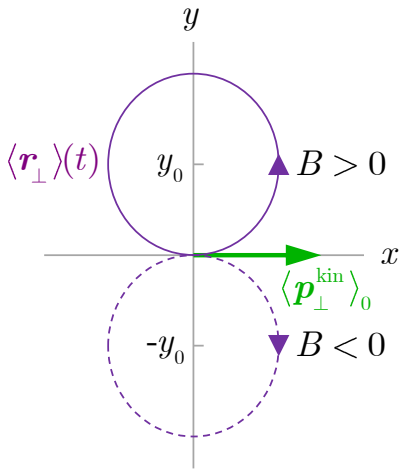

Figure 3.5: **Cyclotron orbit of the expectation value of position $\langle \mathbf{r}_\perp \rangle(t)$.**

With this initial state, the expectation value of the classical orbit centre $\tilde{\mathbf{r}}_\perp$ is $\langle \tilde{\mathbf{r}}_\perp \rangle = \langle \tilde{\mathbf{r}}_\perp \rangle(0) = \langle \mathbf{p}_x^{\text{kin}} \rangle(0)/(m\omega_c)\hat{\mathbf{y}} = y_0\hat{\mathbf{y}}$, where $y_0 = p_c/(|e|B)$. The expectation value of the position $\mathbf{r}_\perp$ is initially $\langle \mathbf{r}_\perp \rangle(0) = \mathbf{0}$, and the initial velocity in the x direction is described by

$$\frac{\partial \langle \mathbf{r}_\perp \rangle(0)}{\partial t} = -\frac{i}{\hbar} \langle [\mathbf{r}_\perp, H_\perp] \rangle (0) = \frac{p_c}{m}\hat{\mathbf{x}}. \tag{3.44}$$

Therefore, upon substitution into (3.42), the particular solution is found to be

$$\langle \mathbf{r}_\perp \rangle(t) = y_0[\sin \omega_c t\hat{\mathbf{x}} + (1 - \cos \omega_c t)\hat{\mathbf{y}}]. \tag{3.45}$$

This trajectory is plotted in 3.5.

3.2.3 Probability density and current density

In this section I present further numerical calculations of the evolution of the probability density and current density. These complement the results of section 3.1 by providing a more detailed picture of how the probability density and current density depend on the initial state of the electron.

Figures 3.6–3.8 illustrate how these quantities depend on the radius of the cyclotron

orbit, which is determined by the momentum p_c. Each of these figures shows a state with a different value of n and ℓ. In each case, the three parts show the evolution of this state for different values of p_c. When $p_c = 0$, there is no cyclotron orbit, and the electron is in a Landau state. This means that the probability density and current density are symmetric under rotation about the z axis. As the value of p_c is increased, the current is increasingly influenced by the cyclotron motion of the electron. When $\ell = 0$ or -1, that is, when there is no canonical angular momentum or else it is in the direction opposite to the magnetic field, the current becomes increasingly dominated by the cyclotron motion. However, when $\ell = 1$, in which case the canonical angular momentum is in the same direction as the magnetic field, this canonical angular momentum has a clear effect on the current density even when $p_c/p_{c\,0} = 3$.

Figure 3.9 shows the evolution of a superposition of two states that have different magnitudes of canonical angular momentum. Unlike the superposition in Fig. 3.3 of section 3.1, which had no net canonical angular momentum, these superpositions have a net canonical angular momentum of magnitude $\hbar$, which may be either parallel or anti-parallel to the magnetic field. It is seen that the motion of the wavefunction is very different in each of these two cases. In the upper panel, where the net canonical angular momentum is anti-parallel to the magnetic field, there is no rotation of the probability density with respect to its centre of mass, and the only rotation is that of the cyclotron orbit. This contrasts to Fig. 3.3 of section 3.1, where there is an internal rotation of the probability density at the Larmor angular velocity. In the lower panel, meanwhile, where the net canonical angular momentum is parallel to the magnetic field, there is an internal rotation at *twice* the Larmor angular velocity, that is, at the cyclotron angular velocity. This means that here the rotation of the centre of mass, and the rotation in the reference frame of the centre of mass, both have the same angular velocity. The dependence of the angular velocity of the internal rotation of the probability density on the canonical angular momentum that is seen here is the same as predicted in [87] and is consistent with the experimental observations of [2].

The rotation in the centre of mass frame can also occur at different fractions of the

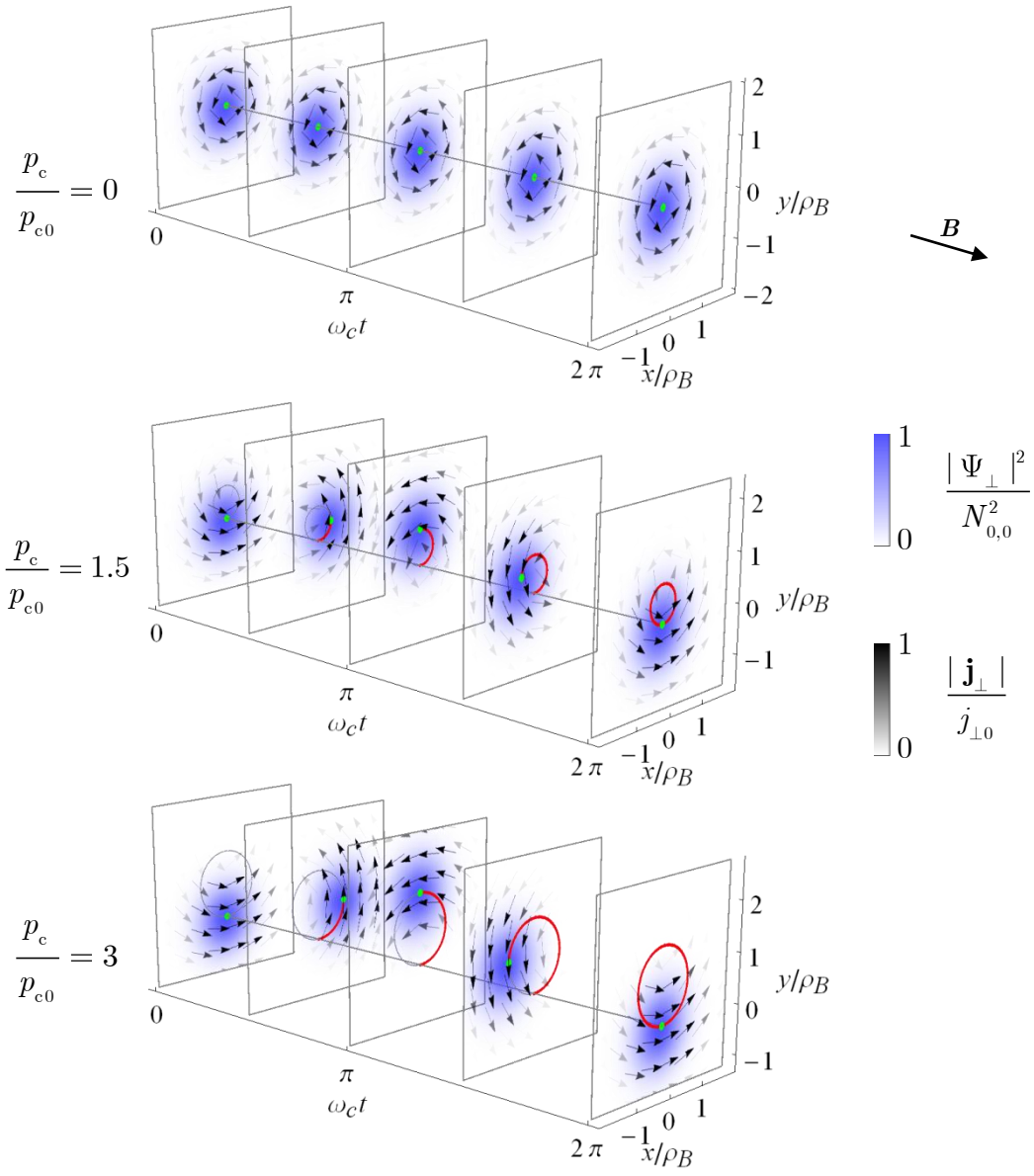

Figure 3.6: **Evolution of the probability density and current density for different values of the cyclotron radius, for a wavefunction with $n = 0$ and $\ell = 0$.** The radius of the cyclotron orbit is determined by the value of the transverse momentum p_c. In this and subsequent images, p_c is quoted relative to the value for a classical particle in a circular orbit with a radius ρ_B and an angular momentum of $\hbar$, $p_{c\,0} = \hbar/\rho_B$.

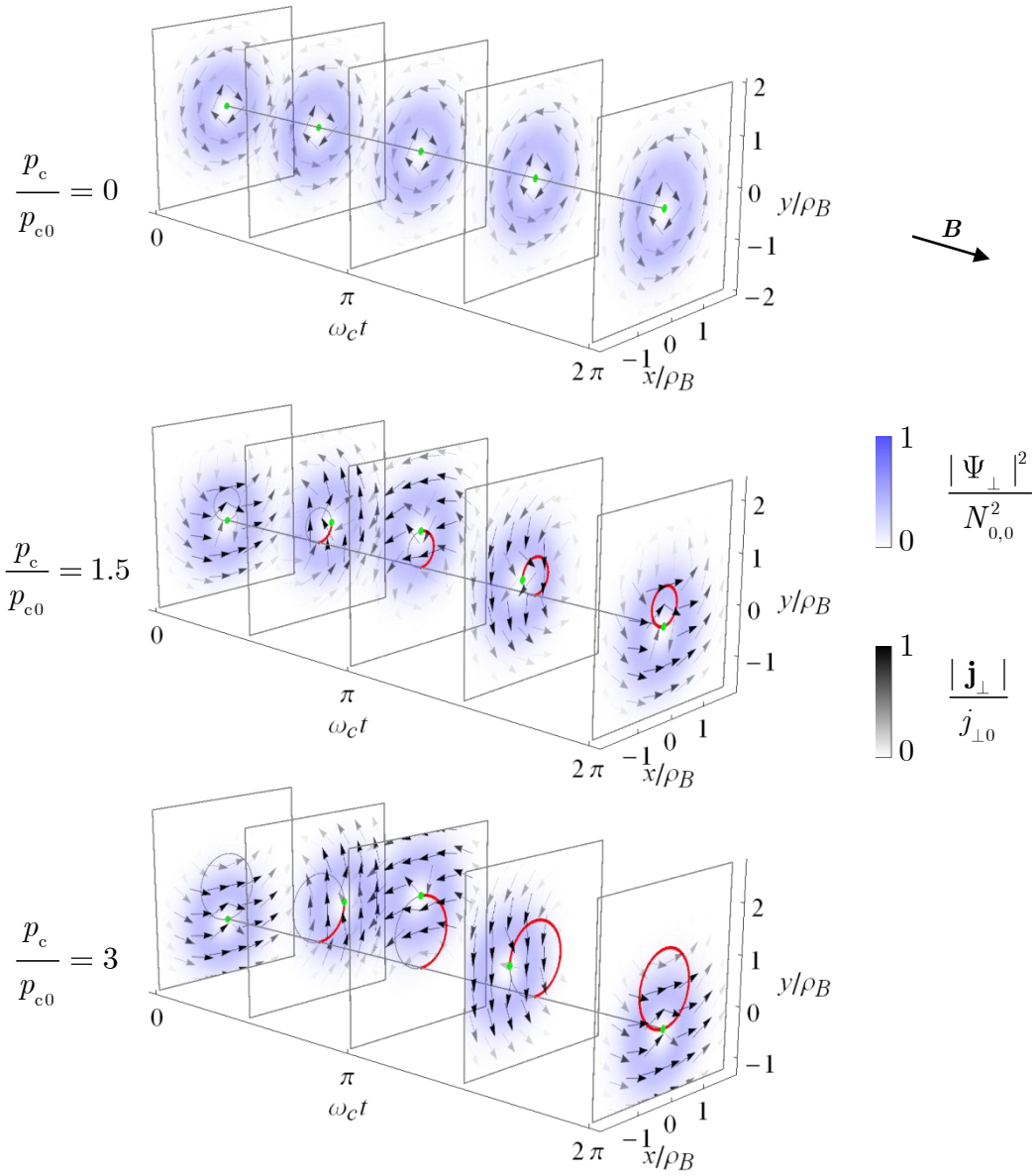

Figure 3.7: **Evolution of the probability density and current density for different values of the cyclotron radius, for a wavefunction with $n = 0$ and $\ell = -1$.**

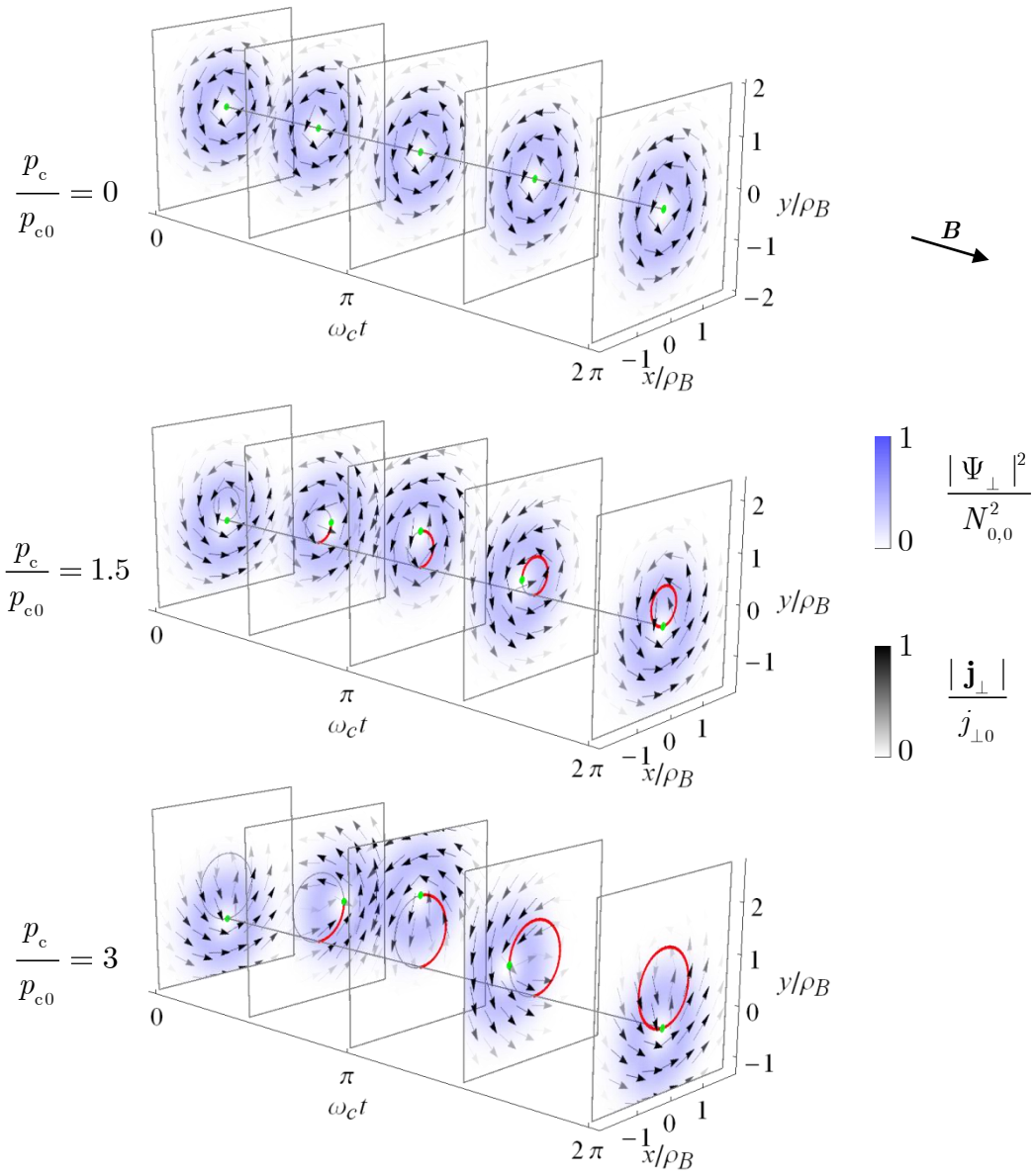

Figure 3.8: **Evolution of the probability density and current density for different values of the cyclotron radius, for a wavefunction with $n = 0$ and $\ell = 1$.**

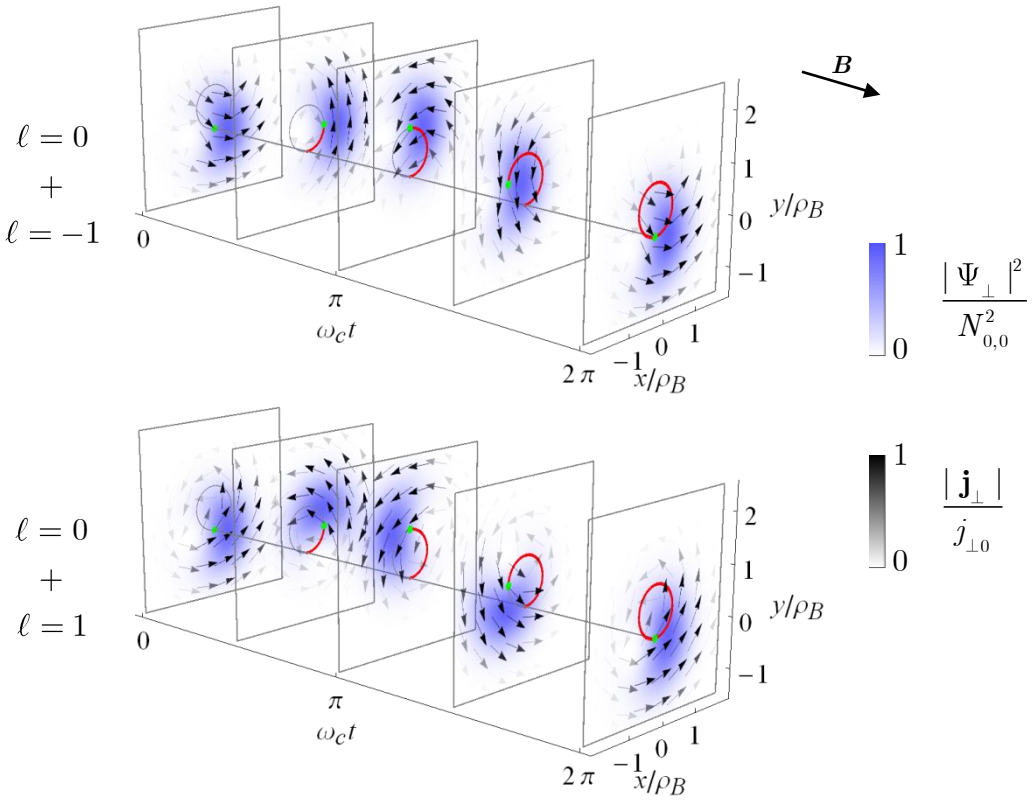

Figure 3.9: **Superpositions of states that have different magnitudes of canonical angular momentum.** In each part the wavefunction is an equally weighted superposition of the labelled values of ℓ, while $n = 0$ and $p_c/p_{c\,0} = 2$. In this and subsequent images the wavefunction of the superposition is normalised to satisfy the condition $\int \mathrm{d}^2\mathbf{r}_\perp \, |\Psi_\perp|^2 = 1$.

cyclotron frequency. This is illustrated by Fig. 3.10. Here, for clarity, p_c has been set to zero, so that there is no cyclotron orbit. As in Fig. 3.9, the two superpositions shown here have a net canonical angular momentum of magnitude $\hbar$, which in one case is parallel to the magnetic field and in the other case is anti-parallel to the field. The difference here though is that the components of the superposition have magnitudes of canonical angular momentum equal to $\hbar$ and $2\hbar$, rather than 0 and $\hbar$. This results in a probability density that is a triangular arrangement of three spots. In the upper panel, where the net canonical angular momentum is anti-parallel to the magnetic field, this pattern rotates at an angular velocity equal to one third of the cyclotron angular velocity. In the lower panel, where this angular momentum is in the same direction as the magnetic field, the rotation is at twice this rate: $2\omega_c/3$. This contrasts with the superpositions considered in [2, 87], which rotate at an angular velocity equal to 0, $\omega_L = \omega_c/2$ or ω_c. Note that the expression for the expectation value of the angular velocity that is derived in [2], and describes rotations at one of these three rates, applies specifically to Landau states, or superpositions of Landau states with different n but the same ℓ.

In general, the probability density does not simply rotate, but also deforms as the wavefunction evolves. This is seen in Fig. 3.4 of section 3.1, where the two components of the superposition have different values of p_c, and so follow different cyclotron orbits. Such a deformation can also occur in the absence of any cyclotron orbit however, when there is a superposition of a larger number of canonical angular momentum components. This is shown in Fig. 3.11. Here the probability density at $t = 0$ again has a triangular pattern, but this time one of the spots is darker than the other two. As time passes, not only does this pattern rotate, but also the spot that is initially darker diminishes in intensity, and at the same time another spot appears on the opposite side of the pattern.

Finally, I will present further examples of superpositions of components that follow different cyclotron orbits. Figure 3.12 shows superpositions similar to that in Fig. 3.4 of section 3.1, but with different choices for the values of ℓ. As in the previous figure, the

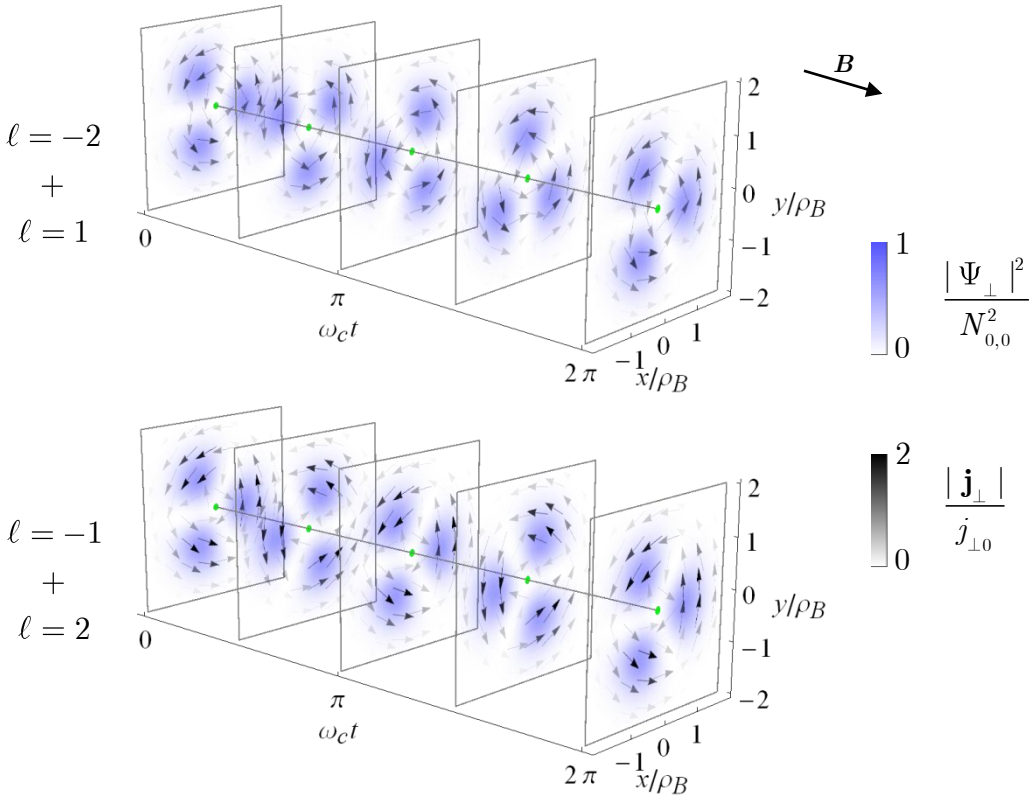

Figure 3.10: **Rotations at different fractions of the cyclotron frequency.** Here p_c is set to 0, so that there is no orbit of the centre of mass, and the internal rotation is clearer. As before $n = 0$, and each part displays a superposition with equal weights of the labelled values of ℓ. In the top image the probability density rotates through an angle of $2\pi/3$ rad, corresponding to an angular velocity of $\omega_c/3$. On the bottom the rotation is through twice this angle, and the angular velocity is therefore $2\omega_c/3$.

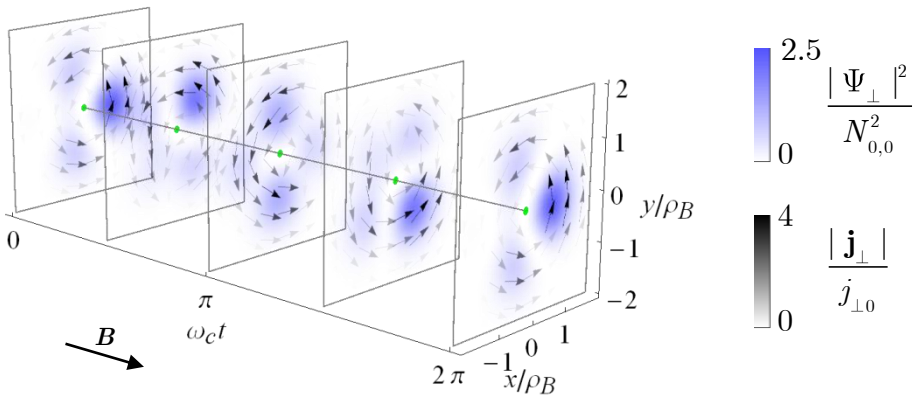

Figure 3.11: **Deformation of the probability density of a more complicated superposition.** This is a superposition with equal weights of the values $\ell = -2, -1, 1$ and 2, with $n = 0$ and $p_c = 0$. Unlike the superpositions of two values of ℓ in the previous figures, here the probability density does not simply rotate with respect to its centre of mass – it deforms as the wavefunction diffracts.

two canonical angular momentum components periodically separate and overlap. The interference pattern formed when they overlap is different depending on the components of the superposition. This could potentially be utilised in interferometry: if one of the components were modified at the point where they are separated, this would be revealed by a change in the interference pattern formed when the components recombine, as illustrated by Fig. 3.13.

3.2.4 Chebyshev polynomial expansion

The numerical calculations I employ are based on an expansion of the time-evolution operator in a series of Chebyshev polynomials. In this section, I describe this expansion in more detail.

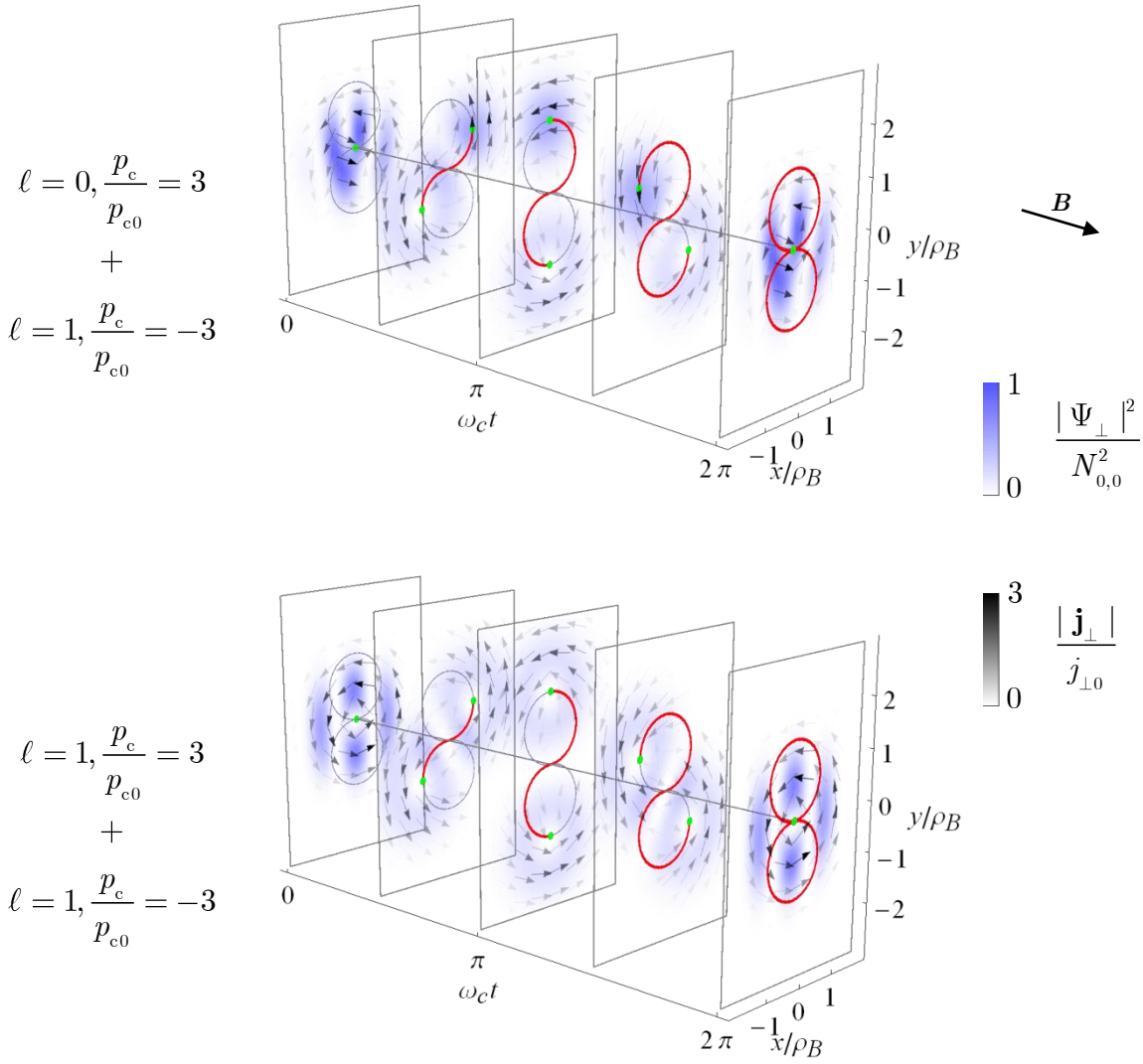

Figure 3.12: **Interference of states that have different values of canonical angular momentum and follow overlapping cyclotron orbits.** In each case $n = 0$.

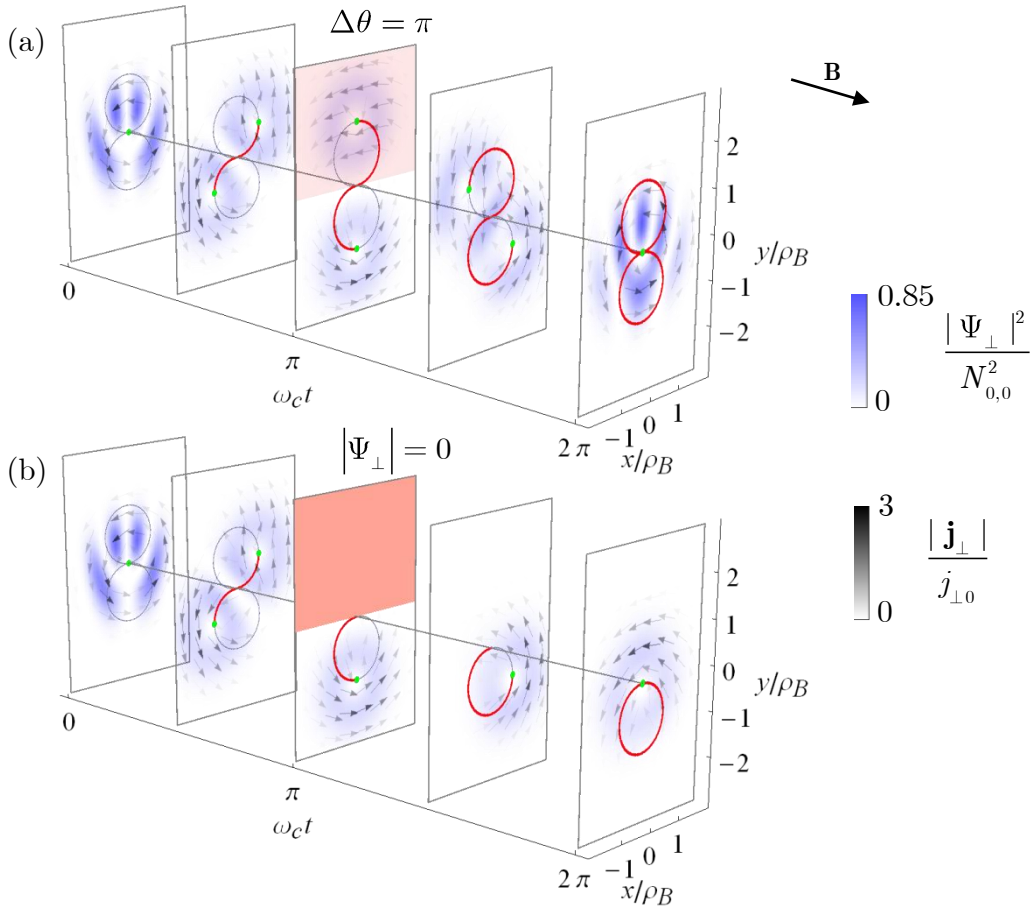

Figure 3.13: **Prototype for a magnetic orbital interferometer.** The initial state is the same as that in Fig. 3.4 of section 3.1: an equally weighted superposition of a wavefunction with $p_c/p_{c\,0} = 3$ and $\ell = -1$ and a wavefunction with $p_c/p_{c\,0} = -3$ and $\ell = 1$. Here, however, after half of a cyclotron period the wavefunction in the region $y > 0$ is modified. In (a), the phase $\arg \Psi_\perp$ in this region is shifted through an angle $\Delta\theta = \pi$, while in (b) the amplitude $|\Psi_\perp|$ in the same region is set to zero. It is seen that the relative phase shift in (a) results in a shift in the interference fringes formed after a complete cyclotron period, while the absorption in (b) eliminates one of the cyclotron components, resulting in a change in the angular momentum of the final state.

It is well known that any function $f(X)$ can be expressed as a series expansion

$$f(X) = \sum_{q=0}^{\infty} \alpha_q P_q(X), \tag{3.46}$$

where P_q is a complete set of polynomials satisfying an orthogonality relation $\langle P_q|P_r\rangle = \delta_{q,r}\langle P_q|P_q\rangle$. The expansion coefficients are

$$\alpha_q = \frac{\langle P_q|f\rangle}{\langle P_q|P_r\rangle}, \tag{3.47}$$

where

$$\langle f|g\rangle = \int_a^b \mathrm{d}X\, w(X) f(X) g(X) \tag{3.48}$$

is a scalar product, with $[a, b]$ the interval on which f is defined and $w(X)$ a weighting function.

While any set of orthogonal polynomials can be used in such an expansion, for numerical calculations it is advantageous to work with Chebyshev polynomials, since in this case the convergence of the series is particularly rapid [148]. The Chebyshev polynomials of the first kind,

$$P_q(X) = T_q(X) = \cos(q \cos^{-1} q), \tag{3.49}$$

are defined on the interval $[a, b] = [-1, 1]$, and are associated with the weighting function $w(X) = 1/\left(\pi\sqrt{1 - X^2}\right)$. They have the orthogonality relation

$$\langle T_q|T_r\rangle = \frac{\delta_{q,r}(1 + \delta_{q,0})}{2} = \begin{cases} \delta_{q,r}, & q = 0 \\ \delta_{q,r}/2, & q \neq 0 \end{cases} \tag{3.50}$$

[148].

Now consider the application to the time-evolution operator that appears in the Schrödinger equation. As described in section 3.2.1, the Hamiltonian should first be scaled such that its eigenvalues are mapped onto the interval $[-1, 1]$ – the domain of the Chebyshev polynomials. This is achieved by the transformation described by (3.19) in section 3.2.1:

$$\tilde{\mathcal{H}} = \frac{\mathcal{H} - b}{a}, \tag{3.51}$$

where $a = (E_{\max} - E_{\min})/2$ and $b = (E_{\max} + E_{\min})/2$, with $E_{\max}$ and $E_{\min}$ being the maximum and minimum energies involved in the problem. The function that must be expanded is the complex exponential

$$f(X) = \exp\left(-i\frac{1}{\hbar}aX\Delta t\right), \tag{3.52}$$

where $X = \tilde{\mathcal{H}}$. Using the Chebyshev polynomials (3.49), the scalar product that appears in the expansion coefficients (3.47) is then

$$\begin{aligned}\langle T_q|f\rangle &= \frac{1}{\pi}\int_{-1}^{1}\mathrm{d}X\,\frac{1}{\sqrt{1-X^2}}\cos\left(q\cos^{-1}q\right)f(X)\\ &= (-1)^q J_q(\frac{1}{\hbar}a\Delta t),\end{aligned} \tag{3.53}$$

where J_q is a Bessel function of the first kind. In evaluating this integral I have first made the change of variables $X = \cos\Phi$, and then used the relations

$$J_q(Z) = \frac{i^{-q}}{\pi}\int_0^{\pi}\mathrm{d}\Phi\,\exp(iZ\cos\Phi)\cos q\Phi \tag{3.54}$$

[151] and $J_q(-Z) = (-1)^q J_q(Z)$. Using this result along with the orthogonality relation (3.50), the expansion coefficients are found to be

$$\alpha_q = \begin{cases}(-1)^q J_q(a\Delta t/\hbar), & q = 0\\ 2(-1)^q J_q(a\Delta t/\hbar), & q \neq 0.\end{cases} \tag{3.55}$$

Note that the series expansion presented here is slightly different from that in [141], where "complex Chebyshev polynomials", defined by $\varphi_q(\omega) = T_q(-i\omega)$, where $\omega \in [-i, i]$, are employed.

As has already been mentioned, the choice of Chebyshev polynomials results in a particularly rapid series convergence. The reason for this is the asymptotic behaviour of the Bessel functions in (3.55), which is described by

$$q \to \infty \Rightarrow J_q\left(\frac{a\Delta t}{\hbar}\right) \to \frac{1}{\sqrt{2\pi q}}\left(\frac{\mathrm{e}a\Delta t}{2q\hbar}\right)^q \tag{3.56}$$

[152]. Here e, in roman font, denotes the mathematical constant. When

$$q > \frac{\mathrm{e}a\Delta t}{2\hbar}, \tag{3.57}$$

so that the argument of the exponent in (3.56) is less than unity, the magnitude of the Bessel function decays exponentially (or, more accurately, faster than this, due to the factor of $q^{-1/2}$). This means that the magnitudes of the coefficients (3.55) decay exponentially whenever the inequality (3.57) is satisfied, as illustrated in Fig. 3.14. Therefore, the error associated with truncating the series at a finite order can be made negligible, by choosing a number of terms

$$M = \frac{\mathrm{e}}{2\hbar} a \Delta t + \delta, \tag{3.58}$$

where δ is an adjustable parameter. This rapid convergence of the series expansion means that, for most applications, the Chebyshev method is the most accurate and efficient technique available for numerically solving the time-dependent Schrödinger equation [153, 142].

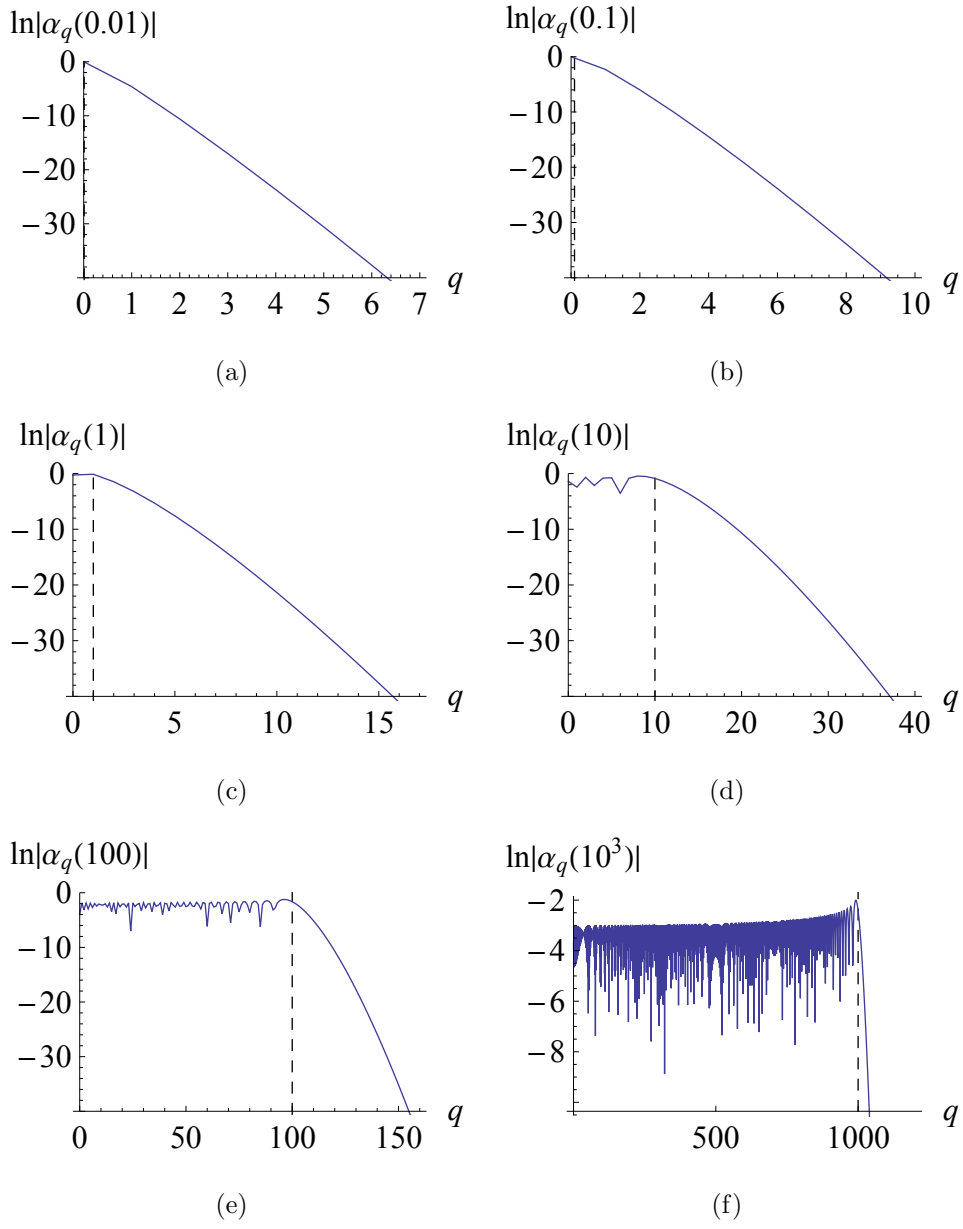

Figure 3.14: **Exponential decay of the magnitude of the Chebyshev expansion coefficients.** Here the logarithm of the coefficient α_q is plotted for different values of the Bessel function argument $a\Delta t/\hbar$. The dashed vertical lines indicate when $q = a\Delta t/\hbar$. It is seen that when $q \gtrsim a\Delta t/\hbar$, the magnitude of the expansion coefficients decays approximately exponentially.

Chapter 4

Is the angular momentum of an electron conserved in a uniform magnetic field?

I show that the diamagnetic angular momentum of an electron moving in a uniform magnetic field can vary with time. Surprisingly this means that the kinetic angular momentum of the electron may vary with time, despite the rotational symmetry of the system. This apparent violation of angular momentum conservation is resolved by including the angular momentum of the surrounding fields.

As in the preceding chapter the main results are presented first, and followed by complementary material.

4.1 Main results

4.1.1 Introduction

As described at the very beginning of this thesis, there is an intimate relation between angular momentum and rotational symmetry. In particular, if a system is symmetric under rotation about a given axis, the angular momentum along that axis will be conserved. This is the case with electron vortex beams in field-free space. These have a cylindrically symmetric wavefunction and maintain a constant orbital angular momentum in the direction of propagation.

Based on the same argument of rotational symmetry it would seem that for an electron exposed to a uniform magnetic field its orbital angular momentum in the direction of the field must be conserved. This is indeed true of the angular momentum about the axis of the classical cyclotron orbit, and the energy eigenstates of the system – the Landau states – also have constant angular momentum.

On the other hand, it is known that the *kinetic* angular momentum of an electron is not necessary constant even when the electron interacts with external fields that are rotationally symmetric [93]. The balance and redistribution of momentum and angular momentum between matter and fields is a fundamental problem of great general interest [11, 15, 60, 154].

Recent investigations of vortex electron states in uniform and quasi-uniform magnetic fields have revealed that the angular velocity of the electron depends not only on the field strength but also on the azimuthal quantum number and the radial position [2, 87, 115]. Furthermore, in these quantum states the average radial position of the electron is not in general constant, but rather changes as the wavefunction diffracts

[76, 86, 115]. This contrasts sharply with the classical orbit in a uniform magnetic field, leading to the question of whether the angular momentum of the electron is in fact conserved.

In this chapter, I show that for an electron in a non-stationary state, the changing radius of the electron's probability distribution in fact gives rise to a time-varying *kinetic* angular momentum. The *canonical* angular momentum however remains constant. The apparent violation of angular momentum conservation is resolved by considering the angular momentum in the fields surrounding the electron. I show that the *total* kinetic angular momentum, including that of the fields, is conserved, as indeed it must be.

4.1.2 Canonical and kinetic angular momenta

I consider an electron moving in a uniform magnetic field, and take the direction of this field to define the z-axis. As in the preceding chapter, I do not consider the effect of spin, the z component of which will be a constant of motion. The (non-relativistic) Hamiltonian for the system can therefore be written in the form

$$H = \frac{1}{2m}(\mathbf{p}^{\mathrm{kin}})^2. \tag{4.1}$$

This is the same as the first term in (2.1). I again choose the vector potential (2.5), meaning that the Hamiltonian (4.1) can be rewritten as

$$H = \frac{1}{2m}(\mathbf{p}^{\mathrm{can}})^2 + \frac{1}{2}m\omega_{\mathrm{L}}^2\rho^2 + \omega_{\mathrm{L}}L_z^{\mathrm{can}}. \tag{4.2}$$

As the Hamiltonian, in the chosen gauge, is independent of ϕ, it commutes with the canonical angular momentum, $[L_z^{\mathrm{can}}, H] = 0$, meaning that L_z^{can} is conserved [76].

Consider an electron wavefunction with cylindrical symmetry so that

$$\Psi = u(\rho, z, t)\mathrm{e}^{i\ell\phi}. \tag{4.3}$$

I make no assumption about the form of the function u, so that in general this will not be an energy eigenstate. This state is however an eigenstate of L_z^{can} and hence the expectation value of its angular momentum has the time-independent value

$$\langle L_z^{\text{can}} \rangle = \ell\hbar. \tag{4.4}$$

This is to be expected as the system is symmetric under rotation about the z-axis, so that according to Noether's theorem the z-component of the angular momentum should be conserved.

As described by (2.16), in the presence of a magnetic field, the kinetic orbital angular momentum differs from its canonical counterpart. The field-dependent contribution to the kinetic angular momentum is associated with a rotation of the electron probability distribution at constant angular velocity ω_{L} – the diamagnetic response of the electron to the external magnetic field.

The expectation value of the kinetic orbital angular momentum can be expressed here as

$$\langle L_z^{\text{kin}} \rangle = \ell\hbar + \langle I_z \rangle \omega_{\text{L}}, \tag{4.5}$$

where I have used the fact that the expectation value of the z-component of the electron's moment of inertia is

$$\langle I_z \rangle = m\langle \rho^2 \rangle. \tag{4.6}$$

This means that the kinetic angular momentum of the electron will be constant only if the radial probability distribution is constant. The squared radius ρ^2 does not commute with the Hamiltonian however, meaning this quantity is not a constant of motion [98]. This means that, in contrast with the classical motion, the mean value $\langle \rho^2 \rangle$ will not, in general, be a constant.

4.1.3 Radial oscillation

It can be seen from the form of the Hamiltonian (4.2) that the radial coordinate exhibits a harmonic motion. This can be understood as the radial diffraction of the electron wavefunction in a harmonic potential generated by the interaction with the magnetic field [76]. The energy associated with the motion perpendicular to the magnetic field remains constant and has the expectation value

$$E_\perp = \left\langle H - \frac{1}{2m}(p_z^{\rm kin})^2 \right\rangle . \tag{4.7}$$

I will obtain the time-dependence of the radial width, and later also of the kinetic orbital angular momentum, from Heisenberg's formalism:

$$\begin{aligned} \frac{\partial^2\langle\rho^2\rangle(t)}{\partial t^2} &= -\frac{1}{\hbar^2}\left\langle \big[[\rho^2, H], H\big] \right\rangle (t) \\ &= -\omega_c^2 \left(\langle\rho^2\rangle(t) - \widetilde{\rho^2} \right) \end{aligned} \tag{4.8}$$

where

$$\widetilde{\rho^2} = \frac{1}{m\omega_{\rm L}^2}\left(E_\perp - \omega_{\rm L}\ell\hbar\right) \tag{4.9}$$

is the constant steady-state value that depends on the energy, the canonical angular momentum and the magnetic field. It can be seen from (4.8) that the mean-square radius oscillates sinusoidally about the value $\widetilde{\rho^2}$ at the cyclotron frequency. Setting $t = 0$ to correspond to a stationary point of this oscillation, I have

$$\langle\rho^2\rangle(t) = \widetilde{\rho^2} + \left(\langle\rho^2\rangle(0) - \widetilde{\rho^2} \right) \cos(\omega_{\rm c} t). \tag{4.10}$$

According to the relation (4.5) this is intrinsically linked to an oscillation of the kinetic angular momentum:

$$\langle L_z^{\rm kin}\rangle(t) = \widetilde{L}_z^{\rm kin} + \left(\langle L_z^{\rm kin}\rangle(0) - \widetilde{L}_z^{\rm kin} \right) \cos(\omega_{\rm c} t), \tag{4.11}$$

where the steady-state value of the kinetic angular momentum

$$\widetilde{L}_z^{\rm kin} = \ell\hbar + m\omega_{\rm L}\widetilde{\rho^2} = \frac{2}{\omega_{\rm c}} E_\perp \tag{4.12}$$

coincides with the classical value of the kinetic angular momentum for an electron with rotational kinetic energy $E_\perp$. In general the angular momentum oscillates sinusoidally about the classical value, with the same frequency, ω_c, as the classical cyclotron motion. Only if the kinetic angular momentum is equal to the classical value does its expectation value remain constant. In this sense (4.12) defines the steady-state value $\widetilde{\rho^2}$.

I can obtain an exact solution for (4.10) in the case when at $t = 0$ the wavefunction (4.3) has the Laguerre-Gaussian form

$$\Psi_{n,\ell}(0) = \mathrm{LG}_{n,\ell} \propto \left(\frac{\rho\sqrt{2}}{\rho_0}\right)^{|\ell|} \exp\left(-\frac{\rho^2}{\rho_0^2}\right) L_n^{|\ell|}\left(\frac{2\rho^2}{\rho_0^2}\right) \times \exp\left[i\left(\ell\phi + k_z z\right)\right], \tag{4.13}$$

where $\ell \in \mathbb{Z}$ and $n = 0, 1, 2, ...$ As with a Landau state the index n specifies the number of radial nodes in the wavefunction, while ρ_0 is the width of the Gaussian envelope. The Laguerre-Gaussian wavefunctions can be used to describe electron vortex beams that have intrinsic orbital angular momentum $\ell\hbar$ [36] as well as electron beams with no intrinsic orbital angular momentum in the case when $\ell = 0$.

The mean-square radius of the Laguerre-Gaussian wavefunction (4.13) is equal to

$$\langle\rho^2\rangle_{n,\ell}(0) = \frac{1}{2}(2n + |\ell| + 1)\rho_0^2 \tag{4.14}$$

[155]. As this depends on the radial index n, it follows that the kinetic angular momentum of the electron also depends on n, which is not the case in the absence of a magnetic field. The steady-state mean-square radius for the same electron energy obtained from (4.7) and (4.12) is

$$\widetilde{\rho^2}_{n,\ell} = \frac{1}{4}(2n + |\ell| + 1)\left[1 + \left(\frac{\rho_\mathrm{B}}{\rho_0}\right)^4\right]\rho_0^2. \tag{4.15}$$

As the phase of the wavefunction (4.13) does not depend on ρ, I have

$$\frac{\partial\langle\rho^2\rangle_{n,\ell}(0)}{\partial t} = \frac{1}{\hbar}\,\mathrm{Im}\left\langle[\rho^2, H]\right\rangle_{n,\ell}(0) = 0, \tag{4.16}$$

meaning that this wavefunction corresponds to a stationary point of the oscillation. The time-evolution of $\langle\rho^2\rangle_{n,\ell}$ can therefore be obtained by substituting (4.14) and (4.15) into (4.10).

In the special case when $\rho_0 = \rho_B$ the Laguerre-Gaussian wavefunctions in (4.13) become the Landau energy eigenstates and I obtain the constant values of $\langle L_z^{\rm kin}\rangle_{n,\ell}$ expected in this case [87]. In general however the angular momentum will oscillate around the classical value, as illustrated in Fig. 4.1(a) for different ratios ρ_0/ρ_B and in Fig. 4.1(b) for different quantum numbers ℓ corresponding to canonical angular momenta $\ell\hbar$. If the canonical angular momentum is in the opposite direction to the magnetic field then the kinetic angular momentum may even change direction, as clearly seen for $\ell = -4$ in Fig. 4.1(b). I note that the moment of inertia increases with the radial quantum number n, resulting in larger amplitude oscillations, and that a reversal of the direction of the magnetic field corresponds to a shift of the phase of the oscillations by 180°.

As we have seen, the kinetic angular momentum may change with time despite the fact that the system is entirely rotationally symmetric – seemingly contradicting Noether's theorem. In order to restore angular momentum conservation I have to include the angular momentum contained in the field. The calculation in the following section was performed with Stephen Barnett.

4.1.4 Field angular momentum

The density of (kinetic) momentum in an electromagnetic field is given by

$$\begin{aligned} \boldsymbol{\mathcal{P}}^{\text{kin field}} &= \mu_0\epsilon_0\mathbf{S} \\ &= \epsilon_0\mathbf{E}\times\mathbf{B}, \end{aligned} \tag{4.17}$$

where $\mathbf{S} = \mathbf{E}\times\mathbf{B}/\mu_0$ is the Poynting vector [156]. The corresponding orbital angular momentum density therefore has the z component

$$\begin{aligned} \mathcal{L}_z^{\text{kin field}} &= (\mathbf{r}\times\boldsymbol{\mathcal{P}}^{\text{kin field}})_z \\ &= \epsilon_0\rho(\mathbf{E}\times\mathbf{B})_\phi. \end{aligned} \tag{4.18}$$

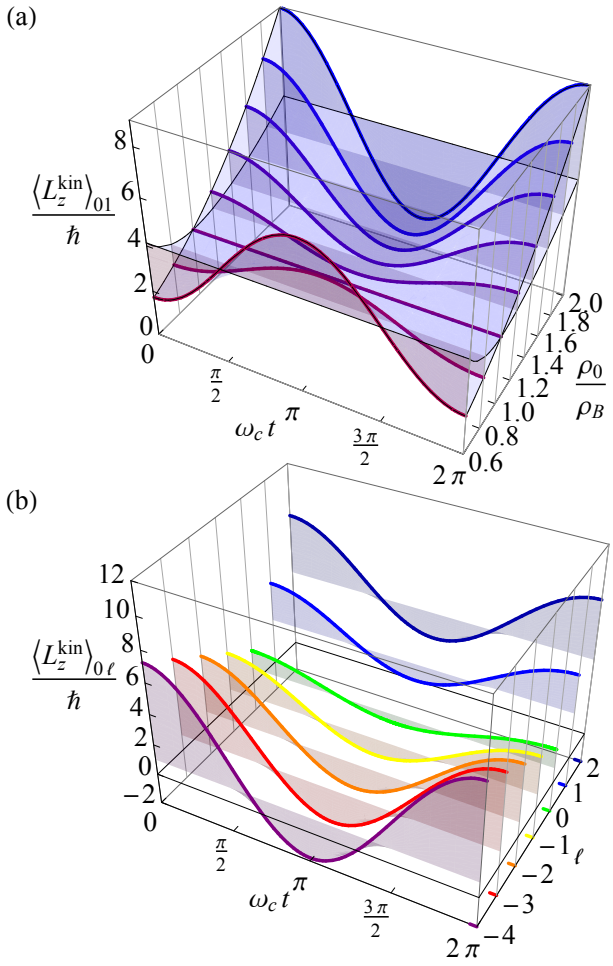

Figure 4.1: **Time-evolution of the expectation value of the electron's kinetic orbital angular momentum for Laguerre-Gaussian states with $n = 0$ and a magnetic field in the positive z-direction ($B > 0$).** This is shown in (a) as a function of the initial width ρ_0 for $\ell = 1$, and in (b) for different values of ℓ assuming $\rho_0 = 1.5\rho_B$. Image created with Sonja Franke-Arnold.

The total kinetic angular momentum in the field can be expressed as

$$\begin{aligned} L_z^{\text{kin field}} &= \int \mathrm{d}V\, \mathcal{L}_z^{\text{kin field}} \\ &= \epsilon_0 \int \mathrm{d}V\, \rho(\mathbf{E}\times\mathbf{B})_\phi \\ &= \epsilon_0 \int \mathrm{d}V\, \rho(-E_\rho B_z + E_z B_\rho). \end{aligned} \tag{4.19}$$

Here this will be evaluated for the uniform external magnetic field and the radial electric field of the electron itself.

In order for the integral in (4.19) to be finite, it must be taken into account that in reality the external magnetic field will not be completely uniform, but rather reverse direction at very large ρ, such that the total flux through the $\mathbf{r}_\perp$ plane is zero:

$$\int \mathrm{d}^2\mathbf{r}_\perp\, B_z(\rho) = \int \mathrm{d}V\, \boldsymbol{\nabla}.\mathbf{B} = 0. \tag{4.20}$$

Here I have used the divergence theorem and also Maxwell's equation $\boldsymbol{\nabla}.\mathbf{B} = 0$. The radial electric field of the electron can be obtained by integrating Gauss's law

$$\boldsymbol{\nabla}.\mathbf{E} = \frac{\varrho}{\epsilon_0} = \frac{e|\Psi|^2}{\epsilon_0}, \tag{4.21}$$

where ϱ is the charge density of the electron, over a cylindrical Gaussian surface. This way, I obtain

$$E_\rho(\rho) = \frac{e}{\epsilon_0 \rho}\int_{\rho'=0}^{\rho} \rho'\,\mathrm{d}\rho'\,|\Psi|^2(\rho'). \tag{4.22}$$

The integral (4.19) then becomes

$$\begin{aligned} L_z^{\text{kin field}} &= -2\pi e \int_{\rho=0}^{\infty} \rho\,\mathrm{d}\rho\, B_z(\rho) \int_{\rho'=0}^{\rho} \rho'\,\mathrm{d}\rho'\,|\Psi|^2(\rho') \\ &= -2\pi e \left[\int_{\rho'=0}^{\rho} \rho'\,\mathrm{d}\rho'\, B_z(\rho') \int_{\rho''=0}^{\rho} \rho''\,\mathrm{d}\rho''|\Psi|^2(\rho'')\right]_{\rho=0}^{\infty} \\ &\quad +2\pi e \int_{\rho=0}^{\infty} \rho\,\mathrm{d}\rho \int_{\rho'=0}^{\rho} \rho'\,\mathrm{d}\rho'\, B_z(\rho')|\Psi|^2(\rho) \\ &= \frac{1}{2} eB\, 2\pi \int_{\rho=0}^{\infty} \rho\,\mathrm{d}\rho\,\rho^2|\Psi|^2(\rho) \\ &= \frac{1}{2} eB\langle\rho^2\rangle. \end{aligned} \tag{4.23}$$

In integrating the first line by parts I have made use of the identity

$$\frac{\partial}{\partial\rho}\int_{\rho'=0}^{\rho} \rho'\,\mathrm{d}\rho'\,|\Psi|^2(\rho') = \rho|\Psi|^2(\rho) \tag{4.24}$$

[157]. I have then used the result (4.20), from which it follows that the term in the square brackets vanishes, and also the fact that in the region of the electron the magnetic field has the uniform value B.

Using (4.5) and (4.23) it is seen that the total kinetic angular momentum including that of the field is equal to the conserved canonical angular momentum:

$$L_z^{\text{kin total}} = \ell\hbar = L_z^{\text{can}}. \tag{4.25}$$

Therefore, when the field is included, the angular momentum of the system has the unique value (4.25), which is conserved.

4.1.5 Discussion

The magnitude of the diamagnetic contribution to the kinetic angular momentum is strongly dependent on the length scale. As can be seen from (4.5), it is characterised by the constant $-e/2 = 7.60 \times 10^{-4}\hbar\,\mathrm{T}^{-1}\mathrm{nm}^{-2}$. In an atomic bound state with rms radius 1 Å, even in a field of strength 1 T the diamagnetic angular momentum is negligible compared to a single unit of canonical angular momentum. However, for unbound electrons, which can be distributed over a much larger area, the diamagnetic angular momentum can become significant, and may be the dominant contribution, both to the electron's kinetic angular momentum and to $E_\perp$. This can certainly be the case in transmission electron microscopes, where the electron beam may have a radius $\langle\rho^2\rangle^{1/2} \sim 1\,\mathrm{nm} - 100\,\mu\mathrm{m}$ and a field $\sim 1\,\mathrm{T}$ is provided by the objective lens. Note that in an electron microscope the radial dynamics occur in a reference frame moving with the electron along the z-axis [36], and so can be observed as a function of the propagation distance [86, 115].

While the creation of electron vortices has aroused a considerable interest in the orbital angular momentum of electron beams [55, 65, 145], little attention has been given

previously to the angular momentum that arises in a magnetic field. Diamagnetic angular momentum is possessed by any electron beam, even those with no canonical orbital angular momentum. The canonical angular momentum is related to symmetry under azimuthal rotation, and is restricted to integer multiples of $\hbar$. In contrast, the diamagnetic contribution, and hence the kinetic angular momentum of the electron, may take any value.

4.2 Complements to section 4.1

In the remainder of this chapter I will expand upon the preceding material by presenting additional detail and further considerations.

First, I provide a detailed derivation of the equation of motion for the mean-square radius of the electron's probability distribution. Like the calculation of the centre of mass in Chapter 3 this is a rather lengthy calculation, and it was only briefly outlined in section 4.1. This calculation starts in the same way as that of the centre of mass, and I make use of the expression I derived previously for the expectation value of an arbitrary operator. Following the derivation of the mean-square radius for an arbitrary initial wavefunction, I consider the particular solution in the case of a Laguerre-Gaussian wavefunction.

It is illuminating to consider the spatial distributions of the probability density and the current density of Laguerre-Gaussian states that have a time-varying radius. I do this here using numerical calculations similar to those in Chapter 3. First, I present simulations for Laguerre-Gaussian wavefunctions of the form used in section 4.1, which do not exhibit any cyclotron motion. I then simulate wavefunctions that also possess a net transverse momentum, and therefore exhibit cyclotron motion, as well as having an oscillating radius.

Following this, I provide additional considerations on the relationship between Laguerre-Gaussian wavefunctions and the Landau states. I discuss both the kinetic angular momentum and the energy of Laguerre-Gaussian wavefunctions in a uniform magnetic field, and illustrate how these vary as a function of the mean-square radius of the probability distribution and the strength of the magnetic field. It is demonstrated how these tend towards, in the appropriate limits, the values for the Laguerre-Gaussian wavefunctions in field-free space and for the Landau states.

Finally, I discuss changes in the angular momentum of the electron as a result of cyclotron radiation. An estimate of the order of magnitude of this effect is presented.

4.2.1 Mean-square radius

In this section I provide additional detail of the derivation of the mean-square radius of the electron that is described in section 4.1.

Arbitrary wavefunction

First, I consider the derivation of the equation of motion for the expectation value $\langle\rho^2\rangle$; that is, (4.8) in section 4.1.

The equation of motion for the evolution of an arbitrary operator $\mathcal{O}$, in a system governed by the Hamiltonian $H_\perp$, was already obtained in the previous chapter. Therefore, all that is required is to substitute $\mathcal{O} = \rho^2$ into (3.27). The commutator of ρ^2 with the

Hamiltonian $H_\perp$ is given by

$$\begin{aligned}
[\rho^2, H_\perp] &= [x^2, H_\perp] + [y^2, H_\perp] \\
&= x[x, H_\perp] + [x, H_\perp]x + y[y, H_\perp] + [y, H_\perp]y \\
&= \frac{2\hbar}{m}\left[\hbar + i(xp_x^{\rm can} + yp_y^{\rm can})\right], \qquad (4.26)
\end{aligned}$$

using the previous results for $[x, H_\perp]$ and $[y, H_\perp]$ in (3.29) and (3.35). The double commutator can therefore be expressed as

$$\begin{aligned}
\left[[\rho^2, H_\perp], H_\perp\right] &= \frac{2i\hbar}{m}\left([xp_x^{\rm can}, H_\perp] + [yp_y^{\rm can}, H_\perp]\right) \\
&= \frac{2i\hbar}{m}\left(x[p_x^{\rm can}, H_\perp] + [x, H_\perp]p_x^{\rm can} + y[p_y^{\rm can}, H_\perp] + [y, H_\perp]p_y^{\rm can}\right) \\
&= 2\hbar^2\left\{\omega_{\rm L}^2(x^2 + y^2) - \frac{1}{m^2}\left[(p_x^{\rm can})^2 + (p_y^{\rm can})^2\right]\right\} \\
&= \hbar^2\left\{\omega_{\rm c}^2\rho^2 - \frac{4}{m}[H_\perp - \omega_{\rm L}L_z^{\rm can}]\right\}, \qquad (4.27)
\end{aligned}$$

where I have made use of the results

$$\begin{aligned}
[p_x^{\rm can}, H_\perp] &= \left[p_x^{\rm can}, \frac{1}{2}m\omega_{\rm L}^2x^2 + \omega_{\rm L}xp_y^{\rm can}\right] \\
&= \frac{1}{2}m\omega_{\rm L}^2[p_x^{\rm can}, x^2] + \omega_{\rm L}[p_x^{\rm can}, xp_y^{\rm can}] \\
&= \frac{1}{2}m\omega_{\rm L}^2\left(x[p_x^{\rm can}, x] + [p_x^{\rm can}, x]x\right) + \omega_{\rm L}\left(x[p_x^{\rm can}, p_y^{\rm can}] + [p_x^{\rm can}, x]p_y^{\rm can} - i\hbar p_y^{\rm can}\right) \\
&= -i\hbar\omega_{\rm L}(m\omega_{\rm L}x + p_y^{\rm can}) \qquad (4.28)
\end{aligned}$$

and

$$\begin{aligned}
[p_y^{\rm can}, H_\perp] &= \left[p_y^{\rm can}, \frac{1}{2}m\omega_{\rm L}^2y^2 - \omega_{\rm L}yp_x^{\rm can}\right] \\
&= \frac{1}{2}m\omega_{\rm L}^2[p_y^{\rm can}, y^2] - \omega_{\rm L}[p_y^{\rm can}, yp_x^{\rm can}] \\
&= \frac{1}{2}m\omega_{\rm L}^2\left(y[p_y^{\rm can}, y] + [p_y^{\rm can}, y]y\right) - \omega_{\rm L}\left(y[p_y^{\rm can}, p_x^{\rm can}] + [p_y^{\rm can}, y]p_x^{\rm can} - i\hbar p_x^{\rm can}\right) \\
&= -i\hbar\omega_{\rm L}(m\omega_{\rm L}y - p_x^{\rm can}). \qquad (4.29)
\end{aligned}$$

This results in the differential equation

$$\frac{\partial^2\langle\rho^2\rangle(t)}{\partial t^2} = -\omega_{\rm c}^2\left(\langle\rho^2\rangle(t) - \tilde{\rho^2}\right), \qquad (4.30)$$

where $\tilde{\rho^2} = \langle H_\perp - \omega_{\rm L}L_z^{\rm can}\rangle/m\omega_{\rm L}^2$, which describes a sinusoidal oscillation of $\langle\rho^2\rangle$ about $\tilde{\rho^2}$ with frequency $\omega_{\rm c}$.

The general solution of this equation of motion can be expressed as

$$\langle\rho^2\rangle(t) = \tilde{\rho^2} + \left(\langle\rho^2\rangle(0) - \tilde{\rho^2}\right)\cos\omega_{\rm c}t + \frac{1}{\omega_{\rm c}}\frac{\partial\langle\rho^2\rangle(0)}{\partial t}\sin\omega_{\rm c}t. \tag{4.31}$$

Setting $t = 0$ to correspond to a stationary point of the oscillation, the second term vanishes; then the result is the same as (4.10) in section 4.1.

Laguerre-Gaussian wavefunction

I now consider the particular solution in the case of a Laguerre-Gaussian wavefunction [22], and set

$$\Psi_\perp(t=0) = \sqrt{\frac{2n!}{\pi(n+|\ell|)!}}\frac{1}{\rho_0}\left(\frac{\rho\sqrt{2}}{\rho_0}\right)^{|\ell|}\exp\left(-\frac{\rho^2}{\rho_0^2}\right)L_n^{|\ell|}\left(\frac{2\rho^2}{\rho_0^2}\right)\exp\left(i\ell\phi\right). \tag{4.32}$$

In this case, $t = 0$ indeed corresponds to a stationary point of the oscillation:

$$\begin{aligned}\frac{\partial\langle\rho^2\rangle_{n,\ell}(0)}{\partial t} &= -\frac{i}{\hbar}\left\langle[\rho^2, H_\perp]\right\rangle_{n,\ell}(0)\\ &= \frac{1}{\hbar}{\rm Im}\left\langle[\rho^2, H_\perp]\right\rangle_{n,\ell}(0)\\ &= \frac{2\hbar}{m}{\rm Im}\left\langle\rho\frac{\partial}{\partial\rho}\right\rangle_{n,\ell}(0)\\ &= 0.\end{aligned} \tag{4.33}$$

Here I have used the fact that the time-derivative of $\langle\rho^2\rangle$ must be real, as well as the fact that the phase of $\Psi_{n,\ell}(0)$ is independent of ρ. As noted in section 4.1, for the Laguerre-Gaussian initial state the mean-square radius is initially $\langle\rho^2\rangle_{n,\ell}(0) = (2n + |\ell| + 1)\rho_0^2/2$ [155].

In order to obtain the steady-state squared radius $\tilde{\rho^2}_{n,\ell}$, the expectation value of the energy, $\langle H_\perp\rangle_{n,\ell}$, must be evaluated. To do this, I use the fact that the wavefunction (4.32) would be an eigenstate of a Hamiltonian

$$H_{\perp\,0} = \frac{1}{2m}\left(\mathbf{p}_\perp^{\rm can}\right)^2 + \frac{1}{2}m\omega_0^2\rho^2, \tag{4.34}$$

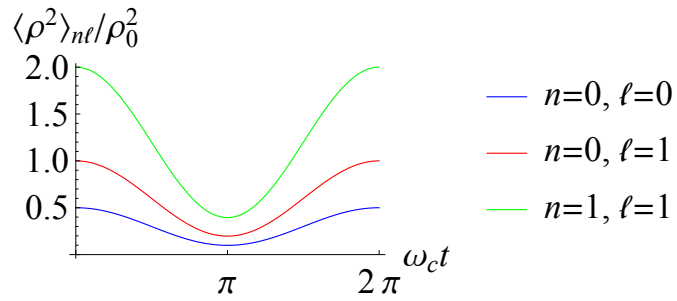

Figure 4.2: **Oscillation of the mean-square radial position of the electron.** Here $\rho_0 = 1.5\rho_{\rm B}$.

where $\omega_0 = 2\hbar/(m\rho_0^2)$, with eigenvalues $(2n + |\ell| + 1)\hbar\omega_0$. Therefore:

$$\begin{aligned}\langle H_\perp\rangle_{n,\ell} &= \langle H_{\perp 0}\rangle_{n,\ell}(0) + \frac{1}{2}m(\omega_{\rm L}^2 - \omega_0^2)\langle\rho^2\rangle(0) + \omega_{\rm L}\langle L_z^{\rm can}\rangle \\ &= (2n + |\ell| + 1)\left[\hbar\omega_0 + \frac{1}{4}m(\omega_{\rm L}^2 - \omega_0^2)\rho_0^2\right] + \ell\hbar\omega_{\rm L} \\ &= \frac{1}{4}m\omega_{\rm L}^2(2n + |\ell| + 1)\left[1 + \left(\frac{\rho_{\rm B}}{\rho_0}\right)^4\right]\rho_0^2 + \ell\hbar\omega_{\rm L}, \end{aligned} \tag{4.35}$$

and so

$$\begin{aligned}\tilde{\rho^2}_{n,\ell} &= \frac{1}{m\omega_{\rm L}^2}\langle H_\perp\rangle_{n,\ell} - \ell\hbar\omega_{\rm L} \\ &= \frac{1}{4}(2n + |\ell| + 1)\left[1 + \left(\frac{\rho_{\rm B}}{\rho_0}\right)^4\right]\rho_0^2. \end{aligned} \tag{4.36}$$

The mean-square radius of the Laguerre-Gaussian probability distribution is therefore given by

$$\langle\rho^2\rangle_{n,\ell}(t) = \frac{1}{4}(2n + |\ell| + 1)\left\{1 + \left(\frac{\rho_{\rm B}}{\rho_0}\right)^4 + \left[1 - \left(\frac{\rho_{\rm B}}{\rho_0}\right)^4\right]\cos(\omega_{\rm c}t)\right\}\rho_0^2. \tag{4.37}$$

The oscillation of the mean-square radius described by (4.37) is illustrated, for different values of n and ℓ, in Fig. 4.2. Note that the value of $\langle\rho^2\rangle(t)$ is independent of the direction of the magnetic field; it is affected only by the magnitude of the field, which determines the value of $\rho_{\rm B}$.

4.2.2 Numerical calculations

In section 4.1 the motion of the electron was characterised by the mean-square radius, as well as the expectation value of the kinetic angular momentum. It is also interesting, however, to examine the corresponding changes in the current density. Here I present the results of numerical calculations of the probability density and current density, which have been performed using the method described in Chapter 3.

Figure 4.3 illustrates the evolution of the probability density and current density for a Laguerre-Gaussian wavefunction that has oscillating width, for different values of ℓ. In contrast to the images in Chapter 3, where the radial distribution remained constant, here the current density acquires a radial component. It is only at the stationary points of the width oscillation that this radial component vanishes, and the current is purely azimuthal. This contrasts with the orbit of a classical particle around the z axis, where the velocity would always be in the azimuthal direction. The intensities of the probability density and current density also vary with time, having the largest values where the mean-square radius is smallest.

It is also worth noting that the cyclotron orbit of the centre of mass and the oscillation of the radial distribution, which up until now have been considered separately, can occur simultaneously. This can be seen by numerically propagating an initial state of the form

$$\Psi_{\perp 0} = N_{n,|\ell|} \left(\frac{\rho\sqrt{2}}{\rho_0}\right)^{|\ell|} \exp\left(-\frac{\rho^2}{\rho_0^2}\right) L_n^{|\ell|}\left(\frac{2\rho^2}{\rho_0^2}\right) \exp\left[i\left(\ell\phi + \frac{p_\mathrm{c}}{\hbar}x\right)\right]. \tag{4.38}$$

This resembles the Laguerre-Gaussian wavefunction used elsewhere in this chapter in that the width ρ_0 can take any value, and resembles the wavefunction in the previous chapter in that there is a transverse momentum p_c. Examples of the evolution of such states are shown in Fig. 4.4. The motion of the electron has three components: the orbit of its centre of mass, the rotation of the probability density with respect to the centre of mass and the radial expansion and contraction of the probability density.

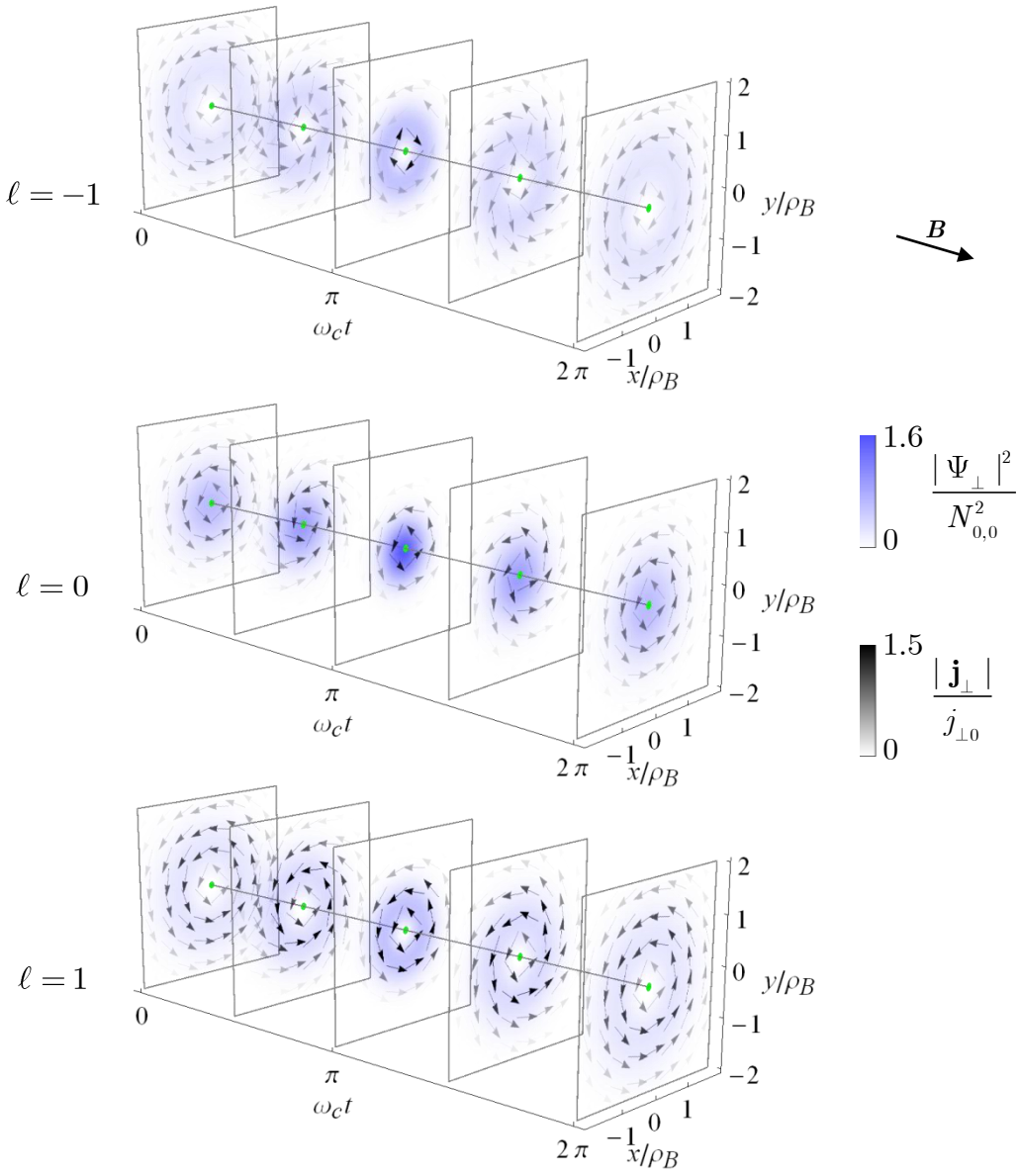

Figure 4.3: **Evolution of the probability density and current density as the radius of the state varies.** Here $n = 0$ and $\rho_0 = 1.25\rho_{\mathrm{B}}$.

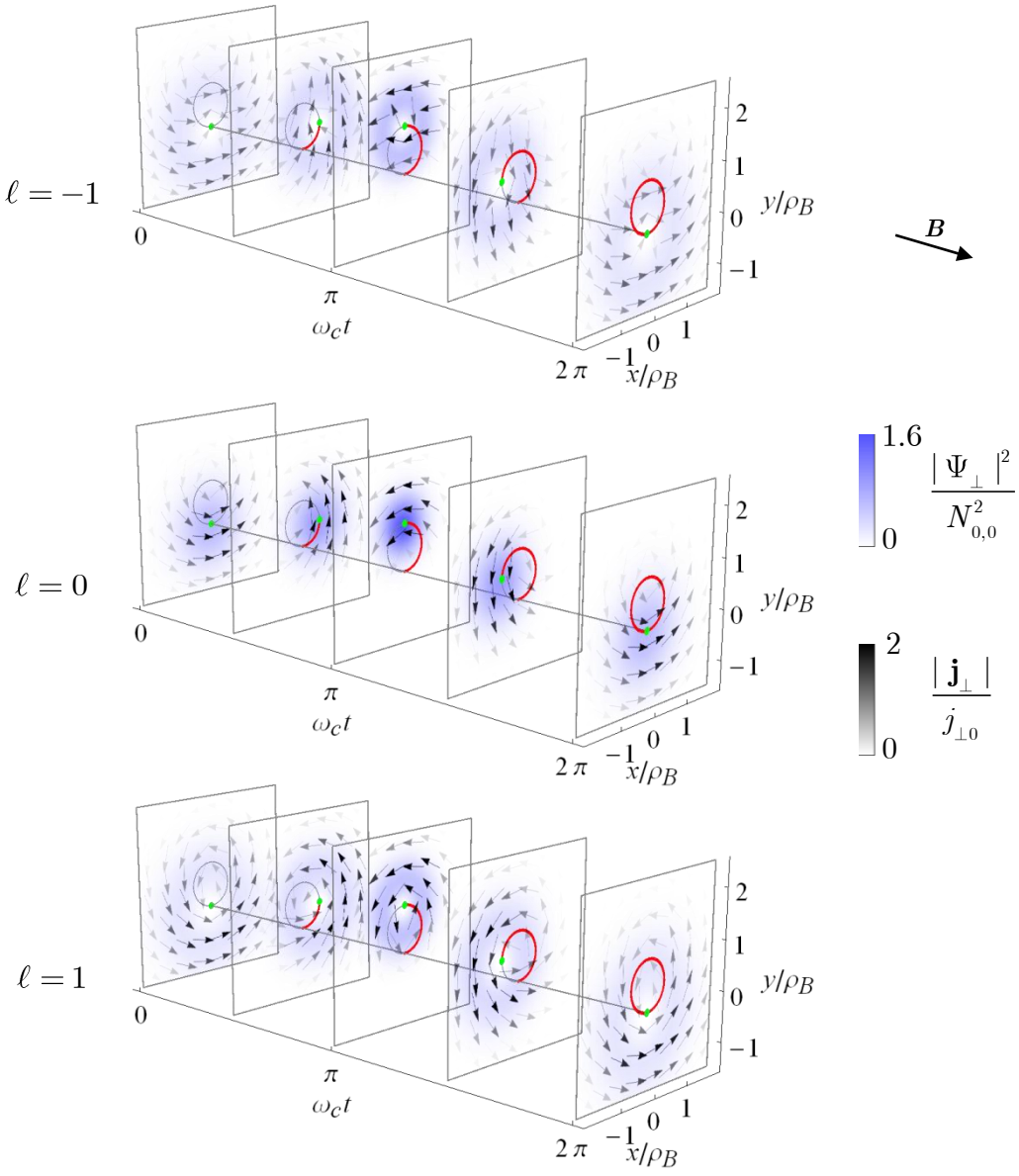

Figure 4.4: **Simultaneous width oscillation and cyclotron motion.** Here $n = 0$, $\rho_0 = 1.25\rho_\mathrm{B}$ and $p_\mathrm{c}/p_{\mathrm{c}0} = 2$.

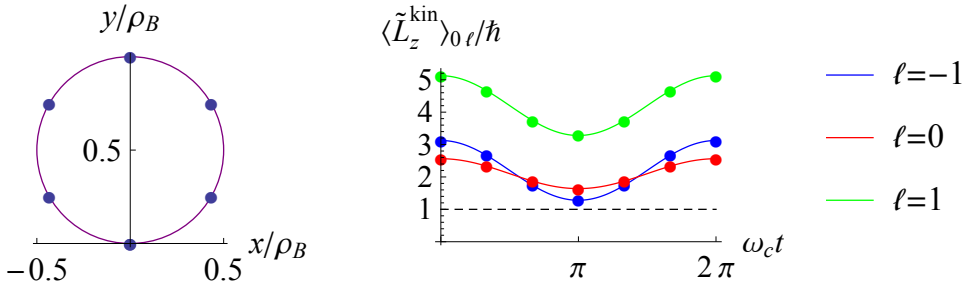

(a) (b)

Figure 4.5: **Centre of mass trajectory and kinetic angular momentum for a state that exhibits both radial oscillation and cyclotron motion.** Here $n = 0$, $B > 0$, $\rho_0 = 1.25\rho_{\mathrm{B}}$ and $p_{\mathrm{c}}/p_{\mathrm{c}\,0} = 2$. In (a) $\langle \mathbf{r}_\perp \rangle(t)$ was calculated for $\ell = 1$. In (b) the angular momentum is calculated with respect to the centre of the cyclotron orbit and the dashed line indicates the constant cyclotron component.

It can be verified that the centre of mass still follows the classical cyclotron orbit in this case by calculating this quantity numerically – the results of such a calculation are shown in Fig. 4.5(a). The value of the kinetic orbital angular momentum with respect to the centre of the cyclotron orbit can also be calculated numerically. As described by (3.12) and (3.13) in section 3.1, this quantity, which is equal to a sum of canonical, cyclotron and diamagnetic components, is constant for a probability distribution with constant mean-square radius. Here, due to the oscillation of the radial distribution, and therefore of the diamagnetic angular momentum, the kinetic angular momentum with respect to the centre of the cyclotron orbit, $\langle \tilde{L}_z^{\mathrm{kin}} \rangle$, also oscillates. This is shown in Fig. 4.5. This indicates that the result (3.12) obtained analytically in section 3.1 for a wavefunction with constant radial distribution also holds when this distribution varies.

4.2.3 Laguerre-Gaussian wavefunctions and the Landau states

As has been shown in section 4.1, the Landau states can be understood as a special type of Laguerre-Gaussian wavefunction, in which the Laguerre-Gaussian radius parameter,

ρ_0, is equal to the magnetic length ρ_B. In this case, the kinetic angular momentum of the Laguerre-Gaussian state has the quantized values described by (2.17). This angular momentum is always in the same direction as the magnetic field, and the allowed values are equally spaced by an interval of $2\hbar$. The minimum allowed magnitude of the angular momentum is equal to $\hbar$ – no Landau state has zero angular momentum.

This is in contrast to the Laguerre-Gaussian states in field-free space, for which the kinetic angular momentum is equal to the canonical angular momentum, and therefore is simply an integer multiplied by $\hbar$. In this case the kinetic angular momentum can have either direction, and may be equal to zero.

As I have shown, however, in general the kinetic angular momentum is not quantized. Both the field-free Laguerre-Gaussian wavefunctions and the Landau states are special examples in this regard. The kinetic angular momentum for Laguerre-Gaussian wavefunctions of different radii is shown in Fig. 4.6. Here the angular momentum is plotted for different values of the ratio $\rho_0/\rho_B = \rho_0\sqrt{|eB|/(4\hbar)}$, which is equal to zero in field-free space, and equal to 1 for a Landau state. The diamagnetic contribution to the kinetic angular momentum, which is proportional to the area of the probability density, increases in magnitude quadratically with ρ_0, in such a way that the Landau angular momenta are obtained when $\rho_0 = \rho_B$. Remarkably, states that otherwise have different values of angular momentum from one another become degenerate where the Landau condition is satisfied.

Similarly, the energy of the state varies as a function of the radius. This is illustrated in Fig. 4.7. Again, the Landau values are obtained when $\rho_0 = \rho_B$. These are the minimum possible values of the energy, which is to be expected, as they represent stationary points of a harmonic motion. Where $\rho_0 > \rho_B$, the energy associated with the diamagnetic angular momentum dominates, and will tend to squeeze the probability distribution to a smaller radius. On the other hand, when $\rho_0 < \rho_B$ the energy associated with the radial momentum of the electron, arising, as described by the un-

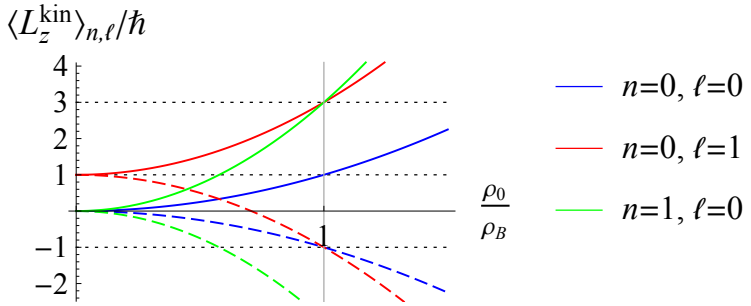

Figure 4.6: **Kinetic angular momentum of Laguerre-Gaussian states of different radii.** This is shown both for $B > 0$ (solid curves) and $B < 0$ (dashed). The horizontal dotted lines indicate the values of the angular momentum for the Landau levels, which occur when $\rho_0 = \rho_{\rm B}$.

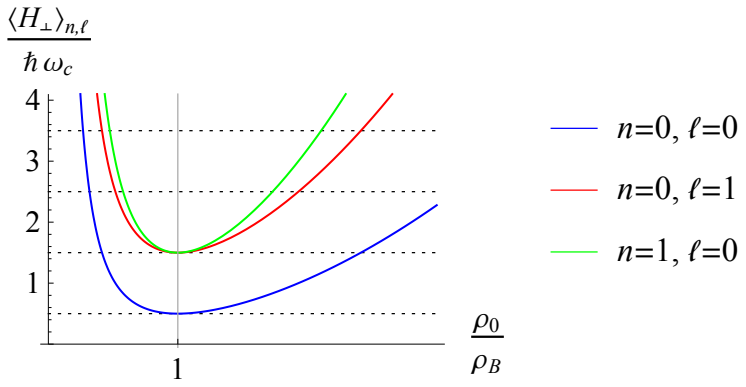

Figure 4.7: **Energy of Laguerre-Gaussian states that have different radii.** As in Fig. 4.6, the values for the Landau states are indicated by the horizontal dotted lines.

certainty principle, from its localisation in space, will dominate. This acts to expand the probability distribution to a large radius, resulting in the harmonic motion I have already described.

4.2.4 Cyclotron radiation

In principle, angular momentum can be lost through the radiation of photons resulting from the orbital motion of the electron [3, 158]. In this section, I show that on the

length scale I have been considering, the probability that a photon will be radiated during the course of a single cyclotron orbit is extremely small. This calculation was performed with Stephen Barnett.

I apply Larmor's formula for the power radiated by an accelerating charge, and consider an electron in a circular orbit with the cyclotron angular velocity ω_c. Larmor's formula reads

$$P = \frac{\mu_0 e^2 a^2}{6\pi c}, \tag{4.39}$$

where a is the electron's acceleration [156]. An electron that is in a circular orbit with a radius ρ has acceleration $a = \rho\omega_c^2$. The energy lost by radiation per rotation period is therefore

$$E_{\mathrm{rad}} = \frac{2\pi}{\omega_c} P = \frac{\mu_0 e^2 \rho^2 \omega_c^3}{3c}. \tag{4.40}$$

Now, as described in section 2.1.2, the electron's energy is quantized in units of $\hbar\omega_c$, meaning that the minimum energy that can be radiated by a photon is $\hbar\omega_c$. The number of photons that can be emitted per cyclotron period is therefore at most

$$\frac{E_{\mathrm{rad}}}{\hbar\omega_c} = \frac{\mu_0 e^2 \rho^2 \omega_c^2}{3\hbar c}. \tag{4.41}$$

For a magnetic field of strength 1 T, and an orbit radius of $\rho = 100\,\mathrm{nm}$, this expression evaluates to 10^{-10}.

Chapter 5

Electron orbital angular momentum Faraday rotation

I show that the diamagnetic rotation of an electron vortex superposition in a uniform magnetic field can be interpreted as a "Faraday effect" for electrons. Whereas in the original Faraday effect the rotation is of optical polarization, here it is a nodal line in the electron's wavefunction that rotates. This can be understood to occur as a result of a canonical orbital angular momentum dependent dispersion of the vortex superposition.

Again the main results are presented first, and followed by complementary material.

5.1 Main results

5.1.1 Introduction

As first reported by Michael Faraday in the middle of the nineteenth century [19], the polarization of light can be affected by magnetic fields. Specifically, Faraday showed that, upon propagation through a suitable medium, in the presence of a longitudinal magnetic field, the plane of polarization of linearly polarized light rotates. Such a medium is referred to as "magneto-active". Now termed the Faraday effect, this phenomenon is of significant historical importance as the first experimental evidence of a connection between light and electromagnetism. Further, the Faraday effect has found numerous applications, including the ultra-sensive detection of magnetic fields [159, 160], and the detection of magnetic fields in outer space [161] and the ionosphere [162].

Faraday rotation can be understood to arise as a consequence of differing propagation speeds for left and right handed circularly polarized light, as illustrated in Fig. 5.1(a). In vacuum, each polarization state has the same velocity. However, with a magneto-active medium in the presence of an external magnetic field, the orbits of the electrons in the medium have an overall handedness that is determined by the magnetic field, resulting in the aforementioned polarization-dependent dispersion of light interacting with these electrons [20].

As noted in Chapter 1, circular polarization of light is associated with the spin angular momentum of photons. Photons can also possess orbital angular momentum, however, associated with an optical vortex. This has led to the question of whether an effect analogous to Faraday rotation exists for optical orbital angular momentum.

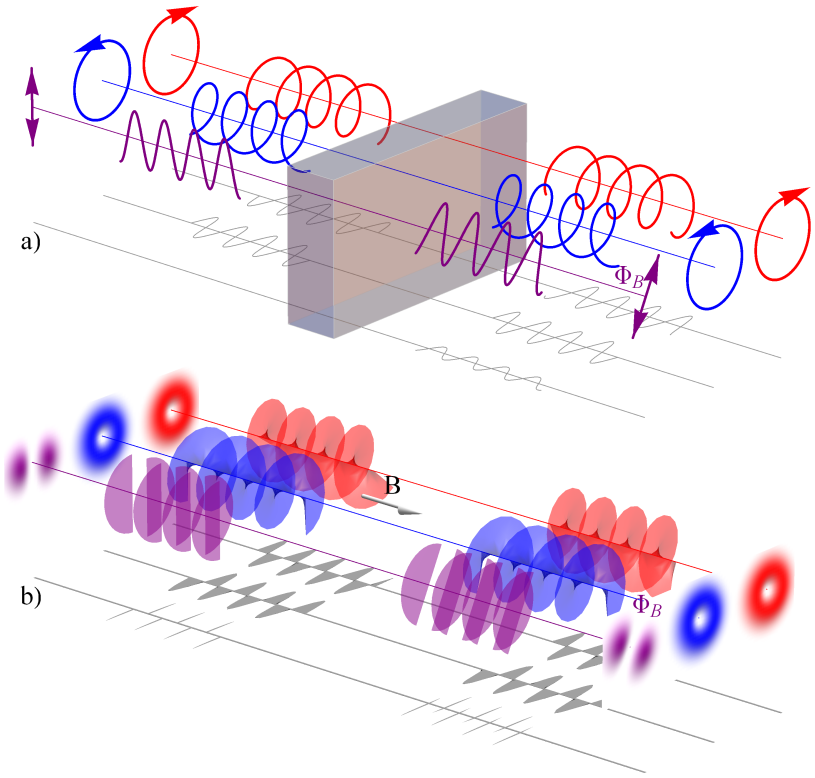

Figure 5.1: **Illustration of the Faraday effect for optical polarization (a) and the analogous rotation of electron vortex superpositions (b).** Image created by Sonja Franke-Arnold. In (a) the left and right circular polarization components propagate at different speeds through a magneto-active medium in a magnetic field, resulting in a rotation of the linear polarization. In (b) the differing propagation speeds of electron vortex states with canonical orbital angular momenta $\ell = \pm 1$ leads to a rotation of the probability density of the superposition.

It can be shown that an *orbital* angular momentum dependent dispersion results in a rotation, not of polarization, but of the intensity distribution of light [27]. That is, image rotation. Such a dispersion can be induced by rotating the medium through which the light propagates [28, 29, 30], and the resulting image rotation has been interpreted as a "mechanical" Faraday effect [31]. However, a similar interaction of light's orbital angular momentum in a stationary medium appears not to exist [32, 33, 34, 35].

Here, I consider the situation for *electron* beams carrying orbital angular momentum. It is known that in a longitudinal magnetic field, even in vacuum, an electron beam does exhibit an image rotation, which arises as a result of a rotation of each electron's probability distribution. Such "Larmor rotation" has already been described throughout this thesis. I now show that, in the specific case of superpositions of vortex states with canonical angular momenta $\ell = \pm 1$, the rotation is in essence a Faraday effect for electrons. Here, instead of optical polarization, it is a nodal line in the electron wavefunction that rotates. This can be understood as arising from the differing propagation speeds of oppositely handed electron vortex states in the magnetic field, as illustrated in Fig. 5.1(b).

5.1.2 Angular momentum dependent phase shift

I begin by considering the energy-momentum relationship for an electron with well-defined canonical orbital angular momentum propagating parallel to a uniform magnetic field. From this I will show that the electron undergoes a phase shift that depends on its total canonical angular momentum, including the orbital component.

As before, I consider a uniform magnetic field parallel to the z axis, described by the cylindrical vector potential (2.5). In contrast to Chapters 3 and 4, here I include the

effect of spin. This aids in comparing and contrasting the electron Faraday effect I describe with that for photons. The appropriate Hamiltonian in this case is (2.6), which it may be helpful to rewrite here as

$$H = -\frac{\hbar^2}{2m}\frac{\partial^2}{\partial z^2} - \frac{\hbar^2}{2m}\nabla_\perp^2 + \frac{1}{2}m\omega_{\rm L}^2\rho^2 + \omega_{\rm L}(L_z^{\rm can} + gS_z). \tag{5.1}$$

The first three terms describe, as before, the kinetic energy in field-free space and also the potential energy of the radial oscillation due to the magnetic field. The final term gives the Zeeman energy, with contributions from both the canonical orbital angular momentum and the spin. Recall that g ($\approx$2) is the gyromagnetic ratio for electron spin.

With this Hamiltonian the time-independent Schrödinger equation $H\psi = E\psi$ can be solved exactly, for eigenstates with given z components of momentum, canonical orbital angular momentum and spin [70]. The eigenfunctions are

$$\begin{aligned}\psi_{n,\ell,s}(\rho,\phi,z) &= \psi_{\perp\, n,\ell}^{\rm Lan}(\rho,\phi)\exp(ik_z z) \\ &= N_{n,|\ell|}R_{n,|\ell|}(\rho)\exp\left[i\left(\ell\phi + k_z z\right)\right]\end{aligned} \tag{5.2}$$

where $\psi_{\perp\, n,\ell}^{\rm Lan}$, defined in (2.11), describes the radial and azimuthal dependence of a Landau state and $R_{n,|\ell|}(\rho)$ is the radial function

$$R_{n,|\ell|}(\rho) = \left(\frac{\rho\sqrt{2}}{\rho_{\rm B}}\right)^{|\ell|}\exp\left(-\frac{\rho^2}{\rho_{\rm B}^2}\right)L_n^{|\ell|}\left(\frac{2\rho^2}{\rho_{\rm B}^2}\right). \tag{5.3}$$

The corresponding energy eigenvalues are

$$\begin{aligned}E &= \frac{\hbar^2 k_z^2}{2m} + E_\perp^{\rm Lan} + \hbar\omega_{\rm L}gs \\ &= \frac{\hbar^2 k_z^2}{2m} + \hbar|\omega_{\rm L}|(2n + |\ell| + 1) + \hbar\omega_{\rm L}(\ell + gs),\end{aligned} \tag{5.4}$$

where $E_\perp^{\rm Lan}$, defined by (2.14), is the energy of the transverse motion in a Landau state. The total energy (5.4) includes, in addition to $E_\perp^{\rm Lan}$, contributions from the electron's longitudinal motion and its spin.

Here I am interested in an electron state that has a well-defined energy E, and wish to calculate the value of the wavenumber k_z. The wavenumber for one of the states (5.2)

with a given energy is obtained by rearranging (5.4) as follows:

$$k_{z\,n,\ell,s} = k_0\sqrt{1 - \frac{1}{E}\left[(2n + |\ell| + 1)\hbar|\omega_{\mathrm{L}}| + (\ell + gs)\hbar\omega_{\mathrm{L}}\right]}. \tag{5.5}$$

Here

$$k_0 = \frac{1}{\hbar}\sqrt{2mE} \tag{5.6}$$

is the wavenumber of the corresponding plane wave energy eigenstate in field-free space. In the magnetic field, the wavenumber depends on the quantum numbers n, ℓ and s, and also on the field. This means that the phase accumulated upon propagation

$$\theta_{n,\ell,s} = k_{z\,n,\ell,s}z, \tag{5.7}$$

depends on these quantities.

From here on I consider the case in which the magnetic energy is small compared to the total energy of the electron. That is, $(2n + |\ell| + 1)\hbar|\omega_{\mathrm{L}}| + (\ell + gs)\hbar\omega_{\mathrm{L}} \ll E$. This would be the case, for example, in a transmission electron microscope. I can then apply a Taylor expansion to (5.5) as follows:

$$k_{z\,n,\ell,s} = k_0\left\{1 - \frac{1}{2E}\left[(2n + |\ell| + 1)\hbar|\omega_{\mathrm{L}}| + (\ell + gs)\hbar\omega_{\mathrm{L}}\right]\right\}. \tag{5.8}$$

Here

$$k_{\mathrm{L}} = \frac{m\omega_{\mathrm{L}}}{\hbar k_0} = -\frac{eB}{2\hbar k_0} \tag{5.9}$$

is the spatial frequency corresponding to the temporal Larmor frequency ω_{L}, for an electron with a longitudinal velocity $\hbar k_0/m$. The phase (5.7) is therefore

$$\theta_{n,\ell,s} = k_0 z - (2n + |\ell| + 1)|k_{\mathrm{L}}|z - (\ell + gs)k_{\mathrm{L}}z. \tag{5.10}$$

The first term here describes the phase evolution for a plane wave in field-free space. The second term depends on the energy of the radial motion in a magnetic field. It is the final term that is of particular interest here – this describes a phase shift, resulting from the Zeeman interaction, that is proportional to the total canonical angular momentum of the electron. This "Zeeman phase" has a sign depending on the relative directions of the angular momentum and the magnetic field. As will now be shown, this phase is revealed in the evolution of vortex superpositions.

5.1.3 Rotation of a vortex superposition

For an electron in one of the angular momentum eigenstates (5.2), the probability density is independent of ϕ, and is invariant upon propagation along the z axis:

$$|\psi_{n,\ell,s}|^2(\rho) = \psi^{\mathrm{Lan}}_{\perp\, n,\ell}(\rho,\phi) = N^2_{n,|\ell|} R_{n,|\ell|}(\rho)^2. \tag{5.11}$$

In order for the Zeeman phase to be revealed, it is necessary to consider instead a superposition of angular momenta. Here I concentrate on superpositions of two states that have the same values for n, s and $|\ell|$, but opposite magnitudes of ℓ – as required for an orbital version of the Faraday effect [27]. That is, a wavefunction:

$$\begin{aligned}
\psi^{\mathrm{superpos}} &= \frac{1}{\sqrt{2}}\left(\psi_{n,\ell,s} + \psi_{n,(-\ell),s}\right) \\
&= \frac{1}{\sqrt{2}} N_{n,|\ell|} R_{n,|\ell|}(\rho) \\
&\quad \times \left\{\exp\left[i\left(\ell\phi + k_{z\,n,\ell,s} z\right)\right] + \exp\left[i\left(-\ell\phi + k_{z\,n,(-\ell),s} z\right)\right]\right\} \\
&= \frac{1}{\sqrt{2}} N_{n,|\ell|} R_{n,|\ell|}(\rho) \\
&\quad \times \left\{\exp\left[i\ell\left(\phi - k_{\mathrm{L}} z\right)\right] + \exp\left[-i\ell\left(\phi - k_{\mathrm{L}} z\right)\right]\right\} \\
&\quad \times \exp\left\{i\left[k_0 z - (2n + |\ell| + 1)|k_{\mathrm{L}}|z + gsk_{\mathrm{L}} z\right]\right\} \\
&= \sqrt{2} N_{n,|\ell|} R_{n,|\ell|}(\rho) \cos\ell(\phi - k_{\mathrm{L}} z) \\
&\quad \times \exp\left\{i\left[k_0 z - (2n + |\ell| + 1)|k_{\mathrm{L}}|z + gsk_{\mathrm{L}} z\right]\right\}.
\end{aligned} \tag{5.12}$$

In contrast to the rotational symmetry of each of its components, this superposition has an amplitude that depends sinusoidally on ϕ. At $z = 0$, its probability density is

$$|\psi^{\mathrm{superpos}}|^2(z=0) = 2N^2_{n,|\ell|} R^2_{n,|\ell|}(\rho) \cos^2\ell\phi. \tag{5.13}$$

This consists of a pattern of $2|\ell|$ lobes separated by lines of zero density, as shown in the top row of Fig. 5.5 in section 5.2. In the case of $|\ell| = 1$, the single line of zero density is analogous to optical linear polarization, as emphasised in Fig. 5.1. Now, as the electron propagates along the z axis the probability density is no longer invariant; rather it evolves as

$$|\psi^{\mathrm{superpos}}|^2(z) = 2N^2_{n,|\ell|} R^2_{n,|\ell|}(\rho) \cos^2\ell[\phi - \Phi_{\mathrm{B}}(z)], \tag{5.14}$$

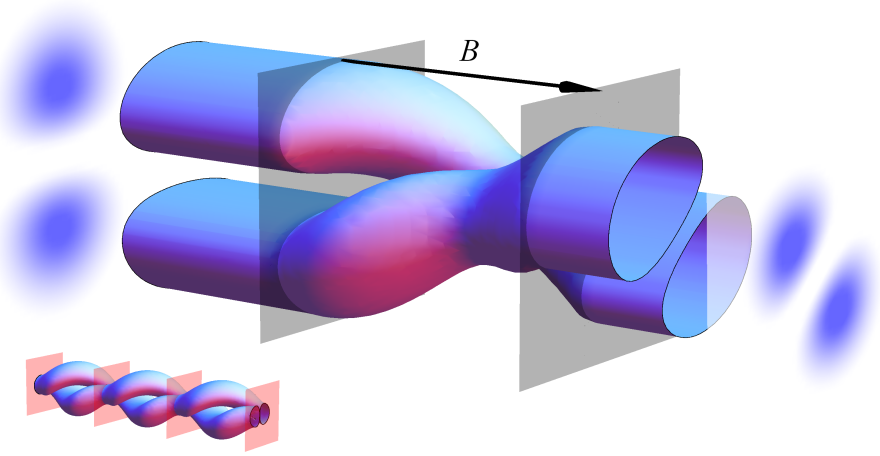

Figure 5.2: **Schematic illustration of the evolution of the probability distribution upon propagation for a superposition of states with $\ell = \pm 1$, where the radial distribution also oscillates.** Here the initial radial distribution has the Laguerre-Gaussian form considered in Chapter 4, with $\rho_0 \neq \rho_B$. The rotation of the probability density has half the frequency of the radius oscillation (see inset). Image created with Sonja Franke-Arnold.

rotating through the angle

$$\Phi_B(z) = k_L z = -\frac{eBz}{2\hbar k_0}. \tag{5.15}$$

Like in the optical Faraday effect this angle is proportional to both the magnetic field and the propagation distance. Here it is also inversely proportional to the longitudinal momentum of the electron.

So far in this chapter I have considered the eigenstates of the Hamiltonian (5.1), which have a fixed radial distribution. As described in the preceding chapter, however, a Laguerre-Gaussian state with a different transverse scale – that is, with a radial width $\rho_0 \neq \rho_B$ – would not be an eigenstate. In such a case the probability density exhibits radial oscillations that occur at the cyclotron frequency, and therefore twice every full rotation. This is illustrated in Fig. 5.2.

5.1.4 Observing the electron Faraday effect

Electron vortex superpositions can be generated using nanofabricated diffraction gratings. We proposed this in [86], at a time when only the generation of eigenstates of L_z^{can} had been reported. A suitable grating pattern can be obtained by interfering the desired vortex superposition with a plane wave $\psi = \exp(ik_x x)$. For a binary absorbing mask, the transmission function can be defined as

$$T = \begin{cases} 1, & \text{if } |2\cos\ell(\phi-\phi_0) + \exp(ik_x x)|^2/3 > 1/2 \text{ and } \rho < a \\ 0, & \text{otherwise.} \end{cases} \tag{5.16}$$

Here $\cos\ell(\phi-\phi_0)$ is the azimuthal dependence of the wavefunction for a vortex superposition that has a density maximum at $\phi = \phi_0$. The radial distribution is specified as a circular aperture of radius a. Such a grating is illustrated in Fig. 5.3(a), with the simulated far-field diffraction pattern (obtained by a Fourier transform calculation) shown in part (b). The desired vortex superposition, here with $|\ell| = 1$, appears in the ± 1 diffraction orders. The generation of vortex superpositions in this manner has now been demonstrated experimentally [115].

In optical Faraday rotation, the rotation angle per unit propagation distance and magnetic field strength in a given material is a constant, known as the Verdet constant of the material. The electron Faraday effect I describe, in contrast, does not have a material dependence, as I consider an electron propagating in vacuum. The electron "Verdet parameter" $\Phi_B/(Bz) = -e/(2\hbar k_0)$ does, however, depend on the longitudinal momentum of the electron. The slower the electron, the longer the time it will be exposed to the field, and the larger the rotation angle will be. The Verdet parameter is plotted in Fig. 5.4, as a function of the energy E, to which k_0 is related by (5.6). As can be seen, the rotation angle diminishes rapidly with increasing energy. As a consequence, measuring Faraday rotation due to a perpendicularly magnetised sample in transmission electron microscopy will be challenging. For $E = 60$ keV, $B = 1$ T and a sample thickness of 100 nm, the rotation angle calculated from (5.15) is 0.06 mrad. It may be better therefore to consider experiments that utilise lower energy electrons, such as photoelectrons.

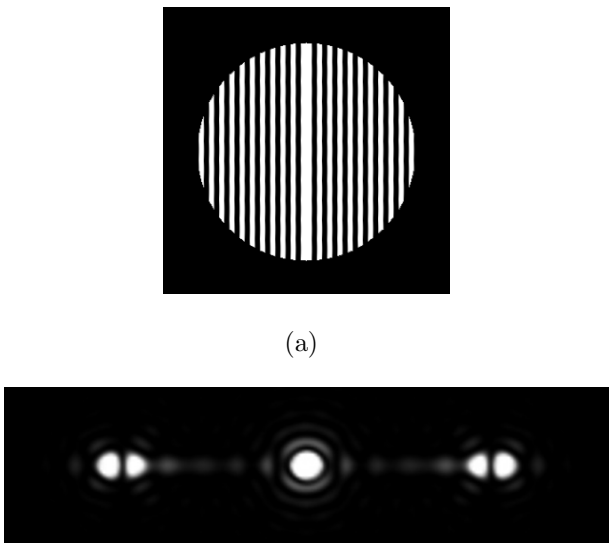

(a)

(b)

Figure 5.3: **Hologram producing a superposition of vortex states with $\ell = \pm 1$.** (a) Grating profile calculated using (5.16) with $\phi_0 = 0$. (b) Simulated far-field diffraction pattern for this grating, with the desired superposition in the ± 1 diffraction orders.

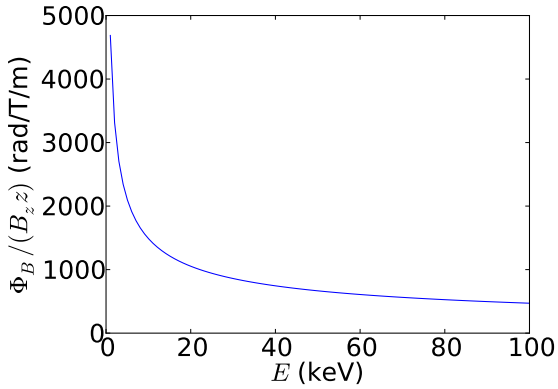

Figure 5.4: **Rotation angle per unit propagation distance and magnetic field strength (the Verdet parameter), as a function of energy.**

5.1.5 Discussion

Although observation of electron Faraday rotation as a result of transmission through a magnetised material is yet to be reported, rotations of vortex superpositions in magnetic lenses have been observed [115]. In light of these experiments it is now clear that, in this context, the Faraday effect described here and the Larmor rotation that is well known in electron optics are one and the same thing. The results of this chapter can therefore be regarded as a reinterpretation of this feature of electron optics.

One reason this is of value is that it bridges a gap between conventional electron optics theory and studies of light's angular momentum. In addition to this, the analogy drawn with optical polarization suggests that Larmor rotation, which in electron imaging is normally considered a background effect, could have practical applications. The most obvious of these is spatially resolved magnetic field measurements. Also, the theoretical approach presented here appears promising for investigating effects that also depend on the spin of the electron.

5.2 Complements to section 5.1

The remainder of this chapter is made up of two sections, each complementing the results that have already been described.

The first of these deals with superpositions of higher order canonical angular momentum states. The electron Faraday effect most closely resembles the rotation of optical polarization for superpositions of states with $|\ell| = 1$. Nonetheless, as noted in section 5.1, the rotation for electrons also occurs with superpositions having $|\ell| > 1$. Here this is discussed further, and it is demonstrated that, where rotation angles are to be

measured, states with $|\ell| = 1$ are advantageous. I also explain why the rotation angle is independent of $|\ell|$.

I then consider more generally the phase change of an electron beam propagating in a magnetic field. Specifically, I derive an expression for the change, due to an arbitrary magnetic field, in the z component of the wavevector, for any paraxial wavefunction. I demonstrate that this formalism provides an alternative means to obtain the ℓ-dependent phase shift described in section 5.1.

5.2.1 Higher order superpositions

The electron Faraday effect is most directly analogous to the rotation of optical polarization in the case of a superposition of two wavefunctions with canonical angular momentum of magnitude $\hbar$. In this case, the nodal line in the wavefunction of the superposition corresponds to the direction of linear polarization. Nonetheless, electron Faraday rotation can be observed with superpositions with larger values of angular momentum as well.

The probability densities for three different superpositions of the form

$$\Psi_{\perp}(t=0) = \frac{1}{\sqrt{2}}\left(\psi^{\mathrm{Lan}}_{\perp\, 0,\ell} + \psi^{\mathrm{Lan}}_{\perp\, 0,-\ell}\right) \tag{5.17}$$

are shown in Fig. 5.5. These are plotted both before propagation in a magnetic field and after rotations through progressively larger angles. Each of the superpositions rotates through the same angle: the rotation angle Φ_{B}, defined by (5.15), is independent of $|\ell|$. The higher order superpositions have more than one nodal line however: these are spaced at an angle of $\pi/|\ell|$. Since the intensity pattern is periodic in ϕ with the period $\pi/|\ell|$, higher order superpositions repeat more quickly. This is seen in Fig. 5.5, where after a rotation through $\Phi_{\mathrm{B}} = \pi/3$ the superposition with $|\ell| = 3$ has returned to its starting orientation. For rotation angles $\sim \pi/|\ell|$ the magnetic field can no longer be

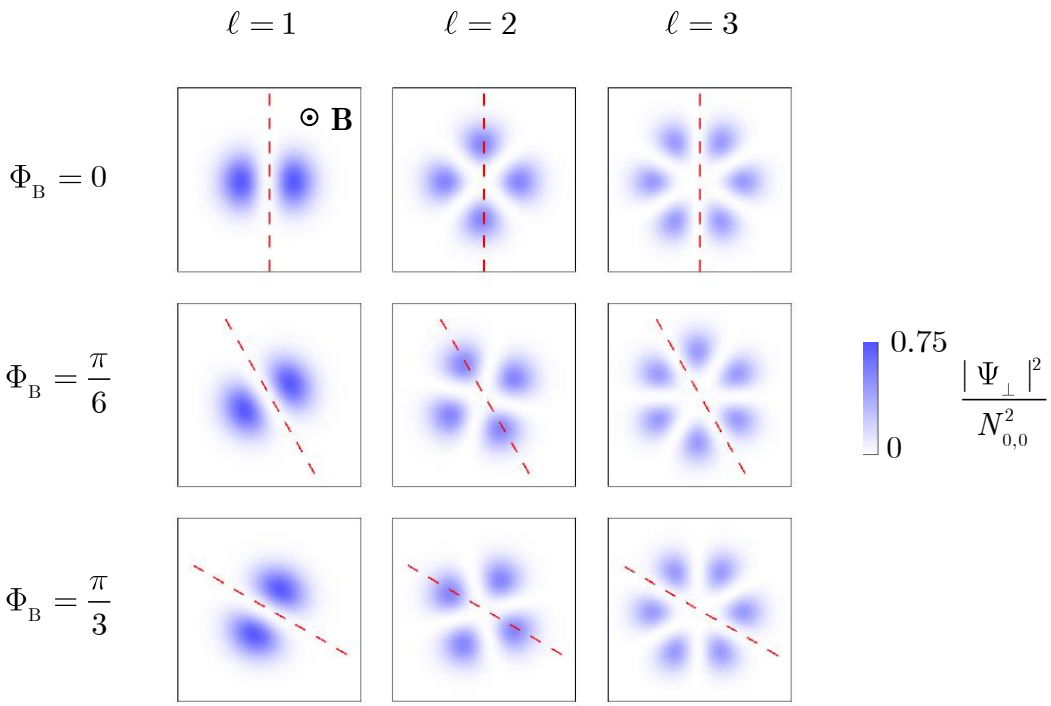

Figure 5.5: **Faraday rotation of superpositions of Landau states with equal and opposite values of canonical angular momentum.** Shown here is the probability density for wavefunctions of the form given by (5.17), with $\ell = 1, 2$ and 3 (left-right), for rotation angles of $\Phi_B = 0, \pi/6$ and $\pi/3$ (top-bottom). Each tile has a side length of $5\rho_B$.

unambiguously inferred from the size of the rotation, meaning that when measuring large rotations the superposition with $|\ell| = 1$ would be most suitable.

It may appear surprising that the rotation angle Φ_B does not depend on the magnitude of ℓ, even though the Zeeman phase shift does. This can be understood, however, by considering the geometry of the twisted phase contours of the wavefunction.

In field-free space, an electron with a canonical angular momentum $\ell\hbar$ and longitudinal momentum $\hbar k_z$ has a wavefunction with a helicoidal phase described by $\theta(\phi, z) = \ell\phi + k_z z$. In general the phase will also depend on the radius ρ, but for the purposes of the discussion here that can be ignored. The surfaces of constant phase are defined by the relation $\theta = 2\pi q + C$, where $q \in \mathbb{Z}$ and C is an arbitrary constant. Using

$k_z = 2\pi/\lambda$, where λ is the wavelength, the phase contours can therefore be described by the expression

$$z = \lambda q - \ell\lambda\frac{\phi}{2\pi}. \tag{5.18}$$

Here I have set $C = 0$. As illustrated in Fig. 5.6, this describes ℓ intertwined helicoids, each of which has a pitch equal to $\ell\lambda$. Since the pitch of the helicoid is proportional to ℓ, an azimuthal rotation of the surface through an angle $\Delta\phi$ is equivalent to a longitudinal translation that is proportional to ℓ:

$$\phi \to \phi + \Delta\phi \Rightarrow z \to z - \ell\lambda\frac{\Delta\phi}{2\pi}. \tag{5.19}$$

This means that a longitudinal phase shift equal to $-\ell\Delta\phi$ corresponds to an azimuthal rotation through the angle $\Delta\phi$. Hence, the Zeeman phase $-\ell\Phi_{\mathrm{B}}$ results in the azimuthal rotation Φ_{B}, which is independent of the value of ℓ.

It should be noted that I am considering here only rotations that arise as a result of the interaction with the magnetic field. If, instead of choosing a superposition in which the two components have the same magnitude of $|\ell|$, an "unbalanced" superposition that has a non-zero net canonical angular momentum were formed, this superposition would exhibit a rotation even in the absence of a magnetic field, as a result of the differing Gouy phases [127, 163, 164] of the superposition components. In a magnetic field, the total rotation of the electron's probability distribution is in general given by the sum of the Faraday (or "Larmor") rotation and the Gouy rotation [87, 99, 115].

5.2.2 General expression for phase shift

The Faraday effect described in the preceding section is associated with the differing phases acquired by vortices with different angular momentum propagating in a uniform magnetic field. In this section I consider the phase change of an arbitrary paraxial electron wavefunction in the presence of an arbitrary magnetic field. I obtain an expression for this phase change in terms of the gradient of the wavefunction and the

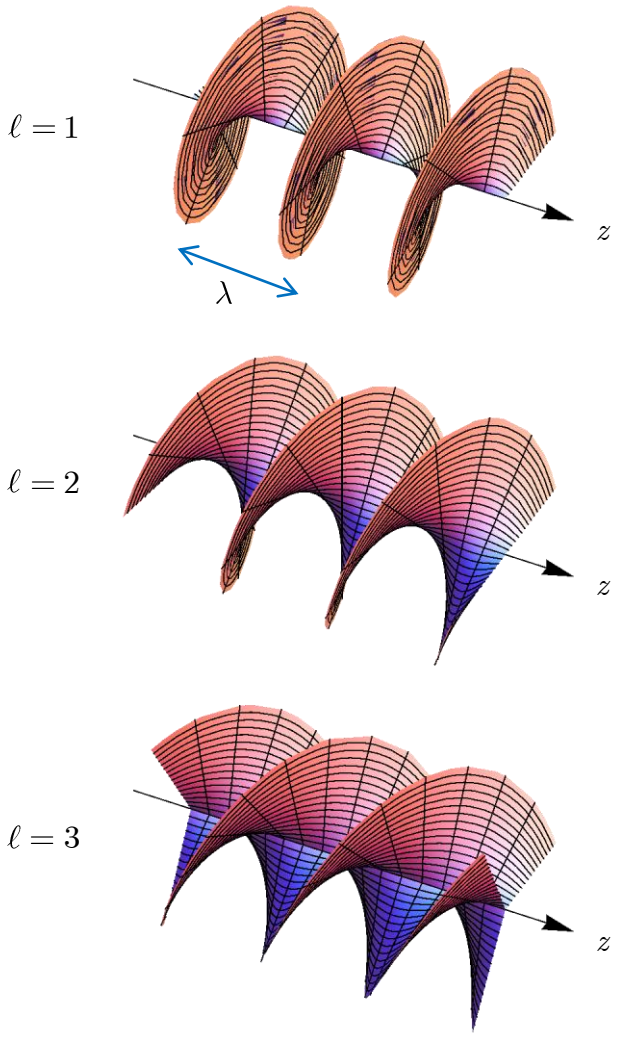

Figure 5.6: **Surfaces of constant phase for Landau wavefunctions with different values of canonical angular momentum.** In each case, $n = 0$, and the phase contour is plotted over a z interval equal to three wavelengths. The pitch of the helicoid is equal to $\ell\lambda$.

vector potential. In the appropriate limit the results of section 5.1 are recovered.

I consider an arbitrary time-independent magnetic field, described by a vector potential $\mathbf{A}(\mathbf{r})$. The electron is assumed to be in an energy eigenstate, with energy E, such that its state is described by the time-independent Schrödinger equation

$$\frac{1}{2m}(\mathbf{p}^{\mathrm{kin}})^2\psi(\mathbf{r}) = E\psi(\mathbf{r}). \tag{5.20}$$

The effect of the electron's spin is not considered here. Choosing the Coulomb gauge, $\boldsymbol{\nabla}.\mathbf{A} = 0$, so that

$$\begin{aligned}(\boldsymbol{\nabla}.\mathbf{A} + \mathbf{A}.\boldsymbol{\nabla})\psi &= 2\mathbf{A}.\boldsymbol{\nabla}\psi + \psi\boldsymbol{\nabla}.\mathbf{A} \\ &= 2\mathbf{A}.\boldsymbol{\nabla}\psi,\end{aligned} \tag{5.21}$$

(5.20) becomes

$$\left[\nabla^2 + k_0^2 - \frac{e}{\hbar}\left(2i\mathbf{A}.\boldsymbol{\nabla} + \frac{eA^2}{\hbar}\right)\right]\psi = 0, \tag{5.22}$$

where $k_0 = \sqrt{2mE}/\hbar$ is the wavenumber of a plane wave that has the energy E. It is convenient when applying the paraxial approximation to express the wavefunction as

$$\psi = u(\mathbf{r})\exp(ik_0 z). \tag{5.23}$$

Substituting this expression into (5.22) yields

$$\frac{\partial^2 u}{\partial z^2} + 2i\left(k_0 - \frac{e}{\hbar}A_z\right)\frac{\partial u}{\partial z} + \nabla_\perp^2 u - \frac{e}{\hbar}\left[2i\mathbf{A}_\perp.\boldsymbol{\nabla}_\perp - A_z\left(2k_0 - \frac{e}{\hbar}A_z\right) + \frac{e}{\hbar}A_\perp^2\right]u = 0. \tag{5.24}$$

In the paraxial approximation, the function u varies slowly with z, meaning that its second derivative, with respect to z, is negligible:

$$\left|\frac{\partial^2 u}{\partial z^2}\right| \ll \left|k_0\frac{\partial u}{\partial z}\right| \tag{5.25}$$

[165]. Here, I also assume that the fractional change in the z component of the kinetic momentum, as a result of the interaction with the magnetic field, is small, so that $|eA_z|/\hbar \ll |k_0|$. I thus arrive at

$$i\frac{\partial u}{\partial z} = -\left(\frac{1}{2k_0}\nabla_\perp^2 + k_{z\,\mathrm{A}}\right)u, \tag{5.26}$$

where

$$k_{z\,\mathrm{A}} = \frac{e}{\hbar}\left(A_z - \frac{i}{k_0}\mathbf{A}_\perp.\boldsymbol{\nabla}_\perp - \frac{e}{2\hbar k_0}A_\perp^2\right) \tag{5.27}$$

is the change, due to the presence of the vector potential, in the z component of the electron's wavevector. The change in the wavevector depends not only on the vector potential, but also on the gradient of the wavefunction, which is related to the electron's momentum. This reflects the dependence of the classical Lorentz force on the velocity of the electron.

The paraxial wave equation (5.26) is equivalent in form to the time-dependent Schrödinger equation. As such, its solution is described by the integral

$$u(z+\Delta z) = Z \exp\left\{ i \int_z^{z+\Delta z} \mathrm{d}z \, \left[\frac{1}{2k_0} \nabla_\perp^2 + k_{z\,\mathrm{A}}(z) \right] \right\} u(z), \tag{5.28}$$

where Z is the equivalent of the time-ordering operator [150]. For a value of Δz that is small enough that terms $\mathcal{O}\left[(\Delta z)^2\right]$ can be ignored, the expression (5.28) simplifies to

$$u(z+\Delta z) = T_\mathrm{A} T_0 u(z), \tag{5.29}$$

where

$$T_0 = \exp\left(i \Delta z \frac{1}{2k_0} \nabla_\perp^2 \right) \tag{5.30}$$

is the field-free propagator, which describes the diffraction of the wavefunction, and

$$T_\mathrm{A} = \exp\left(i \Delta z k_{z\,\mathrm{A}} \right) \tag{5.31}$$

describes the effect of the vector potential. Such an approximation, although normally involving a scalar potential and not a magnetic field, is the basis for both the split operator method of numerically propagating the time-dependent Schrödinger equation [150] and also the related multi-slice method used in electron optics [121, 166].

I will now demonstrate that the formalism developed above reproduces the Zeeman phase shift derived in section 5.1. To do this I first evaluate the propagators (5.30) and (5.31) for a Laguerre-Gaussian wavefunction that can have any radius ρ_0, before subsequently considering the particular case where the electron is in a Landau state.

The Laguerre-Gaussian initial wavefunction is the same as that considered in Chapter 4:

$$u_{n,\ell}(z=0) = \sqrt{\frac{2n!}{\pi(n+|\ell|)!}} \frac{1}{\rho_0} \left(\frac{\sqrt{2}\rho}{\rho_0} \right)^{|\ell|} \exp\left(-\frac{\rho^2}{\rho_0^2} \right) L_n^{|\ell|}\left(\frac{2\rho^2}{\rho_0^2} \right) \exp(i\ell\phi). \tag{5.32}$$

The action of the propagator T_0 on this wavefunction – the evolution of this state in field-free space – is well known:

$$\begin{aligned} T_0 u_{n,\ell}(0) &= \exp\left(i\frac{k_0\rho^2}{2R(z)}\right)\exp[-i(2n+|\ell|+1)\xi(z)]\sqrt{\frac{2n!}{\pi(n+|\ell|)!}} \\ &\quad\times\frac{1}{\rho_z(z)}\left(\frac{\sqrt{2}\rho}{\rho_z(z)}\right)^{|\ell|}\exp\left(-\frac{\rho^2}{\rho_z^2(z)}\right)L_n^{|\ell|}\left(\frac{2\rho^2}{\rho_z^2(z)}\right)\exp(i\ell\phi) \end{aligned} \quad (5.33)$$

[22, 36, 165]. Here $\rho_z(z) = \rho_0\sqrt{1+(z/z_\mathrm{R})^2}$ describes the radius of the probability distribution, where $z_\mathrm{R} = |k_0|\rho_0^2/2$ is the "Rayleigh range" [165], $R(z) = z\left[1+(z_\mathrm{R}/z)^2\right]$ is the wavefront radius of curvature, and $-(2n+|\ell|+1)\xi(z)$ is the Gouy phase, where $\xi(z) = \tan^{-1}(z/z_\mathrm{R})$. Note that if the exponent in the definition (5.23) had the opposite sign, as is the case in [165], then the sign of the first exponent in (5.33) – which depends on $R(z)$ – would be reversed. To first order in a short propagation distance Δz, the above parameters take the values $\rho_z(\Delta z) = \rho_0$, $R(z) = z_\mathrm{R}^2/z$ and $\xi(\Delta z) = z/z_\mathrm{R}$, in which case the expression (5.33) simplifies to

$$T_0 u_{n,\ell}(0) = \exp\left(i\frac{2\Delta z\rho^2}{k_0\rho_0^4}\right)\exp\left[-i(2n+|\ell|+1)\frac{\Delta z}{z_\mathrm{R}}\right]u_{n,\ell}(0). \quad (5.34)$$

In this case the amplitude of the wavefunction is unchanged upon propagation – to first order in Δz, the propagator T_0 affects only the phase. The first exponential in (5.34) describes the curvature of the wavefronts, while the second factor describes the Gouy phase.

The effect of a uniform longitudinal magnetic field on the Laguerre-Gaussian wavefunction can be seen by evaluating the propagator (5.31) using the vector potential (2.5). With this vector potential, (5.31) becomes:

$$T_\mathrm{A} = \exp\left(-k_\mathrm{L}\Delta z\frac{\partial}{\partial\phi}\right)\exp\left(-i\frac{2\Delta z\rho^2}{k_0\rho_\mathrm{B}^4}\right), \quad (5.35)$$

where ρ_B and k_L are defined, respectively, by (2.12) and (5.9). The wavefunction at $z = \Delta z$ is then obtained by substituting (5.34) and (5.35) into (5.29):

$$\begin{aligned} u_{n,\ell}(\Delta z) &= T_\mathrm{A}T_0 u_{n,\ell}(0) \\ &= \exp(-ik_\mathrm{L}\ell\Delta z)\exp\left[i\frac{2\Delta z\rho^2}{k_0}\left(\frac{1}{\rho_0^4}-\frac{1}{\rho_\mathrm{B}^4}\right)\right] \\ &\quad\times\exp\left[-i(2n+|\ell|+1)\frac{\Delta z}{z_\mathrm{R}}\right]u_{n,\ell}(0). \end{aligned} \quad (5.36)$$

The first exponential in (5.36) contains the ℓ-dependent Zeeman phase we described in section 5.1. The second term is related to the wavefront radius of curvature, which is seen to depend here on the magnetic field – the magnetic field acts to produce a curvature of the opposite sign to that which develops due to diffraction. The Gouy phase, described by the final exponential in (5.36), is unaffected by the magnetic field. In the case where $\rho_0 = \rho_{\mathrm{B}}$, meaning that the Laguerre-Gaussian state (5.32) is a Landau state, (5.36) simplifies to

$$u_{n,\ell}(\Delta z) = \exp\left\{-i\left[\ell k_{\mathrm{L}} + (2n + |\ell| + 1)|k_{\mathrm{L}}|\right]\Delta z\right\} u_{n,\ell}(0), \tag{5.37}$$

which is in agreement with (5.7) in section 5.1.

Chapter 6

Summary and outlook

6.1 Summary

I have shown that in a uniform magnetic field the orbital angular momentum of a free electron comprises three components: canonical, cyclotron and diamagnetic. The canonical angular momentum in the direction of the magnetic field is independent of the field. This angular momentum has the same properties as the orbital angular momentum of photons, which do not interact with an external magnetic field. The cyclotron angular momentum, on the other hand, is associated with the motion of a classical charged particle in the magnetic field. Here, this is related to the centre of mass of the electron's probability distribution.

The diamagnetic angular momentum is particularly interesting as it has properties that exist neither for an electron wavefunction in field-free space or for a classical particle. This angular momentum depends on the moment of inertia of the electron's probability distribution. Therefore, it varies with time as the wavefunction diffracts.

The diamagnetic angular momentum also has a minimum allowed magnitude, as a consequence of the uncertainty principle.

The diamagnetic angular momentum is associated with a rotation of the electron's probability density at the Larmor angular velocity. I have shown that this rotation can be observed using electron beams that are in superpositions of states with oppositely handed canonical angular momenta. This rotation can also be understood as arising from a differential phase shift that depends on the canonical angular momentum, and is therefore, in essence, a Faraday effect for electrons.

I have established and illustrated connections between a number of well-known rotational phenomena that are normally considered in separate contexts. This includes optical and electron vortices, cyclotron motion and diamagnetism, as described above, as well as the connection between diamagnetism and Faraday rotation. I hope that this helps to bridge gaps between photon optics, electron optics and condensed matter physics.

One important conclusion to draw is that, where an external magnetic field is present, care must be taken in applying to electrons ideas relating to optical angular momentum. This is because theories developed to describe light take account only of the canonical angular momentum of the electron, and not the additional angular momentum due to the magnetic field. For example, when the centre of mass of an electron's probability distribution is moving in a straight line, along a magnetic field line, it may not be obvious from this distribution that a magnetic field does in fact change the angular momentum of the electron. Also, the diamagnetic angular momentum exists even for "ordinary" electron beams, which do not contain vortices. These are important practical considerations for the utilisation of orbital angular momentum in electron optics, as strong external magnetic fields are used to manipulate electron beams. Of course, the interaction with a magnetic field also presents possibilities for novel technologies that are not possible using photons.

Perhaps what is most interesting of all, however, is that such a simple system – a single electron in a uniform magnetic field – can exhibit such rich and unexpected behaviour.

6.2 Outlook

There are a number of ways in which the ideas contained in this thesis could be developed further or applied. Some promising directions for future research have already been discussed in the results chapters. In what follows, I consider three ideas for future research in more detail.

6.2.1 Vorticity of the current density

The electron states I have described in this thesis have uncertainty in their position and momentum. This means that there is uncertainty in the electron's angular momentum [167], and I have considered the expectation value of this angular momentum, $\langle L_z^{\mathrm{kin}} \rangle$. This is the angular momentum that would be expected to be measured upon averaging over interactions that can occur at all positions within the electron's probability distribution.

What if, though, we are interested in the angular momentum within a specific region of space? For example, what would be the angular momentum transferred to a small absorbing target that occupies only a small region of the electron's probability distribution? A similar situation is encountered in optics, when laser beams carrying orbital angular momentum interact with small particles located within the beam profile [168]. This also recalls rotations in fluids, where the local angular velocity that a small test particle inserted into the fluid would experience is described by the *vorticity* of the

fluid [41].

It seems that the local angular momentum density associated with the diamagnetic current of the electron could be characterised using the concept of vorticity. Indeed, a similar approach has already been taken for optical currents [168, 169]. It has been shown that the angular momentum transferred to a small spherical absorbing particle is proportional to the vorticity of the optical current at the location of the particle [169]. For electrons, though, this current will be influenced by a magnetic field. The electron's current vorticity is equal to

$$\omega_z = \frac{1}{2}\left(\boldsymbol{\nabla}\times\mathbf{j}\right)_z = \frac{1}{2}\boldsymbol{\nabla}_\perp|\Psi|^2\times\frac{\mathbf{j}_\perp}{|\Psi|^2}+\omega_{\mathrm{L}}|\Psi|^2. \tag{6.1}$$

The first term here is associated with a flow of current that is orthogonal to a gradient in the probability density – this current may be due to canonical angular momentum, a magnetic field, or both. The second term, however, describes an additional vorticity that will arise only in the presence of a magnetic field. Interestingly, this vorticity is present even when the probability density does not have a gradient. The dependence of the electron's current vorticity on its probability density, as well as the magnetic field, and how this may appear in experiments, would be an interesting avenue for further investigation.

6.2.2 Angular momentum coupling

It is well known that in atoms the spin and orbital components of an electron's angular momentum are not independent. Rather, when the electron moves under the influence of the atomic nucleus there is a spin-orbit coupling. This can be understood in terms of the relativistic quantum theory developed by Dirac. In fact, electron vortices moving in field-free space are also expected to exhibit spin-orbit coupling [45]. This would occur when the electron has sufficiently high energy (such that the non-relativistic approximation is no longer valid) and also has a large radial component of momentum.

This would be similar to the spin-orbit coupling that is observed with photons in tightly focused light beams [170, 171].

In this thesis I have considered electrons moving in the absence of attractive Coulomb forces, and with sufficiently low energy that the non-relativistic approximation is valid. I have also considered only a magnetic field that is spatially uniform. As described in Chapter 2, under these conditions the spin and orbital components of the electron's angular momentum can be separated. I have also discussed only the component of canonical angular momentum that is in the direction of the magnetic field. As guaranteed by Noether's theorem, this is constant, and independent of the diamagnetic and cyclotron orbits. In a uniform magnetic field the cyclotron and Larmor angular velocities are uniform throughout space.

What, though, about spatially varying magnetic fields? In such fields not only could the orbital angular momentum be coupled to the spin, but also different components of orbital angular momentum could be coupled to one another. Under what conditions could a separate "diamagnetic" contribution to the electron's angular momentum be identified, and, in general, how would this be coupled to the other angular momentum components?

One reason such questions are of interest is that coupling effects could lead to novel means of manipulating the electron's angular momentum. Free electrons could also provide a simple and highly controllable system to investigate angular momentum coupling in atoms and condensed matter.

It would be helpful for performing research in this direction to be able to obtain numerical solutions to the Pauli equation with a non-uniform magnetic field. This would be possible using a modification of the Chebyshev program I have described in this thesis. Spinor wavefunctions could be incorporated in the same manner as in [172], where the Chebyshev method was used to study wavepacket propagation in graphene on the basis

of the Dirac equation. For reasons of numerical efficiency, it would be much preferable to continue to numerically propagate the wavefunction in only two spatial dimensions. This could be achieved by applying the WKB approximation to the motion in the z direction [95], which is valid as long as the field varies slowly compared to the wavelength of the electron. If the Hamiltonian in the reference frame of an electron moving along the z axis were to be considered, then the Hamiltonian would depend on time. Applying the Chebyshev method with a time-dependent Hamiltonian is possible if the propagation is split into a series of short time steps, over which the Hamiltonian can be approximated as uniform [173]. Given that these described changes would increase the required computation time, and that investigating small coupling effects would require high accuracy, it may be necessary to increase the speed of the program. One approach to this would be to exploit the parallel processing capability of a graphics card [143].

Analytical solutions may also be feasible for simple field configurations. For example, consider a magnetic field that is symmetric under rotation about the z axis, but may vary along this axis. As described in section 2.2.3, close to the z axis the longitudinal component of this field can be approximated by its axial value $B_{\mathrm{ax}}(z)$, while the radial component is determined by the gradient of the axial field. Such a magnetic field can be described by the vector potential $\mathbf{A}(\rho, z) = B_{\mathrm{ax}}(z)\rho\hat{\boldsymbol{\phi}}/2$ [93]. With this magnetic field and vector potential, the Hamiltonian of the electron is

$$\begin{aligned} H &= \frac{1}{2m}(\mathbf{p}^{\mathrm{can}})^2 + \frac{1}{2}m\omega_{\mathrm{L}}^2(z)\rho^2 + \omega_{\mathrm{L}}(z)L_z^{\mathrm{can}} + g\omega_{\mathrm{L}}(z)S_z \\ &\quad -\frac{1}{4}g\frac{\mathrm{d}\omega_{\mathrm{L}}(z)}{\mathrm{d}z}\rho\left(\mathrm{e}^{-i\phi}S_+ + \mathrm{e}^{i\phi}S_-\right), \end{aligned} \tag{6.2}$$

where $\omega_{\mathrm{L}}(z) = eB_{\mathrm{ax}}(z)/(2m)$ is the spatially varying Larmor frequency, and $S_+ = S_x + iS_y$ and $S_- = S_x - iS_y$ are the ladder operators. When B_{ax} is constant, this is the same as the Hamiltonian I used in Chapter 5. In general, however, the Larmor angular velocity varies spatially along the z axis. Further, there is a spin-orbit coupling, described by the last term, which is proportional to this variation of the Larmor angular velocity. In investigating the questions discussed in this section, approximate analytical solutions of such a Hamiltonian would likely be of value.

6.2.3 Orbital Stern-Gerlach effect

The Stern-Gerlach experiment was one of the most important in the history of physics, as it confirmed the existence of the electron's spin. Stern and Gerlach passed a beam of neutral atoms through an inhomogeneous transverse magnetic field, and observed a splitting of the beam that was consistent with a dipole force associated with the spin of atomic electrons [174].

Interestingly, a Stern-Gerlach splitting has never been observed for free electrons. Such an experiment has long been discussed, and famously Bohr and Pauli argued that such an observation would be impossible [175]. The important difference between free electrons and the neutral atoms used by Stern and Gerlach is that, as a result of their electrical charge, the electrons will experience a Lorentz force as they move in the magnetic field. This force depends on the velocity of the electron, and Bohr argued that, as a result of the uncertainty of this velocity, there would be a spreading of the electrons' trajectories that would dominate the dipole interaction of the spin. A fully quantum mechanical analysis has revealed, however, that there is no barrier in principle to measuring a splitting associated with the electron's spin [95]. Different experimental geometries have been proposed, and it appears that a measurement is feasible using existing technology, but remains challenging [95, 96, 176, 177].

Here I propose that an analogous splitting may be observed that is associated with the electron's *orbital* angular momentum. This is based on a simple semi-classical argument that concerns the trajectories of a classical particle that is ascribed a magnetic moment of $\boldsymbol{\mu} = -\ell\mu_B\hat{\mathbf{z}}$, which corresponds to an angular momentum of $\ell\hbar\hat{\mathbf{z}}$. Rather than the transverse magnetic field used by Stern and Gerlach, I consider a magnetic field that is longitudinal to the direction of propagation, which I take to be the z axis. As described in Chapter 5, this gives rise to a Zeeman interaction with the orbital magnetic moment: $U = -\boldsymbol{\mu}.\mathbf{B} = \ell\mu_B B_z$. If the magnetic field, and therefore the Zeeman energy, has a transverse gradient, this will result in a transverse dipole force. Here I consider a

magnetic field the strength of which is proportional to the x coordinate: $B_z(x) = \alpha x$. Then, the dipole force is: $\mathbf{F} = -\boldsymbol{\nabla} U = -\ell\mu_B\alpha\hat{\mathbf{x}}$. Solving Newton's equation of motion for an electron that is initially moving in the z direction with velocity v_z, and travels a longitudinal distance L, it is found that the electron experiences a transverse deflection in the x direction of $x_\ell = -\ell\mu_B\alpha L^2/(4E)$, where $E = mv_z^2/2$ is the electron's kinetic energy. This is equivalent to a deflection angle of

$$\theta_\ell \approx \frac{x_\ell}{L} = -\frac{\ell\mu_\mathrm{B}\alpha L}{4E}, \tag{6.3}$$

where a small angle approximation has been applied. Accordingly, it may be expected that a superposition of states with different values of ℓ would display a splitting analogous to that observed by Stern and Gerlach. This is illustrated in Fig 6.1. For a superposition of two states with equal and opposite angular momenta $\pm\ell$, the separation angle would be

$$\Delta\theta_{|\ell|} = 2\theta_{|\ell|}. \tag{6.4}$$

The size of this splitting depends on the magnitude of the orbital angular momentum, the field gradient α, the longitudinal distance for which the electron propagates through the field, L, and the electron's kinetic energy. These quantities could vary greatly depending on the experimental geometry; as an example, though, consider free propagation over a distance of $L = 1\,\mathrm{mm}$, alongside a strip of permalloy providing a field gradient of $\alpha = 10^8\,\mathrm{T\ m^{-1}} = 1\,\mathrm{T}/(10\,\mathrm{nm})$, with $\ell = 100$ and $E = 100\,\mathrm{keV}$. In this case, the separation angle (6.4) would be 3 mrad. Deflections smaller than this, rarely exceeding $100\,\mu$rad, are measured in Lorentz electron microscopy [104].

The above considerations are based on a largely classical model, which does not take into account the uncertainty in the electron's position and velocity. It would be very interesting to find out whether these predictions are borne out in a fully quantum mechanical analysis of the problem. Such an analysis could be performed numerically using an approach along the same lines as discussed in the previous section. If the prediction of a Stern-Gerlach effect for electron orbital angular momentum were borne out by accurate simulations, these could motivate and guide the design of experiments. The observation of such an effect would be of significant fundamental interest, and could also have technological potential for measuring and sorting electron angular momentum

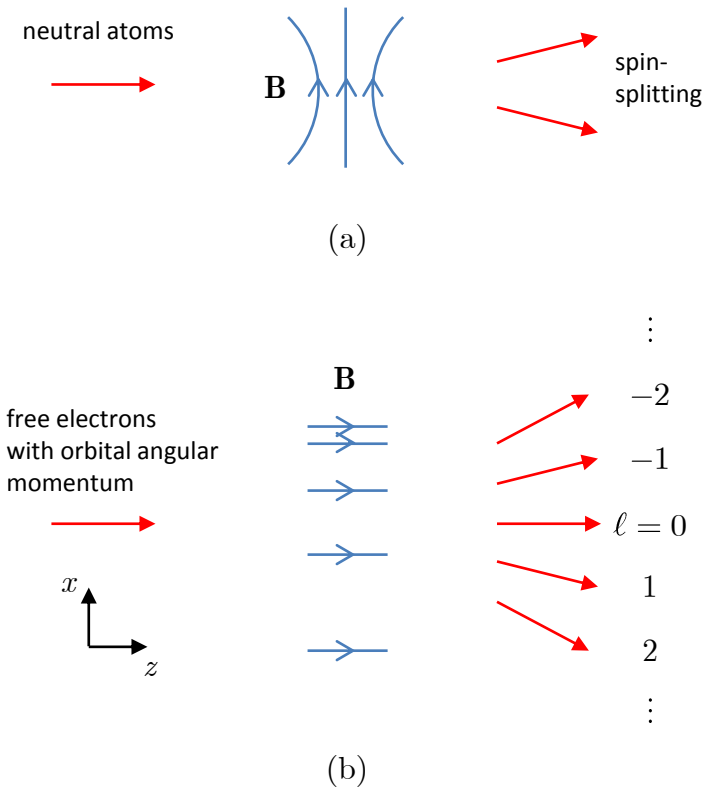

Figure 6.1: **Stern-Gerlach effects for atoms (a) and free electron orbital angular momentum (b).**

in a similar way to devices used in optics [178, 179].

Of course, it is impossible to imagine all the ways that electron orbital angular momentum could prove to be useful or important, and what else may be learned about it. I am very interested to see what the future holds.

Appendix A

Numerical code

The *Mathematica* program I have written to solve the time-dependent Schrödinger equation is described. The code here can also be accessed online at [146].

A.1 Description of *Mathematica* program

Note that \[symbol] indicates where a special character was used in *Mathematica*; for example, \[HBar] would appear in the *Mathematica* notebook interface as $\hbar$. Semicolons are used to suppress output. This code was written for *Mathematica* 9.

A.1.1 Global variables

Here $ is used to indicate a global variable. $Lx and $Ly are the lengths of the simulation area along the x and y axes respectively, while $Nx and $Ny are the corresponding numbers of grid points. $\$m$ and $\$q$ are the mass and charge of the particle for which the Schrödinger equation is being solved. $\$\delta$ is the parameter that determines the accuracy of the Chebyshev expansion, as described in Chapter 3.

```
$Lx=7.5; $Ly=7.5;
$Nx=64; $Ny=64;
$m=1;
$\[HBar]=1;
$q=-1;
$\[Delta]=100;
```

A.1.2 Discretisation

The following functions return the x and y coordinates of the grid points corresponding to the indices i and j, and, similarly, the coordinates k_x and k_y when working in Fourier space. Note that the real space grid is centred on the origin, i.e. x and y lie in the range $-L_x/2 < x < L_x/2$, $-L_y/2 < y < L_y/2$.

```
x[i_] := $Lx/$Nx(i-$Nx/2)
y[j_] := $Ly/$Ny(j-$Ny/2)
kx[i_] := (2\[Pi])/$Lx(i-$Nx/2)
ky[j_] := (2\[Pi])/$Ly(j-$Ny/2)
```

The following functions, based on the in-built *Mathematica* functions Fourier and InverseFourier, implement the discrete Fourier transforms. Here RotateLeft is used since the *Mathematica* functions require the zero frequency to be at the start of the array, rather than in the centre.

```
FT[\[CapitalPsi]_] :=
  ($Lx/Sqrt[2\[Pi]])($Ly/Sqrt[2\[Pi]])
    RotateLeft[Fourier[RotateLeft[\[CapitalPsi],{$Ny/2,$Nx/2}],
      FourierParameters->{-1,-1}],{$Ny/2,$Nx/2}]//N
InverseFT[\[CapitalPsi]FT_] :=
  (Sqrt[2\[Pi]]/$Lx)(Sqrt[2\[Pi]]/$Ly)
    RotateLeft[InverseFourier[RotateLeft[\[CapitalPsi]FT,{$Ny/2,$Nx/2}],
      FourierParameters->{-1,-1}],{$Ny/2,$Nx/2}]//N
```

Spatial derivatives of the wavefunction:

```
GridLaplacian[\[CapitalPsi]_] :=
  InverseFT[Table[-kx[i]^2-ky[j]^2,{i,0,$Nx-1},{j,0,$Ny-1}]
    FT[\[CapitalPsi]]]
GridxDeriv[\[CapitalPsi]_] :=
  InverseFT[Table[I kx[i],{i,0,$Nx-1},{j,0,$Ny-1}]FT[\[CapitalPsi]]]
GridyDeriv[\[CapitalPsi]_] :=
  InverseFT[Table[I ky[j],{i,0,$Nx-1},{j,0,$Ny-1}]FT[\[CapitalPsi]]]
```

Maximum frequency represented on the grid:

```
kxMax[Lx_,Nx_] := \[Pi]Nx/Lx
kyMax[Ly_,Ny_] := \[Pi]Ny/Ly
```

Take any continuous function $f(x, y)$ and represent it on the grid:

```
ToGrid[f_] := Table[f[x[i],y[j]],{i,0,$Nx-1},{j,0,$Ny-1}]//N
```

A.1.3 Wavefunctions and potentials

Introduce cylindrical coordinates:

```
\[Rho][x_,y_] := Sqrt[x^2+y^2]
\[Phi][x_,y_] := If[{x,y}=={0,0},0,ArcTan[x,y]]
```

Here a rotationally symmetric vector potential that describes a uniform magnetic field in the z direction is defined. The symmetry axis of this vector potential is located at (x_0, y_0).

```
CylindricalA[x0_,y0_,B_] :=
  ToGrid[Function[{x,y},
    {-0.5B\[Rho][x-x0,y-y0]Sin[\[Phi][x-x0,y-y0]],
      0.5B\[Rho][x-x0,y-y0]Cos[\[Phi][x-x0,y-y0]],0}]]
```

The following generates a Laguerre-Gaussian wavefunction. The symmetry axis of this wavefunction is located at (x_0, y_0) and the wavefunction has a transverse momentum specified by the wavevector $(k_{x\,0}, k_{y\,0})$.

```
Nn\[ScriptL][n_,\[ScriptL]_] := Sqrt[(2n!)/(\[Pi](n+Abs[\[ScriptL]])!)]
```

```
LG[x0_,y0_,kx0_,ky0_,n_,\[ScriptL]_,\[Rho]0_] :=
  Nn\[ScriptL][n,\[ScriptL]]
    Table[1/\[Rho]0 If[\[ScriptL]!=0,((\[Rho][x[i]-x0,y[j]-y0]Sqrt[2])/
      \[Rho]0)^Abs[\[ScriptL]],1]
      Exp[-(\[Rho][x[i]-x0,y[j]-y0]^2/\[Rho]0^2)]
      LaguerreL[n,Abs[\[ScriptL]],2\[Rho][x[i]-x0,y[j]-y0]^2/\[Rho]0^2]
      Exp[I\[ScriptL]\[Phi][x[i]-x0,y[j]-y0]]Exp[I kx0(x[i]-x0)]
      Exp[I ky0(y[j]-y0)],{i,0,$Nx-1},{j,0,$Ny-1}]//N
```

Strength of uniform B field for which a Laguerre-Gaussian wavefunction with width ρ_0 is a Landau state:

```
B0[\[Rho]0_] := (4$\[HBar])/(Abs[$q]\[Rho]0^2)
```

Width that a Laguerre-Gaussian wavefunction must have, to be a Landau state of a field with strength B:

```
\[Rho]B[B_] := 2Sqrt[$\[HBar]/Abs[$q B]]
```

A.1.4 Time-evolution

These functions are used to calculate the time-evolution of the wavefunction using the Chebyshev method. GeneralCheby works for any Hamiltonian with the form $\mathcal{H}$ defined in section 3.1. For convenience when performing calculations for a uniform

magnetic field a further function ChebyTDSEuniformB is defined, which implements GeneralCheby with the vector potential CylindricalA.

```
a[S2_,S1x_,S1y_,S0_] :=
  (S2(-kxMax[$Lx,$Nx]^2-kyMax[$Ly,$Ny]^2)+2(Max[S1x]kxMax[$Lx,$Nx]+
    Max[S1y]kyMax[$Ly,$Ny])+Max[S0]-Min[S0])/2

b[S2_,S1x_,S1y_,S0_] :=
  (S2(-kxMax[$Lx,$Nx]^2-kyMax[$Ly,$Ny]^2)+Max[S0]+Min[S0])/2

\[ScriptCapitalH][\[CapitalPsi]_,S2_,S1x_,S1y_,S0_] :=
  S2 GridLaplacian[\[CapitalPsi]]+I S1x GridxDeriv[\[CapitalPsi]]+
    I S1y GridyDeriv[\[CapitalPsi]]+S0\[CapitalPsi]

Overscript[\[ScriptCapitalH], ~][\[CapitalPsi]_,S2_,S1x_,S1y_,S0_] :=
  1/a[S2,S1x,S1y,S0](\[ScriptCapitalH][\[CapitalPsi],S2,S1x,S1y,S0]-
    b[S2,S1x,S1y,S0]\[CapitalPsi])

M[S2_,S1x_,S1y_,S0_,\[Eta]_] := Ceiling[a[S2,S1x,S1y,S0]\[Eta]/
  $\[HBar]]+$\[Delta]

GeneralCheby[S2_,S1x_,S1y_,S0_,\[CapitalDelta]t_,\[CapitalPsi]Initial_] :=
  Module[{Tq\[CapitalPsi],TqMinus2\[CapitalPsi],TqMinus1\[CapitalPsi],sum},
    TqMinus2\[CapitalPsi]=\[CapitalPsi]Initial;
    TqMinus1\[CapitalPsi]=Overscript[\[ScriptCapitalH],~][\[CapitalPsi]
      Initial,S2,S1x,S1y,S0];
    sum=BesselJ[0,a[S2,S1x,S1y,S0]\[CapitalDelta]t/$\[HBar]]
      TqMinus2\[CapitalPsi]-2I BesselJ[1,a[S2,S1x,S1y,S0]
        \[CapitalDelta]t/$\[HBar]]TqMinus1\[CapitalPsi];
    Do[Tq\[CapitalPsi]=2Overscript[\[ScriptCapitalH],~][TqMinus1
      \[CapitalPsi],S2,S1x,S1y,S0]-TqMinus2\[CapitalPsi];
```

```
    sum=sum+2(-I)^q BesselJ[q,a[S2,S1x,S1y,S0]\[CapitalDelta]t/
      $\[HBar]]Tq\[CapitalPsi];
    TqMinus2\[CapitalPsi]=TqMinus1\[CapitalPsi];
    TqMinus1\[CapitalPsi]=Tq\[CapitalPsi];,{q,2,M[S2,S1x,S1y,S0,
      \[CapitalDelta]t]}];
    Exp[-I b[S2,S1x,S1y,S0]\[CapitalDelta]t]sum//N]

ChebyTDSEuniformB[\[CapitalPsi]Initial_,B_,\[CapitalDelta]t_] :=
  Module[{Ax,Ay,Az,S2,S1x,S1y,S0},Ax=CylindricalA[0,0,B][[All,All,1]];
    Ay=CylindricalA[0,0,B][[All,All,2]];
    Az=CylindricalA[0,0,B][[All,All,3]];
    S2=-$\[HBar]^2/(2$m);
    S1x=$q$\[HBar]Ax/$m;
    S1y=$q$\[HBar]Ay/$m;
    S0=$q^2(Ax^2+Ay^2)/(2$m);
    GeneralCheby[S2,S1x,S1y,S0,\[CapitalDelta]t,\[CapitalPsi]Initial]]
```

A.1.5 Calculation of observables

Action of operators for the x and y components of kinetic momentum on a wavefunction Ψ:

```
pkinx\[CapitalPsi][\[CapitalPsi]_,A_] := Module[{Ax},Ax=A[[All,All,1]];
  -I $\[HBar] GridxDeriv[\[CapitalPsi]]-$q Ax \[CapitalPsi]]

pkiny\[CapitalPsi][\[CapitalPsi]_,A_]:=Module[{Ay},Ay=A[[All,All,2]];
  -I $\[HBar] GridyDeriv[\[CapitalPsi]]-$q Ay \[CapitalPsi]]
```

Now the x and y components of the current density can be evaluated. These are then combined into a single array containing the vector components $\mathbf{j}_\perp = (j_x, j_y)$; this is required to plot the current using ListVectorPlot.

```
jx[\[CapitalPsi]_,A_]  :=
  Re[Conjugate[\[CapitalPsi]]pkinx\[CapitalPsi][\[CapitalPsi],A]]/$m

jy[\[CapitalPsi]_,A_]  :=
  Re[Conjugate[\[CapitalPsi]]pkiny\[CapitalPsi][\[CapitalPsi],A]]/$m
```

Combine two arrays into an array of 2D vectors, in the form required by ListVectorPlot:

```
Create2DVectors[vxArray_,vyArray_] :=
  MapThread[Function[{vx,vy},{vx,vy}],{vxArray,vyArray},2]

jxy[\[CapitalPsi]_,A_] :=
  Create2DVectors[jx[\[CapitalPsi],A],jy[\[CapitalPsi],A]]
```

It is also convenient to have a function to calculate the absolute value of the current density within the x-y plane, $|\mathbf{j}_\perp|$:

```
Absjxy[\[CapitalPsi]_,A_] := Sqrt[jx[\[CapitalPsi],A]^2
  +jy[\[CapitalPsi],A]^2]
```

Action of the operator for the z component of kinetic orbital angular momentum, with respect to an axis located at (x_0, y_0), on the wavefunction Ψ:

```
LkinzPsi[\[CapitalPsi]_,x0_,y0_,A_] := Module[{Ax,Ay},Ax=A[[All,All,1]];
  Ay=A[[All,All,2]];
  -I $\[HBar] (ToGrid[Function[{x,y},x-x0]]GridyDeriv[\[CapitalPsi]]-
    ToGrid[Function[{x,y},y-y0]]GridxDeriv[\[CapitalPsi]])-
  $q (ToGrid[Function[{x,y},x-x0]]Ay-ToGrid[Function[{x,y},y-y0]] Ax)
    \[CapitalPsi]]
```

Expectation values of the z component of the kinetic orbital angular momentum, and of the x and y coordinates:

```
ExpectationLkinz[\[CapitalPsi]_,x0_,y0_,A_] :=
  Re[Total[Conjugate[\[CapitalPsi]] LkinzPsi[\[CapitalPsi],x0,y0,A],2]/
    Total[Abs[\[CapitalPsi]]^2,2]]

Expectationx[\[CapitalPsi]_] := Total[ToGrid[Function[{x,y},x]]
  Abs[\[CapitalPsi]]^2,2]/Total[Abs[\[CapitalPsi]]^2,2]

Expectationy[\[CapitalPsi]_] := Total[ToGrid[Function[{x,y},y]]
  Abs[\[CapitalPsi]]^2,2]/Total[Abs[\[CapitalPsi]]^2,2]
```

A.1.6 Plotting

It is convenient to have functions to calculate the Larmor angular velocity, the cyclotron period and the radius of the classical cyclotron orbit:

```
\[Omega]L[B_] := -$q B/(2 $m)
T[B_] := 2Pi/(2\[Omega]L[B])
```

```
\[Sigma][B_,pC_] := (Abs[pC]/(2 $m Abs[\[Omega]L[B]]))
```

When using ListDensityPlot it is necessary first to transpose the array to be plotted. It is also preferable to shift the array by one grid point in each direction. These manipulations are achieved with the following function.

```
ProbDensForPlot[\[CapitalPsi]_] :=
  Abs[Transpose[RotateLeft[\[CapitalPsi],{1,1}]]]^2
```

Now the probability density in x-y plane, at a given time, can be plotted. The colour scale on the density plot runs from 0 to intensityScaleMax. The plot area is specified by xLength and yLength, and may be smaller than the simulation area. The parameter yOffest allows the centre of the plot area to be shifted along the y axis – this can be used to centre the plot on the axis of the cyclotron orbit.

```
PlotProbDens[\[CapitalPsi]_,probDensScaleMax_,xLength_,yLength_,
  yOffset_] :=
    ListDensityPlot[ProbDensForPlot[\[CapitalPsi]],BaseStyle->
      {FontSize->10},PlotRange->{{-xLength/2,xLength/2},{-yLength/2
        +yOffset,yLength/2+yOffset},{0,probDensScaleMax}},
        ColorFunction->(Directive[Opacity[Rescale[#,{0,1},
        {0,Max[Abs[\[CapitalPsi]]^2]/probDensScaleMax}]],
        Lighter[Blue,1/3]]&),ColorFunctionScaling->True,DataRange->
        {{-$Lx/2,$Lx/2},{-$Ly/2,$Ly/2}},AspectRatio->
        yLength/xLength,Frame->False,Background->None]
```

The current density is plotted in a similar manner:

```
PlotCurrentDens[\[CapitalPsi]_,A_,currentScaleMax_,xLength_,
  yLength_,yOffset_] :=
    ListVectorPlot[jxy[\[CapitalPsi],A],DataRange->{{-$Lx/2,$Lx/2},
      {-$Ly/2,$Ly/2}},AspectRatio->yLength/xLength,VectorScale->
        {0.06,Scaled[1.8],None},Frame->False,VectorColorFunction->
        (Directive[Opacity[Rescale[#5,{0,1},{0,Max[Absjxy[
        \[CapitalPsi],A]]/currentScaleMax}]],Darker[Red,1]]&),
        VectorColorFunctionScaling->True,VectorPoints->16,
        PlotRange->{{-xLength/2,xLength/2},{-yLength/2+yOffset,
        yLength/2+yOffset}},Background->None]
```

Now a time-series illustrating the evolution of the probability density and current density can be generated. The following functions accept as an argument a list containing the wavefunction at a number of different time steps, which can be generated by applying ChebyTDSEuniformB iteratively using NestList.

```
Surface[\[CapitalPsi]List_,step_,xLength_,yLength_,yOffset_] :=
  Polygon[{{(step-1)/(Length[\[CapitalPsi]List]-1),-xLength/2,
    -yLength/2+yOffset},{(step-1)/(Length[\[CapitalPsi]List]-1),
      xLength/2,-yLength/2+yOffset},{(step-1)/(Length[
        \[CapitalPsi]List]-1),xLength/2,yLength/2+yOffset},{(step-1)
        /(Length[\[CapitalPsi]List]-1),-xLength/2,yLength/2+yOffset}},
        VertexTextureCoordinates->{{0,0},{1,0},{1,1},{0,1}}]

PlotEvolution[\[CapitalPsi]List_,A_,probDensScaleMax_,
  currentScaleMax_,xLength_,yLength_,yOffset_] :=
    Show[
      Map[Function[step,
        Graphics3D[
          Style[
            {Texture[ImageData[
```

```
            Show[PlotProbDens[\[CapitalPsi]List[[step]],
              probDensScaleMax,xLength,yLength,yOffset],
            PlotCurrentDens[\[CapitalPsi]List[[step]],A,
              currentScaleMax,xLength,yLength,yOffset],
                Background->None]]],
          EdgeForm[Gray],Surface[\[CapitalPsi]List,step,xLength,
            yLength,yOffset]},Lighting->{{"Ambient",White}}]]],
              Range[Length[\[CapitalPsi]List]]],
    Graphics3D[{Gray,Line[{{0,0,0},{1,0,0}}]}],
    BoxRatios->{3,1,yLength/xLength},Boxed->False,
    ViewPoint->{1.9,-2,0.7},ImageSize->72*3.125,Background->None,
    Axes->True,AxesEdge->{{-1,-1},Automatic,Automatic},
    AxesLabel->{"Subscript[\[Omega], c]t","x/Subscript[\[Rho], B]",
      "y/Subscript[\[Rho], B]"},
    Ticks->{{{0,0},{0.5,"\[Pi]"},{1,2\[Pi]}},{-1,0,1},{-2,-1,0,1,2}}]
```

A.2 Example of use

A Laguerre-Gaussian wavefunction with $n = 0$, $\ell = 1$ and $\rho_0 = 1$ can be generated as follows:

```
\[CapitalPsi]0 = LG[0,0,0,0,0,1,1];
```

Now a magnetic field will be defined that has strength such that this wavefunction is a Landau state. The corresponding vector potential in the cylindrical gauge is then calculated.

```
B = B0[1];
A = CylindricalA[0,0,B];
```

The maximum values of the probability density and current density that will be displayed in the density plots must be chosen. Examples of such settings are the following:

```
probDensScaleMax = Nn\[ScriptL][0,0]^2;
currentScaleMax = Max[Absjxy[\[CapitalPsi]0,A]];
```

The probability density and probability current density can be plotted together by overlaying one plot on top of the other. This is achieved with the following code, which generates the output shown in Fig. A.1.

```
Show[PlotProbDens[\[CapitalPsi]0,probDensScaleMax,4,4,0],
  PlotCurrentDens[\[CapitalPsi]0,A,currentScaleMax,4,4,0],
    ImageSize->28.45*3]
```

The following code propagates this wavefunction over a time interval equal to a quarter of a cyclotron period.

```
\[CapitalPsi] = ChebyTDSEuniformB[\[CapitalPsi]0,B,T[B]/4];
```

As this wavefunction is a Landau state – one of the energy eigenstates of the system – the magnitude of the wavefunction should be conserved. This can be checked as follows:

```
Max[Abs[Abs[\[CapitalPsi]]-Abs[\[CapitalPsi]0]]]
```

Here the result is:

```
2.79284*10^-6
```

The expectation values of the kinetic orbital angular momentum before and after propagation can also be inspected. (Note that I have set $\hbar = 1$.)

```
ExpectationLkinz[\[CapitalPsi]0,0,0,A]
ExpectationLkinz[\[CapitalPsi],0,0,A]
3.
3.
```

For multiple time steps, it is convenient to apply ChebyTDSEuniformB iteratively using the built-in *Mathematica* function NestList. Here this is done for an initial wavefunction that is the same as Ψ_0 above expect that it also has a net momentum in the x direction that is described by the wavenumber $k_{x\,0} = 2$. This results in a cyclotron motion of the centre of mass. Here there are 4 propagation steps, each equal to a quarter of a cyclotron period.

```
\[CapitalPsi]list = NestList[Function[\[CapitalPsi]i,
  ChebyTDSEuniformB[\[CapitalPsi]i,B,T[B]/4]],LG[0,0,2,0,0,1,1],4];
```

The probability density and current density will now be plotted for Ψlist. Note that here the plot area is shifted along the y axis by an amount $\sigma[B,2\hbar]$, which is the radius

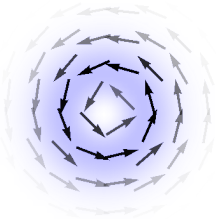

Figure A.1: **Density plot displaying the probability density and current density of a Laguerre-Gaussian wavefunction with $n = 0$ and $\ell = 1$.** This is generated by combining the output of the functions PlotCurrentDens and PlotProbDens.

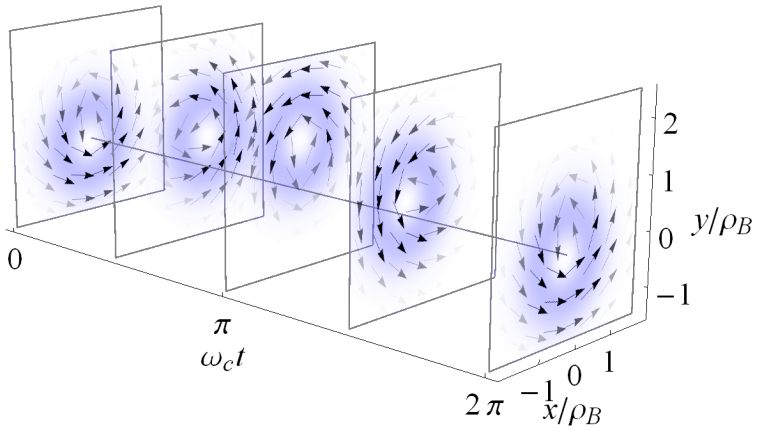

Figure A.2: **Plotting the evolution of the probability density and current density using the PlotEvolution function.** This is shown for a Laguerre-Gaussian wavefunction with $n = 0$, $\ell = 1$ and an x component of transverse momentum equal to $2\hbar/\rho_{\mathrm{B}}$.

of the cyclotron orbit (here equal to 0.5). This means that the plot area is centred on the axis of the cyclotron motion. The output of this code is shown in Fig. A.2.

```
Show[PlotEvolution[\[CapitalPsi]list,A,probDensScaleMax,
  currentScaleMax,4,4,\[Sigma][B,2$\[HBar]]],ImageSize->28.45*10,
    BaseStyle->{FontSize->12}]
```

Appendix B

Journal articles

B.1 Vacuum Faraday effect for electrons

New Journal of Physics
The open-access journal for physics

Vacuum Faraday effect for electrons

Colin Greenshields, Robert L Stamps and Sonja Franke-Arnold[1]
SUPA School of Physics and Astronomy, University of Glasgow,
Glasgow G12 8QQ, UK
E-mail: s.franke-arnold@physics.gla.ac.uk

New Journal of Physics **14** (2012) 103040 (11pp)
Received 10 August 2012
Published 25 October 2012
Online at http://www.njp.org/
doi:10.1088/1367-2630/14/10/103040

Abstract. The optical Faraday effect describes the rotation of linear polarization upon propagation through a medium in the presence of a longitudinal magnetic field. The effect arises from a different phase delay between the right and left handed polarization components of the light. In this paper we predict a Faraday effect for a completely different system: electron vortices. Free electron vortex states were recently observed in transmission electron microscopy experiments, and they introduce new degrees of freedom into the probing of matter with electron beams. We associate a rotation of a vortex superposition with the fact that different phases are acquired by oppositely handed vortices propagating in a magnetic field. We show that, in contrast to the optical Faraday effect, the rotation of the electron beam occurs in vacuum and arises from the intrinsic chirality of the constituent vortex states.

[1] Author to whom any correspondence should be addressed.

Contents

1. The optical Faraday effect and its generalization for electron waves

Michael Faraday reported in 1845 that the polarization of light can be affected by magnetic fields, an effect that now bears his name. Since then, the Faraday effect has found numerous metrological and research applications, including the ultra-sensitive detection of magnetic fields, [1, 2], or of fields generated by electron plasmas in interstellar space and the ionosphere [3, 4].

Faraday noted that the polarization direction of light is rotated after passing through 'heavy glass' exposed to a longitudinal magnetic field. We now understand that the Faraday effect arises from the different speed of propagation of right and left handed circularly polarized light through an optically active medium. The associated difference in accumulated phase between the circular components of linearly polarized light results in a rotation of the polarization direction, shown in figure 1(a).

One of the intriguing properties of light is that it can carry angular momentum: a spin contribution associated with circular polarization ($\pm\hbar$), but also orbital angular momentum (OAM) [5, 6]. While circular polarization describes a rotation of the electric field vector upon propagation, the OAM is a feature of 'twisted' light beams. The OAM can take on arbitrary multiples of $\hbar$ depending on how tightly wound the phase fronts are. These so-called 'vortex beams' have a rotational intensity pattern and are associated with a phase dependence $\exp(\mathrm{i}\,l\phi)$, where l is a non-zero integer and ϕ the azimuthal angle.

Strictly speaking, Faraday rotation is not a relevant concept for optical OAM. The reason is that there is no *intrinsic* mechanism in a gyromagnetic medium to produce the required OAM state dependent dispersion, because selection rules forbid coupling of the OAM to the atomic electron degrees of freedom. This is consistent with results from a recent experiment in which no rotation was observed for a superposition of right and left handed OAM states (a Hermite–Gauss mode) propagating through cholesteric liquid crystals [7]. We note that a relative phase shift between right and left handed OAM components will appear as a rotation of the intensity pattern [8]. Such phase shifts can be induced by spinning the medium through which the light propagates, inducing a 'mechanical' Faraday rotation, as demonstrated recently in a slow light medium [9].

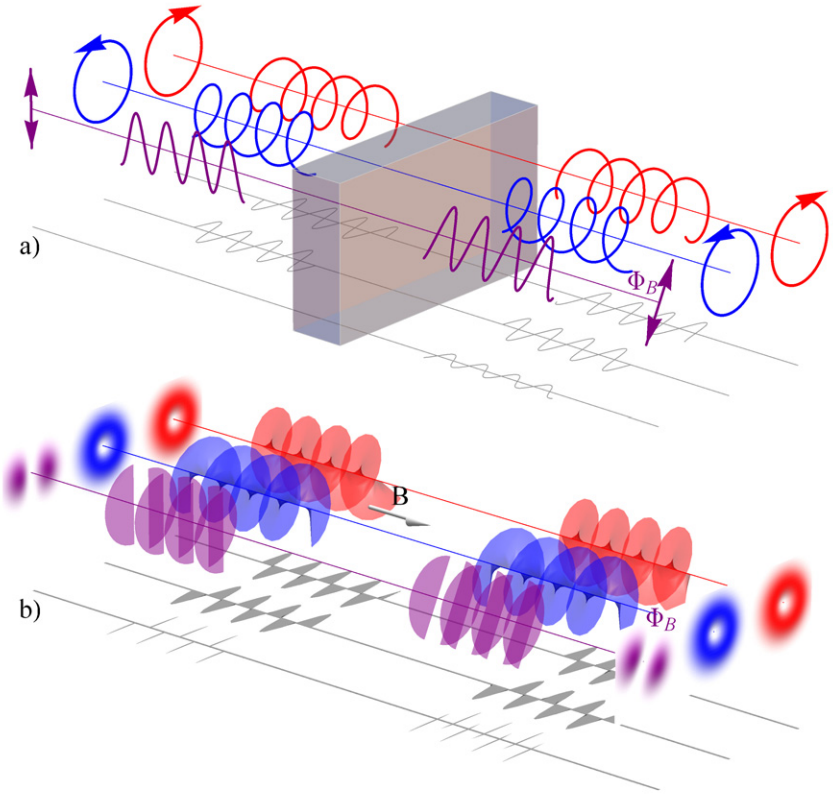

Figure 1. (a) Illustration of the Faraday effect for spin angular momentum, i.e. optical polarization, where the two opposite circular polarization components propagate at different speeds through an optically active medium in a magnetic field. As a result, the linear polarization rotates by an angle proportional to the magnetic field. (b) The analogous effect for transverse beam profiles of electrons, where the different propagation speed of states with opposite OAM in a longitudinal magnetic field leads to image rotation.

Electron vortices are unusual quantum states that have only recently been predicted [10] and produced in transmission electron microscopy (TEM) experiments [11, 12]. Electron vortex beams have the same geometrical properties as their optical counterparts, being characterized by an $\exp(\mathrm{i}\,l\phi)$ angular dependence related to $l\hbar$ units of OAM, but they also produce features that have no analogue in optics. In particular the circulation of charge in an electron vortex beam gives rise to an arbitrarily large orbital magnetic moment (figure 2), distinct from the magnetic moment due to spin [10, 13]. Hence electron vortices can couple to electronic degrees of freedom through dipole selection rules forbidden to optical vortices [14].

Given the analogies (and differences) between optical and electron vortices, the question arises: do electron vortex waves undergo something analogous to an optical Faraday effect? Here we show that there is indeed a Faraday rotation (compare figure 1(b)) arising through Zeeman interaction from propagation *parallel* to a uniform, external magnetic field (i.e. in a geometry where there is no Lorentz force).

2. Electron vortex states

The dynamics of a non-relativistic electron propagating in a magnetic field $\boldsymbol{B}$ (with associated vector potential $\boldsymbol{A}$) is described by the Hamiltonian

$$\hat{H} = \frac{1}{2m}(-\mathrm{i}\hbar\nabla - e\boldsymbol{A})^2 - \boldsymbol{B}\cdot\hat{\boldsymbol{\mu}}_S, \tag{1}$$

where m and $e = -|e|$ are the electron mass and charge, respectively. The Hamiltonian contains the kinetic energy due to the canonical momentum and the Zeeman interaction of the electron spin with an arbitrary external magnetic field $\boldsymbol{B}$. The electron's two-component spinor wavefunction $\tilde{\psi}$ satisfies the Pauli equation $\hat{H}\tilde{\psi} = \mathrm{i}\hbar\frac{\partial}{\partial t}\tilde{\psi}$. Here $\hat{\boldsymbol{\mu}}_S = -g\mu_\mathrm{B}\hat{\boldsymbol{\sigma}}/2$ is the operator for the magnetic moment, $\mu_\mathrm{B} = \hbar|e|/(2m)$ is the Bohr magneton, $g \approx 2$ is the Landé g-factor for electron spin and $\hat{\boldsymbol{\sigma}}$ is the vector of Pauli spin matrices $(\hat{\sigma}_x, \hat{\sigma}_y, \hat{\sigma}_z)$. In agreement with typical parameters in transmission electron microscopes ($\sim$8 nA nm^{-2}), we assume that beam currents are sufficiently low so that Coulomb repulsion can be neglected.

In the case of the uniform magnetic field directed along the z-axis, a suitable choice for the vector potential is $\boldsymbol{A} = (B_z r/2)\hat{\boldsymbol{\phi}}$. Exploiting the cylindrical symmetry of the system, the Hamiltonian can be put in the form

$$\hat{H} = -\frac{\hbar^2}{2m}\frac{\partial^2}{\partial z^2} - \frac{\hbar^2}{2m}\nabla_\perp^2 + \frac{1}{2}m\omega_\mathrm{L}^2 r^2 + \omega_\mathrm{L}(\hat{L}_z + g\hat{S}_z). \tag{2}$$

Here $\omega_\mathrm{L} = |e|B_z/(2m)$ denotes the Larmor frequency, $\hat{L}_z = -\mathrm{i}\hbar\frac{\partial}{\partial\phi}$ and $\hat{S}_z = s\hbar\hat{\sigma}_z$ are the operators for the z component of OAM and spin, respectively, where s is the spin quantum number. The first term gives the kinetic energy of motion along z, which is the same as in field-free space; the second and third terms together give the energy for the transverse motion, and have the form of the Hamiltonian for a harmonic oscillator with characteristic frequency ω_L; the final term gives the Zeeman energy, with contributions from both OAM and spin.

With Hamiltonian (2) the spinor components decouple and we can find monochromatic wave solutions which obey the time independent Schrödinger equation for a scalar wavefunction ψ. This problem can be solved exactly for eigenstates with given z components of OAM and momentum [15]. Separating the degrees of freedom,

$$\psi_{nls}(r, \phi, z) = R_{n|l|}(r)\exp(\mathrm{i}\,l\phi)\exp(\mathrm{i}\,k_{nls}z), \tag{3}$$

we identify the radial modes

$$R_{n|l|}(r) = \sqrt{\frac{2n!}{\pi(n+|l|)!}}\frac{1}{w_\mathrm{B}}\left(\frac{\sqrt{2}r}{w_\mathrm{B}}\right)^{|l|}\mathrm{e}^{-r^2/w_\mathrm{B}^2}L_n^{|l|}\left(\frac{2r^2}{w_\mathrm{B}^2}\right), \tag{4}$$

where $w_\mathrm{B} = 2\sqrt{\hbar/|eB_z|}$ is a characteristic width which depends on the magnitude of the magnetic field, and $L_n^{|l|}$ is an associated Laguerre polynomial. The radial modes are characterized by the OAM quantum number, l, and the radial mode number $n = 0, 1, 2, \ldots$ which denotes the number of radial nodes of the electron density function. The radial profile of a mode with $l = 1$ and $n = 0$ is shown in figure 2. The transverse beam profile, given by $R_{n|l|}(r)\exp(\mathrm{i}\,l\phi)$, is the same as that of the Laguerre–Gauss beams familiar from optical vortices, as was also pointed out in [16].

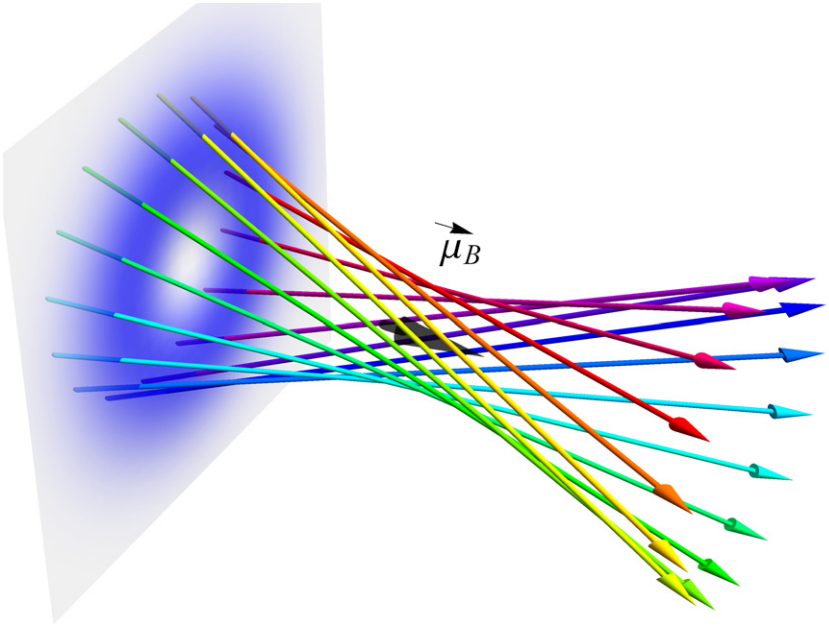

Figure 2. The circulating charge in an electron vortex beam generates a magnetic moment which interacts with external magnetic fields. The electron density function vanishes at the vortex core and the propagation direction is twisted around this core.

Recognizing that the combined second and third terms in (2) describe a two-dimensional harmonic oscillator, which in polar coordinates has energy eigenvalues $\hbar|\omega_L|(2n+|l|+1)$, the eigenvalues for the total energy are the well known Landau levels

$$E = -\frac{\hbar^2 k_{nls}^2}{2m} + \hbar|\omega_L|(2n+|l|+1) + \hbar\omega_L(l+gs). \tag{5}$$

The corresponding allowed wave numbers are then

$$k_{nls} = k_0\sqrt{1-\frac{1}{E}[(2n+|l|+1)\hbar|\omega_L| + (l+gs)\hbar\omega_L]}, \tag{6}$$

where E is the total energy determined by the electron source, and $k_0 = \sqrt{2mE}/\hbar$ is the wave number for a plane (non-vortex) wave propagating freely along the z-axis. For electron vortices, the phase acquired upon propagation depends on the magnetic field. We see from (6) that the geometric path depends upon the direction of the angular momentum through the signs of l and s. This corresponds to a phase $\theta_{nls} = k_{nls}z$ acquired upon propagation which depends (via the Larmor frequency) on the magnetic field and on both the spin and orbital angular momenta.

If the magnetic energy is small compared to the total energy (a situation justified e.g. for electrons in TEM experiments), i.e. $(2n+|l|+1)\hbar|\omega_L| + (l+gs)\hbar\omega_L \ll E$, we can apply the paraxial approximation to the wave numbers (6). The corresponding phase shift accumulated along the trajectory of the vortex then comprises three parts:

$$\theta_{nls} = k_0 z - (2n+|l|+1)|k_L|z - (l+gs)k_L z, \tag{7}$$

where $k_L = \sqrt{\frac{m}{2E}}\mu_B B_z/\hbar$ is a spatial frequency which corresponds to the Larmor temporal frequency ω_L. The first term describes the phase evolution in free space; the second depends on the energy of the transverse motion due to the magnetic field, and the third term arises from the Zeeman interaction with the total angular momentum. In the following it is this latter term which is important, as it causes a different phase shift for vortex states with opposite helicity. We note that electrons in superpositions of left and right spin components should result in a spin Faraday rotation, analogous to optics. Here we concentrate on OAM Faraday rotation for which there is no optical counterpart.

Just like for the optical Faraday effect, the differential phase shifts become observable as a rotation angle for electrons in superpositions of vortex states with opposite handedness. As they originate from the interaction of the magnetic dipole moment with the external field, the electron Faraday effect does not require the mediation of an optically active medium but occurs in vacuum!

3. Considerations on observing the Faraday effect for electrons

Electron vortex states have recently been generated in transmission electron microscopes (TEM) via diffraction from nano-fabricated holograms [12, 17–19]. Using suitably designed holograms, also superpositions of vortex states can be generated (see appendix B). The required shape of the holograms is determined by the interference pattern of the target state with a reference wave function, e.g. a plane or spherical wave, resulting in transverse or longitudinal separation of the diffraction orders respectively.

In order to realize electron Faraday rotation we require electrons in a superposition of two modes with the same spin and radial mode number but opposite vorticity $\pm l$. The probability density then has an azimuthal dependence

$$\frac{1}{2}\left|\psi_{nls} + \psi_{n(-l)s}\right|^2 \propto \cos^2[l(\phi - \Phi_B)], \tag{8}$$

where we define

$$\Phi_B = k_L z = \frac{1}{\hbar}\sqrt{\frac{m}{2E}}\mu_B B_z z. \tag{9}$$

For $n = 0$ this is a petal pattern consisting of $2|l|$ maxima equally spaced around a circle, which after propagating through a region of a longitudinal magnetic field is rotated through the angle Φ_B. The maxima are separated by phase singularity lines, where the phase changes by π and the probability density vanishes. For the case of $l = \pm 1$ the transverse profile, shown in figure 3, is that of the HG_{10} Hermite–Gaussian mode. Here the analogy with optical polarization is clearest, with the $l = \pm 1$ components corresponding to the right and left handed circular polarization states, and the nodal line to the linear polarization.

While the phase change depends on l, the rotation of the intensity pattern is independent of l. The Laguerre–Gauss modes form a complete basis with which an arbitrary wavefunction can be described, and therefore any intensity and phase profile will rotate through the same angle Φ_B [8].

So far we have considered the eigenstates of (2) with a transverse scale determined by the magnetic field strength through the parameter w_B. A beam with the same radial profile but a width $w \neq w_B$ is, however, no longer an eigenstate and will therefore change upon propagation. Solving the paraxial wave equation (see appendix A) we find that the radial profile

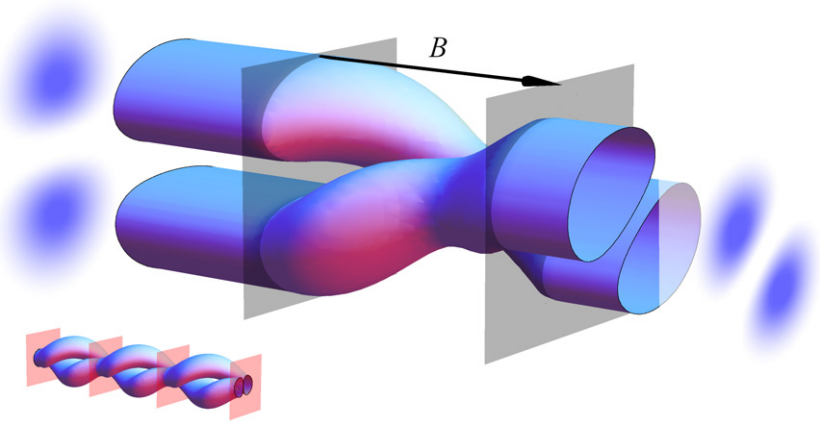

Figure 3. The electron density distribution rotates when propagating through a parallel magnetic field, and at the same time varies its beam waist periodically, with twice the period of the rotation (see inset).

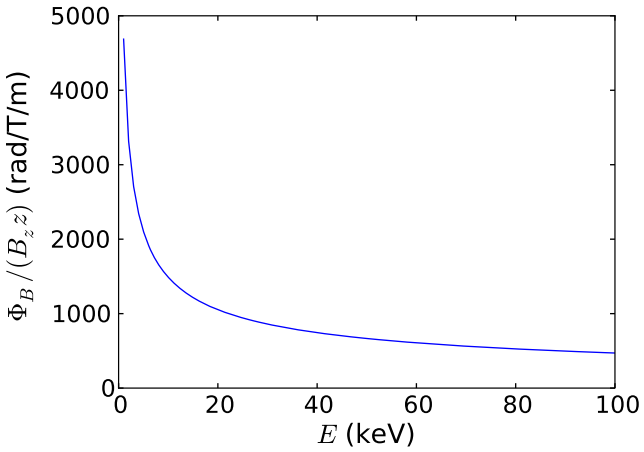

Figure 4. Verdet parameter as a function of energy, i.e. the rotation angle per T and m.

retains the same Laguerre–Gauss form, only now expands and contracts periodically in time, or equivalently with propagation distance (A.7). This contraction happens at twice the Larmor frequency and hence twice every full rotation. The width variation can be understood in terms of the competition between diffraction, which dominates when $w < w_B$, and the confining effect of the magnetic field, which dominates when $w > w_B$. This is illustrated in figure 3.

The rotation angle Φ_B, depends on the initial kinetic energy E of the electrons, as detailed in (9); as slow electrons spend more time in the magnetic field, their rotation angle is larger. While optical Faraday rotation is characterized by the Verdet constant (a proportionality constant of rotation angle per propagation distance and magnetic field strength), the electron 'Verdet' parameter varies with kinetic energy (see figure 4).

Even with low-energy TEM, measuring the proposed deflection due to an interaction with a perpendicularly-magnetized sample remains challenging, in particular the necessity to distinguish Faraday rotation from the usual cycloid motion of an electron beam within

magnetic lenses. Ignoring relativistic corrections, typical values ($E = 60$ keV, sample thickness $= 100$ nm, longitudinal field $B = 1$ T) yields a rotation about the beam axis of 0.06 mrad. In certain geometries differential phase contrast techniques routinely measure deflections of this magnitude, when the rotation can be projected by long camera lengths to give measurable deflections. A more promising experimental approach will be to consider low energy electron beams. Low energy photoelectrons ejected by circularly polarized photons are also known to carry OAM [20] and the subsequent propagation of these electrons through magnetic thin films may also visualize Faraday effects.

4. Conclusions

We have demonstrated that for electron vortex states propagating in a longitudinal magnetic field the Zeeman interaction produces an OAM dependent dispersion. This results in a rotation of the probability density of a superposition of vortex states about the beam axis, analogous to the optical Faraday effect. To the best of our knowledge this is a new concept, it is an effect that is not present in optics, and it may lead to applications in electron spectroscopy. The magnitude of the rotation scales with the magnitude of the magnetic field, and increases with decreasing energy. There are a number of interesting applications which may follow. OAM Faraday rotation provides the possibility of spatially resolved measurements of longitudinal magnetic field components, analogous to the measurement of transverse fields in Lorentz microscopy, by measuring the rotation angle of a vortex superposition. Moreover, we note that in the approximation considered here, spin and OAM are separately conserved. This would not be expected for relativistic non-paraxial beams [13] or spatially varying magnetic fields [21], suggesting a route to investigating intrinsic spin–orbit coupling in an electron vortex beam, via a spin-dependence of the rotation angle.

Acknowledgments

This work was supported by the Future and Emerging Technologies (FET) programme for Research of the European Commission, under the FET Open grant agreement PHORBITECH no. FP7-ICT-255914, and EPSRC Bridging the Gap. CG is supported under a SUPA Prize Studentship. We thank D MacLaren, D McGrouther and S McVitie for stimulating discussions.

Appendix A. Calculation of beam width variation using the paraxial approximation

To find the propagation of a beam with a given beam waist we evaluate the time-independent Schrödinger equation with Hamiltonian (2) as before in the paraxial approximation. We assume a solution of the form

$$\psi(r, \phi, z) = u(r, \phi, z)\, \mathrm{e}^{\mathrm{i}k_0 z}, \tag{A.1}$$

where $u(r, \phi, z)$ is an envelope function which describes the evolution of the beam profile upon propagation. k_0 is as defined in the main text. If u varies sufficiently slowly with z we can use the paraxial approximation

$$\left|\frac{\partial^2 u}{\partial z^2}\right| \ll \left|2k_0 \frac{\partial u}{\partial z}\right|, \left|\nabla_\perp^2 u\right|. \tag{A.2}$$

Then, substituting (A.1) into the Schrödinger equation (now no longer including spin), we arrive at the paraxial wave equation

$$\nabla_\perp^2 u + 2\mathrm{i}\,k_0 \frac{\partial u}{\partial z} - k_0^2 k_\mathrm{L}^2 r^2 u - \frac{2k_0 k_\mathrm{L}}{\hbar}\hat{L}_z u = 0. \tag{A.3}$$

The first two terms here are the same as in the paraxial equation for an optical beam propagating in vacuum, or for an electron beam in field-free space. The third term represents the confining effect of the magnetic field, and the final term gives the Zeeman interaction. For an OAM eigenstate with $u \propto e^{\mathrm{i}l\phi}$, the last term takes a constant value $-2k_0 k_\mathrm{L} l u$. We can then factor out the phase due to the Zeeman interaction by writing

$$u = v\,\mathrm{e}^{-\mathrm{i}lk_\mathrm{L}z}, \tag{A.4}$$

for some function $v(r, \phi, z)$. v then satisfies the equation

$$\nabla_\perp^2 v + 2\mathrm{i}\,k_0 \frac{\partial v}{\partial z} - k_0^2 k_\mathrm{L}^2 r^2 v = 0. \tag{A.5}$$

This equation has the same form as the equation from paraxial optics for a medium with quadratically varying refractive index $n(r) = n_0 - \frac{1}{2}n_2 r^2$, where n_0 and n_2 are constants (see for example [22]), only here $n_2 \to k_\mathrm{L}^2$. Such an optical system supports Laguerre–Gauss type modes which experience a periodic width variation due to the competition between diffraction and the focusing effect produced by the refractive index variation. A similar effect is described in [23], for the propagation of vortex wavepackets in a transverse field.

The solutions can be written [24, 25] as

$$v_{nl}(r, \phi, z) = \sqrt{\frac{2n!}{\pi(n+|l|)!}}\frac{1}{w(z)}\left(\frac{\sqrt{2}r}{w(z)}\right)^{|l|}\mathrm{e}^{-r^2/w^2(z)}L_n^{|l|}\left(\frac{2r^2}{w^2(z)}\right)\mathrm{e}^{\mathrm{i}l\phi}$$
$$\times \exp\left[-\mathrm{i}\frac{k_0 r^2}{2R(z)}\right]\mathrm{e}^{-\mathrm{i}(2n+|l|+1)\xi(z)}, \tag{A.6}$$

where $w(z)$ is the beam width, $R(z)$ is the wavefront radius of curvature and $\xi(z)$ gives the longitudinal phase shift. The equation (A.6) is the same as for the LG modes in free space, except here the functions $w(z)$, $R(z)$ and $\xi(z)$ are different. Choosing $z = 0$ to coincide with one of the minima of $w(z)$, and calling this minimum value w_0, the width function can be written, for the electron beam in a magnetic field, as

$$w(z) = w_\mathrm{B}\sqrt{1 - \left[1 - \left(\frac{w_0}{w_\mathrm{B}}\right)^2\right]\cos(2k_\mathrm{L}z)}. \tag{A.7}$$

Appendix B. Diffraction grating patterns for production of electron vortex superpositions

For interference with a plane wave $\psi \propto \mathrm{e}^{\mathrm{i}k_x x}$, in which case the diffraction orders will be separated transversely, a suitable hologram pattern is generated from

$$|\psi^2|_\mathrm{holo} = \begin{cases} 1 & \text{if } \frac{1}{3}|2\cos l(\phi - \phi_0) + \mathrm{e}^{\mathrm{i}k_x x}|^2 > \frac{1}{2}, \\ 0 & \text{otherwise,} \end{cases} \tag{B.1}$$

where ϕ_0 specifies the orientation of the singularity lines. A grating producing a superposition of $l = 1$ and -1 modes in the first diffraction order is shown in figure B.1(a), where we have

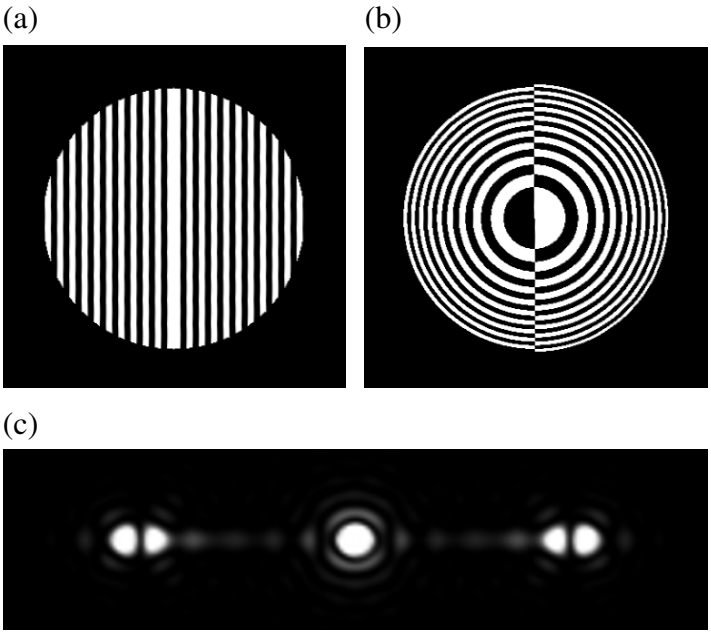

Figure B.1. (a) Hologram grating to produce a superposition of vortex modes with $l = \pm 1$. (b) Grating to produce the same superposition but with the diffraction orders separated longitudinally along the beam axis. (c) Diffraction pattern produced by grating in (a), with the desired superposition in the ± 1 diffraction orders.

chosen $\phi_0 = 0$. Note that the left and right sides of the grating are displaced by half a period with respect to one another, introducing the necessary π phase shift. In a similar way a hologram which separates the diffracted beam components longitudinally rather than transversely could be used [18, 19]. An example of this type of grating is shown in figure B.1(b). This is calculated using the same method, only with the plane wave factor $\psi \propto e^{ik_x x}$ replaced with the spherical wave profile $\psi \propto e^{iCr^2}$, where C is a constant which determines the curvature of the wavefront, and hence the spacing of the diffraction orders. Such grating patterns can be produced in the same way as those already used to generate single vortex modes. We note that gratings which generate superpositions of vortex beams from beams that have flat phasefronts have recently been produced and used to investigate the Gouy phase for electrons [26].

References

[1] Kanorsky S I, Weis A, Wurster J and Hänsch T W 1993 Quantitative investigation of the resonant nonlinear faraday effect under conditions of optical hyperfine pumping *Phys. Rev.* A **47** 1220–6

[2] Labeyrie G, Miniatura C and Kaiser R 2001 Large faraday rotation of resonant light in a cold atomic cloud *Phys. Rev.* A **64** 033402

[3] Warwick J W and Dulk G A 1964 Faraday rotation on decametric radio emissions from jupiter *Science* **145** 380–3

[4] Mendillo M 2006 Storms in the ionosphere: patterns and processes for total electron content *Rev. Geophys.* **44** RG4001

[5] Andrews D L 2008 *Structured Light and its Applications* (New York: Academic)

[6] Franke-Arnold S, Allen L and Padgett M J 2008 Advances in optical angular momentum *Laser Photon. Rev.* **2** 299–313
[7] Löffler W, van Exter M P, 't Hooft G W, Nienhuis G, Broer D J and Woerdman J P 2011 Search for Hermite–Gauss mode rotation in cholesteric liquid crystals *Opt. Express* **19** 12978–83
[8] Allen L and Padgett M J 2007 Equivalent geometric transformations for spin and orbital angular momentum of light *J. Mod. Opt.* **54** 487–91
[9] Franke-Arnold S, Gibson G, Boyd R W and Padgett M J 2011 Rotary photon drag enhanced by a slow-light medium *Science* **333** 65
[10] Bliokh K Y, Bliokh Y P, Savel'ev S and Nori F 2007 Semiclassical dynamics of electron wave packet states with phase vortices *Phys. Rev. Lett.* **99** 190404
[11] Uchida M and Tonomura A 2010 Generation of electron beams carrying orbital angular momentum *Nature* **464** 737–9
[12] Verbeeck J, Tian H and Schattschneider P 2010 Production and application of electron vortex beams *Nature* **467** 301–4
[13] Bliokh K Y, Dennis M R and Nori F 2011 Relativistic electron vortex beams: angular momentum and spin–orbit interaction *Phys. Rev. Lett.* **107** 174802
[14] Lloyd S, Babiker M and Yuan J 2012 Quantized orbital angular momentum transfer and magnetic dichroism in the interaction of electron vortices with matter *Phys. Rev. Lett.* **108** 074802
[15] Landau L D and Lifshitz E M 1977 *Quantum Mechanics: Non-Relativistic Theory* (Oxford: Pergamon)
[16] Bliokh K Y, Schattschneider P, Verbeeck J and Nori F 2012 Electron vortex beams in a magnetic field: a new twist on Landau levels and Aharonov–Bohm states *Phys. Rev. X* at press (arXiv:1204.2780)
[17] McMorran B J, Agrawal A, Anderson I M, Herzing A A, Lezec H J, McClelland J J and Unguris J 2011 Electron vortex beams with high quanta of orbital angular momentum *Science* **331** 192–5
[18] Verbeeck J, Tian H and Béché A 2012 A new way of producing electron vortex probes for STEM *Ultramicroscopy* **113** 83–7
[19] Saitoh K, Hasegawa Y, Tanaka N and Uchida M 2012 Production of electron vortex beams carrying large orbital angular momentum using spiral zone plates *J. Electron Microsc.* **61** 171–7
[20] MacLaren D A *et al* 2009 Asymmetric photoelectron transmission through chirally-sculpted, polycrystalline gold *Phys. Chem. Chem. Phys.* **11** 8413–6
[21] Gallup G A, Batelaan H and Gay T J 2001 Quantum-mechanical analysis of a longitudinal Stern–Ggerlach effect *Phys. Rev. Lett.* **86** 4508–11
[22] Siegman A E 1986 *Lasers* (Mill Valley, CA: University Science Books)
[23] Gallatin G M and McMorran B 2012 Propagation of vortex electron wave functions in a magnetic field *Phys. Rev.* A **86** 012701
[24] Tien P K and Gordon J P 1965 Focusing of a light beam of Gaussian field distribution in continuous and periodic lens-like media *Proc. IEEE* **53** 129–36
[25] Newstein M and Rudman B 1987 LaGuerre-Gaussian periodically focusing beams in a quadratic index medium *IEEE J. Quantum Electron.* **23** 481–2
[26] McMorran B J, Agrawal A, Anderson I M, Herzing A, Lezec H J, McClelland J J and Unguris J 2011 Electron beams carrying quantized orbital angular momentum *Laser Science, OSA Technical Digest* paper LWL1 (Washington, DC: Optical Society of America)

B.2 Is the angular momentum of an electron conserved in a uniform magnetic field?

Is the Angular Momentum of an Electron Conserved in a Uniform Magnetic Field?

Colin R. Greenshields, Robert L. Stamps, Sonja Franke-Arnold, and Stephen M. Barnett*
SUPA School of Physics and Astronomy, University of Glasgow, Glasgow G12 8QQ, United Kingdom
(Received 25 July 2014; published 9 December 2014)

We show that an electron moving in a uniform magnetic field possesses a time-varying "diamagnetic" angular momentum. Surprisingly this means that the kinetic angular momentum of the electron may vary with time, despite the rotational symmetry of the system. This apparent violation of angular momentum conservation is resolved by including the angular momentum of the surrounding fields.

DOI: 10.1103/PhysRevLett.113.240404 PACS numbers: 03.65.-w, 11.30.-j, 41.75.-i, 42.50.Tx

Introduction.—There is an intimate relation between angular momentum and rotational symmetry, as encapsulated by Noether's theorem [1]. In particular, if a system is symmetric under rotation about a given axis, the angular momentum along that axis will be conserved. This is the case with free electron vortices, which in the last few years were predicted and observed in electron microscopes [2–5]. Electron vortex beams in field-free space have a cylindrically symmetric wave function and maintain a constant orbital angular momentum in the direction of propagation [2].

Based on the same argument of rotational symmetry it would seem that for an electron exposed to a uniform magnetic field its orbital angular momentum in the direction of the field must be conserved. This is indeed true of the angular momentum about the axis of the classical cyclotron orbit, and, furthermore, the energy eigenstates of an electron in a uniform magnetic field—the Landau states—have constant angular momentum [6,7].

On the other hand, it is known that the *kinetic* angular momentum of an electron, which describes its mechanical motion, is not necessarily constant even when the electron interacts with external fields which are rotationally symmetric [8]. The balance and redistribution of momentum and angular momentum between matter and fields is a fundamental problem of great general interest [9–12].

Recent investigations of vortex electron states in uniform and quasiuniform magnetic fields have revealed that the angular velocity of the electron depends not only on the field strength but also on the azimuthal quantum number and the radial position [7,13,14]. Furthermore, in these quantum states the average radial position of the electron is not in general constant, but rather changes as the wave function diffracts [14–16]. This contrasts sharply with the classical orbit in a uniform magnetic field, leading to the question of whether the angular momentum of the electron is in fact conserved.

In this Letter, we show that for an electron in a nonstationary state, the changing radius of the electron's probability distribution in fact gives rise to a time-varying *kinetic* angular momentum. The *canonical* angular momentum however remains constant. The apparent violation of angular momentum conservation is resolved by considering the angular momentum in the fields surrounding the electron. We show that the *total* kinetic angular momentum, including that of the fields, is conserved, as indeed it must be.

Results.—We consider an electron moving in a uniform magnetic field, and take the direction of this field to define the z axis. The (nonrelativistic) Hamiltonian for this system can be written in the form

$$H = \frac{1}{2m}(\mathbf{p}^{\mathrm{kin}})^2, \tag{1}$$

where $\mathbf{p}^{\mathrm{kin}} = m\mathbf{v} = \mathbf{p}^{\mathrm{can}} - e\mathbf{A}$ is the kinetic momentum, $\mathbf{p}^{\mathrm{can}} = -i\hbar\nabla$ is the canonical momentum, $e = -|e|$ is the charge of the electron, and m its mass. We choose a vector potential which in cylindrical polar coordinates (ρ, ϕ, z) has the form

$$\mathbf{A} = \frac{B\rho}{2}\hat{\boldsymbol{\phi}} \Rightarrow \mathbf{B} = \nabla \times \mathbf{A} = B\hat{\mathbf{z}}. \tag{2}$$

We note, for later reference, that this choice of vector potential corresponds to the Coulomb gauge, in that $\nabla \cdot \mathbf{A} = 0$. The Hamiltonian (1) can then be rewritten as [17]

$$H = \frac{1}{2m}(\mathbf{p}^{\mathrm{can}})^2 + \frac{1}{2}m\omega_L^2\rho^2 + \omega_L L_z^{\mathrm{can}}, \tag{3}$$

where $\omega_L = -eB/(2m)$ is the Larmor frequency and

$$L_z^{\mathrm{can}} = (\mathbf{r} \times \mathbf{p}^{\mathrm{can}})_z = -i\hbar\frac{\partial}{\partial\phi} \tag{4}$$

is the z component of canonical orbital angular momentum. As the z component of linear momentum $p_z^{\mathrm{kin}} = p_z^{\mathrm{can}}$ commutes with the Hamiltonian, the motion of the electron

in the z direction is unaffected by the magnetic field. This means that for an electron beam propagating along the z axis we need only consider the z component of angular momentum. Furthermore, as the Hamiltonian, in our chosen gauge, is independent of ϕ it commutes with the canonical angular momentum $[L_z^{\mathrm{can}}, H] = 0$ and, hence, L_z^{can} is conserved [15].

Consider an electron wave function with cylindrical symmetry so that

$$\Psi = u(\rho, z, t)e^{i\ell\phi}. \tag{5}$$

We make no assumption about the form of the function u, so that in general this will not be an energy eigenstate. This state is, however, an eigenstate of L_z^{can} and hence the expectation value of its angular momentum has the time-independent value

$$\langle L_z^{\mathrm{can}} \rangle = \ell\hbar. \tag{6}$$

This is eminently reasonable as the system is symmetric under rotation about the z axis, so that according to Noether's theorem the z component of the angular momentum should be conserved.

In the presence of a magnetic field, the kinetic orbital angular momentum differs from its canonical counterpart:

$$L_z^{\mathrm{kin}} = (\mathbf{r} \times \mathbf{p}^{\mathrm{kin}})_z = L_z^{\mathrm{can}} + m\omega_L\rho^2 \tag{7}$$

[8], where we have used the definition of the kinetic linear momentum and the specific form of the vector potential (2). We see that the field-dependent contribution to the kinetic angular momentum is associated with a rotation of the electron probability distribution at constant angular velocity ω_L. This is consistent with Larmor's theorem [18] and can be interpreted as a diamagnetic response of the electron to the external magnetic field [19].

The expectation value of the kinetic orbital angular momentum can be expressed as

$$\langle L_z^{\mathrm{kin}} \rangle = \ell\hbar + \langle I_z \rangle \omega_L, \tag{8}$$

where we have used the fact that the expectation value of the z component of the electron's moment of inertia is

$$\langle I_z \rangle = m\langle \rho^2 \rangle. \tag{9}$$

This means that the kinetic angular momentum of the electron will be constant only if the radial probability distribution is constant. The squared radius ρ^2 does not commute with the Hamiltonian, however, meaning this quantity is not a constant of motion [6]. This means that, in contrast with the classical motion, the mean value $\langle \rho^2 \rangle$ will not, in general, be a constant.

It can be seen from the form of the Hamiltonian (3) that the radial coordinate exhibits a harmonic motion. This can be understood as the radial diffraction of the electron wave function in a harmonic potential generated by the interaction with the magnetic field [15]. The energy associated with the motion perpendicular to the magnetic field remains constant and has the expectation value

$$E_\perp = \left\langle H - \frac{1}{2m}(p_z^{\mathrm{kin}})^2 \right\rangle. \tag{10}$$

We will obtain the time behavior of the radial width, and later also of the kinetic orbital angular momentum, from Heisenberg's formalism:

$$\begin{aligned} \frac{\partial^2 \langle \rho^2 \rangle(t)}{\partial t^2} &= -\frac{1}{\hbar^2}\langle [[\rho^2, H], H] \rangle(t) \\ &= -\omega_c^2(\langle \rho^2 \rangle(t) - \tilde{\rho^2}), \end{aligned} \tag{11}$$

where $\omega_c = 2\omega_L = -eB/m$ is the classical cyclotron frequency and $\tilde{\rho^2} = (E_\perp - \omega_L\ell\hbar)/(m\omega_L^2)$ is the constant steady-state value which depends on the energy, the canonical angular momentum, and the magnetic field. It can be seen from (11) that the mean-square radius oscillates sinusoidally about the value $\tilde{\rho^2}$ at the cyclotron frequency. Setting $t = 0$ to correspond to a stationary point of this oscillation, we have

$$\langle \rho^2 \rangle(t) = \tilde{\rho^2} + (\langle \rho^2 \rangle(0) - \tilde{\rho^2})\cos(\omega_c t). \tag{12}$$

According to the relation (8) this is intrinsically linked to an oscillation of the kinetic angular momentum:

$$\langle L_z^{\mathrm{kin}} \rangle(t) = \tilde{L}_z^{\mathrm{kin}} + (\langle L_z^{\mathrm{kin}} \rangle(0) - \tilde{L}_z^{\mathrm{kin}})\cos(\omega_c t), \tag{13}$$

where the steady-state value of the kinetic angular momentum

$$\tilde{L}_z^{\mathrm{kin}} = \ell\hbar + m\omega_L\tilde{\rho^2} = \frac{2}{\omega_c}E_\perp \tag{14}$$

coincides with the classical value of the kinetic angular momentum for an electron with rotational kinetic energy $E_\perp$. In general, the angular momentum oscillates sinusoidally about the classical value, with the same frequency ω_c as the classical cyclotron motion. Only if the kinetic angular momentum is equal to the classical value does its expectation value remain constant. In this sense (14) defines the steady-state value $\tilde{\rho^2}$.

We can obtain an exact solution for (12) in the case when at $t = 0$ the wave function (5) has the Laguerre-Gaussian form

$$\begin{aligned} \Psi_{n,\ell}(0) = \mathrm{LG}_{n,\ell} \propto &\left(\frac{\rho\sqrt{2}}{\rho_0}\right)^{|\ell|} \exp\left(-\frac{\rho^2}{\rho_0^2}\right) L_n^{|\ell|}\left(\frac{2\rho^2}{\rho_0^2}\right) \\ &\times \exp\left[i(\ell\phi + k_z z)\right], \end{aligned} \tag{15}$$

where $\ell \in \mathbb{Z}$, $n = 0, 1, 2, \ldots$, and $L_n^{|\ell|}$ is an associated Laguerre polynomial. The index n specifies the number of radial nodes in the wave function, while ρ_0 is the width of the Gaussian envelope. The Laguerre-Gaussian wave functions can be used to describe electron vortex beams which have intrinsic orbital angular momentum $\ell\hbar$ [2] as well as electron beams with no intrinsic orbital angular momentum in the case when $\ell = 0$.

The mean-square radius of the Laguerre-Gaussian wave function (15) is equal to

$$\langle \rho^2 \rangle_{n,\ell}(0) = \frac{1}{2}(2n + |\ell| + 1)\rho_0^2 \tag{16}$$

[20]. As this depends on the radial index n, it follows that the kinetic angular momentum of the electron also depends on n, which is not the case in the absence of a magnetic field. The steady-state mean-square radius for the same electron energy obtained from (10) and (14) is

$$\tilde{\rho^2}_{n,\ell} = \frac{1}{4}(2n + |\ell| + 1)\left[1 + \left(\frac{\rho_B}{\rho_0}\right)^4\right]\rho_0^2, \tag{17}$$

where $\rho_B^2 = 2\hbar/(m|\omega_L|) = 4\hbar/|eB|$. As the phase of the wave function (15) does not depend on ρ, we have

$$\frac{\partial \langle \rho^2 \rangle_{n,\ell}(0)}{\partial t} = \frac{1}{\hbar}\mathrm{Im}\langle [\rho^2, H] \rangle_{n,\ell}(0) = 0, \tag{18}$$

meaning that this wave function corresponds to a stationary point of the oscillation. The time evolution of $\langle \rho^2 \rangle_{n,\ell}$ can therefore be obtained by substituting (16) and (17) into (12).

In the special case when $\rho_0 = \rho_B$ the Laguerre-Gaussian wave functions in (15) become the Landau energy eigenstates and we obtain the constant values of $\langle L_z^{\mathrm{kin}} \rangle_{n,\ell}$ expected in this case [7]. In general, however, the angular momentum will oscillate around the classical value, as illustrated in Fig. 1(a) for different ratios ρ_0/ρ_B and in Fig. 1(b) for different quantum numbers ℓ corresponding to canonical angular momenta $\ell\hbar$. If the canonical angular momentum is in the opposite direction to the magnetic field then the kinetic angular momentum may even change direction, as clearly seen for $\ell = -4$ in Fig. 1(b). We note that the moment of inertia increases with the radial quantum number n, resulting in larger amplitude oscillations, and that a reversal of the direction of the magnetic field corresponds to a shift of the phase of the oscillations by 180°.

As we have seen, the kinetic angular momentum may change with time despite the fact that the system is entirely rotationally symmetric—seemingly contradicting Noether's theorem. In order to restore angular momentum conservation we have to include the angular momentum contained in the field.

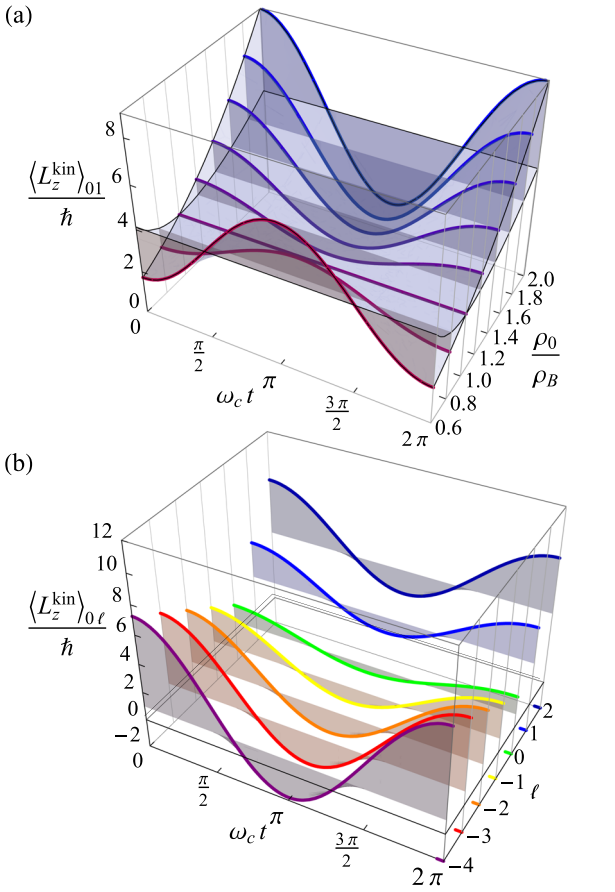

FIG. 1 (color online). Time evolution of the expectation value of the electron's kinetic orbital angular momentum for Laguerre-Gaussian states with $n = 0$ and a magnetic field in the positive z direction ($B > 0$). This is shown in (a) as a function of the initial width ρ_0 for $\ell = 1$, and in (b) for different values of ℓ assuming $\rho_0 = 1.5\rho_B$.

The combination of the externally imposed magnetic field and the electric field of the electron itself gives rise to a nonzero angular momentum density $\varepsilon_0 \mathbf{r} \times (\mathbf{E} \times \mathbf{B})$ [11]. The z component of the field angular momentum is

$$\begin{aligned} L_z^{\mathrm{kin\,field}} &= \int dV \varepsilon_0 [\mathbf{r} \times (\mathbf{E} \times \mathbf{B})]_z \\ &= \int dV \varepsilon_0 (\nabla \cdot \mathbf{E})(\mathbf{r} \times \mathbf{A}^{\perp})_z \end{aligned} \tag{19}$$

[21], where $\mathbf{A}^{\perp}$ is the (manifestly gauge invariant) transverse part of the vector potential, defined by $\nabla \cdot \mathbf{A}^{\perp} = 0$. In rewriting the second line we have used the fact that the electric field of the electron is longitudinal, that is, $\nabla \times \mathbf{E} = \mathbf{0}$. To complete our resolution we need only note that the first Maxwell equation is

$$\nabla \cdot \mathbf{E} = \frac{\varrho}{\varepsilon_0} = \frac{e}{\varepsilon_0}|\Psi|^2, \tag{20}$$

where ϱ is the charge density, so that

$$L_z^{\text{kin field}} = \frac{eB}{2}\langle\rho^2\rangle. \tag{21}$$

Using (8) and (21) the *total* kinetic angular momentum of the electron plus the field is, therefore,

$$L_z^{\text{kin total}} = \ell\hbar = L_z^{\text{can}}, \tag{22}$$

which is conserved, as it should be. Adding the kinetic angular momentum of the field to that of the electron has restored the unique and conserved total angular momentum.

Effect of gauge transformations.—We have worked throughout in the Coulomb gauge and uncovered the result that the canonical angular momentum of the electron is equal to the total angular momentum (with the value $\ell\hbar$). We can and should ask what we would have found had we worked in a different gauge. The kinetic angular momentum of the field is, as we have seen, gauge invariant. To underline this point, we note that it depends only on the magnetic field B and the mean-square radius $\langle\rho^2\rangle$, both of which are gauge invariant. Making a gauge transformation does change, however, both the vector potential and the phase of the wave function. The natural way to introduce a gauge transformation in quantum theory is through a local change in the phase of the wave function:

$$\Psi \to e^{i\chi(\mathbf{r},t)}\Psi. \tag{23}$$

In this case, the action of our canonical momentum operator on the state changes to

$$\mathbf{p}^{\text{can}}\Psi \to -i\hbar\nabla e^{i\chi(\mathbf{r},t)}\Psi = e^{i\chi(\mathbf{r},t)}(-i\hbar\nabla + \hbar\nabla\chi)\Psi. \tag{24}$$

This change is counterbalanced by the corresponding transformation of the vector potential

$$\mathbf{A} \to \mathbf{A} + \frac{\hbar}{e}\nabla\chi \tag{25}$$

so that the kinetic momentum $\mathbf{p}^{\text{kin}}$ is unchanged. The z component of the canonical angular momentum is similarly changed by a gauge transformation to

$$L_z^{\text{can}} \to -i\hbar\frac{\partial}{\partial\phi} + \hbar\frac{\partial\chi}{\partial\phi}. \tag{26}$$

Interestingly, the expectation value of this quantity for our cylindrically symmetric state will still be $\ell\hbar$, as $|e^{i\chi(\mathbf{r},t)}\Psi|^2 = |\Psi|^2$ is independent of ϕ, and, in particular, $\langle\hbar\partial\chi/\partial\phi\rangle = 0$.

Discussion.—The magnitude of the diamagnetic contribution to the kinetic angular momentum is strongly dependent on the length scale. As can be seen from (8), it is characterized by the constant $-e/2 = 7.60\times 10^{-4}\hbar\ \text{T}^{-1}\,\text{nm}^{-2}$. In an atomic bound state with rms radius 1 Å, even in a field of strength 1 T the diamagnetic angular momentum is negligible compared to a single unit of canonical angular momentum. However, for unbound electrons, which can be distributed over a much larger area, the diamagnetic angular momentum can become significant, and may be the dominant contribution, both to the electron's kinetic angular momentum and to $E_\perp$. This can certainly be the case in transmission electron microscopes, where the electron beam may have a radius $\langle\rho^2\rangle^{1/2} \sim 1$ nm–100 μm and a field $\sim$1 T is provided by the objective lens. Note that in an electron microscope the radial dynamics occur in a reference frame moving with the electron along the z axis [2], and so can be observed as a function of the propagation distance [14,16].

While the creation of electron vortices has aroused a considerable interest in the orbital angular momentum of electron beams [22–24], little attention has been given previously to the angular momentum which arises in a magnetic field. Our diamagnetic angular momentum will occur with any electron beam, even those with no canonical orbital angular momentum. The canonical angular momentum is a manifestation of the cylindrical symmetry and is restricted to integer multiples of $\hbar$. In contrast, the diamagnetic contribution, and hence the kinetic angular momentum of the electron, may take any value.

It is interesting to ask why our electron carries two distinct angular momenta and where each of these might be expected to appear in experiment. The total angular momentum contains a part L_z^{kin} that may be ascribed to the electron, and a second part $L_z^{\text{kin field}}$ that depends on *both* the externally imposed magnetic field and the electric field due to the electron. This latter part may be assigned either to the field, which gives the kinetic momentum, or to the electron, giving the canonical momentum. This situation is reminiscent of the linear momentum of a photon in a dielectric medium, where two rival momenta, due to Abraham and Minkowski, are the kinetic and canonical momenta [25]. As with the photon, we can associate the canonical and kinetic momenta of the electron with wavelike and particlelike properties, respectively. Hence, an electron interference pattern should reveal the $e^{i\ell\phi}$ dependence associated with the canonical angular momentum [26]. Absorption of an electron by an initially neutral target, however, should transfer the kinetic angular momentum of the electron to the rotational motion of the target, with the remaining angular momentum retained by the electric field of the now charged target.

C. G. is supported by a SUPA Prize Studentship. We also acknowledge support from the UK EPSRC under Program Grants No. EP/I012451/1 and No. EP/L002922/1, and Bridging the Gap.

*Stephen.Barnett@glasgow.ac.uk

[1] E. Noether, Nachrichten der Königlichen Gesellschaft der Wissenschaften zu Göttingen, Math.-phys. Klasse **2**, 235 (1918); D. E. Neuenschwander, *Emmy Noether's Wonderful Theorem* (Johns Hopkins, Baltimore, MD, 2011).
[2] K. Y. Bliokh, Y. P. Bliokh, S. Savel'ev, and F. Nori, Phys. Rev. Lett. **99**, 190404 (2007).
[3] M. Uchida and A. Tonomura, Nature (London) **464**, 737 (2010).
[4] J. Verbeeck, H. Tian, and P. Schattschneider, Nature (London) **467**, 301 (2010).
[5] B. J. McMorran, A. Agrawal, I. M. Anderson, A. A. Herzing, H. J. Lezec, J. J. McClelland, and J. Unguris, Science **331**, 192 (2011).
[6] C. Li and Q. Wang, Physica (Amsterdam) **269B**, 22 (1999).
[7] K. Y. Bliokh, P. Schattschneider, J. Verbeeck, and F. Nori, Phys. Rev. X **2**, 041011 (2012).
[8] P. W. Hawkes and E. Kasper, *Principles of Electron Optics* (Academic Press, San Diego, 1996), Vol. 1, p. 24.
[9] E. J. Konopinski, Am. J. Phys. **46**, 499 (1978).
[10] J. M. Aguirregabiria and A. Hernandez, Eur. J. Phys. **2**, 168 (1981).
[11] H. J. Lipkin and M. Peshkin, Phys. Lett. **118B**, 385 (1982).
[12] S. M. Lloyd, M. Babiker, and J. Yuan, Phys. Rev. A **88**, 031802 (2013).
[13] P. Schattschneider, Th. Schachinger, M. Stöger-Pollach, S. Löffler, A. Steiger-Thirsfeld, K. Y. Bliokh, and F. Nori, Nat. Commun. **5**, 4586 (2014).
[14] G. Guzzinati, P. Schattschneider, K. Y. Bliokh, F. Nori, and J. Verbeeck, Phys. Rev. Lett. **110**, 093601 (2013).
[15] G. M. Gallatin and B. McMorran, Phys. Rev. A **86**, 012701 (2012).
[16] C. Greenshields, R. L. Stamps, and S. Franke-Arnold, New J. Phys. **14**, 103040 (2012).
[17] I. Bialynicki-Birula, Z. Bialynicka-Birula, and C. Śliwa, Phys. Rev. A **61**, 032110 (2000).
[18] L. Brillouin, Phys. Rev. **67**, 260 (1945); S. P. Heims and E. T. Jaynes, Rev. Mod. Phys. **34**, 143 (1962).
[19] C. Kittel, *Introduction to Solid State Physics* (Wiley, Hoboken, NJ, 2004).
[20] R. L. Phillips and L. C. Andrews, Appl. Opt. **22**, 643 (1983).
[21] C. Cohen-Tannoudji, J. Dupont-Roc, and G. Grynberg, *Photons and Atoms: Introduction to Quantum Electrodynamics* (Wiley, New York, 1997), p. 45.
[22] S. M. Lloyd, M. Babiker, and J. Yuan, Phys. Rev. Lett. **108**, 074802 (2012).
[23] I. P. Ivanov and D. V. Karlovets, Phys. Rev. Lett. **110**, 264801 (2013).
[24] J. Verbeeck, G. Guzzinati, L. Clark, R. Juchtmans, R. Van Boxem, H. Tian., A. Béché, A. Lubk, and G. Van Tendeloo, C.R. Phys. **15**, 190 (2014).
[25] S. M. Barnett, Phys. Rev. Lett. **104**, 070401 (2010); S. M. Barnett and R. Loudon, Phil. Trans. R. Soc. A **368**, 927 (2010).
[26] G. Guzzinati, L. Clark, A. Béché, and J. Verbeeck, Phys. Rev. A **89**, 025803 (2014).

B.3 Parallel axis theorem for free-space electron wavefunctions

New Journal of Physics
The open access journal at the forefront of physics

Deutsche Physikalische Gesellschaft DPG
IOP Institute of Physics

Published in partnership with: Deutsche Physikalische Gesellschaft and the Institute of Physics

OPEN ACCESS

RECEIVED
14 April 2015

REVISED
15 July 2015

ACCEPTED FOR PUBLICATION
11 August 2015

PUBLISHED
9 September 2015

PAPER

Parallel axis theorem for free-space electron wavefunctions

Colin R Greenshields, Sonja Franke-Arnold and Robert L Stamps

SUPA School of Physics and Astronomy, University of Glasgow, Glasgow G12 8QQ, UK

E-mail: Sonja.Franke-Arnold@glasgow.ac.uk **and** Robert.Stamps@glasgow.ac.uk

Keywords: free electron vortices, orbital angular momentum, cyclotron motion

Abstract

We consider the orbital angular momentum of a free electron vortex moving in a uniform magnetic field. We identify three contributions to this angular momentum: the canonical orbital angular momentum associated with the vortex, the angular momentum of the cyclotron orbit of the wavefunction, and a diamagnetic angular momentum. The cyclotron and diamagnetic angular momenta are found to be separable according to the parallel axis theorem. This means that rotations can occur with respect to two or more axes simultaneously, which can be observed with superpositions of vortex states.

1. Introduction

In classical mechanics, an electron moving in a uniform magnetic field follows a circular orbit in the plane perpendicular to the field, as dictated by the Lorentz force. This so-called cyclotron motion, which occurs even in the absence of a central potential, plays a role in areas as diverse as particle physics [1, 2], electron microscopy [3], plasma physics [4], and also in microwave ovens [5].

Electrons can also possess quantized canonical orbital angular momentum which does not depend on the presence of a magnetic field. This is well known in the case of bound states in atoms and quantum dots [6], in which there is a confining potential, however recently it was discovered that *free* electrons can be imprinted with orbital angular momentum. Electron vortex beams [7–10], generated, for example, in electron microscopes, have twisted wavefronts, and resemble freely propagating atomic orbitals. The understanding, manipulation and exploitation of this angular momentum for a range of technological applications is currently a very active area of investigation [11–21].

In a magnetic field, an electron can possess both canonical orbital angular momentum, *and* angular momentum arising from the interaction with the field. If the magnetic field is uniform, the canonical angular momentum in the direction of the field is independent of the field and is constant [22]. Meanwhile, the magnetic field induces an additional current within the electron's wavefunction which gives rise to a diamagnetic angular momentum [23–26]. Manipulating the canonical and diamagnetic orbital angular momenta of free electrons recently led to the first direct imaging of Landau states [27, 28]. In addition to the diamagnetic rotation of an electron's wavefunction, however, in a magnetic field there will generally also be a cyclotron orbit of the centre of mass of the wavefunction [22, 29]. The angular momentum associated with this cyclotron motion has not previously been considered.

In this paper, we show that the total orbital angular momentum of the electron is described by the parallel axis theorem. This angular momentum comprises the canonical and diamagnetic components, which are associated with rotation relative to the centre of mass of the wavefunction, and a cyclotron component which has expectation value equal to that for the classical orbit. Interestingly, for free electrons all three of these components can have similar magnitude. This means that the trajectory of the electron is strongly dependent on how these angular momenta add and subtract. Further, we show that different cyclotron orbits can be superposed, leading to rotations with respect to multiple parallel axes, and periodic interference. Our results suggest novel means of structuring electron beams for use in specific applications, such as probing magnetic and chiral materials.

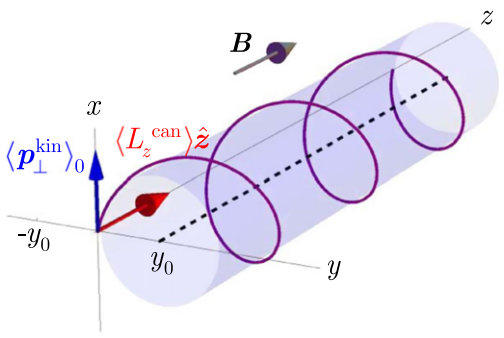

Figure 1. Cyclotron trajectory of the centre of mass of the wavefunction. This orbit occurs with respect to the axis $y = y_0$, the position of which depends on the initial transverse momentum $\langle \boldsymbol{p}_\perp^{\rm kin}\rangle_0$ as well as the magnetic field. Also indicated is the direction of the canonical orbital angular momentum $\langle L_z^{\rm can}\rangle\hat{\boldsymbol{z}}$.

2. Model

We consider an otherwise free electron moving under the influence of a uniform magnetic field. We take the direction of this magnetic field to define our z axis, and consider the motion of the electron within the x–y plane. The electron may also be moving in the z direction, however the component of its momentum in this direction is a constant of motion [25], and will not affect our results. We consider non-relativistic energies, meaning that the spin angular momentum is also constant, and can be separated from the orbital motion of the electron [30]. In what follows, we shall consider only the electron's orbital angular momentum. The magnetic field $\boldsymbol{B} = B\hat{\boldsymbol{z}}$ can be described by the cylindrically symmetric vector potential $\boldsymbol{A} = B\rho\hat{\boldsymbol{\phi}}/2$, where ρ and ϕ are cylindrical polar coordinates. This choice of gauge is convenient as it allows us to exploit the rotational symmetry of the magnetic field. Our Hamiltonian is therefore

$$H = \frac{\left(\boldsymbol{p}_\perp^{\rm kin}\right)^2}{2m} = \frac{1}{2m}\left[\left(\boldsymbol{p}_\perp^{\rm can}\right)^2 + \frac{1}{4}e^2B^2\rho^2 - eBL_z^{\rm can}\right], \tag{1}$$

where $\boldsymbol{p}_\perp^{\rm kin} = m\boldsymbol{v}_\perp = \boldsymbol{p}_\perp^{\rm can} - e\boldsymbol{A}_\perp$ is the component of the electron's kinetic momentum in the plane perpendicular to the magnetic field, $\boldsymbol{p}_\perp^{\rm can} = -\mathrm{i}\hbar\,\boldsymbol{\nabla}_\perp$ is the corresponding canonical momentum component, $L_z^{\rm can} = \rho p_\phi^{\rm can} = -\mathrm{i}\hbar\,\partial/\partial\phi$ is the z-component of the canonical orbital angular momentum, $e = -|e|$ is the electron's charge, and m its mass.

We are interested in the evolution of non-stationary states of the system, described by the time-dependent Schrödinger equation

$$\mathrm{i}\hbar\frac{\partial\Psi\left(\boldsymbol{r}_\perp, t\right)}{\partial t} = H\Psi\left(\boldsymbol{r}_\perp, t\right), \tag{2}$$

where $\boldsymbol{r}_\perp = (\rho, \phi)$ is the position of the electron in the plane perpendicular to the magnetic field. Note that if the electron is moving along the z axis with a velocity v_z, the Schrödinger equation (2) describes the state of the electron after a propagation distance of $z = v_z t$ [27].

An electron with momentum transverse to the magnetic field will exhibit cyclotron motion. This is conventionally described in a classical context. Here we will derive the cyclotron motion by assuming an electron wavefunction

$$\Psi(t=0) = \Psi_0 = u(\rho)\exp\left[\mathrm{i}\left(\ell\phi + \frac{p_{\rm c}}{\hbar}x\right)\right], \tag{3}$$

where $\ell \in \mathbb{Z}$. We have defined the x axis as the direction of the transverse kinetic momentum at $t = 0$. This state has a rotationally symmetric probability density $|\Psi_0|^2 = |u(\rho)|^2$, and an expectation value of canonical angular momentum $\langle L_z^{\rm can}\rangle = \ell\hbar$. We shall see that the momentum $\langle \boldsymbol{p}_\perp^{\rm kin}\rangle_0 = p_{\rm c}\hat{\boldsymbol{x}}$ results in a cyclotron orbit of the wavefunction.

Note that in our model the canonical orbital angular momentum is not collinear with the instantaneous direction of propagation of the wavefunction. This is illustrated in figure 1. The angular momentum is in the direction of the magnetic field, while the kinetic momentum has a component perpendicular to the magnetic field. This contrasts with vortex states, either in field-free space or in a magnetic field, which are energy eigenfunctions, as these have momentum and angular momentum which are collinear [29, 31]. Electrons in non-stationary states can have angular momentum at an arbitrary angle to their direction of propagation,

however [22, 32, 33]. Here, as a result of the cyclotron orbit, the *time-averaged* expectation value of kinetic momentum is collinear with the angular momentum $\langle L_z^{\text{can}} \rangle$.

3. Electron trajectories and angular momentum

In the following we will show that the different forms of angular momentum give rise to rotations with respect to more than one axis. This can be seen by examining the 'trajectories' associated with the electron's probability distribution and current density.

First, we will consider the expectation value of the electron's position, which is equivalent to the centre of mass of its probability distribution. Differentiating twice with respect to time, we obtain the equation of motion

$$\begin{aligned}\frac{\partial^2 \left\langle \boldsymbol{r}_\perp \right\rangle (t)}{\partial t^2} &= -\frac{1}{\hbar^2}\left\langle \left[\left[\boldsymbol{r}_\perp, H\right], H\right]\right\rangle (t), \\ &= -\omega_c^2 \left\langle \boldsymbol{r}_\perp - \left[x + p_y^{\text{kin}}/(eB)\right]\hat{\boldsymbol{x}} - \left[y - p_x^{\text{kin}}/(eB)\right]\hat{\boldsymbol{y}}\right\rangle (t), \\ &= -\omega_c^2 \left(\left\langle \boldsymbol{r}_\perp \right\rangle (t) - y_0 \hat{\boldsymbol{y}}\right),\end{aligned} \tag{4}$$

where $\omega_c = -eB/m$ is the cyclotron angular velocity and $y_0 = p_c/(|e|B)$. Here we have used the fact that the quantity $\left[x + p_y^{\text{kin}}/(eB)\right]\hat{\boldsymbol{x}} + \left[y - p_x^{\text{kin}}/(eB)\right]\hat{\boldsymbol{y}}$, which is the centre of the orbit of a classical particle which has position $\boldsymbol{r}_\perp$ and momentum $\boldsymbol{p}_\perp^{\text{kin}}$ [34], has the constant expectation value $y_0\hat{\boldsymbol{y}}$. The initial position and velocity of the centre of mass of the probability distribution are given by $\langle \boldsymbol{r}_\perp \rangle (0) = \boldsymbol{0}$ and

$$\frac{\partial \left\langle \boldsymbol{r}_\perp \right\rangle (0)}{\partial t} = -\frac{\mathrm{i}}{\hbar}\left\langle \left[\boldsymbol{r}_\perp, H\right]\right\rangle (0) = \frac{p_c}{m}\hat{\boldsymbol{x}} \tag{5}$$

respectively, and substituting these into (4) yields the trajectory

$$\langle \boldsymbol{r}_\perp \rangle (t) = y_0\left[\sin \omega_c t \hat{\boldsymbol{x}} + \left(1 - \cos \omega_c t\right)\hat{\boldsymbol{y}}\right]. \tag{6}$$

This trajectory, illustrated in figure 1, is a circular orbit with radius

$$\sigma = |y_0| = \left|\frac{p_c}{eB}\right| \tag{7}$$

and angular velocity ω_c—the cyclotron orbit of a classical particle with the momentum p_c. The trajectory of the centre of mass of the probability distribution is therefore independent of the canonical angular momentum of the electron.

The canonical angular momentum is instead associated with a circulation of current within the electron's probability distribution. This can be seen by examining the probability current density $\boldsymbol{j}_\perp(\boldsymbol{r}_\perp, t) = \text{Re}(\Psi^* \boldsymbol{p}_\perp^{\text{kin}} \Psi)/m$. To do so we have solved the time-dependent Schrödinger equation (2) numerically using the Chebyshev method [35–37], as described in appendix A. We must first specify the radial distribution, $u(\rho)$, of the initial wavefunction (3). Here we will set this to be the same as that of a Landau state—one of the energy eigenstates of the system:

$$u(\rho) = u_{n,|\ell|}^{\text{Lan}}(\rho) = N_{n,|\ell|}\left(\frac{\rho\sqrt{2}}{\rho_B}\right)^{|\ell|} \exp\left(-\frac{\rho^2}{\rho_B^2}\right) L_n^{|\ell|}\left(\frac{2\rho^2}{\rho_B^2}\right), \tag{8}$$

where $n = 0, 1, 2, \ldots$ is the radial quantum number, $L_n^{|\ell|}$ is an associated Laguerre polynomial, $\rho_B = \sqrt{4\hbar/|eB|}$ is the width of the Gaussian envelope and $N_{n,|\ell|} = \sqrt{2n!/[\pi(n + |\ell|)!]}/\rho_B$ is a normalization constant. This means that if $p_c = 0$, the electron would be in a Landau state. An arbitrary radial distribution could be decomposed in terms of the eigenfunctions $u_{n,|\ell|}^{\text{Lan}}$.

The time-evolution of the probability density $|\Psi|^2$ and the current density $\boldsymbol{j}_\perp$ are shown in figure 2. Here the transverse momentum p_c has been chosen such that the radius of the cyclotron orbit is approximately equal to the width of the probability distribution. In (a) and (b) the electron has no net canonical orbital angular momentum, while in (c) and (d) it has a canonical orbital angular momentum $\ell = 1$. The evolution of these states is shown for different directions of the magnetic field, which result in different directions of the cyclotron orbit. Whereas the probability density follows a straightforward classical orbit, the current density is seen to depend in a non-trivial manner on both the wavefunction and the magnetic field. In particular, in contrast to the classical cyclotron trajectory, and also to orbital angular momentum eigenstates in the absence of a magnetic field, the current distribution here is not rotationally symmetric. The rotational symmetry of the probability distribution, with respect to its centre of mass, is preserved, however. This reflects the fact that the magnetic field

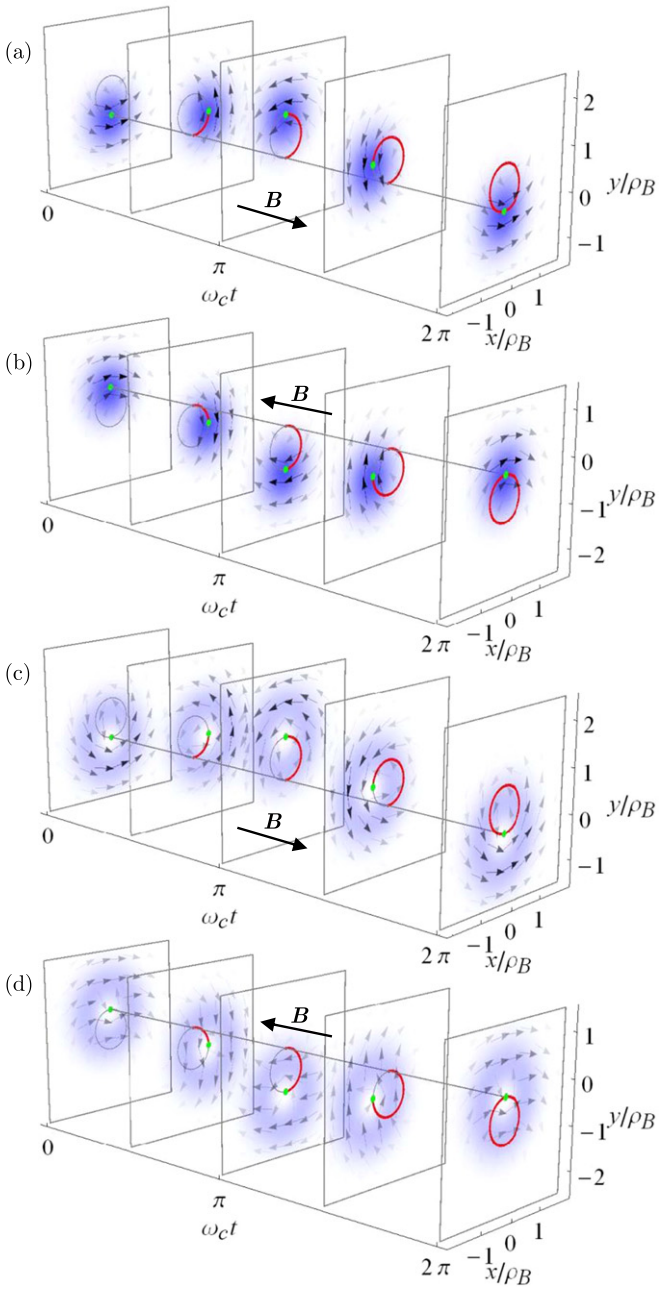

Figure 2. Probability density $|\Psi|^2$ and current density $\boldsymbol{j}_\perp$ for wavefunctions with canonical orbital angular momentum $\ell = 0$ (a), (b) and $\ell = 1$ (c), (d), for opposite directions of the magnetic field. In each case the transverse momentum is $p_c = 2\hbar/\rho_B$ and the wavefunction has the radial distribution $u^{\mathrm{Lan}}_{0,|\ell|}$. The red arcs indicate the trajectory of the centre of mass of the probability distribution, which is highlighted in green.

is rotationally symmetric, and the canonical angular momentum L_z^{can} is conserved. This means that the canonical orbital angular momentum of the electron is associated with a rotation axis at the centre of mass of the probability distribution, and is independent of the cyclotron orbit.

More surprising, perhaps, is that rotations in fact occur with respect to the cyclotron axis *and* the centre of mass axis even when the electron does not possess any net canonical angular momentum. This is as a result of the diamagnetic angular momentum that any electron wavefunction possesses in the presence of a magnetic field [23, 24]. This angular momentum arises as a result of the circulating current the magnetic field induces within the wavefunction, and is associated with a rotation of the probability density at the Larmor angular velocity $\omega_{\mathrm{L}} = \omega_{\mathrm{c}}/2 = -eB/(2m)$ [27, 38]. The diamagnetic angular momentum is equal to $L_z^{\mathrm{dia}} = I'\omega_{\mathrm{L}}$, where

$$I' = m\langle \rho'^2 \rangle \tag{9}$$

is the moment of inertia of the electron's probability distribution, in the reference frame of its centre of mass [25]. Here $\rho' = |\boldsymbol{r}_\perp - \langle \boldsymbol{r}_\perp \rangle|$ is the radial coordinate in this reference frame. This angular momentum has the

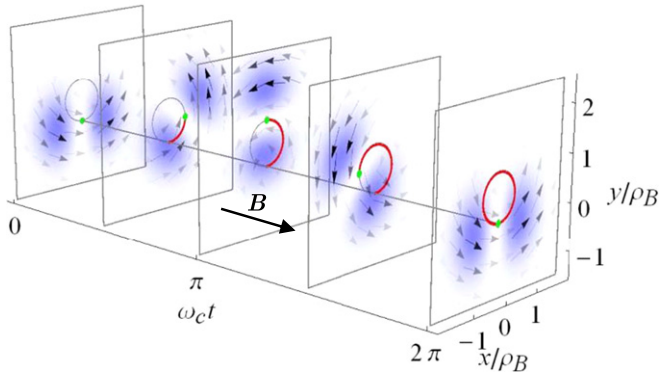

Figure 3. Probability density and current density for an equally weighted superposition of wavefunctions which both have transverse momentum $p_c = 2\hbar/\rho_B$, but have opposite values of canonical angular momentum $\ell = \pm 1$. The constituent states have the same radial distributions as in figure 2.

same direction as the external magnetic field, meaning that the associated magnetic moment, $\mu_z^{\text{dia}} = eL_z^{\text{dia}}/(2m)$, opposes the external field, in accordance with Lenz's law. In contrast to cyclotron motion, the diamagnetic rotation depends on there being an extended probability distribution, and vanishes in the classical limit. For the Landau radial distribution $u_{n,\ell}^{\text{Lan}}$, the mean square radius is $\langle \rho'^2 \rangle_{n,\ell}^{\text{Lan}} = (2n + |\ell| + 1)\rho_B^2/2$, and the diamagnetic angular momentum therefore takes the quantized values $L_z^{\text{dia, Lan}} = \text{sign}(B)(2n + |\ell| + 1)\hbar$ [29]. The effect of the diamagnetic angular momentum becomes clear when we consider a superposition of opposite values of canonical orbital angular momentum, such as that shown in figure 3. As this superposition has no net canonical angular momentum, the rotation of the electron's probability density with respect to its centre of mass is due entirely to the diamagnetic angular momentum. Previously we have interpreted this as a form of Faraday rotation for electrons [30].

In general, the orbital angular momentum with respect to the centre of mass axis will be given by a sum of canonical and diamagnetic contributions. The motion is thus described by two independent rotations: the cyclotron orbit, and the rotation around the instantaneous centre of mass axis due to the canonical and diamagnetic angular momenta.

4. Parallel axis theorem

The rotation of the electron's wavefunction is reminiscent of a classical rigid body. We will explore this analogy further by considering the kinetic angular momentum of the electron, which is the total mechanical angular momentum it possesses while moving in the magnetic field. This angular momentum has the z component

$$L_z^{\text{kin}} = \rho p_\phi^{\text{kin}} = L_z^{\text{can}} - \frac{1}{2}eB\rho^2, \tag{10}$$

with an expectation value of

$$\langle L_z^{\text{kin}} \rangle = \ell\hbar + I\omega_{\text{L}} \tag{11}$$

for any state with a canonical orbital angular momentum $\ell\hbar$. Here $I = m\langle \rho^2 \rangle$ is the moment of inertia of the electron's probability distribution for rotation with respect to the z axis. Just as with a rigid body, we can use the parallel axis theorem to express the moment of inertia I as a sum of two components:

$$I = m\rho_0^2 + I', \tag{12}$$

where $\rho_0 = |\langle \boldsymbol{r}_\perp \rangle| = \sqrt{2(1 - \cos\omega_c t)}\ \sigma$, with σ defined by (7), is the radial coordinate of the centre of mass, and I' is the moment of inertia with respect to the centre of mass axis, given by (9). These two components correspond to the cyclotron orbit of the wavefunction and its diamagnetic angular momentum respectively. The total kinetic angular momentum of the electron, which we obtain from (11) and (12), can therefore be expressed as

$$\langle L_z^{\text{kin}} \rangle = \ell\hbar + L_z^{\text{cyclo}} + L_z^{\text{dia}}, \tag{13}$$

where $L_z^{\text{cyclo}} = m\omega_{\text{L}}\rho_0^2 = (1 - \cos\omega_c t)m\omega_c\sigma^2$ is the angular momentum associated with the cyclotron orbit. While the relation between the kinetic and canonical angular momenta in (10) is true also for a classical point particle [39], the decomposition into separate cyclotron and diamagnetic components which follows from (12) is only meaningful for an extended probability distribution.

Unlike the canonical and diamagnetic components, the cyclotron angular momentum depends on our choice of reference axis. A natural choice is to consider the angular momentum with respect to the centre of the cyclotron motion. In this reference frame, which we reach by making the transformation $y \rightarrow \tilde{y} = y - y_0$, the cyclotron angular momentum has the constant value

$$\tilde{L}_z^{\text{cyclo}} = m\omega_c\sigma^2. \tag{14}$$

Irrespective of the reference frame, of course, the total kinetic angular momentum will be equal to the sum of the three components described.

One may expect that the cyclotron angular momentum, which exists classically, would be the dominant contribution to the electron's kinetic angular momentum. However, this need not be the case, as can be seen by considering typical parameters for free electrons in electron microscopes. For example, if an electron beam which is initially propagating parallel to a magnetic field is transmitted through a diffraction grating with a period $d = 100$ nm, the first diffraction order will have a net transverse momentum of $p_c = \hbar\,(2\pi/d) = h/d$, which corresponds to an energy of $p_c^2/(2\,m) = h^2/(2md^2) = 0.15$ meV. In a magnetic field of $B = 1$ T, the resulting cyclotron orbit, which has radius 41 nm, will have an angular momentum of $2.6\hbar$. This is of the same order of magnitude as the canonical angular momentum of the lowest order vortex states, and considerably smaller than that of vortex beams recently generated with a winding number of $\ell = 200$ [21]. Indeed, in a given magnetic field, the cyclotron angular momentum can in principle have any size, ranging from zero to macroscopic values, depending on the net transverse momentum p_c. The diamagnetic angular momentum can also take a wide range of values, as the mean square radius of the probability distribution is varied [25], although this has a lower limit due to the uncertainty principle and a maximum due to the requirement of spatial coherence. This means that the different rotations we have described can indeed occur on the same length scale, justifying the choices of parameters in our figures.

5. Superposition of cyclotron orbits

So far we have considered rotations with respect to two different axes—the cyclotron axis, as well as the centre of mass axis. The position of the cyclotron axis was defined by the transverse momentum p_c which appears in a plane wave factor in the wavefunction (3). Suppose, however, that we have a superposition of different transverse momenta. Arbitrary distributions of transverse momentum could be created using appropriately designed holograms [40–43]. A simple example would be the following superposition of two momenta, $p_{c,1}$ and $p_{c,2}$, which may also be associated with different canonical orbital angular momenta, ℓ_1 and ℓ_2:

$$\Psi_0 = \frac{u^{\text{Lan}}_{n,|\ell|}(\rho)}{\sqrt{2}}\exp\left[\mathrm{i}\left(\ell_1\phi + \frac{p_{c,1}}{\hbar}x\right)\right] + \frac{u^{\text{Lan}}_{n,|\ell_2|}(\rho)}{\sqrt{2}}\exp\left[\mathrm{i}\left(\ell_2\phi + \frac{p_{c,2}}{\hbar}x\right)\right]. \tag{15}$$

This is similar to the wavefunction formed when a plane wave is transmitted through a forked diffraction grating [10]. For the discussion here the particular form of the radial distribution is not important, and the Landau function has been chosen with numerical efficiency in mind. The evolution of such a state, here with equal and opposite values of both the transverse momentum and canonical angular momentum, is shown in figure 4. It can be seen that there are now two cyclotron orbits, which have different rotation axes. These are associated with different directions of the initial momentum p_c. As a result, the two components of the superposition move apart, before re-combining and interfering.

Taken together, the cyclotron orbits in figure 4 describe a rotation, with respect to the z axis, at the Larmor angular velocity ω_L. This is consistent with the predictions of classical electron optics regarding image formation in rotationally symmetric magnetic lenses [3]. Interestingly, though, in our case the axis of the Larmor rotation is not defined by a symmetry of the magnetic field—a uniform magnetic field is rotationally symmetric with respect to an infinite number of axes. Rather, here the Larmor rotation occurs with respect to the centre of mass of the electron's probability distribution. This is the case both in figure 3, where the centre of mass follows a cyclotron orbit, and in figure 4, where the centre of mass is stationary. Further, it must be remembered that we are considering here a single electron which is in a state of superposition. This means, for example, that if one of the two cyclotron components in figure 4 underwent an interaction which modified its phase, this could be detected through its effect on the subsequent interference pattern.

6. Summary and outlook

In summary, we have shown that in a magnetic field an electron can rotate around more than one axis simultaneously. The wavefunction of the electron follows a cyclotron orbit, and superposed onto this is a rotation around the instantaneous centre of mass. The rotation with respect to the centre of mass axis arises as a

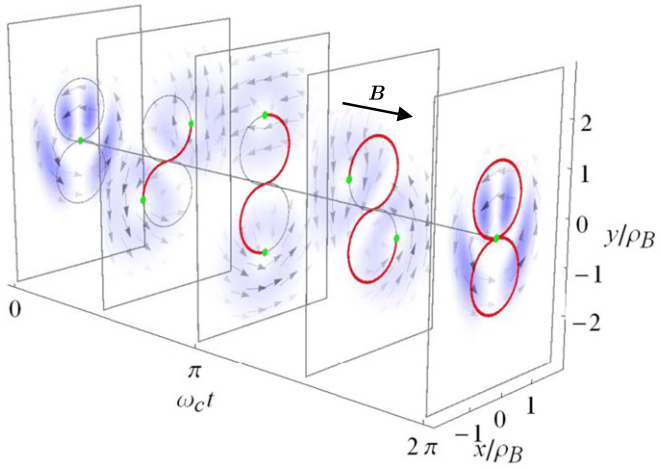

Figure 4. Probability density and current density for an equally weighted superposition of a wavefunction with $p_c = 3\hbar/\rho_B$ and $\ell = -1$ and a wavefunction with $p_c = -3\hbar/\rho_B$ and $\ell = 1$. The constituent states have the same radial distributions as in figures 2 and 3. The centre of mass of the superposition remains stationary in the x–y plane, while the individual components follow the cyclotron trajectories indicated.

result of the diamagnetic angular momentum, as well as any canonical orbital angular momentum the electron possesses. The kinetic angular momentum of the electron is therefore described by the parallel axis theorem.

Our results show that canonical orbital angular momentum and cyclotron motion provide separate degrees of freedom for shaping electron current distributions. This could allow electron beams to be structured for use in specific applications. For example, the symmetry of the current distribution could be optimized to probe specific transitions in materials [40, 44]. It may also be possible to utilize cyclotron trajectories in novel forms of interferometry. Moreover, here we have only considered the case in which the canonical angular momentum and magnetic field are parallel, so that the rotation is confined to a plane. With canonical angular momentum and magnetic fields which are in different directions to one another, the angular momentum and current density could be shaped in three dimensions.

Further, if the angular momenta were in different directions, it appears that they would become coupled. Canonical orbital angular momentum which is at an angle to a uniform magnetic field would be expected to precess around the direction of the field [22, 33]. The canonical angular momentum is also not conserved when the rotational symmetry of the magnetic field is broken, such as in astigmatic magnetic lenses [45–47]. Not only this, but in non-uniform magnetic fields the spin and orbital degrees of freedom of an electron with non-relativistic velocity are no longer independent [12, 48]. The nature of the coupling between all of these angular momenta is an interesting avenue for future investigation.

Acknowledgments

CG is supported by a SUPA Prize Studentship. We also acknowledge support from the UK EPSRC under Grant No. EP/M024423/1. CG thanks Konstantin Bliokh for stimulating discussions prior to the commencement of this work.

Appendix A. Numerical solution of Schrödinger equation

The time-dependent Schrödinger equation can be solved numerically with high accuracy and efficiency by expanding the time-evolution operator in a series of Chebyshev polynomials. In this appendix, we describe how this method can be applied to the two-dimensional Schrödinger equation for an electron interacting with an external magnetic field. For generality, we shall consider here a Hamiltonian of the form

$$\mathcal{H}(x, y) = S_2\left(\frac{\partial^2}{\partial x^2} + \frac{\partial^2}{\partial y^2}\right) + \mathrm{i}S_{1x}(x, y)\frac{\partial}{\partial x} + \mathrm{i}S_{1y}(x, y)\frac{\partial}{\partial y} + S_0(x, y) \tag{16}$$

[37] . In the case of the Hamiltonian used in the main text, we would have $S_2 = -\hbar^2/(2m)$, $S_{1x} = -\hbar eBy/(2m)$, $S_{1y} = \hbar eBx/(2m)$ and $S_0 = e^2B^2(x^2 + y^2)/(8m)$. The *Mathematica* code we have used to perform these calculations has been made available online at [49].

Since the Hamiltonian (16) is independent of time, we can write the solution of the Schrödinger equation as

$$\Psi(t + \Delta t) = \exp\left(-\frac{\mathrm{i}}{\hbar}\mathcal{H}\Delta t\right)\Psi(t). \tag{17}$$

In order to evaluate this numerically, first we must represent the wavefunction, and the coefficients S_2 etc., on a two-dimensional grid. If this grid covers an area $L_x \times L_y$, and contains $N_x \times N_y$ points, then the maximum spatial frequencies represented are $k_{x,\max} = \pi N_x/L_x$ and $k_{y,\max} = \pi N_y/L_y$. The maximum and minimum values of energy represented on the grid are then

$$\begin{aligned} E_{\max} = &- S_2\left(k_{x,\max}^2 + k_{y,\max}^2\right) + \mathrm{Max}\left(S_{1x}\right)k_{x,\max} \\ &+ \mathrm{Max}\left(S_{1y}\right)k_{y,\max} + \mathrm{Max}\left(S_0\right) \end{aligned} \tag{18}$$

and

$$E_{\min} = -\left[\mathrm{Max}\left(S_{1x}\right)k_{x,\max} + \mathrm{Max}\left(S_{1y}\right)k_{y,\max}\right] + \mathrm{Min}\left(S_0\right). \tag{19}$$

Let us now introduce a new operator

$$\tilde{\mathcal{H}} = \frac{\mathcal{H} - b}{a}, \tag{20}$$

where $a = (E_{\max} - E_{\min})/2$ and $b = (E_{\max} + E_{\min})/2$. This operator has eigenvalues represented on the grid which lie in the range $[-1,\ 1]$. We can then expand the time-evolution operator in a series of Chebyshev polynomials $T_q(\tilde{\mathcal{H}})$:

$$\begin{aligned} \Psi(t + \Delta t) &= \exp\left(-\frac{\mathrm{i}}{\hbar}b\Delta t\right)\exp\left(-\frac{\mathrm{i}}{\hbar}a\tilde{\mathcal{H}}\Delta t\right)\Psi(t) \\ &\approx \exp\left(-\frac{\mathrm{i}}{\hbar}b\Delta t\right)\sum_{q=0}^{M}\alpha_q(a\Delta t)\,T_q\left(\tilde{\mathcal{H}}\right)\Psi(t). \end{aligned} \tag{21}$$

Chebyshev polynomials are chosen as these minimize the error associated with truncating the expansion at a finite order M [35]. The expansion coefficients are given by

$$\alpha_q(a\Delta t) = \begin{cases} (-\mathrm{i})^q J_q(a\Delta t/\hbar), & q = 0 \\ 2(-\mathrm{i})^q J_q(a\Delta t/\hbar), & q \neq 0 \end{cases} \tag{22}$$

where J_q is a Bessel function. For $q > \mathrm{e}a\Delta t/(2\hbar)$, where e, in roman font, denotes the mathematical constant, the magnitudes of these coefficients decay exponentially with increasing q [50, 51]. This means that the error due to truncating the series at order M, which can be estimated by $|\alpha_M(a\Delta t)|$, can be made arbitrarily small. If we set

$$M = \frac{\mathrm{e}}{2\hbar}a\Delta t + \delta, \tag{23}$$

δ can be adjusted so that this error is less than machine precision. The numerical error resulting from the Chebyshev expansion is then negligible.

In order to evaluate the individual terms in the expansion (21), the action of the Chebyshev polynomial $T_q(\tilde{\mathcal{H}})$ on the initial wavefunction $\Psi(t)$ must be calculated. Using the recurrence relation for the Chebyshev polynomials, we obtain

$$T_q\left(\tilde{\mathcal{H}}\right)\Psi(t) = 2\tilde{\mathcal{H}}T_{q-1}\left(\tilde{\mathcal{H}}\right)\Psi(t) - T_{q-2}\left(\tilde{\mathcal{H}}\right)\Psi(t), \tag{24}$$

for $q > 0$, with the initial conditions $T_0(\tilde{\mathcal{H}})\Psi(t) = \Psi(t)$ and $T_1(\tilde{\mathcal{H}})\Psi(t) = \tilde{\mathcal{H}}\Psi(t)$. The action of the Hamiltonian on the wavefunction can be efficiently calculated by evaluating the spatial derivatives in Fourier space [50, 52]. That is,

$$\begin{aligned} \mathcal{H}\Psi(t) \approx &\, S_2\mathrm{FT}^{-1}\left[\left(-k_x^2 - k_y^2\right)\mathrm{FT}\Psi\right] + \mathrm{i}S_{1x}\mathrm{FT}^{-1}\left(\mathrm{i}k_x\mathrm{FT}\Psi\right) \\ &+ \mathrm{i}S_{1y}\mathrm{FT}^{-1}\left(\mathrm{i}k_y\mathrm{FT}\Psi\right) + S_0\Psi, \end{aligned} \tag{25}$$

where k_x, k_y are the coordinates in Fourier space and FT denotes a discrete Fourier transform and FT^{-1} the corresponding inverse transform.

References

[1] Lawrence E O and Livingston M S 1932 The production of high speed light ions without the use of high voltages *Phys. Rev.* **40** 19–37
[2] Veksler V 1945 A new method of acceleration of relativistic particles *J. Phys. Acad. Sci. USSR* **9** 153–8
[3] Hawkes P W and Kasper E 1996 *Principles of Electron Optics* (San Diego: Academic)
[4] Erckmann V and Gasparino U 1994 Electron cyclotron resonance heating and current drive in toroidal fusion plasmas *Plasma Phys. Control. Fusion* **36** 1869–962
[5] Vollmer M 2004 Physics of the microwave oven *Phys. Educ.* **39** 74–81
[6] Millo O, Katz D, Cao Y and Banin U 2001 Imaging and spectroscopy of artificial-atom states in core/shell nanocrystal quantum dots *Phys. Rev. Lett.* **86** 5751
[7] Bliokh K Y, Bliokh Y P, Savel'ev S and Nori F 2007 Semiclassical dynamics of electron wave packet states with phase vortices *Phys. Rev. Lett.* **99** 190404
[8] Uchida M and Tonomura A 2010 Generation of electron beams carrying orbital angular momentum *Nature* **464** 737–9
[9] Verbeeck J, Tian H and Schattschneider P 2010 Production and application of electron vortex beams *Nature* **467** 301–4
[10] McMorran B J, Agrawal A, Anderson I M, Herzing A A, Lezec H J, McClelland J J and Unguris J 2011 Electron vortex beams with high quanta of orbital angular momentum *Science* **331** 192–5
[11] Bliokh K Y, Dennis M R and Nori F 2011 Relativistic electron vortex beams: angular momentum and spin–orbit interaction *Phys. Rev. Lett.* **107** 174802
[12] Karimi E, Marrucci L, Grillo V and Santamato E 2012 Spin-to-orbital angular momentum conversion and spin-polarization filtering in electron beams *Phys. Rev. Lett.* **108** 044801
[13] Lloyd S, Babiker M and Yuan J 2012 Quantized orbital angular momentum transfer and magnetic dichroism in the interaction of electron vortices with matter *Phys. Rev. Lett.* **108** 074802
[14] Lloyd S M, Babiker M, Yuan J and Kerr-Edwards C 2012 Electromagnetic vortex fields, spin, and spin–orbit interactions in electron vortices *Phys. Rev. Lett.* **109** 254801
[15] Hemsing E, Knyazik A, Dunning M, Xiang D, Marinelli A, Hast C and Rosenzweig J B 2013 Coherent optical vortices from relativistic electron beams *Nat. Phys.* **9** 549–53
[16] Ivanov I P and Karlovets D V 2013 Detecting transition radiation from a magnetic moment *Phys. Rev. Lett.* **110** 264801
[17] Béché A, Van Boxem R, Van Tendeloo G and Verbeeck J 2014 Magnetic monopole field exposed by electrons *Nat. Phys.* **10** 26–29
[18] Asenjo-Garcia A and García de Abajo F J 2014 Dichroism in the interaction between vortex electron beams, plasmons, and molecules *Phys. Rev. Lett.* **113** 066102
[19] Hayrapetyan A G, Matula O, Aiello A, Surzhykov A and Fritzsche S 2014 Interaction of relativistic electron-vortex beams with few-cycle laser pulses *Phys. Rev. Lett.* **112** 134801
[20] Matula O, Hayrapetyan A G, Serbo V G, Surzhykov A and Fritzsch S 2014 Radiative capture of twisted electrons by bare ions *New J. Phys.* **16** 053024
[21] Grillo V, Gazzadi G C, Mafakheri E, Frabboni S, Karimi E and Boyd R W 2015 Holographic generation of highly twisted electron beams *Phys. Rev. Lett.* **114** 034801
[22] Gallatin G M and McMorran B 2012 Propagation of vortex electron wave functions in a magnetic field *Phys. Rev.* A **86** 012701
[23] Landau L 1930 Diamagnetismus der metalle *Z. Phys.* **64** 629–37
[24] Darwin C G 1931 The diamagnetism of the free electron *Math. Proc. Camb. Phil. Soc.* **27** 86–90
[25] Greenshields C R, Stamps R L, Franke-Arnold S and Barnett S M 2014 Is the angular momentum of an electron conserved in a uniform magnetic field? *Phys. Rev. Lett.* **113** 240404
[26] Babiker M, Yuan J and Lembessis V E 2015 Electron vortex beams subject to static magnetic fields *Phys. Rev.* A **91** 013806
[27] Schattschneider P, Schachinger Th, Stöger-Pollach M, Löffler S, Steiger-Thirsfeld A, Bliokh K Y and Nori F 2014 Imaging the dynamics of free-electron Landau states *Nat. Commun.* **5** 4586
[28] Schachinger T, Löffler S, Stöger-Pollach M and Schattschneider P 2015 Peculiar rotation of electron vortex beams *Ultramicroscopy* **158** 17–25
[29] Bliokh K Y, Schattschneider P, Verbeeck J and Nori F 2012 Electron vortex beams in a magnetic field: a new twist on Landau levels and Aharonov–Bohm states *Phys. Rev.* X **2** 041011
[30] Greenshields C, Stamps R L and Franke-Arnold S 2012 Vacuum Faraday effect for electrons *New J. Phys.* **14** 103040
[31] Lloyd S M, Babiker M and Yuan J 2013 Mechanical properties of electron vortices. *Phys. Rev.* A **88** 031802(R)
[32] Bliokh K Y and Nori F 2012 Spatiotemporal vortex beams and angular momentum *Phys. Rev.* A **86** 033824
[33] Bialynicki-Birula I, Bialynicka-Birula Z and Śliwa C 2000 Motion of vortex lines in quantum mechanics *Phys. Rev.* A **61** 032110
[34] Li C and Wang Q 1999 The quantum behaviour of an electron in a uniform magnetic field *Physica* **269B** 22–27
[35] Tal-Ezer H and Kosloff R 1984 An accurate and efficient scheme for propagating the time dependent Schrödinger equation *J. Chem. Phys.* **81** 3967–71
[36] van Dijk W, Brown J and Spyksma K 2011 Efficiency and accuracy of numerical solutions to the time-dependent Schrödinger equation *Phys. Rev.* E **84** 056703
[37] Dziubak T and Matulewski J 2012 An object-oriented implementation of a solver of the time-dependent Schrödinger equation using the CUDA technology *Comput. Phys. Commun.* **183** 800–12
[38] Guzzinati G, Schattschneider P, Bliokh K Y, Nori F and Verbeeck J 2013 Observation of the Larmor and Gouy rotations with electron vortex beams *Phys. Rev. Lett.* **110** 093601
[39] Reimer L and Kohl H 2008 *Transmission Electron Microscopy: Physics of Image Formation* (*Springer Series in Optical Sciences* vol 36) (Berlin: Springer)
[40] Verbeeck J, Guzzinati G, Clark L, Juchtmans R, van Boxem R, Tian H, Béché A, Lubk A and van Tendeloo G 2014 Shaping electron beams for the generation of innovative measurements in the (S)TEM *C. R. Phys.* **15** 190–9
[41] Voloch-Bloch N, Lereah Y, Lilach Y, Gover A and Arie A 2013 Generation of electron airy beams *Nature* **494** 331–5
[42] Grillo V, Karimi E, Gazzadi G C, Frabboni S, Dennis M R and Boyd R W 2014 Generation of nondiffracting electron Bessel beams *Phys. Rev.* X **4** 011013
[43] Harvey T R, Pierce J S, Agrawal A K, Ercius P, Linck M and McMorran B J 2014 Efficient diffractive phase optics for electrons *New J. Phys.* **16** 093039
[44] Rusz J, Idrobo J and Bhowmick S 2014 Achieving atomic resolution magnetic dichroism by controlling the phase symmetry of an electron probe *Phys. Rev. Lett.* **113** 145501

[45] Schattschneider P, Stöger-Pollach M and Verbeeck J 2012 Novel vortex generator and mode converter for electron beams *Phys. Rev. Lett.* **109** 084801
[46] Clark L, Béché A, Guzzinati G, Lubk A, Mazilu M, van Boxem R and Verbeeck J 2013 Exploiting lens aberrations to create electron-vortex beams *Phys. Rev. Lett.* **111** 064801
[47] Petersen T C, Weyland M, Paganin D M, Simula T P, Eastwood S A and Morgan M J 2013 Electron vortex production and control using aberration induced diffraction catastrophes *Phys. Rev. Lett.* **110** 033901
[48] Gallup G A, Batelaan H and Gay T J 2001 Quantum-mechanical analysis of a longitudinal Stern–Gerlach effect *Phys. Rev. Lett.* **86** 4508–11
[49] Greenshields C 2015 *Mathematica* program for the numerical solution of the time-dependent Schrödinger equation in the presence of a magnetic field (http://dx.doi.org/10.5525/gla.researchdata.199)
[50] Wang J B and Scholz T T 1998 Time-dependent approach to scattering by Chebyshev-polynomial expansion and the fast-Fourier-transform algorithm *Phys. Rev.* A **57** 3554–9
[51] Weiße A and Fehske H 2008 Chebyshev expansion techniques *Computational Many-Particle Physics* (*Lecture Notes in Physics* vol 739) (Berlin: Springer) pp 545–577
[52] Kosloff D and Kosloff R 1983 A Fourier method solution for the time dependent Schrödinger equation as a tool in molecular dynamics *J. Comput. Phys.* **52** 35–53

Bibliography

[1] B. J. McMorran, A. Agrawal, I. M. Anderson, A. A. Herzing, H. J. Lezec, J. J. McClelland, and J. Unguris. Electron vortex beams with high quanta of orbital angular momentum. *Science*, 331:192–195, 2011.

[2] P. Schattschneider, Th. Schachinger, M. Stöger-Pollach, S. Löffler, A. Steiger-Thirsfeld, K. Y. Bliokh, and F. Nori. Imaging the dynamics of free-electron Landau states. *Nat. Commun.*, 5:4586, 2014.

[3] O. Heaviside. The radiation from an electron describing a circular orbit. *Nature (London)*, 69:293–294, 1904.

[4] D. M. Brink and G. R. Satchler. *Angular Momentum.* Oxford University Press, 3rd edition, 1993.

[5] E. Noether. Invariante Variationsprobleme. *Nachrichten der Königlichen Gesellschaft der Wissenschaften zu Göttingen, Math.-Phys. Klasse*, pages 235–257, 1918.

[6] D. E. Neuenschwander. *Emmy Noether's Wonderful Theorem.* Johns Hopkins, Baltimore, MD, 2011.

[7] C. Cohen-Tannoudji, J. Dupont-Roc, and G. Grynberg. *Photons and Atoms: Introduction to Quantum Electrodynamics*, page 45. Wiley, New York, 1997.

[8] J. H. Poynting. The wave motion of a revolving shaft, and a suggestion as to the angular momentum in a beam of circularly polarised light. *Proc. R. Soc. London A*, 82:560–567, 1909.

[9] R. A. Beth. Mechanical detection and measurement of the angular momentum of light. *Phys. Rev.*, 50:115–125, 1936.

[10] C. Cohen-Tannoudji, B. Diu, and F. Laloë. *Quantum Mechanics*. Wiley-VCH, Weinheim, 2005.

[11] E. J. Konopinski. What the electromagnetic vector potential describes. *Am. J. Phys.*, 46:499–502, 1978.

[12] U. Leonhardt. Optics: Momentum in an uncertain light. *Nature (London)*, 444:823–824, 2006.

[13] S. M. Barnett. Resolution of the Abraham-Minkowski dilemma. *Phys. Rev. Lett.*, 104:070401, 2010.

[14] S. M. Barnett and R. Loudon. The enigma of optical momentum in a medium. *Phil. Trans. R. Soc. A*, 368:927–939, 2010.

[15] H. J. Lipkin and M. Peshkin. Angular momentum paradoxes with solenoids and monopoles. *Phys. Lett. B*, 118:385–390, 1982.

[16] G. G. Lombardi. Feynman's disk paradox. *Am. J. Phys.*, 51:213–214, 1983.

[17] M. Peshkin. The Aharonov-Bohm effect: Why it cannot be eliminated from quantum mechanics. *Phys. Rep.*, 80:375–386, 1981.

[18] F. Wilczek. Magnetic flux, angular momentum, and statistics. *Phys. Rev. Lett.*, 48:1144–1146, 1982.

[19] M. Faraday. On the magnetization of light and the illumination of magnetic lines of force. *Phil. Trans. R. Soc. Lon.*, 136:1–20, 1846.

[20] M. Freiser. A survey of magnetooptic effects. *IEEE Trans. Magn.*, 4:152–161, 1968.

[21] L. Allen, M. W. Beijersbergen, R. J. C. Spreeuw, and J. P. Woerdman. Orbital angular momentum of light and the transformation of Laguerre-Gaussian laser modes. *Phys. Rev. A*, 45:8185–8189, 1992.

[22] A. M. Yao and M. J. Padgett. Orbital angular momentum: origins, behavior and applications. *Adv. Opt. Photon.*, 3:161–204, 2011.

[23] V. I. Bazhenov, M. V. Vasnetsov, and M. S. Soskin. Laser beams with wave front screw dislocations. *JETP Lett.*, 52:429–431, 1990.

[24] N. R. Heckenberg, R. McDuff, C. P. Smith, H. Rubinsztein-Dunlop, and M. J. Wegener. Laser beams with phase singularities. *Opt. Quant. Electron.*, 24:S951–S962, 1992.

[25] J. F. Nye and M. V. Berry. Dislocations in wave trains. *Proc. R. Soc. London A*, 336:165–190, 1974.

[26] D. L. Andrews. *Structured light and its applications.* Academic Press, Palo Alto, CA, 2008.

[27] L. Allen and M. Padgett. Equivalent geometric transformations for spin and orbital angular momentum of light. *J. Mod. Optic.*, 54:487–491, 2007.

[28] M. Padgett, G. Whyte, J. Girkin, A. Wright, L. Allen, P. Öhberg, and S. M. Barnett. Polarization and image rotation induced by a rotating dielectric rod: an optical angular momentum interpretation. *Opt. Lett.*, 31:2205–2207, 2006.

[29] J. B. Götte, S. M. Barnett, and M. Padgett. On the dragging of light by a rotating medium. *Proc. R. Soc. London A*, 463:2185–2194, 2007.

[30] S. Franke-Arnold, G. Gibson, R. W. Boyd, and M. J. Padgett. Rotary photon drag enhanced by a slow-light medium. *Science*, 333:65–67, 2011.

[31] G. Nienhuis, J. P. Woerdman, and I. Kuščer. Magnetic and mechanical Faraday effects. *Phys. Rev. A*, 46:7079–7092, 1992.

[32] M. Babiker, C. R. Bennett, D. L. Andrews, and L. C. Dávila Romero. Orbital angular momentum exchange in the interaction of twisted light with molecules. *Phys. Rev. Lett.*, 89:143601, 2002.

[33] D. L. Andrews, L. C. Dávila Romero, and M. Babiker. On optical vortex interactions with chiral matter. *Opt. Comm.*, 237:133–139, 2004.

[34] F. Araoka, T. Verbiest, K. Clays, and A. Persoons. Interactions of twisted light with chiral molecules: An experimental investigation. *Phys. Rev. A*, 71:055401, 2005.

[35] W. Löffler, M. P. van Exter, G. W. 't Hooft, G. Nienhuis, D. J. Broer, and J. P. Woerdman. Search for Hermite-Gauss mode rotation in cholesteric liquid crystals. *Opt. Express*, 19:12978–12983, 2011.

[36] K. Y. Bliokh, Y. P. Bliokh, S. Savel'ev, and F. Nori. Semiclassical dynamics of electron wave packet states with phase vortices. *Phys. Rev. Lett.*, 99:190404, 2007.

[37] M. Uchida and A. Tonomura. Generation of electron beams carrying orbital angular momentum. *Nature (London)*, 464:737–739, 2010.

[38] J. Verbeeck, H. Tian, and P. Schattschneider. Production and application of electron vortex beams. *Nature (London)*, 467:301–304, 2010.

[39] I. Bialynicki-Birula, Z. Bialynicka-Birula, and C. Śliwa. Motion of vortex lines in quantum mechanics. *Phys. Rev. A*, 61:032110, 2000.

[40] L. Ph. H. Schmidt, C. Goihl, D. Metz, H. Schmidt-Böcking, R. Dörner, S. Yu. Ovchinnikov, J. H. Macek, and D. R. Schultz. Vortices associated with the wave function of a single electron emitted in slow ion-atom collisions. *Phys. Rev. Lett.*, 112:083201, 2014.

[41] G. K. Batchelor. *An Introduction to Fluid Dynamics*. Cambridge University Press, 1967.

[42] K. W. Madison, F. Chevy, W. Wohlleben, and J. Dalibard. Vortex formation in a stirred Bose-Einstein condensate. *Phys. Rev. Lett.*, 84:806–809, 2000.

[43] M. W. Zwierlein, J. R. Abo-Shaeer, A. Schirotzek, C. H. Schunck, and W. Ketterle. Vortices and superfluidity in a strongly interacting Fermi gas. *Nature (London)*, 435:1047–1051, 2005.

[44] A. L. Fetter. Rotating trapped Bose-Einstein condensates. *Rev. Mod. Phys.*, 81:647–691, 2009.

[45] K. Y. Bliokh, M. R. Dennis, and F. Nori. Relativistic electron vortex beams: angular momentum and spin-orbit interaction. *Phys. Rev. Lett.*, 107:174802, 2011.

[46] S. M. Lloyd, M. Babiker, J. Yuan, and C. Kerr-Edwards. Electromagnetic vortex fields, spin, and spin-orbit interactions in electron vortices. *Phys. Rev. Lett.*, 109:254801, 2012.

[47] H. C. Ohanian. What is spin? *Am. J. Phys.*, 54:500–505, 1986.

[48] J. Harris, V. Grillo, E. Mafakheri, G. C. Gazzadi, S. Frabboni, R. W. Boyd, and E. Karimi. Structured quantum waves. *Nature Phys.*, 11:629–634, 2015.

[49] D. B. Williams and C. B. Carter. *Transmission Electron Microscopy.* Springer, Berlin, 2009.

[50] T. R. Harvey, J. S. Pierce, A. K. Agrawal, P. Ercius, M. Linck, and B. J. McMorran. Efficient diffractive phase optics for electrons. *New J. Phys.*, 16:093039, 2014.

[51] V. Grillo, G. C. Gazzadi, E. Mafakheri, S. Frabboni, E. Karimi, and R. W. Boyd. Holographic generation of highly twisted electron beams. *Phys. Rev. Lett.*, 114:034801, 2015.

[52] A. Tonomura, J. Endo, T. Matsuda, T. Kawasaki, and H. Ezawa. Demonstration of single-electron buildup of an interference pattern. *Am. J. Phys.*, 57:117–120, 1989.

[53] A. Tonomura. *The Quantum World Unveiled by Electron Waves.* World Scientific, Singapore, 1998.

[54] J. Verbeeck, P. Schattschneider, S. Lazar, M. Stöger-Pollach, S. Löffler, A. Steiger-Thirsfeld, and G. Van Tendeloo. Atomic scale electron vortices for nanoresearch. *Appl. Phys. Lett.*, 99:203109, 2011.

[55] S. Lloyd, M. Babiker, and J. Yuan. Quantized orbital angular momentum transfer and magnetic dichroism in the interaction of electron vortices with matter. *Phys. Rev. Lett.*, 108:074802, 2012.

[56] J. Rusz and S. Bhowmick. Boundaries for efficient use of electron vortex beams to measure magnetic properties. *Phys. Rev. Lett.*, 111:105504, 2013.

[57] P. Schattschneider, B. Schaffer, I. Ennen, and J. Verbeeck. Mapping spin-polarized transitions with atomic resolution. *Phys. Rev. B*, 85:134422, 2012.

[58] A. Asenjo-Garcia and F. J. García de Abajo. Dichroism in the interaction between vortex electron beams, plasmons, and molecules. *Phys. Rev. Lett.*, 113:066102, 2014.

[59] J. Verbeeck, H. Tian, and G. Van Tendeloo. How to manipulate nanoparticles with an electron beam? *Adv. Mater.*, 25:1114–1117, 2013.

[60] S. M. Lloyd, M. Babiker, and J. Yuan. Mechanical properties of electron vortices. *Phys. Rev. A*, 88:031802(R), 2013.

[61] E. Karimi, L. Marrucci, V. Grillo, and E. Santamato. Spin-to-orbital angular momentum conversion and spin-polarization filtering in electron beams. *Phys. Rev. Lett.*, 108:044801, 2012.

[62] V. Grillo, L. Marrucci, E. Karimi, R. Zanella, and E. Santamato. Quantum simulation of a spin polarization device in an electron microscope. *New J. Phys.*, 15:093026, 2013.

[63] I. P. Ivanov. Colliding particles carrying nonzero orbital angular momentum. *Phys. Rev. D*, 83:093001, 2011.

[64] I. P. Ivanov and V. G. Serbo. Scattering of twisted particles: Extension to wave packets and orbital helicity. *Phys. Rev. A*, 84:033804, 2011.

[65] I. P. Ivanov and D. V. Karlovets. Detecting transition radiation from a magnetic moment. *Phys. Rev. Lett.*, 110:264801, 2013.

[66] N. Voloch-Bloch, Y. Lereah, Y. Lilach, A. Gover, and A. Arie. Generation of electron Airy beams. *Nature (London)*, 494:331–335, 2013.

[67] V. Grillo, E. Karimi, G. C. Gazzadi, S. Frabboni, M. R. Dennis, and R. W. Boyd. Generation of nondiffracting electron Bessel beams. *Phys. Rev. X*, 4:011013, 2014.

[68] J. Rusz, J. Idrobo, and S. Bhowmick. Achieving atomic resolution magnetic dichroism by controlling the phase symmetry of an electron probe. *Phys. Rev. Lett.*, 113:145501, 2014.

[69] E. O. Lawrence and M. S. Livingston. The production of high speed light ions without the use of high voltages. *Phys. Rev.*, 40:19–37, 1932.

[70] L. D. Landau and E. M. Lifshitz. *Quantum Mechanics: Nonrelativistic Theory*. Pergamon, Oxford, 1977.

[71] A. Landé. Über den anomalen Zeemaneffekt (Teil I). *Z. Physik*, 5:231–241, 1921.

[72] K. Hentschel. Paschenback effect. In D. Greenberger, K. Hentschel, and F. Weinert, editors, *Compendium of Quantum Physics*, pages 468–470. Springer, Berlin, 2009.

[73] P. Zeeman. XXXII. On the influence of magnetism on the nature of the light emitted by a substance. *Philos. Mag. Series 5*, 43:226–239, 1897.

[74] B. H. Bransden and C. J. Joachain. *Physics of Atoms and Molecules*. Longman, Harlow, 1983.

[75] R. Cade. Larmor's theorem in quantum mechanics. *Am. J. Phys.*, 18:114–115, 1950.

[76] G. M. Gallatin and B. McMorran. Propagation of vortex electron wave functions in a magnetic field. *Phys. Rev. A*, 86:012701, 2012.

[77] M. Faraday. On new magnetic actions, and on the magnetic condition of all matter. *Phil. Trans. R. Soc. Lon.*, 136:21–62, 1846.

[78] C. Kittel. *Introduction to Solid State Physics*. Wiley, Hoboken, NJ, 8th edition, 2004.

[79] P. Langevin. Magnétisme et théorie des électrons. *Ann. Chim. Phys.*, 5:70–127, 1905.

[80] D. Jiles. *Magnetism and Magnetic Materials*. Chapman and Hall, London, 2nd edition, 1998.

[81] L. Landau. Diamagnetismus der metalle. *Z. Phys.*, 64:629–637, 1930. English translation: Diamagnetism of metals. In D. ter Haar, editor, *Collected Papers of L. D. Landau*, pages 31–38. Pergamon, London, 1965.

[82] C. G. Darwin. The diamagnetism of the free electron. *Math. Proc. Cambridge Phil. Soc.*, 27:86–90, 1931.

[83] C. Kittel. *Quantum Theory of Solids*. Wiley, New York, 2nd edition, 1987.

[84] D. Shoenberg. *Magnetic Oscillations in Metals*. Cambridge University Press, 1984.

[85] Z. F. Ezawa. *Quantum Hall Effects*. World Scientific, Singapore, 2013.

[86] C. Greenshields, R. L. Stamps, and S. Franke-Arnold. Vacuum Faraday effect for electrons. *New J. Phys.*, 14:103040, 2012.

[87] K. Y. Bliokh, P. Schattschneider, J. Verbeeck, and F. Nori. Electron vortex beams in a magnetic field: a new twist on Landau levels and Aharonov-Bohm states. *Phys. Rev. X*, 2:041011, 2012.

[88] K. Hashimoto, T. Champel, S. Florens, C. Sohrmann, J. Wiebe, Y. Hirayama, R. A. Römer, R. Wiesendanger, and M. Morgenstern. Robust nodal structure of Landau level wave functions revealed by Fourier transform scanning tunneling spectroscopy. *Phys. Rev. Lett.*, 109:116805, 2012.

[89] S. Nomura, L. Samuelson, M.-E. Pistol, K. Uchida, N. Miura, T. Sugano, and Y. Aoyagi. Landau level formation in semiconductor quantum dots in a high magnetic field. *Appl. Phys. Lett.*, 71:2316–2318, 1997.

[90] S. Peil and G. Gabrielse. Observing the quantum limit of an electron cyclotron: QND measurements of quantum jumps between Fock states. *Phys. Rev. Lett.*, 83:1287–1290, 1999.

[91] E. Bauer. Low energy electron microscopy. *Rep. Prog. Phys.*, 57:895, 1994.

[92] S. Anders, H. A. Padmore, R. M. Duarte, T. Renner, T. Stammler, A. Scholl, M. R. Scheinfein, J. Stöhr, L. Séve, and B. Sinkovic. Photoemission electron microscope for the study of magnetic materials. *Rev. Sci. Instrum.*, 70:3973–3981, 1999.

[93] P. W. Hawkes and E. Kasper. *Principles of Electron Optics*. Academic Press, Palo Alto, CA, 1996.

[94] D. Hanneke, S. Fogwell, and G. Gabrielse. New measurement of the electron magnetic moment and the fine structure constant. *Phys. Rev. Lett.*, 100:120801, 2008.

[95] G. A. Gallup, H. Batelaan, and T. J. Gay. Quantum-mechanical analysis of a longitudinal Stern-Gerlach effect. *Phys. Rev. Lett.*, 86:4508–4511, 2001.

[96] S. McGregor, R. Bach, and H. Batelaan. Transverse quantum Stern-Gerlach magnets for electrons. *New J. Phys.*, 13:065018, 2011.

[97] M. Babiker, J. Yuan, and V. E. Lembessis. Electron vortex beams subject to static magnetic fields. *Phys. Rev. A*, 91:013806, 2015.

[98] C. Li and Q. Wang. The quantum behaviour of an electron in a uniform magnetic field. *Physica (Amsterdam)*, 269B:22–27, 1999.

[99] T. Schachinger, S. Löffler, M. Stöger-Pollach, and P. Schattschneider. Peculiar rotation of electron vortex beams. *Ultramicroscopy*, 158:17–25, 2015.

[100] P. A. M. Dirac. Quantised singularities in the electromagnetic field. *Proc. R. Soc. London A*, 133:60–72, 1931.

[101] Y. Aharonov and D. Bohm. Significance of electromagnetic potentials in the quantum theory. *Phys. Rev.*, 115:485–491, 1959.

[102] H. Busch. Über die Wirkungsweise der Konzentrierungsspule bei der Braunschen Röhre. *Arch. Elektrotech.*, 18:583–594, 1927.

[103] L. Reimer and H. Kohl. *Transmission Electron Microscopy: Physics of Image Formation*, volume 36 of *Springer Series in Optical Sciences*. Springer, Berlin, 2008.

[104] A. K. Petford-Long and J. N. Chapman. Lorentz microscopy. In *Magnetic Microscopy of Nanostructures*, NanoScience and Technology, pages 67–86. Springer, Berlin, 2005.

[105] H. Lichte and M. Lehmann. Electron holography—basics and applications. *Rep. Prog. Phys.*, 71:016102, 2008.

[106] M. Peshkin and A. Tonomura. *The Aharonov-Bohm Effect*, volume 340 of *Lecture Notes in Physics*. Springer, Berlin, 1989.

[107] A. Tonomura, N. Osakabe, T. Matsuda, T. Kawasaki, J. Endo, S. Yano, and H. Yamada. Evidence for Aharonov-Bohm effect with magnetic field completely shielded from electron wave. *Phys. Rev. Lett.*, 56:792–795, 1986.

[108] N. Osakabe, T. Matsuda, T. Kawasaki, J. Endo, A. Tonomura, S. Yano, and H. Yamada. Experimental confirmation of Aharonov-Bohm effect using a toroidal magnetic field confined by a superconductor. *Phys. Rev. A*, 34:815–822, 1986.

[109] P. Schattschneider, M. Stöger-Pollach, and J. Verbeeck. Novel vortex generator and mode converter for electron beams. *Phys. Rev. Lett.*, 109:084801, 2012.

[110] L. Clark, A. Béché, G. Guzzinati, A. Lubk, M. Mazilu, R. Van Boxem, and J. Verbeeck. Exploiting lens aberrations to create electron-vortex beams. *Phys. Rev. Lett.*, 111:064801, 2013.

[111] T. C. Petersen, M. Weyland, D. M. Paganin, T. P. Simula, S. A. Eastwood, and M. J. Morgan. Electron vortex production and control using aberration induced diffraction catastrophes. *Phys. Rev. Lett.*, 110:033901, 2013.

[112] A. Béché, R. Van Boxem, G. Van Tendeloo, and J. Verbeeck. Magnetic monopole field exposed by electrons. *Nature Phys.*, 10:26–29, 2014.

[113] A. M. Blackburn and J. C. Loudon. Vortex beam production and contrast enhancement from a magnetic spiral phase plate. *Ultramicroscopy*, 136:127–143, 2014.

[114] P. Schattschneider, S. Löffler, M. Stöger-Pollach, and J. Verbeeck. Is magnetic chiral dichroism feasible with electron vortices? *Ultramicroscopy*, 136:81–85, 2014.

[115] G. Guzzinati, P. Schattschneider, K. Y. Bliokh, F. Nori, and J. Verbeeck. Observation of the Larmor and Gouy rotations with electron vortex beams. *Phys. Rev. Lett.*, 110:093601, 2013.

[116] W. Ehrenberg and R. E. Siday. The refractive index in electron optics and the principles of dynamics. *Proc. Phys. Soc. B*, 62:8–21, 1949.

[117] W. Glaser and P. Schiske. Elektronenoptische Abbildung auf Grund der Wellenmechanik. *Ann. Phys.*, 447:240–280, 1953.

[118] K. Hasegawa, Y. Saitoh, N. Tanaka, and M. Uchida. Propagation dynamics of electron vortex pairs. *J. Phys. Soc. Jpn*, 82:073402, 2013.

[119] J. Verbeeck, H. Tian, and A. Béché. A new way of producing electron vortex probes for STEM. *Ultramicroscopy*, 113:83–87, 2012.

[120] K. Saitoh, Y. Hasegawa, N. Tanaka, and M. Uchida. Production of electron vortex beams carrying large orbital angular momentum using spiral zone plates. *J. Electron Microsc.*, 61:171–177, 2012.

[121] G. Pozzi. A multislice approach to magnetic electron lens theory. *Ultramicroscopy*, 30:417–424, 1989.

[122] W. Glaser. Strenge Berechnung magnetischer Linsen der Feldform $H = H_0/[1 + (z/a)^2]$. *Z. Phys.*, 117:285–315, 1941.

[123] S. A. Khan and R. Jagannathan. Quantum mechanics of charged-particle beam transport through magnetic lenses. *Phys. Rev. E*, 51:2510–2515, 1995.

[124] H. A. Ferwerda, B. J. Hoenders, and C. H. Slump. Fully relativistic treatment of electron-optical image formation based on the Dirac equation. *Opt. Acta*, 33:145–157, 1986.

[125] P. W. Hawkes. Aberration correction past and present. *Phil. Trans. R. Soc. A*, 367:3637–3664, 2009.

[126] J. Arlt. Handedness and azimuthal energy flow of optical vortex beams. *J. Mod. Optic.*, 50:1573–1580, 2003.

[127] J. Hamazaki, Y. Mineta, K. Oka, and R. Morita. Direct observation of Gouy phase shift in a propagating optical vortex. *Opt. Express*, 14:8382–8392, 2006.

[128] K. Saitoh, Y. Hasegawa, K. Hirakawa, N. Tanaka, and M. Uchida. Measuring the orbital angular momentum of electron vortex beams using a forked grating. *Phys. Rev. Lett.*, 111:074801, 2013.

[129] G. Guzzinati, L. Clark, A. Béché, and J. Verbeeck. Measuring the orbital angular momentum of electron beams. *Phys. Rev. A*, 89:025803, 2014.

[130] L. Clark, A. Béché, G. Guzzinati, and J. Verbeeck. Quantitative measurement of orbital angular momentum in electron microscopy. *Phys. Rev. A*, 89:053818, 2014.

[131] R. Shiloh, Y. Tsur, R. Remez, Y. Lereah, B. A. Malomed, V. Shvedov, C. Hnatovsky, W. Krolikowski, and A. Arie. Unveiling the orbital angular momentum and acceleration of electron beams. *Phys. Rev. Lett.*, 114:096102, 2015.

[132] N. H. Dekkers and H. de Lang. Differential phase contrast in a STEM. *Optik*, 41:452–456, 1974.

[133] N. Shibata, S. D. Findlay, Y. Kohno, H. Sawada, Y. Kondo, and Y. Ikuhara. Differential phase-contrast microscopy at atomic resolution. *Nature Phys.*, 8:611–615, 2012.

[134] A. Lubk and J. Zweck. Differential phase contrast: An integral perspective. *Phys. Rev. A*, 91:023805, 2015.

[135] J. N. Chapman. The investigation of magnetic domain structures in thin foils by electron microscopy. *J. Phys. D: Appl. Phys.*, 17:623, 1984.

[136] J. N. Chapman, I. R. McFadyen, and S. McVitie. Modified differential phase contrast Lorentz microscopy for improved imaging of magnetic structures. *IEEE Transactions on Magnetics*, 26:1506–1511, 1990.

[137] M. R. Teague. Deterministic phase retrieval: a Green's function solution. *J. Opt. Soc. Am.*, 73:1434–1441, 1983.

[138] K. Ishizuka and B. Allman. Phase measurement of atomic resolution image using transport of intensity equation. *J. Electron Microsc.*, 54:191–197, 2005.

[139] A. Lubk, G. Guzzinati, F. Börrnert, and J. Verbeeck. Transport of intensity phase retrieval of arbitrary wave fields including vortices. *Phys. Rev. Lett.*, 111:173902, 2013.

[140] K. Y. Bliokh and F. Nori. Spatiotemporal vortex beams and angular momentum. *Phys. Rev. A*, 86:033824, 2012.

[141] H. Tal-Ezer and R. Kosloff. An accurate and efficient scheme for propagating the time dependent Schrödinger equation. *J. Chem. Phys.*, 81:3967–3971, 1984.

[142] W. van Dijk, J. Brown, and K. Spyksma. Efficiency and accuracy of numerical solutions to the time-dependent Schrödinger equation. *Phys. Rev. E*, 84:056703, 2011.

[143] T. Dziubak and J. Matulewski. An object-oriented implementation of a solver of the time-dependent Schrödinger equation using the CUDA technology. *Comp. Phys. Comm.*, 183:800–812, 2012.

[144] C. R. Greenshields, R. L. Stamps, S. Franke-Arnold, and S. M. Barnett. Is the angular momentum of an electron conserved in a uniform magnetic field? *Phys. Rev. Lett.*, 113:240404, 2014.

[145] J. Verbeeck, G. Guzzinati, L. Clark, R. Juchtmans, R. Van Boxem, H. Tian, A. Béché, A. Lubk, and G. Van Tendeloo. Shaping electron beams for the generation of innovative measurements in the (S)TEM. *C. R. Physique*, 15:190–199, 2014.

[146] C. Greenshields. *Mathematica* program for the numerical solution of the time-dependent Schrödinger equation in the presence of a magnetic field [data collection]. http://dx.doi.org/10.5525/gla.researchdata.199, 2015.

[147] J. B. Wang and T. T. Scholz. Time-dependent approach to scattering by Chebyshev-polynomial expansion and the fast-Fourier-transform algorithm. *Phys. Rev. A*, 57:3554–3559, 1998.

[148] A. Weiße and H. Fehske. Chebyshev expansion techniques. In *Computational Many-Particle Physics*, volume 739 of *Lecture Notes in Physics*, pages 545–577. Springer, Berlin, 2008.

[149] D. Kosloff and R. Kosloff. A Fourier method solution for the time dependent Schrödinger equation as a tool in molecular dynamics. *J. Comp. Phys.*, 52:35–53, 1983.

[150] D. J. Tannor. *Introduction to Quantum Mechanics: A Time Dependent Perspective*. University Science Books, Herndon, VA, 2007.

[151] NIST Digital Library of Mathematical Functions. http://dlmf.nist.gov/10.9.E2, Version 1.0.9.

[152] NIST Digital Library of Mathematical Functions. http://dlmf.nist.gov/10.19.E1, Version 1.0.9.

[153] C. Leforestier et al. A comparison of different propagation schemes for the time dependent Schrödinger equation. *J. Comp. Phys.*, 94:59–80, 1991.

[154] J. M. Aguirregabiria and A. Hernandez. The feynman paradox revisited. *Eur. J. Phys.*, 2:168–170, 1981.

[155] R. L. Phillips and L. C. Andrews. Spot size and divergence for Laguerre Gaussian beams of any order. *Appl. Opt.*, 22:643–644, 1983.

[156] D. J. Griffiths. *Introduction to Electrodynamics*. Addison Wesley, Boston, MA, 3rd edition, 1998.

[157] G. Woan. *The Cambridge Handbook of Physics Formulas*, page 40. Cambridge University Press, 2003.

[158] D. M. Asner et al. Single-electron detection and spectroscopy via relativistic cyclotron radiation. *Phys. Rev. Lett.*, 114:162501, 2015.

[159] S. I. Kanorsky, A. Weis, J. Wurster, and T. W. Hänsch. Quantitative investigation of the resonant nonlinear Faraday effect under conditions of optical hyperfine pumping. *Phys. Rev. A*, 47:1220–1226, 1993.

[160] G. Labeyrie, C. Miniatura, and R. Kaiser. Large Faraday rotation of resonant light in a cold atomic cloud. *Phys. Rev. A*, 64:033402, 2001.

[161] J. W. Warwick and G. A. Dulk. Faraday rotation on decametric radio emissions from Jupiter. *Science*, 145:380–383, 1964.

[162] M. Mendillo. Storms in the ionosphere: patterns and processes for total electron content. *Rev. Geophys.*, 44(RG4001), 2006.

[163] J. Courtial. Self-imaging beams and the Gouy effect. *Opt. Comm.*, 151:1–4, 1998.

[164] S. M. Baumann, D. M. Kalb, L. H. MacMillan, and E. J. Galvez. Propagation dynamics of optical vortices due to Gouy phase. *Opt. Express*, 17:9818–9827, 2009.

[165] A. E. Siegman. *Lasers*. University Science Books, Sausalito, CA, 1986.

[166] E. J. Kirkland. *Advanced Computing in Electron Microscopy*. Springer, New York, 2nd edition, 2010.

[167] S. Franke-Arnold, S. M. Barnett, E. Yao, J. Leach, J. Courtial, and M. Padgett. Uncertainty principle for angular position and angular momentum. *New J. Phys.*, 6:103, 2004.

[168] A. Bekshaev, K. Y. Bliokh, and M. Soskin. Internal flows and energy circulation in light beams. *J. Opt.*, 13:053001, 2011.

[169] M. V. Berry. Optical currents. *J. Opt. A: Pure Appl. Opt.*, 11:094001, 2009.

[170] Y. Zhao, J. S. Edgar, G. D. M. Jeffries, D. McGloin, and D. T. Chiu. Spin-to-orbital angular momentum conversion in a strongly focused optical beam. *Phys. Rev. Lett.*, 99:073901, 2007.

[171] K. Y. Bliokh, M. A. Alonso, E. A. Ostrovskaya, and A. Aiello. Angular momenta and spin-orbit interaction of nonparaxial light in free space. *Phys. Rev. A*, 82:063825, 2010.

[172] V. Krueckl and T. Kramer. Revivals of quantum wavepackets in graphene. *New J. Phys.*, 11:093010, 2009.

[173] C. P. Koch, José P. Palao, R. Kosloff, and F. Masnou-Seeuws. Stabilization of ultracold molecules using optimal control theory. *Phys. Rev. A*, 70:013402, 2004.

[174] W. Gerlach and O. Stern. Das magnetische Moment des Silberatoms. *Z. Phys.*, 9:353–355, 1922.

[175] B. M. Garraway and S. Stenholm. Does a flying electron spin? *Contemp. Phys.*, 43:147–160, 2002.

[176] B. M. Garraway and S. Stenholm. Observing the spin of a free electron. *Phys. Rev. A*, 60:63–79, 1999.

[177] J. Larson, B. M. Garraway, and S. Stenholm. Transient effects on electron spin observation. *Phys. Rev. A*, 69:032103, 2004.

[178] G. C. G. Berkhout, M. P. J. Lavery, J. Courtial, M. W. Beijersbergen, and M. J. Padgett. Efficient sorting of orbital angular momentum states of light. *Phys. Rev. Lett.*, 105:153601, 2010.

[179] M. P. J. Lavery, D. J. Robertson, G. C. G. Berkhout, G. D. Love, M. J. Padgett, and J. Courtial. Refractive elements for the measurement of the orbital angular momentum of a single photon. *Opt. Express*, 20:2110–2115, 2012.